UNIVERSITEIT
STELLENBOSCH
UNIVERSITY

Petrogenesis of the syntectonic Matok Pluton in the Limpopo Belt (South Africa) and its implications on the geodynamic environment

by
Mafusi Rapopo

Thesis submitted to the Faculty of Science, Stellenbosch University, in fulfilment of the requirements for the degree of
Masters in Geology
2011

Supervisors: Prof. Gary Stevens and Dr Jean-Francois Moyen

DECLARATION

I, Mafusi Rapopo, hereby declare that the work presented in this thesis is my own and where other people's work has been used, such thoughts and contributions have been attributed, and appropriately cited. I have not previously submitted any part of this work at any university for the award of a degree.

December.....2011

ABSTRACT

The ~2.67 Ga Matok pluton comprises calc-alkaline pyroxene (px)-bearing and px-free granitoids. The pluton was constructed by means of two episodes of intrusion each of which had co-magmatic px-bearing and px-free granitoid groups. All the granitoid groups (px-bearing and px-free) are characterised by non-porphyritic and porphyritic varieties. The phenocrysts in both episodes of intrusion are plagioclase ± alkali feldspar and are aligned parallel to the trend of the Limpopo Belt, attesting to a syntectonic emplacement. The time gap between the first and second intrusion is insignificant and magma was most likely stored in the chamber after the first intrusion. Petrography and geochemical signature of both px-bearing and px-free granitoid samples have been studied and a petrogenetic model which accounts for the coeval px-bearing and px-free granitoids is proposed. The relevance of the syntectonic emplacement of the Matok pluton in the Limpopo Belt is also addressed.

Px-bearing granitoids always have clinopyroxene but orthopyroxene is not always present. Magnetite and ilmenite are present in both px-bearing and px-free granitoids but are more abundant in the px-bearing granitoids and subordinate in the px-free granitoids. Plagioclase in both px-bearing and px-free granitoids is of oligoclase (An_{12-30}) composition but is relatively more calcic and increases in modal abundance in the px-bearing granitoids. Alkali feldspar is more dominant in the px-free granitoids. Hornblende is present in all the px-bearing granitoids and the px-free granitoids with ≤71 wt.% SiO_2 but is absent in the px-free granites with >71 wt.% SiO_2. Both magmatic epidote and titanite occur exclusively in the px-free granitoids with ≤71 wt.% SiO_2 and are absent in all the px-bearing granitoids as well as the px-free granites with >71 wt.% SiO_2.

Px-bearing granitoids are mainly of dioritic and granodioritic and have subordinate granitic composition while px-free granitoids are mainly of granitic and granodioritic and have subordinate dioritic composition. All the rocks define well correlated variation of SiO_2 with the rest of the major elements. However, there is always a hiatus between the granites with >71 wt.% SiO_2 and all other rocks. Px-bearing and px-free granitoids at the same SiO_2 concentrations tend to have approximately equal concentrations of MgO, CaO and TiO_2, whereas K_2O concentration is distinctively higher for the px-free granitoids. The distribution of the high field strength elements (HFSE; Nb, Ta, Zr and Hf) and rare earth elements (REE) is similar in both px-bearing and px-free granitoids. On contrary, Th, U, Cs and Rb are characteristically higher in the px-free granitoids. All granitoids are characterised by negative anomalies of the HFSE (Nb, Ta and Ti) and the LILE (Th, U and Sr) on primitive mantle normalised diagrams.

On the one hand, concentrations of compatible elements (Cr, Ni and Mg) in the Matok pluton granitoids are rather low for a mantle source. On the other hand, all the granitoids have superchondtritic Nb/Ta ratios that overlap with those of the Ventersdorp continental flood basalts which extruded in the Kaapvaal Craton at ~2.7 Ga. The continental crust typically has subchondritic Nb/Ta ratio, and superchondtritic Nb/Ta ratios are widely accepted to resemble a mantle source. The implication is that the Matok pluton granitoids had inherited the superchondtritic Nb/Ta ratio from their source; juvenile underplated mafic magmas that had ponded owing to the impact of the Ventersdorp mantle plume. The large volumes of ponded magmas probably induced the high grade metamorphism in the Limpopo Belt.

All the granitoids of the Matok pluton are probably products of one partial melting event. One possible way to account for the co-existence of px-bearing and px-free granitoids in the Matok pluton is by means of, at least, two magma chambers; one which was filled with anhydrous magma and the other which was filled with hydrous magma. An alternative model would be that in which there was only one chamber. In the one chamber scenario, the magma was hydrodynamically sorted into zones that differed mostly in fH_2O and concentrations of highly fluid-mobile elements but conserved the uniformity in fluid immobile elements. Regardless of the number of chambers, magma batches intruded in the form of feeder dikes which minimally interacted, thus avoiding the hydration of pyroxene in the px-bearing granitoids.

SELELEKELA

Plutone ya Matok e fumanehang profinsing ya Limpopo sebakeng seo ho digeologist se tsebahalang ka hore ke Lebanta la Limpopo e ile ya aheya dilemong tse 2.67 biliyone tse fetileng. Plutone ena eile ya aheya ka mekgahlelo e mmeli, mme mokgahlelo ka mong o ne o bopilwe ka majwe a nang le pyroxene le a senang yona. Majwe kaofela ke a mofuta wa calc-alkaline. Phapang e kgolo dipakeng tsa mefuta ena e mmedi ya majwe ke boteng ba pyroxene le boteng ba epidote le titanite majweng a nang le pyroxene le a senang pyroxene ka ho latellana. Ha e le diminerale tse ding kaofela tsona ha likgethe mofuta wa lejwe; liteng mefuteng ya majwe ka bobedi.

Kgonahalo ya hore plutone ya Matok e ahwe ka mefuta ena e mmedi (px-bearing and px-free) e tlile ka mekgoa e mmedi kapa o mong wa mekgwa ena yo ka bobedi e ka etsahalang. (1)Tlaase semelong sa *lesheleshele moralla* (magma) hone ho ena le didiba tse pedi, seseng se tshetse lesheleshele le chesang haholo ebile le le metsi a fokolang (anhydrous magma) ha se seng se ne se tshetse lesheleshele le metsi a mangata (hydrous magma). Ho tloheng moo didibeng tse pedi ho tla moo plutone ea Matok eleng teng kajeno masheleshele ana a ne a tla ka mokgwa wa di-dike tseo kaofela phello ya tsona e neng e le sebakeng se le seng-plutone ya Matok.

(2) Mokgwa wa bobedi ke haeba ho ne ho ena le sediba se le seng sa *lesheleshele moralla*, mme ka sedibeng ka moo ho ne ho ena le maqulwana (zones) a neng a fapane ka bongata ba metsi. Ho tloha sedibeng moo masheleshele ana a ne a tloha ka bona boqulwana boo entse ele ka mokhwa wa di-dike, mme kaofela phello ya di-dike ene ele plutone ya Matok.

Kaofela majwe a plutone ya Matok a na le feldspar eo boholo ba nako e patlameng ho ya nqa bophirimela-bochabela (W-E), e leng nqa eo Lebanta la Limpopo le phatlaletseng ka teng. Hona ho tiisa hore plutone ya Matok e aheile nakong yo Lebanta la Limpopo le neng le ntse le aheya le lona. Ke dilemong tse kabang 2.7 biliyone tse fetileng ha dikarolong tse ding tsa Cratone ya Kaapvaal ho ne ho aheya majwe a moralla a Ventersdorp. Majwe ana ke a hlahang tlaase botebong ba lefatshe (mantle), mme a susumeditswe ke plumo. Karolo boholo ya *lesheleshele moralla* hae ya ka ya nyoloha ho fihla hodimo lefatsheng. Empa mofuthu o mongata ho nyoloha *leshelesheleng* moo ke ona oileng wa 'pheha' majwe ho phatlalla le Lebanta la Limpopo. Ho nyoloha hona ha plumo ho etsahetse ka nako e lengwe le ho tsukutleha ho hoholo ho potapota le Cratone ya Kalahari, mme bobedi diketsahalo tsena diile tsa tswala Lebanta la Limpopo. Hobane plutone ya Matok e aheile hanghang ka mora hore *leshelesheleshele la moralla* le dule tlaase ho lekgapetla la lefatshe (crust), dielemente tse ratang haholo diminerale tsa ditemperetjha tse hodimo diile tsa feela jwalo di nkile lefa hotswa *lesheleshele moralleng* la Ventersdorp.

ACKNOWLEDGEMENTS

I would like to thank my supervisors Professor Gary Stevens and Dr Jean-Francois Moyen for granting me the opportunity to carry-out this research. Thank you for your guidance, patience and support. I am also appreciative to Ms Madelaine Frazenburg for her patience and assistance with the scanning electron microscope. My thanks also go to Ms Loxie Conradie and Mr George Oliver - thank you both for your cooperation and assistance. I am also indebted to the two examiners without whose constructive criticism, recommendations, thorough investigation and marking, this thesis would have been substandard.

I sincerely would like to express my genuine gratitude to the South African National Research Foundation (NRF) without whose grant to Gary Stevens this research would have only been a dream.

And to all the postgraduate students at the geology department whom during my studies have come and gone and to the present ones, I am greatly grateful for your acquaintance. To you guys and all other friends I have made at Stellenbosch University, bai´e dankie vir jou kameraadlik/geselskap- julle kê´rels is sters!

Last but not least I would like to thank my family for their support and trust in me. I know you have always kept me in your prayers. To especially my mother mme Manako - thank you for the infinite love and all the sacrifices you have had to make from the day I was created. And to you my siblings and aunts - thank you for your endless love and compassion. Ke le rata haholo ho feta dithaba!

TABLE OF CONTENTS

LIST OF FIGURES

1. INTRODUCTION

The Neoarchaean syntectonic Matok pluton in the high-grade Limpopo Belt of southern Africa comprises suites of pyroxene-bearing and pyroxene-free granitoids all of which according to the classification of Peccerillo and Taylor (1976) are calc-alkaline. Granitoids in general may be products of partial melts derived from the continental crust, the mantle or from a combination of both mantle and crust (Chappell et al., 1987; Chappell and White1992; Ajaji et al., 1998; Ma et al., 1998; Caprarelli and Leitch, 1998; Eklund et al., 1998; Küster and Harms, 1998; Bakkali et al., 1998; Bonin et al., 1998; Ferré et al., 1998; Grigoriev and Pshenichny, 1998). The factors which are used to suggest a source and tectonic settings for granitoids include mineral assemblages and geochemical characteristics. Granitoids derived as partial melts of the crust tend to be peraluminous and comprise the high Al-bearing minerals such as garnet, magmatic muscovite ± cordierite ± kyanite/sillimanite (Barbarin, 1999). Conversely, mantle-only derived granitoids tend to be alkaline or peralkaline in addition to molar $Al_2O_3<Na_2O + K_2O$ while granitoids derived from a combination of mantle and crust tend to be metaluminous and calc-alkaline with molar $Al_2O_3>Na_2O + K_2O$ (Barbarin, 1999). Although mantle-only and mantle + crust derived granitoids may both be amphibole and pyroxene-bearing, these minerals tend to be sodic in the former and calcic in the latter. While experimental evidence has shown that many granitoid magmas have the potential to crystallise orthopyroxene at or near the liquidus (Nany, 1983; Frost and Lindsley, 1992) its fate through to the solidus is hampered by the hydrous nature that granitoid magmas typically evolve into (Frost and Frost, 2008). This fact may explain why granitoid rocks are typically devoid of pyroxene. The presence of orthopyroxene in granitoid rocks hence reflects unusually high temperature and anhydrous magmas for rocks with granitoid composition.

The interesting feature about the Matok pluton is the mutual existence of orthopyroxene-bearing and pyroxene-free granitoids, at the same crustal level. Contrary to orthopyroxene-bearing granitoids, pyroxene-free granitoids reflect hydrous magmatic systems. The close spatial and temporal association of both pyroxene-bearing and pyroxene-free granitoids in one pluton hence presents an astounding occurrence and the petrogenetic implication of which is yet to be resolved. Furthermore, the fact that even the orthopyroxene-bearing granitoids of the Matok pluton are calc-alkaline presents a yet another attractive aspect which needs to be explained; calc-alkaline granitoids are popularly perceived to reflect a subduction environment (e.g. Cribb and Barton, 1997; Percival and Mortensen, 2002; El Aouli et al., 2010) and by implication a hydrous magmatic environment.

Before a petrogenetic model and tectonic setting for the Matok pluton can be proposed, it is first important to provide a summary of the current petrogenetic models of orthopyroxene-bearing granitoids and calc-alkaline granitoids. The model for orthopyroxene-bearing granitoids will be discussed first and then calc-alkaline granitoids' model will follow.

1.1. Models of tectonic setting of pyroxene-bearing granitoids

It has been common among many researchers to classify all the orthopyroxene-bearing granitoids (enderbites, charnoenderbites, mangerite, jotunite and charnockites) generally as 'charnockites'. Caution against this generalisation is well argued for in the paper by Frost and Frost (2008). The recommendation is that, instead of bringing up new terms which noticeably lead to some confusion, the prefix "Opx" may simply be added to an IUGS-based igneous rock classification to emphasise that the granitoid comprises a higher temperature mineral, orthopyroxene (Opx). Though Opx-bearing granitoids (*sensu lato* charnockites) form by both igneous and metamorphic processes, important features such as sharp field contacts, the presence of enclaves, preservation of igneous textures and appropriate mineral composition may attest to the igneous origin of such rocks (e.g. Newton, 1992; Bohlender, 1992; Percival and Mortensen, 2002; Tomson et al., 2006). Geodynamic environments proposed for igneous Opx-bearing granitoids include (Frost and Frost, 2008):

(i) Calcic to calc-alkalic metaluminous magmatism which may be (but not necessarily, especially in the Archaean) arc related.
(ii) Rifting-related tholeiitic magmatism which tends to produce ferroan-metaluminous granitoids with nearly no crustal component.
(iii) The minor but equally important alkali to alkali-calcic 'Caledonian-type' granitoids which form due to delamination of a continental crust that had been thickened due to collisional orogeny.
(iv) Typically weakly to moderately peraluminous granitoids which form by extraction of melt owing to granulite facies metamorphism and/ or intrusion of hot ferroan magmas.

Although the above tectonic environments have been suggested for pyroxene (px)-bearing granitoids, it is by no means implied that the plutons concerned are composed exclusively of pyroxene-bearing rocks. In some plutons (as in the Matok), both px-bearing granitoid suites and their equivalent px-free suites are present (e.g. Frost et al., 2000; Glebovitsky et al., 2001; Percival and Mortensen, 2002; Rajesh 2007, 2008). The intrusive relationships between these two end-members (px-bearing and px-free) are often ambiguous with regard to time-space relationships (e.g. Tomson et al., 2006; Frost and Frost, 2008).

Theoretically, the survival of a px-bearing member in a pluton comprising both px-bearing and px-free granitoids requires that the px-bearing members are cumulate to prevent the inevitable reaction to biotite (Johannes and Holtz, 1990; Frost and Frost, 2008).

1.2. Definition and classification of calc-alkaline granitoids

Sub-alkaline rocks are classified into calc-alkaline and tholeiitic suites, both of which may have a mantle component (Barbarin, 1999; Best and Christiansen, 2001). In order to distinguish between calc-alkaline and tholeiitic rocks, at least three different discrimination diagrams have been used. These are; (i) the K_2O vs. SiO_2 (Peccerillo and Taylor, 1976), (ii) FeO*/MgO (where FeO* = total Fe) vs. SiO_2 wt % (Miyashiro, 1974) and (iii) the AFM diagram ((Na_2O+K_2O) vs. FeO* vs. MgO; Kuno, 1968). Although many rocks labelled calc-alkaline are (abusively) commonly dubbed subduction-related, rocks classified as calc-alkaline by one discrimination diagram are not always classified so by the other discrimination diagrams (Arculus, 2003). In addition, none of the above discrimination diagrams has "calc" as one of the variables. Alkalis are represented in both the Peccerillo and Taylor (1976) and Kuno (1968) diagrams. However, the suitability of Miyashiro (1974) and Kuno (1968) diagrams is hampered particularly by the presence of FeO as one of the variables. Saturation of an Fe-Ti oxide phase in magma may influence and have a profound impact on the FeO/MgO ratio and FeO concentrations in a petrogenetic trend of a suite of rocks (Arculus, 2003). For this reason the K_2O vs. SiO_2 diagram is probably the most appropriate for distinguishing between calc-alkaline and tholeiitic rocks. The Matok pluton rocks plot, according to the classification of Peccerillo and Taylor (1976), in the calc-alkaline field.

Very often, rocks classified in terms of major elements as calc-alkaline show negative anomalies of Nb, Ta and Ti on primitive-mantle-normalised diagrams. Many of these rocks in addition outcrop in orogenic belts. This has led many researchers to contend that negative anomalies of Nb, Ta and Ti relative to the LILE signify subduction, either active at the time of granitoid emplacement or primordial (e.g. Tatsumi and Ishizaka, 1982; Stern et al., 1989; O'Brien et al., 1995; Sajona et al., 1996; Ma et al., 1998; Caprarelli and Leitch 1998; Eklund et al., 1998; Bakkali et al., 1998; Ferré et al., 1998; Ajaji et al., 1998; Barbarin, 1999; Stevenson et al., 1999; Pearce et al., 2000; Percival and Mortensen, 2002; Kalfoun et al., 2002; Tomson et al., 2006; Niu and O'Hara, 2009). While the knowledge of isotopic data of such granitoids may be crucial, it is also popularly accepted that a subduction-related source with a larger contribution from the continental crust may produce the porphyritic K-rich and K-feldspar calc-alkaline granitoids (KCG) while a mantle-dominated source may produce the ACG- amphibole-rich calc-alkaline granitoids (DePaolo and Farmer, 1984; Barbarin, 1999). This distinction necessitates that at the same level of SiO_2 saturation, an ACG has higher CaO than a KCG while KCG in turn

has higher K_2O than the ACG (Barbarin, 1999). Notwithstanding these perceptions however, there are calc-alkaline granitoids that have formed in an intracontinental setting with no indication of subduction either at the time of magmatism or any time before then (e.g. Roberts and Clemens, 1993; Eyal et al., 2004; Mišković and Francis, 2006; Rajesh, 2008; Scarrow et al., 2009). This suggests that calc-alkaline granitoids do not always imply subduction-related magmatism.

1.3. The research problem and objectives of this study

Field evidence in the Matok pluton clearly shows that both px-bearing and px-free granitoids were emplaced at the same crustal level; i.e. no tectonic features such as faults are seen in-between the px-bearing and px-free granitoids. Additionally, field evidence suggests co-magmatism between px-free (hydrous) and px-bearing (anhydrous) granitoids. Both the emplacement at the same crustal level and co-magmatism of hydrous and anhydrous magmas should have led to the interaction of magmas of px-bearing and px-free granitoids. This interaction should have led to hydration of pyroxene to biotite ± hornblende. Understanding the mechanism by which both rock suites (px-bearing and px-free) happen to be co-magmatic and the manner in which magmas of the px-bearing granitoids escaped hydration by magmas of the px-free granitoids forms the specific thrust of this thesis.

The high-grade Limpopo Belt is observed to have been subjected to episodic high-grade metamorphism spaning from the Neoarchaean to the Proterozoic (McCourt and Vearncombe, 1987, 1992; Barton and van Reenen, 1992a; Holzer et al., 1999; Kröner et al., 1999; Boshoff et al., 2006; Buick et al., 2006; Buick et al., 2007; Millonig et al., 2008; Gerdes and Zeh, 2009). The heat source of these high-grade metamorphic events is yet to be resolved. The syntectonic nature of the Matok pluton thus holds the potential to complement the deformation and metamorphism studies, thus resolving the heat source problem in the Limpopo Belt. Specifically, it will be possible to say if the high grade metamorphism observed in the Limpopo Belt provoked partial melting or vice versa. The objectives of studying the Matok pluton are therefore as follows:

(i) To present mineralogical, petrographic and geochemical features of the Matok pluton in order to propose petrogenetic processes that may have lead to spatially and temporally related px-bearing and px-free granitoids. Ultimately this involves understanding of the crystallisation controlling parameters which in turn determine the fate of pyroxene crystallisation in granitoid magma and its subsequent endurance through to and below the solidus. This will also determine whether both px-bearing and px-free varieties were derived from similar or distinct sources.

(ii) To use the geochemistry of the Matok pluton to evaluate the most likely source region composition as well as to suggest the heat source most likely to have triggered partial melting.

(iii) To use the geochemical signature of the Matok pluton jointly with the current knowledge about structural and metamorphism nature of the Limpopo Belt to constrain the possible geodynamic setting of the region at the time of Matok pluton emplacement.

2. GEOLOGICAL BACKGROUND

The geological events that may have paved a way to the Matok pluton emplacement can be better understood if geological processes that happened before its emplacement are highlighted. The term 'Kalahari Craton' is used in the literature to refer to the union of the southern African Archaean crustal entities; Kaapvaal Craton, Zimbabwe Craton and the Limpopo Belt (Griffin et al., 2003; Hin et al., 2009). Owing to the controversy regarding the origin of the Limpopo Belt (and its relatively smaller size compared to the adjacent cratons) it has thus been common among researchers to refer to these geological provinces of the Kalahari Craton separately as the Kaapvaal and Zimbabwe Cratons and Limpopo Belt (see Fig. 1a). The oldest rocks in the Kalahari Craton are the 3.8 Ga Sand River Gneisses (Tankard et al., 1982) which crop out in the Central Zone (CZ) of the Limpopo Belt. Some researchers rather consider the 3.7-3.2 Ga Ancient Gneiss Complex of Swaziland (Tankard et al. 1982; Kröner and Tegtmeyer, 1994) and the 3.5-3.2 Ga Barberton Greenstone Belt in South Africa (Armstrong et al., 1990) (both in the Kaapvaal Craton) as the oldest nuclei of the rocks in the region. Again, this is because of the dispute regarding the origin of the Limpopo Belt. Despite the controversy around the origin of the Limpopo Belt however, it has been argued on isotopic, trace element and structural grounds that the Southern Marginal Zone (SMZ) of the Limpopo Belt (see Fig. 1b) represents the same lithologies as those in the Kaapvaal Craton, though now at higher deformation and metamorphism rates (Mason, 1973; du Toit et al., 1983; van Reenen, et al., 1987; van Reenen, et al., 1992; Smit et al., 1992; Kreissig et al., 2000, 2001; Perchuk et al., 2000a). If this link between the SMZ and the Kaapvaal Craton be true, then the geological history of the Kaapvaal Craton prior to the Matok pluton emplacement may equally give an insight on the geological processes that may have paved a way for the Matok pluton emplacement.

The time period 3.7-3.1 Ga has been suggested to evidence the initial formation of a 'rigid' crust and to actually record the early separation of the continental lithosphere from the mantle to form the Kaapvaal Craton (de Wit et al., 1992). The ending of this initial stage of Kaapvaal Craton formation at 3.25-3.1 Ga saw extensive granitoid plutonism which was mostly in the south-eastern, eastern and northern parts of the Craton (Tankard et al., 1982). The second stage of the craton development at 3.1-2.6 Ga (de Wit et al., 1992) was marked by the stabilisation of the cratonic keel from which conditions became favourable to the establishment of sedimentary basins (the Witwatersrand Basin), rifting events, and yet another episode of granitoid plutonism (Tankard et al., 1982; de Wit et al., 1992; Elworthy et al., 2000; Eriksson et

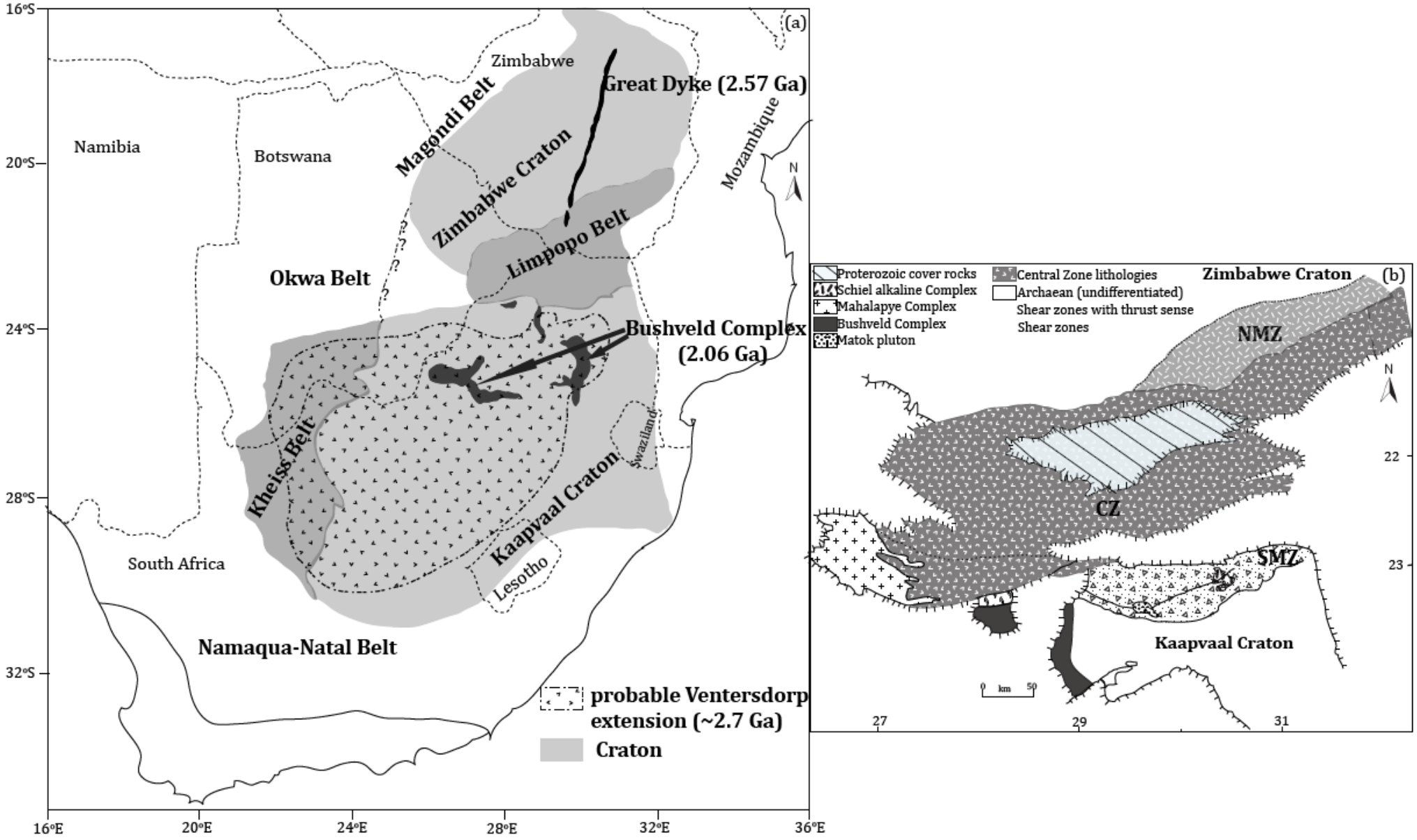

Figure 1. Regional geology of the Kalahari Craton (Limpopo Belt, Zimbabwe and Kaapvaal Cratons). (a) modified from James et al., (2003); McCourt and Vearncombe (1992); Strik et al. (2007) and (b) after Roering et al. (1992a).

al., 2001; Eglington and Armstrong, 2004; Silver et al., 2004). By this time the locus of granitoid plutonism had shifted towards the west, remained in the northern parts of the Kaapvaal Craton and became extensive in the Limpopo Belt (Eglington and Armstrong, 2004). It was during this second stage of Kaapvaal Craton establishment that the mantle plume-originated ~ 2.7 Ga Ventersdorp continental flood basalts extruded (Crow and Condie, 1988; Marsh et al., 1992; Nelson et al., 1992; van der Westhuizen et al., 1991). Also important to mention is the Great Dyke of Zimbabwe which was emplaced at 2575±0.7 Ma (Wingate, 2000; Oberthür et al., 2002) (see Fig. 1a for location). Both the Ventersdorp continental flood basalts and Great Dyke are expressions of rifting environment (Silver et al., 2004). The Limpopo Belt orogenic process and granitoid plutonism across the Kalahari Craton coincided with the time interval between the Ventersdorp continental flood basalts and Great Dyke emplacement. The emplacement of the Great Dyke is more intriguing because it implies brittle fracturing in the crust but was then again contemporaneous with the emplacement of the Chilimanzi and Razi granite Suites and some enderbitic plutons in Zimbabwe Craton (Frei et al., 1999) as well as granulite facies metamorphism in the Northern Marginal Zone of the Limpopo Belt (NMZ). All these other 'heating' events (except the Great Dyke) would have provoked a ductile, rather than brittle, crust (Oberthür et al., 2002).

2.1. The Limpopo Belt

The high-grade ENE-WSW trending Limpopo Belt cropping-out 'in-between' the Zimbabwe and the Kaapvaal Cratons, is differentiated from the cratons by its granulite facies metamorphism relative to the typically amphibolite-facies rocks of the cratons (de Wit et al., 1992; Roering et al., 1992a, b). Seismic data suggest the distribution of the (high-grade) structurally deformed rocks in the SMZ and the NMZ to be confined to upper crust at less than 8.5km (de Beer and Stettler, 1992; Durrheim et al., 1992; Stuart and Zengeni, 1987). There is also no indication of mid-crustal *decollemént* in the Limpopo Belt but the crust is rather 3.5 to 6 km shallower than in the Kaapvaal and Zimbabwe Cratons (de Beer and Stettler, 1992). The exposed total surface of the Limpopo Belt is a length of ~690 km and width of 170km and 220km in the west and the centre respectively (Tankard et al., 1982). The tectonic relations of the belt, to Zimbabwe and Kaapvaal Cratons, in the eastern- and westernmost parts is hampered by the poor outcrop exposure (Tankard et al., 1982; McCourt and Vearncombe, 1992) but it has been suggested that the belt dies out into Zimbabwe Craton in the eastern Botswana (Key and Hutton, 1976).

The decision to subdivide the Limpopo Belt into SMZ, CZ and NMZ (see Fig. 1b) was motivated by the discovery that the timing of high-grade metamorphism and deformation had not always been uniform across the three zones (e.g. Cox et al., 1965; Mason, 1973; van Reenen et al., 1992; McCourt and Vearncombe, 1992; Rollinson, 1993; Kramers et al., 2001). The northernmost boundary of the Limpopo Belt is generally accepted as the southward dipping North Limpopo Thrust Zone, the thrusting of which occurred diachronously between > 2669 ± 67 and ~ 2517 ± 55 Ma and generally younging to the east (McCourt and Vearncombe, 1992; de Beer and Stettler 1992; Durrheim et al., 1992; Stuart and Zengeni, 1987; Kamber and Biino 1995; Kamber et al., 1995a; Blenkinsop et al., 1995; Holzer et al., 1999; Frei et al., 1999; Vinyu et al., 2001; Oberthür et al., 2002). Beyond the North Limpopo Thrust Zone in the Zimbabwe Craton, however, similar deformational features to those in the NMZ are present (Coward et al., 1976).

The boundary between the SMZ and the Kaapvaal Craton is controversial and was initially suggested to be gradational (Mason, 1973) but later on proposed to be sharp and defined by the ~ 5km wide Hout River Shear Zone (HRSZ; Smit et al., 1992; Smit and van Reenen, 1997). The HRSZ is northward dipping (de Beer and Stettler 1992; Durrheim et al., 1992; McCourt and Vearncombe, 1992). Field and seismic evidence suggest the NMZ thrusting over the Zimbabwe Craton and the SMZ thrusting over Kaapvaal Craton (Durrheim et al., 1992; Smit et al., 1992; De Beer and Stettler 1992; Perchuk et al., 2000a). The volumetrically larger CZ (Fig. 1b) is adjoined to the two marginal zones by near vertical inward dipping strike-slip shear faults (de Beer and Stettler 1992; McCourt and Vearncombe, 1992; Kamber et al., 1995a; Perchuk et al., 2000a).

It was initially suggested that the formation of Limpopo Belt was due to Neoarchaean collision between Kaapvaal and Zimbabwe Cratons with N-S subduction (Tankard et al., 1982; de Wit et al., 1992; van Reenen et al., 1992; Roering et al., 1992a; Smit and van Reenen, 1997). This model however fails to account for the inward dipping HRSZ and the North Limpopo Thrust Zone. On the basis of the dip directions of the shear zones, McCourt and Vearncombe (1987, 1992) suggested an alternative model in which the CZ is an ancient micro-continent which came from the northeast to southwest as an overriding plate and subsequently collided with the then unified Zimbabwe and Kaapvaal Cratons, during the Neoarchaean.

The 3.8 Ga Sand River (ortho)Gneiss, cropping-out in the CZ but lacking in the marginal zones had undergone granulite facies metamorphism by ~3.2Ga (Tankard et al., 1986; McCourt and Vearncombe, 1992). A subsequent granulite facies metamorphism in the CZ is recorded by the 3.6-3.2 Ga dominantly sedimentary sequence of the Beit Bridge Complex (Tankard et al.,

1982) at 2.7-2.5 Ga (Holzer et al., 1999; Boshoff et al., 2006). This episode coincided with granulite facies metamorphism in the two marginal zones and with granitoid plutonism across the Limpopo Belt as well as in the Kaapvaal and Zimbabwe Cratons (Hickman, 1978; McCourt and Vearncombe, 1992; Kamber and Biino, 1995; Berger and Rollinson 1997; Holzer et al., 1999; Zeh et al., 2004). The NMZ records at least two episodes of granulite facies metamorphism during the Neoarchaean; one at ~2.7 Ga and another at ~2.52 Ga (Hickman, 1978; Kamber and Biino, 1995). It has been suggested that even the CZ possibly experienced two granulite facies metamorphism during the Neoarchaean (Hickman, 1978; Berger et al., 1995; Buick et al., 2006; Kamber and Biino, 1995). The SMZ on the other hand had experienced a single clockwise P-T loop with granulite facies metamorphism at ~2.69 Ga (Stevens and van Reenen, 1992a; Barton et al., 1992; Kreissig et al., 2001).

The third and final granulite facies metamorphism event at ~2.0 Ga was recorded in the CZ but not observed in the two marginal zones (Kamber et al., 1995a, b; Holzer et al., 1998; Holzer et al., 1999; Boshoff et al., 2006; Buick et al., 2007; Mouri et al., 2008; Gerdes and Zeh, 2009). This event was however not regional within the CZ; only the eastern and westernmost parts of the CZ had undergone granulite facies metamorphism while the central parts had undergone amphibolite facies metamorphism and hydration (Buick et al., 2007; Millonig et al., 2008; Gerdes and Zeh, 2009). Although all the major shear and thrust zones in the Limpopo Belt were established during the Neoarchaean, some minor strike-slip shear zones in the NMZ were reactivated at ~2.0 Ga (e.g. Kamber et al., 1995a, b). It is this tectono-metamorphic event at 2.0 Ga that prompted subsequent workers to suggest that the inferred collision of either Zimbabwe and Kaapvaal Craton or the CZ with Zimbabwe + Kaapvaal Cratons took place during the Proterozoic (Holzer et al., 1999).

***In conclusion*:** The wide spread 2.7 – 2.5 Ga granulite facies metamorphism experienced across the three zones of the Limpopo Belt is compatible with a regional source of heat during the Neoarchaean. While other workers suggest the high-temperature metamorphism in the Limpopo Belt was due to the heat that emanated from the intrusive granitoids (Kröner et al., 1999; Millonig et al., 2008), there is no consensus as to what then triggered partial melting to produce the granitoids. Moreover, high-grade metamorphism, in many instances, slightly predates granitoid plutonism. The syntectonic nature of the Matok pluton thus has a bearing on the tectonic evolution of the Limpopo Belt and by implication may provide solution to the source of heat that triggered metamorphism in the Limpopo Belt during the Neoarchaean. The SMZ had, during the Neoarchaean, much lower geothermal gradient such that the granulite facies metamorphism observed was improbable even if crustal thickening were considered (Kramers et al., 2001). Though there is evidence for *in situ* melt generation in the form of

migmatites in the SMZ the derived partial melts were too low to form plutonic bodies (Kreissig et al., 2001; Kramers et al., 2001; Perchuk et al., 2000a; Stevens and van Reenen, 1992b). On contrary, both the NMZ and CZ had high enough geothermal gradients such that the observed granulite facies metamorphism and crustal anatexis may have been probable (Berger and Rollinson, 1997; Kröner et al., 1999; Kramers et al., 2001). However, there are also areas in the NMZ which were only at amphibolite facies, were never considerably thickened (Frei et al., 1999) and as such could not have experienced *in situ* partial melting and granitoid intrusions without 'external' heat input.

2.2. The Neoarchaean granitoids in the Kalahari Craton

The Neoarchaean granitoids in the Kalahari Craton were emplaced practically contemporaneous with the establishment of the Limpopo Belt (Phaup, 1973; Tankard et al., 1982; Holzer et al., 1999; Frei et al., 1999; Vinyu et al., 2001; Blenkinsop et al., 2004; Rigby et al., 2008). Magmatic fabric of many of the Neoarchaean granitoids in the Limpopo Belt is parallel to the trend of the Limpopo Belt, attesting to a syn-to post tectonic emplacement (e.g. Frei et al., 1999; McCourt and Armstrong, 1998). In the SMZ, the ~ 2674 Ma Matok pluton preserves magmatic mineral foliation parallel to the trend of the Limpopo Belt and in addition has metapelitic xenoliths which had undergone granulite facies metamorphism at ~2.69 Ga (Barton et al., 1992; Retief et al., 1990; Bohlender, 1992; Kreissig et al., 2001). In the CZ, the Bulai pluton has granulite facies phases as well as non-deformed granitic phases (McCourt and Armstrong, 1998; Kröner et al., 1999; Zeh et al., 2007; Millonig et al., 2008). The ~2620 Ma granitic phase of the Bulai pluton has xenoliths of the Beit Bridge Complex which were subjected to granulite facies metamorphism at 2644 ±8 Ma (Millonig et al., 2008). Similarly, the NMZ has the 2.67-2.52 Ga Razi granite Suite which outcrops along the North Limpopo Thrust Zone younging to the east (Frei et al., 1999), thus also attesting to a syn-tectonic emplacement. Many of these Neoarchaean plutons in the Limpopo Belt comprise both Opx-bearing granitoids and their (hydrous) px-free equivalents (Frei et al., 1999; Barton et al., 1992; Bohlender, 1992; Bohlender et al., 1992; Berger and Rollinson, 1997; Kampunzu et al., 2003; Millonig et al., 2007). However, the granitoids of the northern parts of the Limpopo Belt and Zimbabwe Craton are dominantly enderbitic while those in the southern and central parts of the Limpopo Belt are modestly enderbitic (Barton et al., 1992; Berger et al, 1995; Mkweli et al. 1995; Frei et al., 1999).

2.3. Previous work in the SMZ and the Matok pluton

A retrograde orthoamphibole isograd had been postulated to run through the SMZ dividing the SMZ into granulite facies and amphibolite facies domains to the north and south

respectively (van Reenen, 1986; Smit et al. 1992; Baker et al., 1992; Smit and van Reenen, 1997). The retrogressed southern domain (at amphibolite facies) of the SMZ was supposedly achieved by influx of externally (mantle) derived CO_2-rich fluids into the formerly granulite facies rocks and preserve no evidence for the former existence of granulite facies assemblages (van Reenen, 1986; van Reenen et al., 1988; van Schalkwyk and van Reenen, 1992; see also Rigby et al., 2008). However, the stable isotopic data ($\delta^{13}C$ and $\delta^{18}O$) show no differences between the granulite and amphibolite facies rocks; the $\delta^{13}C$ values inherent to the graphitic metasediments are inconsistent with a mantle source of carbon (Vennemann and Smith, 1992; Hoernes and van Reenen, 1992), thus ruling out the opinion of externally derived fluids.

The lack of isotopic and field evidence to suggest a subzone of hydration within the SMZ accommodates an alternative viewpoint that the inferred isograd should rather be the boundary between the Limpopo Belt and the Kaapvaal Craton (Mason, 1973; Tankard et al., 1982). This information in turn accommodates the perspective that the establishment of the HRSZ was concurrent with ~2.69 Ga peak metamorphism in the SMZ (Kreissig et al., 2001), rather than forming a sharp break in metamorphic grade as Smit et al. (1992) and Smit and van Reenen (1997) had suggested. Furthermore, parts of the Kaapvaal Craton adjacent to and south of the HRSZ are very similar to and actually do record similar metamorphic grade to the southern parts of the SMZ (Perchuk et al., 2000a). The dominant lithologies in the SMZ are the px-bearing tonalitic gneisses named Baviaanskloof Gneiss and the granulitic metapelitic gneisses named Bandelierkop Formation (Smit and van Reenen, 1997; Perchuk et al., 2000a; Kramers et al., 2001).

Despite the outcrop being limited, Bohlender (1992) conducted detailed geological mapping of the Matok pluton and compiled the map shown in Figure 2. The pluton consists of suites of px-bearing and px-free granitoids ranging from diorites through granodiorites to granites. The px-bearing granitoids were classified as enderbites and charnoenderbites while the px-free granitoids were classified into several units from which Bohlender (1992) identified at least nine phases each with similar but different proportions of minerals (Fig. 2). Although a few of the enderbite phases have been found as 'xenoliths' in the px-free granitoids (Bohlender, 1992), the map also reveals that there are enclaves of G1 (a px-free hornblende-granodiorite) in enderbite (to the north of Fig. 2). Barton et al. (1992) had suggested that intrusions in the Matok pluton were episodic and that the first intrusion comprised only the px-bearing granitoids while the second intrusion comprised the non-deformed px-free granitoids. On contrary, Bohlender (1992) has mapped px-free granitoids with a gneissic fabric (G5; Fig. 2). On the basis of U-Pb

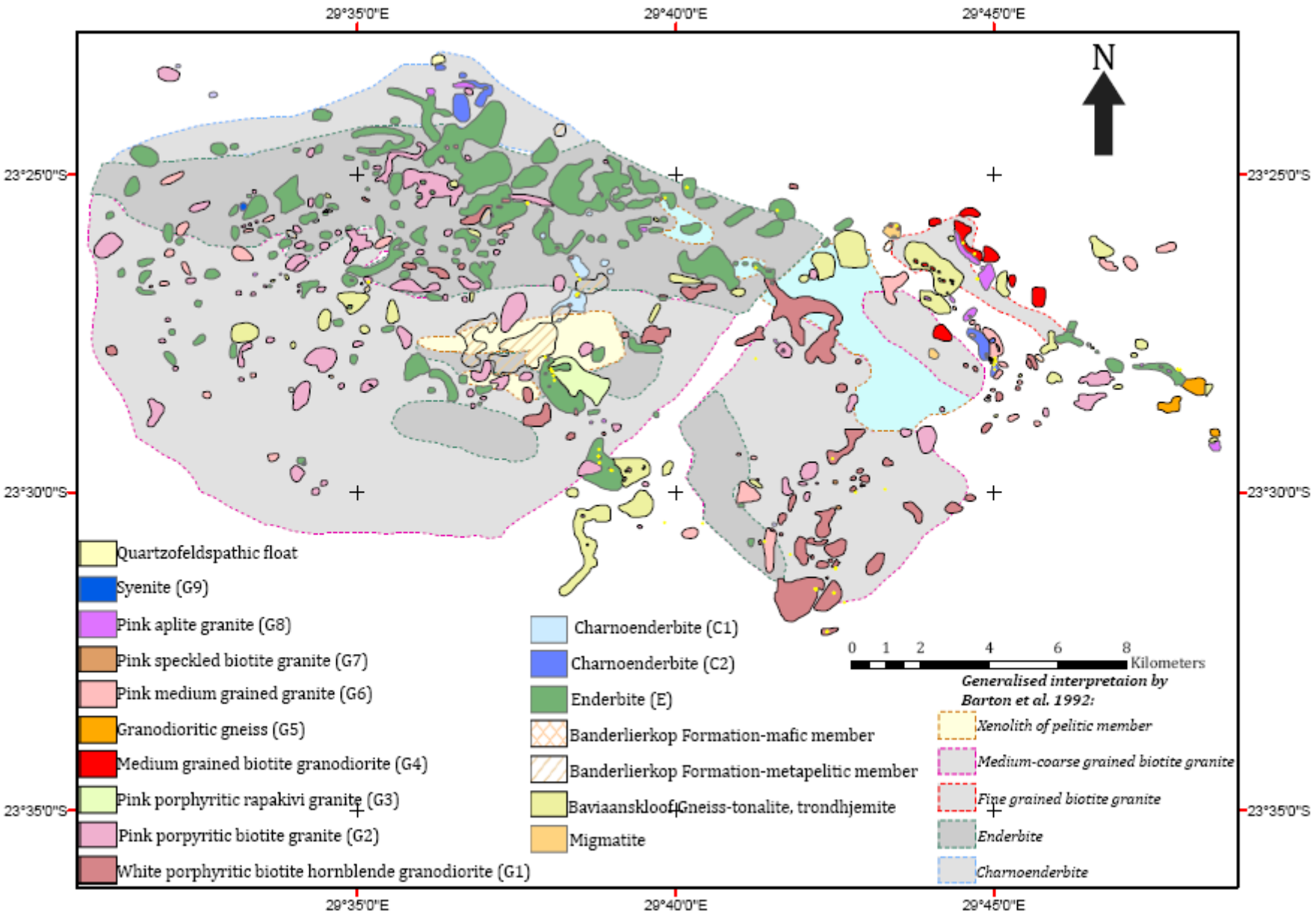

Figure 2. Geological map of the Matok pluton. The different units (e.g. G1, G2 etc) are after Bohlender (1992), the pluton outline and the 'generalised interpretation' (legend on the far bottom right) are after Barton et al. (1992).

zircon dating, Barton et al. (1992) suggested the intrusion age of px-bearing granitoids at 2671 ±2 Ma and that of px-free granitoids in the time range 2667-2664 Ma. This led these authors and Bohlender et al. (1992) to propose that the Matok pluton intruded along the clockwise P-T loop experienced by the SMZ with the px-bearing granitoids emplaced during peak metamorphic conditions while the px-free granitoids were emplaced during retrogression. On another note, Retief et al. (1990) obtained a SHRIMP age of 2674 +44/-46 for the px-free granitoids of the Matok pluton, similar to the age of px-bearing granitoids from Barton et al. (1992). The pitfall to the Barton et al. (1992) ages for the px-free granitoids is that no age uncertainties were presented and therefore there is no reason not to surmise a similar age for both px-bearing and px-free granitoids.

An ample amount of bulk rock and mineral major element geochemistry of the Matok pluton were presented by Bohlender (1992). A few trace element data were presented and a petrogenetic model based on such data had not yet been presented. Hence the importance of this study to utilise a comprehensive trace element database in conjunction with major elements to propose a petrogenetic model.

3. FIELD OBSERVATIONS FROM THIS STUDY

Field evidence suggests at least two episodes of magmatic injection in the Matok pluton. Both episodes were marked by clear intrusive contacts with the country rocks of the intensely banded Baviaanskloof Gneiss and metapelites of Bandelierkop Formation. Granitoids of the first intrusion in the Matok pluton evidence a mild gneissic development prior to the intrusion of the second episode. Most of the first intrusion granitoids are px-bearing and a few are px-free. The fact that both px-bearing and px-free granitoids are represented in this first episode of intrusion demonstrates that the first intrusion was not typified only by px-bearing granitoids as previously suggested by Barton et al. (1992). A mild gneissic development (Fig. 3a) in turn, compared to the granulitic Baviaanskloof orthoGneiss, attests to emplacement after the main granulite-facies forming event in the SMZ. Granitoids of the second intrusion episode were not affected by metamorphic event as evidenced by the absence of metamorphic textures. Px-bearing xenoliths of the first intrusion episode were found in the younger granitoids of the second intrusion (Fig. 3b).

While the presence versus the absence of pyroxene in the Matok pluton granitoids remains the central subject to this thesis, it is important to highlight that each of the px-bearing and px-free granitoid groups are characterised by phases with similar mineralogical textures but at different mineralogical proportions. Although quantifying the contact relationships between the different phases of the Matok pluton is often hindered by the limited outcrop exposure (see Fig. 2), a few localities do actually provide intrusive relationships between granitoids of the second episode.

Co-magmatism of two px-bearing granitoids is portrayed typically in the form of a gradational contact between the two granitoids with a slight difference in mineral proportions as well as a slight difference in grain size (Fig. 3c). Similarly, there is evidence for co-magmatism between magmas of px-bearing and px-free granitoids (Fig. 3d, e). Where this is the case, px-free granitoids are often more porphyritic than px-bearing granitoids (Fig. 3e). Rarely, the contact between a px-bearing and px-free granitoid ranges from sharp to gradational (Fig. 3d). Likewise, there is evidence for mingling of hydrous magma batches of two px-free phases at different mineral proportions (Fig. 3f). The exceptions in the intrusive relationships are the aplite granites and dikes which clearly post-date intrusions of all other rock types of the Matok pluton.

Figure 3. Field relations of the different rock types of the Matok pluton.(a) subsolidus deformation in the px-bearing granitoid of the first intrusion, (b)xenolith of a px-bearing granitoid in a px-free granitoid, (c) co-magmatic two px-bearing granitoids with different grain size and mineral proportions, (d) co-magmatic px-bearing and px-free granitoids, suggesting a zoned magma with a vein associated with the latter 'intruding' the former, (e) magma mixing of px-bearing and px-free granitoids, (f) magma mixing of two px-free granitoids with difference in maficity.

The px-bearing granitoids are generally more mafic than the px-free granitoids. Both granitoid types range from porphyritic to non-porphyritic varieties. Phenocrysts (up to 4 centimetres) of both plagioclase and alkali feldspar are present in both px-bearing and px-free granitoids and are typical aligned roughly ENE-WSW; parallel to the trend of the Limpopo Belt. The px-bearing granitoids are however dominated by plagioclase phenocrysts as opposed to alkali feldspar phenocrysts. Even the gneissic (first intruded) granitoids do have feldspar phenocrysts aligned ENE-WSW. A small scale shearing (shear zone ≤5 cm) event, postdating the emplacement of the pluton is recorded in the non-deformed granitoids.

4. MINERALOGY OF THE MATOK PLUTON

4.1. Nomenclature

Due to the hydrous nature that granitoid magmas characteristically evolve into, the occurrence of orthopyroxene is rare in granitic rocks. Even so, many granitic rocks do hold evidence for a prior presence of orthopyroxene, and this is commonly evidenced by biotite-quartz intergrowth which most probably represents the reaction of orthopyroxene with the melt to liberate biotite and quartz (e.g. René et al., 2008). This fact therefore raises the possibility that even the px-free granitoids of the Matok pluton may have had orthopyroxene at the liquidus. In this study the criterion used to differentiate px-bearing from px-free granitoids is the answer to the question "did the rock contain pyroxene at the solidus"? It will be suggested later in this chapter why, if both granitoid suites (px-bearing and px-free) had pyroxene at the liquidus, the pyroxene of px-free granitoids did not to survive to the solidus; i.e. what was the control factor.

Although nomenclature of the Matok pluton granitoids by Bohlender (1992) has been retained in Figure 2 (e.g. enderbites, charnoenderbites) the rest of this project will refer to the px-bearing rocks according to the recommendation by Frost and Frost (2008) (see section 1.1). In the px-bearing granitoids, clinopyroxene is always present but orthopyroxene is not. As a result, the prefix "px" instead of "Opx" has been adopted to denote the presence of pyroxene. Likewise the prefix "px-free" is adopted to indicate that the rocks are devoid of pyroxene. For example px-diorite and px-free diorite will be adopted to indicate respectively the presence and absence of pyroxene in a diorite.

The gneissic px-bearing rocks that have been sampled are all (and solely) of dioritic composition. In the subsequent sections when it is crucial to clarify the difference between diorites of the first intrusion and the second intrusion, the terms px-diorites1, px-diorites2 and px-free diorites will be adopted to refer, respectively, to px-diorites of the first intrusion, px-diorites of the second intrusion and px-free diorites of the second intrusion. To distinguish between pyroxene-bearing and pyroxene-free granodiorites, the terms px-granodiorites and px-free granodiorites will appropriately be used. Only two samples of pyroxene-bearing granites were sampled and these will be referred to as px-granites. As will be discussed in chapters five and six the granites with >71 wt% SiO_2 do not concur with the geochemical trends defined by all other granitoids of the Matok pluton. For this reason, the terms px-free granites with ≤71 wt% SiO_2 and px-free granites with >71 wt% SiO_2 will accordingly be adopted.

When it is not necessary to make use of the above terminology, the broad terms px-bearing granitoids and px-free granitoids will be used to highlight the differences between granitoids with and without pyroxene respectively. This will apply mostly when crystallisation parameters are inferred between the px-bearing versus px-free granitoids, i.e. when it becomes necessary to account for how px-bearing suites and px-free suites characterised one pluton.

4.2. Petrography

The details of petrographic observations as identified by optical microscope on the polished thin sections are presented with an emphasis on the minerals present, their textural relationships, crystal habit, size, the presence of inclusions and the degree to which the observed phases are considered to be in textural equilibrium. Attention will also be drawn to evaluate the mineralogical differences and similarities between the px-bearing and px-free granitoids and provide a preview assessment of a possibility of either crystal fractionation or different sources to account for the characteristic mineralogy of the Matok pluton. Due to the differences in modal proportions of minerals within each of the px-bearing and px-free granitoid groups, mineral percentages will be given in ranges. A more detailed petrography and mineral modal abundance pertaining to individual rocks is presented in Appendix A.

The most important petrographic variation between the px-bearing and px-free granitoid groups of the Matok pluton is the presence of pyroxene exclusively in the former and the presence of magmatic epidote and titanite exclusively in the latter. As stated earlier, two generations of px-bearing granitoids exist in the Matok pluton- the gneissic (px-diorites1) and granitoids of the second intrusion (px-diorites2, px-granodiorites and px-granites). To highlight the impact of metamorphic overprint in the px-diorites1, petrographic descriptions for the px-bearing granitoids will accordingly be divided up into granitoids of the first episode (px-diorites1) and that of the second intrusion episode (px-diorites2, px-granodiorites and px-granites combined). Also, because the px-free granites with >71 wt.% SiO_2 either plot off the geochemical trend or are separated by a hiatus from all other granitoids, the petrographic description of the px-free granitoids is divided into px-free granites with >71 wt.% SiO_2 and all other px-free granitoids with ≤71 wt.% SiO_2 (dioritic, granodioritic and granitic inclusive).

This separation is more important because it allows for an assessment of the degree to which the px-diorites1 have been altered, and also evaluate the extent to which magmatic processes such as crystal fractionation could possibly be accountable to the fate of px-free granites with >71 wt.% SiO_2.

The rocks are classified to be fine grained when the overall grain size is less than 1mm, medium grained when the grain size is in the range 1-5mm and coarse grained when the size is

greater than 5mm. The term phenocryst is applied to euhedral to subhedral crystals which are set in a finer grained matrix. The modal proportions of mineral phases, given in brackets, are estimated by visual observation.

4.2.1. Px-bearing granitoids

The rocks classified under this group have either pristine pyroxene preserved or have evidence for having had magmatic pyroxene which may have subsequently been altered to amphibole and/ or biotite at subsolidus conditions. The latter situation is evidenced by relics of pyroxene crystals in proximity with the subsolidus amphibole or biotite crystals. Where petrographic studies indicate pyroxene to have been destroyed by a sub-solidus reaction, such rocks are included in this group. However, where the destruction of pyroxene is indicated to have occurred in the magmatic state, such rocks are classified under the px-free granitoid group.

4.2.1.1. Px-diorites1 (gneissic)

These rocks range from fine- to coarse-grained with both porphyritic and non-porphyritic varieties present. The phenocrysts are chiefly plagioclase, but alkali feldspar phenocrysts are rare. In most samples, the mafic minerals are fairly equigranular, when not defining the subsolidus foliation. More commonly, the rocks are traversed by micro-veinlets which are filled mostly with quartz, brown and green biotite ± hornblende ± opaque minerals. The opaque minerals and apatite form the smallest of all grains. One sample (Mat 19) which was taken near a shear zone has traces of muscovite, chlorite, titanite and epidote as subsolidus phases that had formed at the expense of hornblende, biotite and plagioclase. Epidote is found exclusively along the edges of hornblende. Important to note is the fact that other than in this sample no epidote was found in the px-bearing granitoids.

Ortho- and clinopyroxene (traces -7%) form anhedral grains which are typically less than 3 mm in size. In most samples both ortho- and clinopyroxene are fairly equigranular at ~ 0.4 mm. More commonly, the presence of orthopyroxene is evidenced by minute relics, or fragmentary grains which occasionally occur in subsolidus biotite while relics of clinopyroxene occur in hornblende. Pyroxene occurs both as an inclusion in the feldspar and as an interstitial phase.

Plagioclase (35-70 %) and alkali feldspar (0-7 %) occur mainly as smaller (< 1.5 mm) crystals with anhedral to euhedral habit. In porphyritic rocks, feldspar phenocrysts (which may be in the order of 2 cm) typically host minute inclusions of ortho- and clinopyroxene, green biotite, hornblende and opaque minerals. A myrmekitic texture is common. Albite twinning is

also common in the less sericitised grains. Deformational twinning, undulose extinction and sericitisation of both plagioclase and alkali feldspar are also common. Sericitisation is mostly preferentially incurred at the core while the rims are relatively fresh.

Hornblende (2-37%) occurs as anhedral to subhedral grains with an average size of 1.5 mm. A large number of grains inferred to be of magmatic origin are fragmentary, owing to their replacement by subsolidus biotite. In some samples, hornblende occurs as a relatively equigranular (~0.15 mm) interstitial phase between the felsic minerals, possibly suggesting 'autorecrystallisation' of former pyroxene crystals, as judged by the few samples in which pristine pyroxene is preserved as an interstitial phase between felsic minerals. A few grains are prismatic, also mimicking the shape of clinopyroxene which they replaced. There are also a significant number of hornblende grains defining the subsolidus foliation in the affected rocks. Orthoamphibole is rarely observed and has anhedral grains which occur as pseudomorphs after orthopyroxene.

Biotite (2-15%) commonly defines the gneissocity but forms mainly anhedral randomly oriented grains when not defining the gneissocity. An intergrowth with quartz is common, and seemingly formed at the expense of orthopyroxene in a magmatic environment. Some biotite grains are fragmentary, possibly suggesting the incomplete replacement of pyroxene and occasionally of hornblende.

Both magnetite and ilmenite (traces - 3%) occur mainly as microlite magmatic inclusions in all other minerals and rarely alongside mafic minerals defining the gneissocity. Magnetite (and rarely ilmenite) also occurs as an interstitial phase. Rarely, ilmenite grains rimmed by thin slice of titanite and/ or apatite are found. Both titanite and apatite rimming ilmenite are subsolidus. Even when ilmenite is an inclusion in plagioclase or hornblende, such rimming by titanite and/ or apatite may be present. Other than this occasional occurrence of thin titanite rim around ilmenite, no other titanite is present in the px-bearing granitoids. Traces of apatite occur as perfectly hexagonal inclusions in plagioclase and hornblende.

Quartz (15-25%) forms anhedral grains most of which are free of inclusions. Both relatively larger (~2mm) and smaller grains are present. Most of the smaller grains are products of recrystallisation. Deformation-induced subgrain development is common.

4.2.1.2. Px-bearing granitoids of the second intrusion (px-diorites2, px-granodiorites and px-granites)

These rocks also range from fine- to coarse-grained with both porphyritic and non-porphyritic varieties being present. Both plagioclase and alkali feldspar occur as the phenocrysts. Felsic minerals are much larger than the mafic minerals and in many samples, the mafic minerals tend to be equigranular.

Both orthopyroxene (0 - 15%) and clinopyroxene (traces – 15%) exhibit euhedral to anhedral crystals that range from less than 200 μm to ~ 3.5 mm. Both minerals occur commonly as interstitial between the felsic minerals (Fig. 4a, b) and less commonly as inclusions in plagioclase. Various shapes ranging from prismatic to equant are exhibited, with the prismatic grains being mainly subhedral (Fig. 4c). Rarely, a lamellar intergrowth of the two pyroxenes is present with orthopyroxene being the host. In many of these rocks, the pyroxene has been partially or nearly completely replaced by anhedral amphibole and/or biotite (Fig. 4b, c, d) at subsolidus conditions. Though there is this evidence for pyroxene replacement, no gneissic development, both on thin section and in the field was observed in these rocks.

Plagioclase (38 - 75 %) occurs both as phenocrysts of up to ~ 4 cm and as smaller grains with an average size of ~1.5 mm. The phenocrysts range from subhedral to euhedral while the smaller grains range from euhedral through subhedral to anhedral. Occasionally, tabular crystals of plagioclase are present and occur mainly as inclusions in other big crystals of plagioclase. Both antiperthitic and myrmekitic textures are observed. Inclusions of ilmenite and rare allanite microlites are present in the plagioclase. Sericitisation is common and typically at the core while the rim is fresh (Fig. 4e), though cases where it is spread across the entire grain are also present. In some samples, plagioclase typically exhibits undulose extinction, subgrain development as well as deformation twinning. K-feldspar (traces – 20%) is present in subordinate amounts to plagioclase and occurs mainly as anhedral crystals which rarely show Carlsbad twinning. Phenocrysts of K-feldspar are rare. The proportion of alkali feldspar increases with increasing leucocratic character of the rocks. Quartz (10 - 25 %) grains range from smaller to up to 1.5 mm and rarely up to 4 mm. It is relatively fresh, occasionally hosts inclusions of tiny magnetite, albite and allanite crystals, but is more commonly free of inclusions.

Biotite (1 - 15 %) occurs mainly as anhedral grains typically < 1 mm and rarely up to 4 mm. It variously occurs either intergrown with quartz or as skeletal grains with an incomplete orthopyroxene replacement. In other cases it has completely replaced the pyroxene, but the overall interstitial nature of the pyroxene being preserved and in this case suggesting the biotite

as an interstitial phase. In some samples, two populations of magmatic biotite can be distinguished. One is the smaller (< 0.3 mm) euhedral type which commonly occurs as an inclusion in plagioclase and occasionally seems to have been in equilibrium with pyroxene, suggesting magmatic origin. The other is the larger (up to 4 mm) anhedral (less commonly skeletal) grains commonly intergrown with quartz and possibly suggesting orthopyroxene replacement in a magmatic environment. Biotite intergrowth with hornblende is also common. Where this is the case, the biotite has pseudo-120° cleavage intersection which is typical of

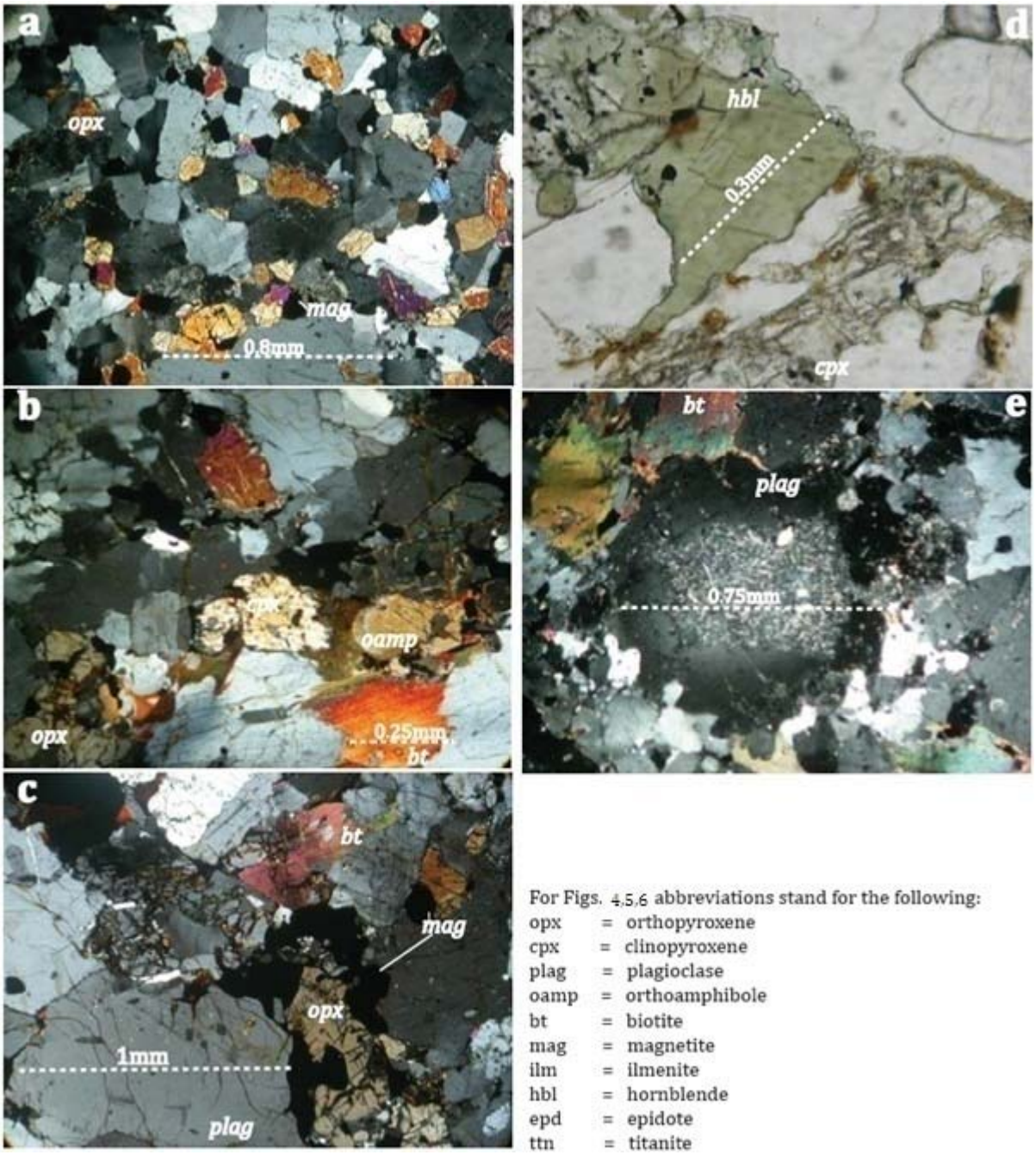

Figure 4. Mineral textural relationships of the px-bearing granitoids of the Matok pluton.

hornblende, suggesting biotite formation at the expense of hornblende, possibly at magmatic conditions.

Hornblende (traces - 30%) forms predominantly anhedral and less commonly euhedral grains that range from micron scale to ~3.5 mm. A small population of euhedral to subhedral hornblende grains occurs intergrown with quartz with no evidence of former existence of clinopyroxene around or within the hornblende grain. These grains are inferred to be magmatic replacement of pyroxene, rather than subsolidus phases. There are also anhedral hornblende grains with core of clinopyroxene and these make most of the hornblende in these rocks. Both magmatic and subsolidus hornblende grains host inclusions of zircon, apatite, magnetite and ilmenite.

Both magnetite and ilmenite (traces - 3 %) occur either as minute crystal (typically <200 μm) inclusions in plagioclase, alkali-feldspar, pyroxene, hornblende and quartz or as non-inclusions and rarely as interstitial phases between felsic minerals. An ilmenite-magnetite intergrowth is present. Both magnetite and ilmenite also rarely occur intergrown with or as thin slices around minute hornblende and/ or biotite grains - these are possibly subsolidus. In addition to magnetite and ilmenite, the trace minerals, apatite, zircon, pyrite, chalcopyrite monazite and allanite are also inclusion phases in plagioclase, alkali feldspar, ortho- and clinopyroxene, hornblende and biotite. Apatite in turn occurs as an inclusion phase in ilmenite and allanite. Rarely, ilmenite grains are rimmed by thin slice of apatite. Even when ilmenite is an inclusion in plagioclase, the apatite rim may be present. The rimming apatite is probably subsolidus.

The generalised crystallisation sequence suggests the following succession from the early to the last mineral to crystallise:

apatite - zircon – chalcopyrite – pyrite - ilmenite - magnetite – allanite – monazite - plagioclase - clinopyroxene ~ orthopyroxene - hornblende – alkali feldspar - biotite – quartz

4.2.2. Px-free granitoids

Some biotite-quartz intergrowth has been interpreted to resemble a magmatic orthopyroxene replacement in the px-bearing granitoid group. There is also a proof of pyroxene presence in those rocks. Some of the rocks classified under the px-free granitoid group also have the biotite-quartz intergrowth which is also interpreted to indicate a magmatic state replacement of orthopyroxene. However, there is no evidence for pyroxene presence in this group. As such, all the pyroxene that had crystallised initially is interpreted to have been

consumed before the solidus temperature. A complementary criterion used for this criterion is the existence of magmatic epidote and titanite, both of which are lacking in the px-bearing granitoids. Similar to the px-bearing granitoids, the px-free granitoids range from non-porphyritic to porphyritic varieties, with both plagioclase and alkali feldspar occurring as phenocrysts. Likewise, the overall texture ranges from fine to coarse grained, but there are less finely grained and more of the coarse grained rocks.

4.2.2.1. Px-free diorites, granodiorites and granites with ≤71 wt. % SiO_2

Feldspar consists of both plagioclase (17 – 62%) and alkali feldspar (5 - 52%) crystals ranging from euhedral through subhedral to anhedral. Smaller grains are typically < 5 mm and dominantly anhedral while phenocrysts are subhedral to euhedral and may range up to 4 cm. Both myrmekitic and perthitic textures are present and in a few samples antiperthitic texture is also present. Cases where a myrmekitic plagioclase is an inclusion in perthitic alkali feldspar are also common. Carlsbad twinning in alkali feldspar is also commonly observed. In some samples, both plagioclase and alkali feldspar exhibit undulose extinction. Sericitisation is common and nearly always accompanied by epidote ± titanite ± biotite microlite inclusions in both plagioclase and alkali feldspar.

Quartz (10 - 29%) occurs as anhedral grains majority of which have developed subgrains. It is commonly intergrown with biotite, suggesting orthopyroxene reaction with the melt. It is rarely found as small inclusion in K-feldspar. Rare biotite and pyrite microlite inclusions were found in quartz; otherwise quartz is fairly free of inclusions. In some samples, two quartz populations can be distinguished; one is defined by the commonly intergrown with biotite grains (up to 4 mm in size) and the other is the typically <0.05 mm population that evidently resembles recrystallisation. This recrystallised quartz has a tendency to accumulate along grain boundaries of bigger crystals. Even in the presence of recrystallised quartz the overall texture of the rocks is magmatic.

Both biotite (3 - 30%) and hornblende (traces - 27%) occur as anhedral to euhedral grains which may range up to 5mm. Symplectitic biotite (Fig. 5a) and hornblende (Fig. 5b) are interpreted to resemble replacement of pyroxene in a magmatic environment. Both biotite and hornblende tend to define a glomeropophyritic intergrowth with epidote, titanite, ± ilmenite (Figs. 5c, d, e). The biotite that occurs in the above association (glomeropophyritic intergrowth) is commonly prismatic and not symplectitic. Hornblende occasionally hosts inclusions of small (< 0.1 mm) biotite and ilmenite crystals. An occasional embayment of apatite onto hornblende is present. Small plagioclase, apatite, zircon, ilmenite and magnetite inclusions in biotite have been found especially where biotite is not intergrown with other mafic minerals. The smallest

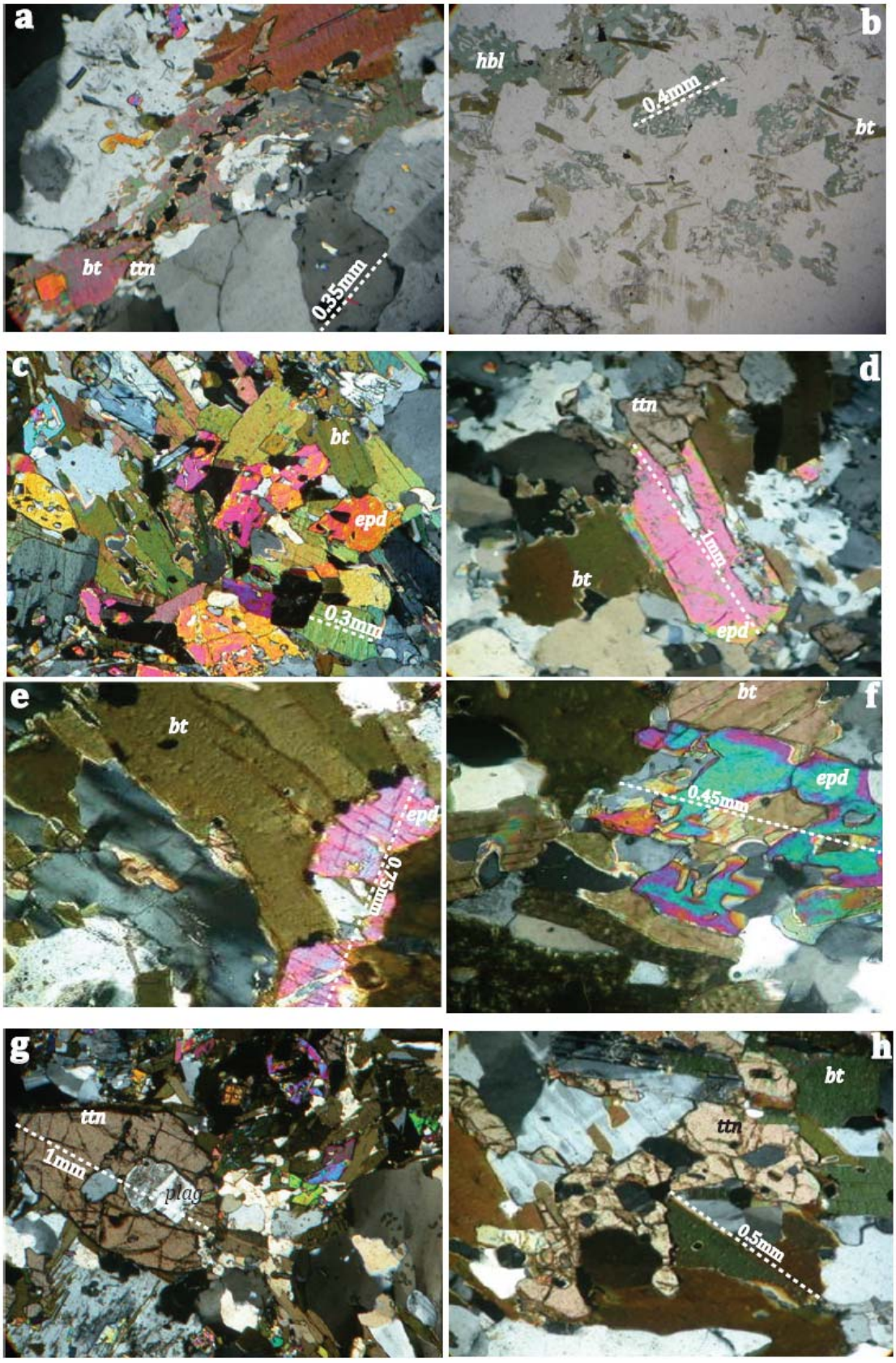

Figure 5. Mineral textural relationships of the px-free granitoids of the Matok pluton - mineral symbols are as in Fig. 4.

(typically < 0.05 mm) biotite grains in turn occur poikilitically enclosed in plagioclase and K-feldspar and are commonly also intergrown with tiny epidote crystals. The orientation of biotite crystallite inclusions in the feldspar is mainly random. Instances where this inclusion biotite occurs along cleavage in the host feldspar have been found. An incomplete replacement of hornblende by biotite is also occasionally seen where the biotite pseudomorph after amphibole still preserve the ~120^{o} cleavage intersection of the proto amphibole. All the biotite except the one occurring as inclusion in the feldspar is interpreted to be magmatic.

Magnetite and ilmenite (traces - 1%) are present but subordinate to their quantity in the px-bearing granitoids. Both minerals are inclusion phases in plagioclase and also occur intergrown with other mafic minerals. Similar to the px-bearing granitoids, ilmenite has been found where it is rimmed by thin slice of titanite and/ or apatite. Even when ilmenite occurs as an inclusion in plagioclase, it may have the thin slice of titanite rim.

Titanite (traces - 5 %) forms typically ≤ 2.5 mm grains that range from being anhedral to euhedral, the latter which commonly preserve the perfect wedge shape. Fresh magmatic grains are abundant but a subsolidus alteration to leucoxene is also common such that where this is the case the grains look nearly opaque under the microscope. Bigger titanite grains host plagioclase inclusions (Fig. 5g), suggesting the latter to have contributed towards the formation of the former in a magmatic environment. The presence of euhedral titanite (Fig. 5g) complemented by euhedral crystal face of epidote against biotite (Fig. 5c) but a vermicular texture against plagioclase and quartz attests to a magmatic origin for both epidote and titanite (Long et al., 2005). Although most of the anhedral titanite is probably subsolidus, the one that is intergrown with biotite and quartz (Fig. 5h) is interpreted to be magmatic, regardless of the anhedral habit. This titanite typically has no core ilmenite; the texture which is suggested to signify a subsolidus formation of titanite in the Matok pluton granitoids. Conversely, the small (<0.1mm) titanite grains which occur as inclusions in hornblende, plagioclase and K-feldspar or rimming ilmenite or filling-in voids within the host minerals (Fig. 6a) are subsolidus.

Epidote (traces - 4%) occurs in three distinct generations that can be distinguished in terms of textural relationships. The first generation of epidote is that of euhedral to subhedral (up to 1mm in size) grains which may be symplectitic to well-developed (Figs. 5c-f). In the symplectitic grains, the euhedral habit can be traced. This epidote is commonly intergrown with or partially enclosed by biotite and is nearly always zoned. Such textural relationships of epidote have been interpreted to confirm the magmatic origin of epidote (Tulloch, 1979; Evans and Vance, 1984; Zen and Hammarstrom, 1984; Sial et al., 2008). Generally, the abundance of this symplectitic epidote decreases with increasing hornblende abundance across the samples.

The second generation of epidote comprises euhedral to anhedral optically zoned microlites (< 0.10 μm) that occur preferentially as inclusions in plagioclase and alkali feldspar. Most commonly, this epidote forms trails within the host feldspar. Orientation of the non-trailing microlites is random. From textural relationships, the host feldspars are in equilibrium with the rest of the magmatic minerals and as such, the epidote crystallites were more likely produced by influx of Fe^{3+}-rich final stage melts. Moreover, these epidote inclusions are mostly in the feldspar grains that had suffered sericitisation (Fig. 6b). An alkali feldspar that hosts inclusions of magmatic epidote is commonly suggested to have crystallised rapidly and just before the solidus, so that the epidote did not dissolve (Sial et al., 1999; Sial et al., 2008). In the case of the Matok pluton where plagioclase also has hundreds of inclusions of epidote microlites, it is improbable that plagioclase could have also crystallised just before the solidus, hence supporting the contention that this epidote is secondary (subsolidus), and that the euhedral habit of these epidote microlites does not mean they are magmatic (e.g. Keane and Morrison, 1997). Traces of allanite, monazite, tourmaline and apatite 'needles' are found as inclusion phases in plagioclase and along cleavage planes in biotite as well as in quartz. These are suggested to be subsolidus and were formed at the same time that the subsolidus epidote described above was formed.

The third and minor generation of epidote is that which occurs in rocks which were sampled along shear zone. This epidote typically occurs along grain boundaries of hornblende and is interpreted to also be subsolidus.

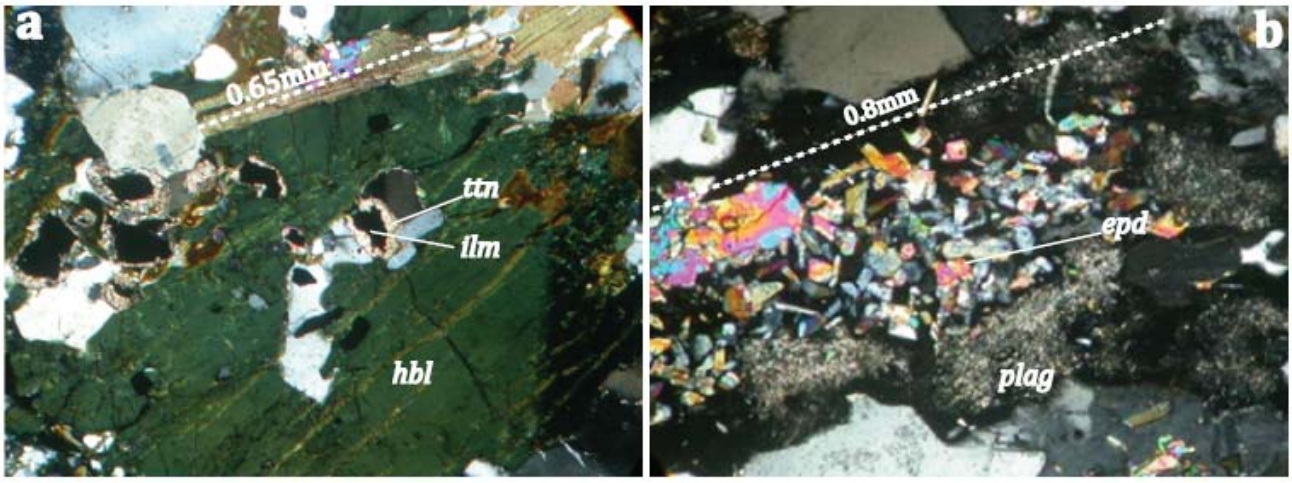

Figure 6. Subsolidus alteration in the px-free granitoids of the Matok pluton - mineral symbols are as in Fig. 4.

Similar to the px-bearing granitoids, accessory phases of pristine crystals of zircon, apatite, chalcopyrite, pyrite, magnetite ± magmatic ilmenite are hosted in the major minerals (feldspars, hornblende and biotite). Magmatic apatite exhibit sector zoning.

The general crystallisation sequence suggests the following succession from the early to the last mineral to crystallise:

apatite - zircon – chalcopyrite – pyrite - ilmenite - magnetite - plagioclase –hornblende –alkali feldspar - titanite – epidote - biotite - quartz

4.2.2.2. Px-free granites with >71 wt. % SiO_2

Both porphyritic and non-porphyritic varieties are present with the phenocrysts being plagioclase and alkali feldspar. Mafic minerals are generally < 2 mm while felsic minerals tend to be larger. Compared to other px-free granitoids described above, these granites are virtually devoid of hornblende and magmatic epidote but rarely have traces of titanite.

Plagioclase (5 -29%) and alkali feldspar (28 - 59 %) exhibit subhedral to anhedral grains ranging from micron scale to phenocrysts of up to ~ 1 cm. In some samples, only phenocrysts of alkali feldspar (and not plagioclase) are found. Myrmekitic, granophyric and perthitic textures are present. A rare alkali feldspar overgrowth on myrmekitic plagioclase is present. Recrystallisation, deformational twinning, undulose extinction and sericitisation of both plagioclase and alkali feldspar are common. In most samples alkali feldspar is dominated by microcline but some grains do preserve calsbard twinning. Quartz (29 - 45%) forms anhedral grains with variable size ranging from micron scale to an average of 3mm. More commonly quartz has developed of subgrains and recrystallisation.

Biotite (1 - 12%) forms mainly anhedral and rarely subhedral grains that are generally < 2 mm in diameter. The smallest biotite grains are inclusions in plagioclase. In many cases, two distinct populations of biotite can be distinguished. One is the subhedral, typically prismatic (with no preferred orientation) variety which is found nearly always intergrown with quartz ± microcline, possibly suggesting the reaction of pyroxene with melt to liberate biotite and quartz. The second generation of biotite occurs nearly always in the vicinity of altered titanite, and possibly suggesting titanite contribution towards the formation of the biotite, at subsolidus conditions.

Ilmenite and magnetite (traces) occur as small (typically < 0.1 mm) grains that may be interstitial or inclusions in the feldspars. Rimming of ilmenite by a thin slice of titanite is common. Even the ilmenite that is an inclusion in the feldspar may have a titanite rim. Titanite (traces - 1%) forms subhedral to anhedral grains which are more commonly <0.3 mm. Nearly all the titanite grains have at least some bit of ilmenite relics on them, attesting to the replacement of the latter by the former, at subsolidus conditions.

Accessory phases of apatite and zircon occur as small grains (typically less than 0.02 mm) which are more commonly inclusions in the feldspars. Zircon inclusions in quartz have also been found. In one sample (Mat 63) epidote traces are found. This epidote is texturally similar to the subsolidus epidote described above.

Discussion:

Although it is well documented that crystallisation of orthopyroxene (in basalts + andesites) occurs at slightly higher temperature than clinopyroxene (e.g. Bowen, 1928), the dominance of clinopyroxene over orthopyroxene in the Matok pluton granitoids more likely points to the calc-alkaline nature rather than relatively lower liquidus temperatures. Moreover, when orthopyroxene is not found in a sample while clinopyroxene is, magmatic epidote and titanite are not found, reiterating that the absence of orthopyroxene is simply to do with the calc-alkaline nature of the Matok pluton. The calc-alkaline nature of the Matok magmas would have favoured the stabilisation of Ca-bearing minerals in preference to Mg- and Fe-bearing minerals of the same group.

Besides the differences in mineral modal proportions within each of the px-bearing and px-free granitoid groups, no differences in textural relationships have been observed within each group. Even the px-free granites with > 71wt.% SiO_2 which lack hornblende and magmatic epidote do show textural similarity of other minerals as in the rest of the px-free granitoids. Both px-bearing and px-free granitoids have common accessory minerals apatite, zircon, chalcopyrite and pyrite which mutually occur as inclusions in the rest of the major minerals, suggesting a similarity in initial mineral assemblages between the two granitoid suites.

The general absence of oscillatory zoning, the scarce twinning in the feldspar as well as its inclusion of microlites of secondary epidote ± biotite ± titanite would suggest that most of the feldspar in the px-free granitoids is metamorphic. The feldspars are rather in equilibrium with all other magmatic minerals. Moreover, even the alkali feldspar that shows calsbard twinning does have inclusions of epidote, biotite and titanite microcrystallites. Carlsbad twinning is known to occur in igneous alkali feldspar, but not in metamorphic feldspar (Deer et al., 1992; Wintsch and Yi, 2002).

Comparison of feldspar presence between the px-bearing and px-free granitoids reveals that the former tend to have higher proportion of plagioclase and less alkali feldspar than the px-free granitoids. This is compatible with plagioclase fractionation. However, one other equally important mineral present in both groups is hornblende. Generally, both the px-bearing granitoids and all the px-free granitoids with ≤ 71 wt.% SiO_2 have subequal proportions of

hornblende, suggesting the nonexistent hornblende fractionation to link the px-bearing and px-free granitoids. On the other hand, the px-free granites with > 71 wt.% SiO_2 do not have hornblende and therefore hornblende fractionation is not ruled out in their case. Alternatively, the fact that these px-free granites with > 71 wt.% SiO_2 do not have magmatic epidote may suggest that crystallisation parameters were simply not conducive to magmatic epidote, and hornblende crystallisation. Because these granites have the least amounts of calcium, it is possible that the early-crystallised plagioclase had confiscated all the Ca. A possibility also holds that these granites are residual differentiates (via hornblende fractionation) from magmas of the px-bearing granitoids.

The mere dominance of hydrous mafic minerals in the px-free granitoids denotes them to have had a higher fluid content than the magmas of the px-bearing granitoids. A higher amount of water dissolved in a melt induces shifts in oxidation state (Marzouki et al., 1979) which in turn may favour stabilisation of hydrous and Fe^{3+}-bearing minerals. Above the epidote stability field, magnetite is the main Fe^{3+}- capturing phase whereas the onset of epidote stability will result in epidote incorporating the Fe^{3+} (e.g. Sial et al., 1999). Magmatic epidote and titanite coexistence with orthopyroxene, magnetite and ilmenite requires relatively high fO_2 conditions (Wones, 1989; Schmidt and Thompson, 1996; Sial et al., 1999; Nakada, 1991; Xirouchakis et al., 2001; Broska et al., 2007; Sial et al., 2008). Both magmatic epidote and titanite are never found with ortho- and clinopyroxene and the modal abundances of magnetite and ilmenite decrease in the px-free granitoids of the Matok pluton. The incompatible behaviour of magmatic epidote and titanite with orthopyroxene, clinopyroxene ± magnetite ± ilmenite in the Matok pluton therefore suggests the relatively low fO_2 in the magma batches that produced the px-bearing granitoids. On the other hand, the evolution of the px-free granitoid magma batches led conditions conducive to higher fO_2 (and fH_2O) and hence the establishment of magmatic epidote and titanite.

The hydrous nature of px-free granitoid magma batches encouraged a prolonged crystallisation duration relative to the px-bearing granitoids. This prolonged duration ultimately saw all the pyroxene reacting with the melt to liberate hornblende, biotite ± epidote in a magmatic environment. In addition, the prolonged magmatic history favoured the separation of residual melt from crystals. These residual melts associated with px-free granitoids magma batches later led to the secondary epidote microlites discussed above. It can therefore fairly be surmised that, although this epidote is interpreted as subsolidus, the time of their crystallisation was at the solidus temperature “just” before the 'frozen' state of the rocks. The fact that feldspar of the px-bearing granitoids does not contain epidote crystallite inclusions even when sericitised (e.g. Fig. 4e) supports the contention that these inclusions were only associated with

infiltration of later stage residual melts associated with the px-free granitoids and were not a product of metamorphism long after crystallisation.

In order to envisage the establishment of magmatic epidote, hornblende and biotite at the expense of pyroxene, the following series of reactions are feasible:

Opx + cpx + plagioclase + magnetite + ilmenite + melt = hornblende + epidote + titanite + biotite + quartz (1)

Opx + cpx + plagioclase + magnetite + ilmenite + melt = epidote + biotite + titanite + quartz (2)

Hornblende + titanite + alkali feldspar + melt = epidote + biotite + quartz + ilmenite (3)

Hornblende + alkali feldspar + magnetite + melt = epidote + biotite + quartz (4)

Reaction 1 is substantiated by minute inclusions of magnetite found in magmatic epidote and hornblende. Also, reactions 1 and 2 substantiate contribution of plagioclase, ilmenite and magnetite towards the formation of titanite (Fig. 5g) and highlight why magnetite and ilmenite are subordinate in the px-free granitoids. The absence of pyroxene or its relicts in the px-free granitoids reiterates the fact that reactions 1 and 2 occurred in the magmatic environment, where due to an increased fluid content, the pyroxene had become unstable and reacted out.

Magmatic hornblende is present in both px-bearing and px-free granitoids. The suggested prolonged magmatic state and higher fluid content of the px-free granitoid magmas may have led to some early crystallised hornblende to react with the melt to liberate epidote (reactions 3 and 4). In turn, this would explain why some epidote grains are more resorbed than others (Fig. 5f vs. 5d) and why occasionally epidote is found with a 120^{o} cleavage intersection, as if it pseudomorphed hornblende (Fig. 5e). The severely resorbed epidote grains (Fig. 5f) may possibly be linked to reaction 1, which suggests a concurrent hornblende-epidote crystallisation and the less resorbed grains (Figs. 5d, e) may indicate conditions of reactions 3 and 4. The possibility of reaction 3 where titanite in turn may have contributed its Ti to the formation of biotite is supported by observation that some biotite grains occur only in close proximity to titanite (and quartz; Fig. 5h).

4.3. Mineral chemistry

This section outlines the characteristic mineral chemistry of the different rock types of the Matok pluton. Mineralogical major element variation within and between the px-bearing and px-free granitoid groups will be assessed. The emphasis is made on the difference in

chemical composition of minerals that occur mutually in both px-bearing and px-free granitoids. All the mineral chemical analyses are presented in Appendix B.

When present, Opx is partitioned into an average of ~ En_{51}:Fe_{49} (Fig. 7a). The Mg# (calculated as atomic Mg/(Mg+Fe^{2+})) of clinopyroxene on the other hand is variable in the range 0.47-0.77 but overall, the Ca-end-member constitutes an average of ~49% of clinopyroxene (Fig. 7a). Chemical analyses revealed that in both clino- and orthopyroxene, zoning (if present) is not uniform. Also, no systematic differences in pyroxene of the gneissic and px-bearing granitoids of the second intrusion were detected.

Crystallisation of magmatic epidote and titanite is more favourable under relatively oxidising conditions (Wones, 1989; Schmidt and Thompson, 1996; Sial et al., 1999; Nakada, 1991; Xirouchakis et al., 2001a; Broska et al., 2007; Sial et al., 2008). In order to assess if the presence of these two minerals in the px-free granitoids and their absence in the px-bearing granitoids denotes a difference in oxidising conditions, it is important to analyse the ferric/ferrous iron ratio (Fe^{3+}/Fe^{2+}) of mafic minerals that occur in both groups of granitoids. The Fe^{3+}/Fe^{2+} ratio of ilmenite (calculated according to Droop, 1987) does not distinguish between px-bearing and px-free granitoids (Fig. 7b). However, subtle differences exist in the Mn distribution which tends to be higher for ilmenite of the px-free granitoids.

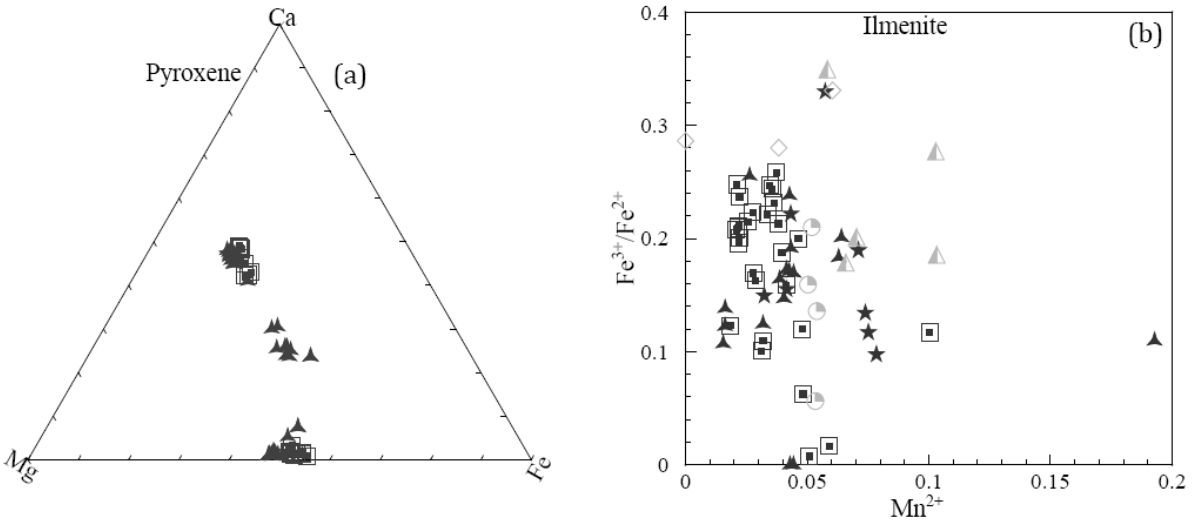

Figure 7. Composition of (a) pyroxene and (b) ilmenite for the rocks of the Matok pluton. Dark coloured symbols represent px-bearing granitoids and light grey symbols represent px-free granitoids. Data are supplemented with analyses from Bohlender (1992).

Assuming the theoretical (Droop, 1987) distribution of Fe^{3+} and Fe^{2+} in hornblende and biotite to hold true, the Fe^{3+}/Fe^{2+} ratio of total Fe was calculated on the basis of 23 and 22 oxygen atoms for hornblende and biotite respectively. The Fe^{3+}/Fe^{2+} ratio of hornblende (of the inferred magmatic origin) does not distinguish between px-bearing and px-free granitoids and

is by large constant with an increase Mg#. Nonetheless, the Mg# of hornblende of the px-bearing granitoids tends to be higher than that of px-free granitoids (Fig. 8a). The total Al content (Al^T) of hornblende in calc-alkaline rocks is important as it often holds information about the pressure of crystallisation (Hammarstrom and Zen, 1986; Hollister et al., 1987; Anderson and Smith, 1995; Liang et al., 2009). In the Matok pluton, the total Al content of hornblende yields a narrow range of about 1.4 to 2.2 cations per unit formula and does not differentiate between px-bearing and px-free granitoids. Similarly, the total alkalies (Na + K) distribution in hornblende does not distinguish between px-bearing and px-free granitoids and is confined to ~0.7 to 0.85 cations per unit formula (Fig. 8b). Overall, the (Na + K) distribution is constant over the confined total Al content in the hornblende of both px-bearing and px-free granitoids alike.

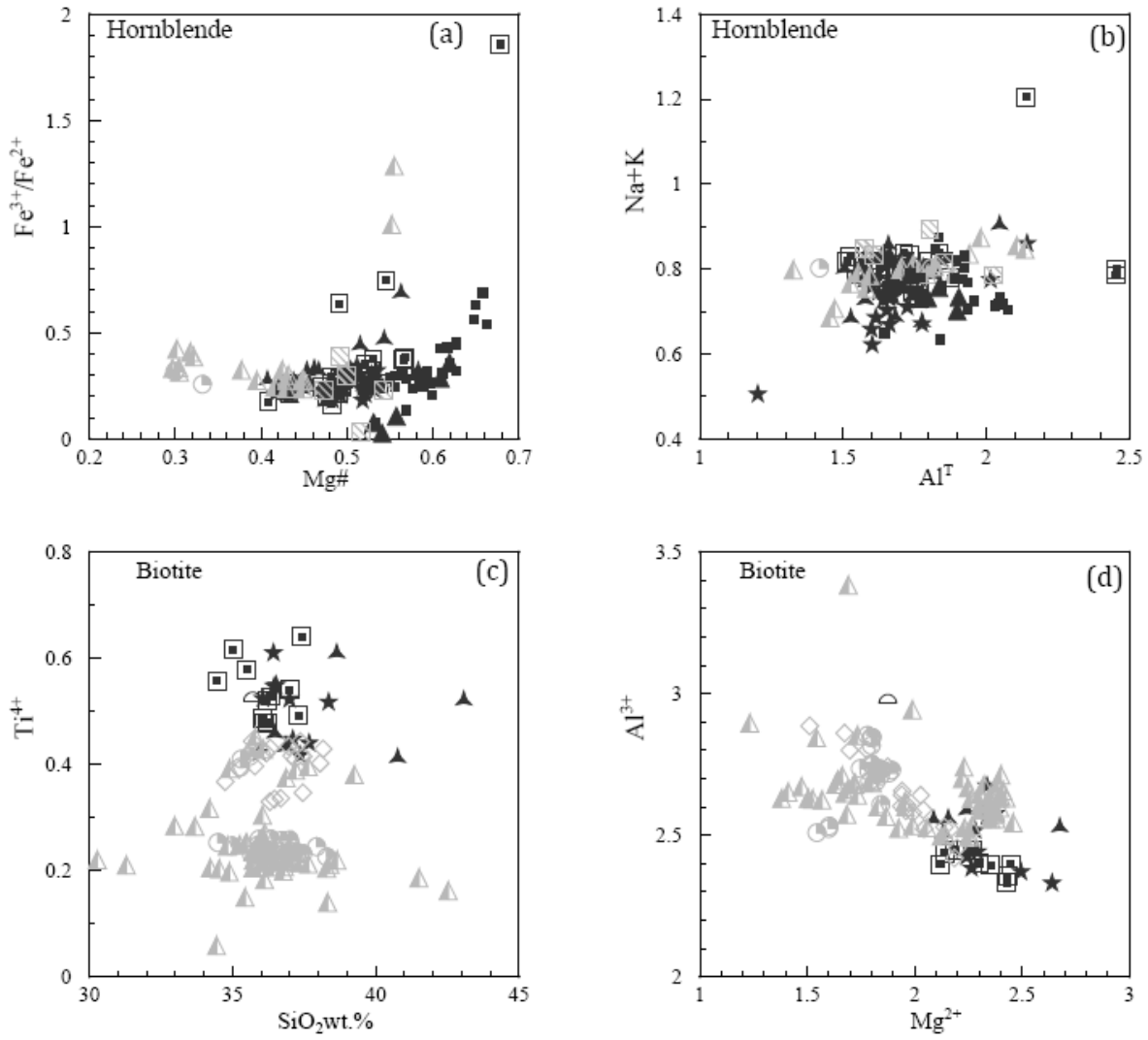

Figure 8. Variation of (a) Fe^{3+}/Fe^{2+} with Mg# (calculated as atomic Fe^{2+}/ (Fe^{2+} +Mg)), (b) Na+K with total aluminium per unit formula (Al^T) for hornblende, (c) Ti per unit formula with SiO_2 and (d) total aluminium (Al^{3+}) with Mg per unit formula for biotite in the Matok pluton granitoids. Dark coloured symbols represent px-bearing granitoids and light grey symbols represent px-free granitoids. Hornblende data are supplemented with analyses from Bohlender (1992).

An attempt to evaluate if there is any difference in the Fe^{3+}/Fe^{2+} ratio of magmatic biotite of px-bearing and px-free granitoids was fruitless. Assuming a total of 16 cations and 22 oxygen atoms yielded less than 16 cations for all the biotite. For this reason and according to Droop (1987) equation, it was assumed that all the Fe in biotite is in ferrous state. As such, the Fe^{3+} content of biotite cannot be used to delineate oxidation states of magmas of px-bearing and px-free granitoids. Ti is an element which can be coordinated in the octahedral site of biotite (Deer et al., 1992) and its solubility in biotite increases with increase in temperature (Nachit et al., 2005). From Figure 8c it is clear that biotite of the px-bearing granitoids has distinctively higher Ti per unit formula than that of px-free granitoids. It is also worth mentioning that a small population of biotite of px-free granitoids has just about similar Ti per unit formula as for the px-bearing granitoids (Fig. 8c). The cationic Mg^{2+} shows, generally, negative correlation with Al per unit formula and tends to be relatively higher for biotite of px-bearing granitoids (Fig. 8d).

In both px-bearing and px-free granitoids plagioclase composition is virtually all oligoclase (An_{10-30}; Fig. 9a), and though there is overlap in the composition, average values for the analyses performed give An_{24} and An_{20} for px-bearing and px-free granitoids respectively. The alkali feldspar exhibits overlapping proportions of K to Na in all the granitoids and shows an average of Or_{90}:Ab_{10} and Or_{92}:Ab_8 for px-bearing granitoids and px-free granitoids respectively. Contrary to plagioclase which is slightly less anorthitic (and more albitic) for px-free granitoids (Fig. 9b), the alkali feldspar composition shows no systematic distinction between px-bearing and px-free granitoids (Fig. 9c).

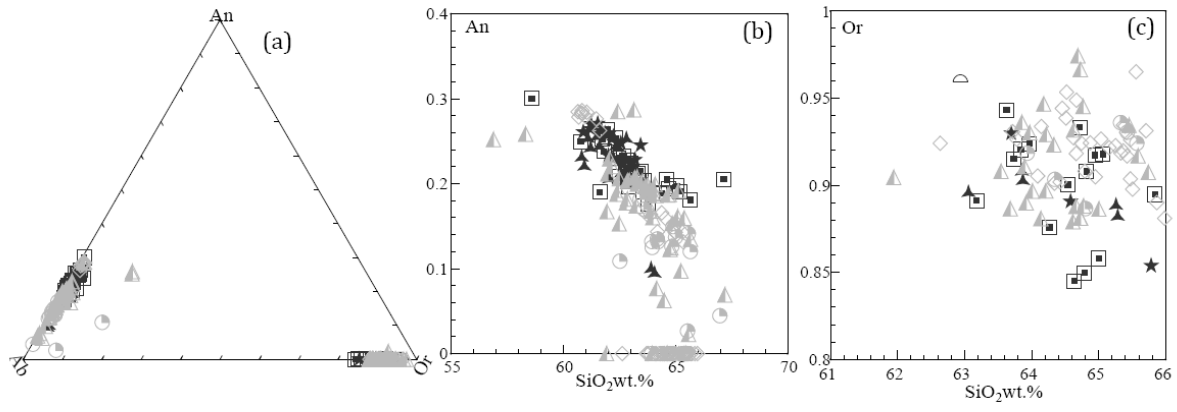

Figure 9. Composition of feldspar in the rocks of the Matok pluton. (a) shows plagioclase and alkali feldspar composition; An is for anorthite, Ab for albite and Or for orthoclase. In (b) the plagioclase Ca (the anorthite end member) content variation with mineral SiO_2 is shown, and in (c) the alkali feldspar orthoclase content variation with mineral SiO_2 is shown. Dark coloured symbols represent px-bearing granitoids and light grey symbols represent px-free granitoids.

The different generations of epidote distinguished in terms of textural relationships can also be classified in terms of their Ps (pistacite; $Fe^{3+}/(Fe^{3+}+Al^{3+})$) content (Fig. 10). The epidote

that is commonly intergrown with biotite, titanite ± hornblende has Ps content of Ps_{26-33} and TiO_2 < 0.2wt.% (Fig. 10a, b), compatible with the definition of magmatic epidote as proposed by Tulloch (1979), Evans and Vance (1984), and Zen and Hammarstrom (1984). Although TiO_2 content of epidote inclusions in feldspar is also < 0.2wt.%, the pistacite content is in the range Ps_{10-27}, (average of Ps_{23}), lower than the proposed Ps_{25} content of magmatic epidote and thus supporting the view that it is secondary. Even though this epidote inclusion in feldspar is commonly zoned on optical microscope, SEM resolution was not able to detect such zoning. Contrarily, minor Fe^{3+} zoning was detected in the magmatic epidote and shows a typical decrease from core to the rim. The assumption is that all iron in epidote is Fe^{3+}.

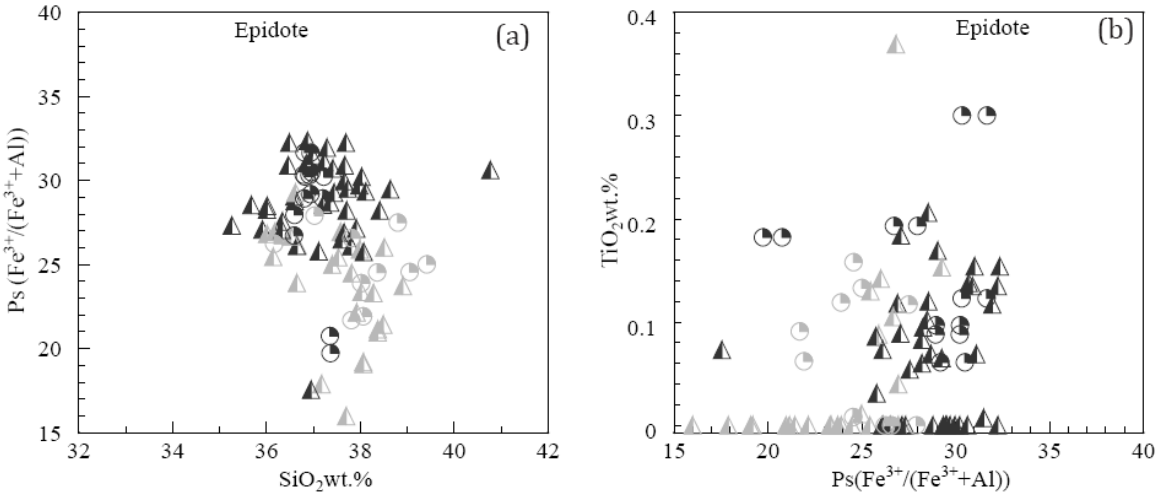

Figure 10. Variation of (a) SiO_2 and (b) TiO_2 of epidote with its pistacite (Ps) content in the px-free granitoids of the Matok pluton. The convention in all the plots in this work is to plot px-bearing rocks with dark colours. Magmatic epidote is present only in the px-free granitoids. In order to highlight the difference in epidote composition of magmatic and secondary origin, the two epidote varieties are in this figure distinguished by colour. Epidote of the inferred magmatic origin is shown in black and the epidote that occurs as inclusions in feldspar (secondary) is shown in grey.

Discussion:

Orthopyroxene contains just about equal proportions of enstatite and ferrosillite. The Mg# of clinopyroxene on the other hand averages ~0.66. This behaviour points to a possibility of early formation of clinopyroxene (i.e. before orthopyroxene). It is therefore emphasised that the dominance of clinopyroxene over orthopyroxene in the px-bearing granitoids is possibly due to the calc-alkaline nature of the rocks, rather than implying lower liquidus temperatures.

The Fe^{3+}/Fe^{2+} ratio of ilmenite in both px-bearing and px-free granitoids is similar. Crystallisation sequence suggests that ilmenite was one of the earliest phases to crystallise in both px-bearing and px-free granitoid magmas. Ilmenite therefore crystallised under similar

oxidation state in both px-bearing and px-free granitoids. Likewise, the similarity in the Fe^{3+}/Fe^{2+} ratio of magmatic hornblende for both px-bearing and px-free granitoids suggests crystallisation under similar oxidation state. Although alkali feldspar is more dominant in the px-free granitoids, the comparable alkalies partitioning into hornblende of both px-bearing and px-free granitoids attests to the insignificance of concurrent crystallisation with alkali feldspar. The higher Ti content of biotite of px-bearing granitoids attests to crystallisation at higher temperatures than in the px-free granitoids. This in turn supports the proposal that the px-free granitoid magma had a prolonged history which in turn saw progression towards biotite forming later at the expense of pyroxene ± hornblende under lower temperature conditions.

To sum up, the similarity in the Fe^{3+}/Fe^{2+} ratio of ilmenite and hornblende of both px-bearing and px-free granitoids is consistent with both granitoid types having had, initially, similar fO_2. However the magmas of the px-free granitoids underwent a protracted history which, in addition to higher fH_2O, saw the establishment of magmatic epidote and titanite. The lower Ti content of biotite of the px-free granitoids attests to crystallisation at relatively lower temperatures than the biotite in the px-bearing granitoids.

4.4. Geothermobarometric and fO_2 calculations

The metapelitic granulites of the Bandelierkop Formation in the SMZ record peak pressure-temperature (P-T) conditions of ≤9.5 kbar - 850^{0}C (van Reenen, 1983; Stevens and van Reenen, 1992a, b). Following retrogression, the SMZ P-T path culminated at isobaric conditions of ~6 kbar and a temperature of ~ 600^{0}C (van Reenen, 1986). Both the px-bearing and px-free granitoids of the Matok pluton were emplaced sometime during this metamorphic history (Barton et al., 1992).

Opx-bearing granitoids (*sensu lato* charnockites) typically record liquidus temperatures as high as ~1000^{o}C and are known to occur commonly in high pressure regimes (Grantham et al., 1996; Duchesne and Wilmart, 1997; Percival and Mortensen, 2002; Rajesh, 2007; Frost and Frost, 2008). Bearing in mind the 9.5 - 6 kbar pressure estimates in the SMZ (Stevens and van Reenen, 1992a, b; van Reenen, 1986), the hornblende-plagioclase thermometer of Holland and Blundy (1994) which produce the uncertainty of ± 75^{0}C was employed in the pressure range of 5-10 kbar. Temperature ranges of 722-735, 747-757, 730-740 and 680-684^{0}C were obtained for px- diorites1, px- diorites2 and px-granodiorites, px-free granodiorites and px-free granites respectively. An alternative geothermometer (a two-feldspar thermometer) of Stormer and Whitney (1977) was used to compare the results with that of Holland and Blundy and the derived average temperatures are 754, 740, 730 and 701^{0}C for px-diorites1, px-diorites2 and

px-granodiorites, px-free granodiorites and px-free granites respectively. While the Holland and Blundy geothermometer gives slightly lower temperatures for the px- diorites1 than the rest of the granitoids, an important observation is that the px- diorites2, px-granodiorites and px-free granodiorites are equally suited by the two geothermometers. However, all these temperatures are significantly lower than the typical liquidus temperature of Opx-bearing granitoids (see above). This possibly means that the onset of hornblende crystallisation occurred appreciably below the liquidus temperature.

The pressure of crystallisation of calc-alkaline granitoids is commonly estimated by the use of the total Al content of hornblende. The equation characterising this relationship predicts a positive correlation between the pressure of crystallisation and Al content of hornblende (Hammarstrom and Zen, 1986; Hollister et al., 1987; Liang et al., 2009). The total Al in hornblende of both px-bearing granitoids and px-free granitoids is largely similar and will predictably give similar pressure. The Al-in-hornblende geobarometer of Hammarstrom and Zen (1986) modified by Anderson and Smith (1995) to account for the effects of fO_2 in the assemblage; quartz-plagioclase-hornblende-alkali-feldspar-biotite-ilmenite/magnetite is the most applicable to the assemblages of the Matok pluton granitoids. The use of Anderson and Smith geobarometer, which has an uncertainty of ± 0.6 kbar, yields pressure estimates ranging from ~8.6 to ~3.3 kbar. The pressure average for all the granitoids is ~4.5 kbar in the temperature range of 680-757℃. The obtained pressure average is significantly lower than that suggested for the SMZ (see above) and therefore possibly suggests that the emplacement was not really at great depths.

The equation of Wones (1989) was used to estimate the fO_2 for the Matok pluton granitoids in order to establish if different values can be obtained for px-bearing and px-free granitoids. On the basis of pressures derived from the Al-in hornblende geobarometry and temperatures derived by the equation of Holland and Blundy (1994), the derived log fO_2 is in the range -3.8 to -7.0. While the stability of magmatic epidote in tonalitic melts may be established at higher pressures of ~ 10 kbar (Zen and Hammarstrom, 1984; Zen, 1985; Anderson and Smith, 1995), the pressure can be lowered to ~ 5 kbar or ~ 3 kbar when fO_2 is buffered by the NNO (Farrow and Barr, 1992; Sial et al., 2008) or haematite-magnetite (Schmidt and Thomson 1996). This suggests that the most influential parameters to determine the stability of magmatic epidote are rather fO_2 and fH_2O (e.g. Brandon et al., 1996). Similarly, the stability of titanite is favoured under high fO_2 and fH_2O conditions (Nakada, 1991; Broska et al., 2005). The fact that all the Matok pluton granitoids yield similar fO_2 implies no difference in oxidation states of both px-bearing and px-free granitoid groups. Assuming that the hornblende of the px-free granitoids records magmatic temperatures, it is suggested that both epidote and titanite crystallised at the

late stages of magmatic history of the px-free granitoids. This implies that the high fO_2 conditions were rather achieved towards late stages of crystallisation.

5. MAJOR ELEMENT CHARACTERISTICS

The aim of this chapter is to present and evaluate geochemical signature of the Matok pluton. The geochemical similarity and variation in the distribution of major elements between px-bearing and px-free granitoids will be explored. The next chapter will then present the distributions of trace elements. Major oxide concentrations were determined by the inductively coupled plasma (ICP)-emission spectrometry while the trace elements were determined by the ICP -mass spectrometry technique. Details of sample preparation and analytical conditions are presented in Appendix B.

Major element oxides of calc-alkaline granitoids can be used to quantitatively investigate the role of partial melting and subsequent crystallisation processes in influencing the characteristic geochemical signature. The MgO, Cr, Ni, concentration and Mg# play a decisive role in speculating on the origin of the magma as their quantity may provide information about the source. Specifically, rocks with at least 8 wt.% MgO, 400 ppm of Ni and 1000 ppm of Cr may signify a mantle origin (Best and Christiansen, 2001). In a number of studies, rocks with less than ~6 wt.% MgO are suggested for a source region that had a mantle wedge component (e.g. Halla, 2005; Kovalenko et al., 2005; Lobach-Zhuchenko et al., 2005; Steenfelt et al., 2005).

The type of protolith in the genesis of granitoids is also measured by the alumina saturation index (ASI; $Al_2O_3/(K_2O+Na_2O+CaO)$). When the ASI is greater than unity, the source is commonly characterised by sedimentary rocks or the magmas may have assimilated pelitic rocks enroute to (or at) the level of emplacement (e.g. Best and Christiansen, 2001). However, because amphibole is relatively poor in Al_2O_3, its extensive fractionation may also give rise to the more evolved rocks having ASI of >1 (Clarke, 1992). Extensive mineral fractionation may link the more evolved granitoids to more mafic parental magmas. The testimony for the 'liquid line of descent' which links the granitoids to a more mafic parent is normally based on the correlative major element oxide trends on Harker diagrams. However, this correlation may only be substantiated if trace element and isotopic data support the model of major elements.

The rocks of the Matok pluton range from diorites through granodiorites to granites according to the classification scheme of Cox et al. (1979). Major element oxide analyses are reported in Table 1 and Harker variation diagrams illustrated in Figure 11. All the rocks of the Matok pluton define a compositional continuum on the basis of major element oxides. Important to note in Figure 11 is the fact that all the major element oxides define well correlated trends (excluding Na_2O and Al_2O_3) with SiO_2 and that there is a small gap in between the granites with >71 wt.% SiO_2 and all the other rocks. Px-bearing granitoids collectively have SiO_2 in the range 53.71 - 68.39 wt.% while px-free granitoids have 61.70 - 74.88 wt.% SiO_2. The

MgO content ranges from 4.61 - 1.13 wt.% in all the px-bearing granitoids combined and 2.92 - 0.06 wt.% in the px-free granitoids. Mafic enclaves found in px-bearing granitoids have 3.51 - 1.99 wt.% MgO while the ones in px-free granitoids have 2.90 - 1.18 wt.% MgO. A negative correlation between MgO and SiO_2 is defined by all the rock types (Fig. 11a). Variation of CaO and SiO_2 also defines a negative correlation throughout the whole granitoid suite (Fig. 11b). When px-free granitoids are more mafic (in terms of SiO_2 saturation) than px-bearing granitoids, the former has higher CaO composition. This may suggest that the low temperature assemblage (px-free granitoids) may not be linked to the px-bearing granitoids by fractionation of Ca-bearing minerals.

Variation of FeO* (all Fe calculated as Fe^{3+}) with SiO_2 shows a negative correlation across all the rock types (Fig. 11c). Beside pyroxene being unique to the px-bearing granitoids, the other Fe-bearing minerals are ilmenite and magnetite. These latter two minerals are also present, though minor in the px-free granitoids. Mineral chemistry reveals that the Fe content of both ilmenite and magnetite of both the px-bearing and px-free granitoids is insignificantly variable. Additionally, FeO* content of both biotite and hornblende is generally higher for px-free granitoids than for px-bearing granitoids. This means that the higher FeO* content of px-bearing granitoids can be accounted for by the trio; pyroxene, magnetite and ilmenite. In turn, this feature would tend to produce an inflection point, a steep decreasing FeO with increasing SiO_2 in the px-bearing granitoids and a gentler decreasing (or increasing) trend in the px-free granitoids; but this is not the case. The implication is that the FeO* versus SiO_2 trend is inconsistent with control by fractionation of Fe-minerals.

TiO_2 versus SiO_2 shows an overall negative correlation. Within this trend however, a couple of distinctive fields may be allotted (Fig. 11d). From the illustrated fields it is observed that the topmost field shows a constant TiO_2 with increasing SiO_2 for some of the px-diorites1 and px-diorites2. Px-granodiorites and px-free granodiorites at similar SiO_2 content also tend to have similar TiO_2. While ilmenite is more abundant in the px-bearing granitoids, biotite and hornblende Ti concentration for px-free granitoids is smaller than that in px-bearing granitoids. The modal abundance of titanite, which is present in px-free granitoids and absent in the px-bearing granitoids is insignificant to make a huge influence on the TiO_2 versus SiO_2 plot. Therefore, the overlapping Ti concentrations for px-granodiorites and px-free granodiorites argue against fractionation of a Ti-bearing phase between the two groups of granitoids.

Table 1. Major and trace element data for the granitoids of the Matok pluton. Analytical procedures are explained in Appendix B2. nd stands for concentrations below the detection limits. The hyphens are written where the element concerned was contaminated as explained in Appendix B2.

Rock type	Pyroxene-bearing															
	Diorites1							Diorites2								
Sample	Mat 16	Mat 19	Mat 44	Mat 45	Mat 50	Mat 60	Mat 67	Mat 28	Mat 29	Mat 17	Mat 18	Mat 26	Mat 46	Mat 51	Mat 52	Mat 66
Major elements (wt.%)																
SiO_2	56.38	58.87	60.97	62.65	60.23	59.2	56.61	57.26	61.06	53.71	57.25	60.53	61.5	61.49	62.95	60.58
TiO_2	1.81	1.9	1.52	1.44	1.47	1.49	2.43	1.95	1.5	1.94	1.82	1.91	2.02	1.78	1.36	1.83
Al_2O_3	13.98	14.09	14.29	14.02	14.32	14.5	13.53	13.63	14.12	14.91	14.7	13.79	13.28	13.91	13.85	13.88
Fe_2O_3	10.16	8.95	7.67	6.93	7.78	8.01	10.93	10.03	7.4	9	8.94	9.51	8.88	7.78	6.43	9.2
MnO	0.15	0.12	0.11	0.1	0.11	0.11	0.16	0.12	0.1	0.14	0.14	0.14	0.1	0.12	0.09	0.12
MgO	4.06	2.44	2.49	2.09	2.88	3.19	2.82	3.49	2.63	4.61	3.29	2.03	2.09	2.41	1.75	1.86
CaO	6.06	5.36	5.2	4.44	5.45	5.92	6.15	6.27	5.18	6.96	5.87	5.19	4.7	4.72	4.03	4.13
Na_2O	3.84	3.79	3.95	3.92	3.99	3.81	3.63	3.39	3.95	3.42	3.81	3.87	3.83	3.63	3.78	4.07
K_2O	1.05	1.48	1.95	2.33	2.14	2.01	1.78	1.76	1.99	1.91	1.88	1.42	1.63	2.61	2.99	2.26
P_2O_5	0.88	0.77	0.62	0.6	0.61	0.64	1.12	0.99	0.66	0.91	0.8	0.73	0.8	0.8	0.54	0.61
Cr_2O_3	0.025	0.007	_	_	_	_	_	0.015	0.01	0.033	0.017	0.008	_	_	_	0.014
LOI	1.1	1.7	0.9	1.1	0.6	0.8	0.4	0.5	1	2.1	1.1	0.4	0.9	0.4	1.9	1
Sum	99.5	99.51	99.66	99.61	99.62	99.67	99.55	99.41	99.61	99.63	99.62	99.55	99.7	99.62	99.63	99.52
Trace elements (ppm)																
Sc	21	19	15	16	16	16	24	20	16	18	18	22	23	15	13	18
Ni	_	_	21.5	18.3	25.4	38.3	18.1	_	_	_	_	_	17.7	24.5	17.5	13.1
Co	29.1	_	20.7	18.2	21.5	22.6	25.6	27.4	19.5	_	_	_	19.7	19.2	13.8	18.9
V	177	156	157	137	159	146	217	176	137	170	151	180	181	160	110	136
Cs	1.7	0.4	0.9	0.7	1.3	0.9	0.2	0.7	0.9	1.5	1.4	nd	1.4	1.3	1.3	0.2
Ba	1045	1116	931	1166	1003	759	1200	1381	1018	635	1048	984	490	1348	1284	1311
Rb	20.2	26.1	68.2	65.1	90.9	65.2	30	37.7	65.7	66	56.2	14	67.5	67.6	67.5	48.7
Sr	866.4	739.9	606.5	589.5	632.4	572.1	719.1	800.4	622	751.8	686.5	563.5	479.1	748.6	545.2	679.9
Nb	20.2	28.9	20	24.6	19.1	18.5	28	24.9	18.5	17.6	21.4	22.3	37.6	25	23.9	32.8
Ta	0.9	1.1	1	1.2	0.8	0.8	1.4	1.2	0.8	0.9	1	1	1.7	1.1	1.1	1.5
Zr	400.3	737.5	376.6	439.7	414.5	383.4	554.9	399.3	382.7	222.9	406.2	579.7	474.4	59.7	414.3	854.8
Hf	9.6	18	9.1	11	9.7	9.3	13.5	9.1	8.8	5.2	10.3	13.9	11.5	2	9.6	18
Th	1	2.5	1.4	2.8	1.9	1.2	1.2	1.5	1.2	1.3	1.5	0.5	0.6	2.6	3.2	2.6
U	0.3	0.6	0.3	0.5	0.4	0.4	0.4	0.3	0.2	0.3	0.4	0.2	0.5	0.4	0.7	0.4
Y	54.4	61.9	53	66.2	46.8	44.5	74.4	54.5	44.3	38.5	51	53.7	67.7	55.4	54.9	70.1
La	78.6	97.7	66.1	82.8	66.5	60.2	96.5	88.5	62.6	50.3	70.4	57.3	43.8	79.9	76.8	102.6
Ce	177.8	225.5	150.3	183	147.8	132.4	222.8	192.8	135	117.3	159.8	138.2	120.9	175.6	172.9	223.4
Pr	23.97	28.77	18.95	23.71	18.6	16.74	29.15	25.35	17.94	14.67	20.63	18.66	18.01	22.26	21.79	29.15
Nd	100.9	114.2	76.9	95.5	75	67.3	124.8	102.4	70.5	60.4	83.5	77.4	82	88.4	87.2	125.2
Sm	16.61	18.6	12.92	16.08	12.28	11.32	20.37	16.85	12.61	10.61	13.89	13.53	16.28	15.01	14.34	19.72
Eu	4.13	3.7	2.91	2.97	2.63	2.68	4.83	4.17	2.8	2.48	3.31	3.29	2.47	3.18	2.96	4.38
Gd	13.36	15.33	11.1	13.9	10.01	9.71	16.74	13.79	10.58	9.72	11.9	12.49	15.07	12.32	11.78	16.05
Tb	1.99	2.34	1.74	2.19	1.55	1.48	2.44	2.08	1.61	1.45	1.86	1.95	2.36	1.9	1.82	2.41
Dy	10.29	12.25	9.49	11.83	8.58	7.97	13.31	10.77	8.6	8.22	9.73	10.26	13.19	10.41	9.92	13.27
Ho	1.93	2.28	1.83	2.33	1.6	1.56	2.61	1.99	1.65	1.48	1.89	1.93	2.49	1.93	1.88	2.55
Er	5.25	6.09	5.13	6.28	4.47	4.45	7.1	5.5	4.37	3.91	5.02	5.33	6.63	5.28	5.33	7.31
Tm	0.78	0.92	0.79	0.96	0.7	0.67	1.07	0.86	0.7	0.58	0.78	0.79	0.96	0.77	0.8	1.08
Yb	4.76	5.43	4.65	5.59	4.05	3.94	6.29	5	4.13	3.66	4.6	4.74	5.34	4.58	4.75	6.5
Lu	0.68	0.79	0.69	0.8	0.59	0.59	0.95	0.74	0.58	0.54	0.69	0.71	0.78	0.65	0.69	0.94
Ga	18.3	19.5	18.3	17.8	18.9	17.9	20.1	20.7	18.5	17.5	18.7	18.9	19.6	18.9	18.5	19.7
Sn	2	3	3	3	2	2	3	3	2	2	2	2	3	3	3	3
W	21.5	_	nd	nd	nd	nd	0.6	18.5	26.4	_	_	_	0.5	0.8	0.7	nd
Mo	1	0.9	4.5	4.5	3.4	3.8	4	1.9	1	1.4	2.1	2.1	6.5	5.5	4.3	4.2
Cu	37.5	16.4	20.4	20.3	22.2	23	27.5	27.8	20.8	32	28	19.1	27.2	30.3	17.4	40.8
Zn	70	80	54	47	57	72	56	64	65	58	66	44	54	64	51	45
Pb	4.2	5.8	7.6	10.8	6.7	2.8	3.6	1.4	6.1	9.4	5.3	1.5	4.3	10.4	4.6	5.7

Table 1 continued

Rock type	Pyroxene-bearing									Pyroxene-free					
	Granodiorite							Granites		Diorite		Granodiorites			
Sample	Mat 27	Mat 57	Mat 58	Mat 59	Mat 62	Mat 68	Mat 53	Mat 54	Mat 55	Mat 10	Mat 11	Mat 3	Mat 8	Mat 9	Mat 12
Major elements (wt.%)															
SiO_2	65.79	64.34	68.39	67.51	66.32	64.76	62.57	72.42	70.79	62.6	61.7	65.93	66.34	63.63	65.61
TiO_2	1.15	1.35	0.96	0.99	1.16	1.33	1.65	0.17	0.85	1.35	1.39	1.23	1.22	1.22	0.99
Al_2O_3	14.29	13.77	13.57	13.75	13.82	13.94	14.01	15.33	13.91	14.22	14.18	13.64	13.3	14.2	14.2
Fe_2O_3	6.16	6.27	4.73	5.07	5.59	6.44	7.28	1.12	4.21	6.54	7.36	5.95	6.07	5.94	5.06
MnO	0.09	0.09	0.06	0.07	0.08	0.08	0.1	0.01	0.04	0.08	0.09	0.07	0.09	0.07	0.07
MgO	1.38	1.81	1.13	1.31	1.54	1.5	1.88	0.66	1.05	2.54	2.73	1.51	1.42	2.38	1.92
CaO	3.21	3.94	2.72	3.14	3.33	3.46	4.37	1.63	2.43	4.21	4.24	3.27	3.18	3.87	3.52
Na_2O	4.55	3.42	3.71	3.9	3.75	3.66	3.81	5.73	3.73	4.08	4.07	3.55	3.67	4.28	3.97
K_2O	1.75	3.63	3.55	3.16	3.26	3.22	2.89	2.1	2.09	2.53	2.67	3.32	3.32	2.58	3.19
P_2O_5	0.52	0.54	0.31	0.34	0.4	0.39	0.66	0.08	0.23	0.57	0.62	0.47	0.45	0.5	0.44
Cr_2O_3	0.009	_	_	_	_	_	_	_	_	0.016	0.014	0.005	0.008	0.02	0.018
LOI	0.8	0.5	0.5	0.4	0.3	0.8	0.4	0.5	0.3	0.9	0.6	0.6	0.5	0.9	0.6
Sum	99.66	99.62	99.64	99.65	99.6	99.55	99.59	99.73	99.63	99.62	99.69	99.55	99.58	99.61	99.6
Trace elements (ppm)															
Sc	10	13	14	11	11	14	14	1	7	13	14	12	12	12	10
Ni	_	19	12.8	16.6	17.1	12.9	15.1	8	12.1	_	_	_	_	_	_
Co	_	14.1	8.4	11	11.8	12.7	15.2	2.7	7.5	15.8	18.4	12.9	12.6	14.6	12.4
V	89	109	70	83	103	109	124	29	63	106	116	91	86	100	79
Cs	0.3	0.7	0.5	0.5	0.5	0.6	0.8	0.5	0.6	1.4	2.6	2.6	1.7	2.5	2.3
Ba	717	1365	1451	1232	1527	1599	1351	1202	1436	1008	631	1308	1386	997	1087
Rb	26.1	68.1	75.5	66.5	84.9	74.3	55.5	26.2	62.5	85.9	109.6	104.5	81.7	105.4	111.6
Sr	375.9	510	378.6	408.8	514.1	487.3	651.1	940.2	358.1	560.3	497.7	486.7	494.2	541.8	514.2
Nb	18.8	29.6	24.4	21	28.6	26.5	25.1	2.2	20.8	20	18.9	24.3	25.6	17.7	17.2
Ta	0.9	1.2	1	0.8	1.3	1.2	1.1	0.2	0.6	1	0.7	1.2	0.9	0.7	1
Zr	402.4	484.3	510.6	503.4	500.5	778.9	547.2	88.5	516	487.5	453.3	576.3	525.6	442.5	384.7
Hf	9.1	11.9	12.5	12.4	11.8	17.6	12.8	2.4	12.9	12.6	11.3	13.7	13.9	11.1	9.4
Th	0.8	1.4	2.8	2.1	1.1	4.9	1.6	5	12.8	3.4	2.6	6.9	6.9	2.8	4.1
U	0.3	0.5	0.3	0.4	0.3	0.4	0.7	0.6	1.2	0.3	0.9	0.7	0.6	0.5	1.4
Y	31.6	70.4	56.3	51.8	60.5	61.2	57.2	4.5	38.9	47.6	50	50.2	53.3	45.8	42.6
La	53.8	80.5	79.4	77.9	62.6	138.7	78.1	15	123.2	67.6	56.1	76.6	95.3	74.4	56.5
Ce	124.5	194.1	175.1	170.6	149.5	288.3	175.5	26.6	253.2	147.3	125.7	189.2	201.1	158.3	122.9
Pr	16.06	25.78	21.99	21.08	19.81	32.97	22.62	2.74	29.49	18.53	16.49	20.94	23.58	19.39	15.96
Nd	64.6	103.6	86.2	82.4	81.4	125.8	91.8	9.1	106.4	72.8	68	81.7	90	74.4	60.1
Sm	10.54	17.53	14.64	13.92	14.27	18.27	15.17	1.54	15.54	12.18	12.1	13.68	14.99	12	10.3
Eu	1.48	2.79	2.54	2.18	2.54	3.11	3.28	0.54	2.23	2.43	2.01	2.3	3.04	2.39	2.25
Gd	8.63	14.02	12.41	11.42	11.76	13.98	12.11	1.2	10.7	9.89	10.51	11.14	12.2	9.84	8.46
Tb	1.27	2.25	1.95	1.79	1.94	2.04	1.89	0.18	1.57	1.6	1.65	1.73	1.84	1.55	1.34
Dy	6.12	12.37	10.61	9.76	10.72	11.13	10.08	0.93	7.8	8.49	9.04	9.24	9.85	8.09	7.34
Ho	1.13	2.42	2.03	1.85	2.1	2.13	2.02	0.15	1.34	1.63	1.69	1.72	1.82	1.57	1.43
Er	2.93	6.93	5.54	5.14	6.2	5.85	5.58	0.35	3.5	4.67	4.58	4.8	4.92	4.3	3.81
Tm	0.42	1.02	0.8	0.75	0.96	0.88	0.85	0.04	0.48	0.69	0.69	0.73	0.76	0.68	0.63
Yb	2.56	6.15	4.42	4.32	5.8	5.2	4.92	0.23	2.73	4	4.17	4.23	4.63	3.99	3.83
Lu	0.37	0.87	0.63	0.62	0.84	0.75	0.72	0.04	0.38	0.6	0.62	0.64	0.64	0.56	0.58
Ga	17.3	18.1	18.2	18.5	18.1	19.3	18	13	18.4	18.9	19.8	18	19	18.1	18.3
Sn	2	3	2	2	3	2	2	nd	nd	2	2	2	2	2	3
W	_	nd	nd	nd	0.6	nd	0.6	nd	nd	23.6	11.1	15.4	42	59	42.5
Mo	1.9	3.6	5.8	5.5	7.5	5.2	3.5	7.4	6.4	1.5	1	3.4	1.7	1.6	1.3
Cu	14.2	26.8	11.4	15.9	13.5	18	19.3	34.9	9.4	21.1	20	13.7	14.5	20.2	16.6
Zn	57	55	39	50	45	66	59	23	46	76	99	83	92	79	69
Pb	5.2	3.6	2.9	2.3	3.9	8.9	3	82.7	3.4	2.4	2.3	4.3	5.3	2.4	3.1

Table 1 continued

Rock type	Pyroxene-free															
	Granodiorites									Granites						
Sample	Mat 21	Mat 22	Mat 4	Mat 13	Mat 14	Mat 30	Mat 34	Mat 38	Mat 70	Mat 1	Mat 7	Mat 31	Mat 33	Mat 39	Mat 42	Mat 36
Major elements (wt.%)																
SiO_2	65.19	65.82	64.39	63.4	65.8	66.33	67.4	66.32	60.27	69.13	68.4	67.7	69.05	68.17	68.86	70.39
TiO_2	1.24	1.36	1.2	1.06	0.96	0.86	0.99	1.15	1.37	0.89	0.99	0.82	0.84	1.08	0.99	0.81
Al_2O_3	13.9	13.6	13.94	14.47	14.55	13.83	13.36	13.55	14.74	13.31	13.31	14.24	13.63	13.38	13.06	13.28
Fe_2O_3	5.82	6.33	6.6	6.02	4.93	5.75	5.54	5.53	7.48	4.52	4.74	4.25	4.1	4.91	5.18	3.99
MnO	0.07	0.08	0.08	0.08	0.06	0.08	0.06	0.08	0.1	0.06	0.06	0.05	0.05	0.06	0.09	0.06
MgO	1.6	1.22	1.54	2.15	1.63	1.12	1.04	1.4	2.92	0.87	1.16	1.11	1.16	0.91	0.81	0.74
CaO	3.66	3.32	2.64	3.89	3.47	2.84	2.48	2.83	4.41	2.46	2.49	2.15	2.25	2.22	2.57	1.86
Na_2O	3.75	3.82	3.63	3.88	4.26	3.41	3.8	3.14	4.04	3.95	3.52	3.67	3.93	3.29	4.15	3.84
K_2O	3.11	3.18	3.6	3.16	2.94	4.05	3.27	3.58	2.81	3.35	3.74	4.58	3.59	4.59	3.03	3.71
P_2O_5	0.48	0.31	0.64	0.49	0.39	0.35	0.39	0.62	0.64	0.28	0.37	0.36	0.34	0.24	0.25	0.25
Cr_2O_3	0.005	0.005	0.007	0.013	0.01	0.004	0.004	_	_	0.007	0.003	0.005	0.005	_	_	0.003
LOI	0.7	0.5	1.3	1	0.6	0.9	1.3	1.4	0.9	0.6	0.8	0.7	0.7	0.7	0.6	0.6
Sum	99.52	99.55	99.54	99.63	99.61	99.53	99.61	99.63	99.67	99.43	99.6	99.65	99.65	99.52	99.56	99.54
Trace elements (ppm)																
Sc	12	13	11	13	9	14	8	12	17	9	10	8	8	9	11	9
Ni	_	_	_	_	_	_	_	17.5	37.1	_	_	_	_	8.7	4.4	_
Co	13.1	11.1	_	_	_	_	_	12.1	18.7	7.3	9.7	9.4	9.2	9	5.8	6.3
V	91	78	88	89	72	65	66	101	133	52	74	62	73	79	47	47
Cs	1.4	0.3	3.5	3	1.9	2.2	1.6	1.6	3.4	0.3	2.1	2.1	2	0.8	nd	0.2
Ba	1363	1561	1098	992	1323	1474	1069	1242	689	2084	1302	1197	1201	1914	1899	2144
Rb	75	41.5	129	123.7	95.5	104.6	99.6	115.1	132.7	58.6	109.3	129.3	103.6	96.2	50.2	67.1
Sr	576	513.9	435.7	488.2	543.7	475.7	439.3	395.1	521.5	530.2	434.7	402.6	428.2	456.3	462.2	407.5
Nb	22.6	25.4	26	22.2	15.9	25.3	19	25.2	23.6	27.1	24.7	18.7	17.3	21.4	24.9	24.8
Ta	0.9	0.9	1.2	1.6	1	2.5	1.1	1.2	1.2	1	1.7	0.7	1	1	1	1
Zr	451.2	853.9	560.3	441.3	340.2	435.9	429.2	552.5	557.6	657.1	511.9	449.1	396.3	995.6	642	599.8
Hf	10.4	19.1	13.2	11.4	8.5	11.8	11	13.9	12.7	16	13.6	10.6	10.8	24.7	14.7	15.7
Th	5.8	1.6	7.3	5.4	5.2	11.8	9.1	4.9	5.5	5	6.7	4.9	4.8	3.3	3.3	6.7
U	0.7	0.4	2	1.7	1.2	1.5	0.7	0.5	1.4	0.3	1	0.8	1.2	0.6	0.2	0.4
Y	51.5	52.8	41.6	49.6	38.4	66.3	32.8	64.4	56.3	62.5	50.9	31.9	34.6	54.1	51.9	51.1
La	106.9	71.4	73.8	60.6	65.4	110.5	92.8	105.1	70.1	120.1	90	39.1	58.6	66.3	81.6	128.9
Ce	213.2	155.8	167.9	147.5	138.3	227	187.9	198.4	159.5	246.3	186.1	86.2	126.4	166.6	178.8	266.5
Pr	24.91	20.69	20.88	18.69	16.72	27.63	20.5	28.75	20.5	30.42	22.63	11.33	16.05	19.98	23.09	31.31
Nd	90.6	84.3	80.9	74.2	63.6	102.2	70	114.7	84.9	110.1	84.5	45.7	58.6	78.9	91.6	110
Sm	14.21	14.7	13.41	12.51	10.68	16.59	9.49	18.77	13.9	17.38	13.69	9.62	9.74	13.59	15.06	16.45
Eu	3.01	3.21	2.66	2.39	2.3	3.88	2.29	2.57	2.44	3.69	2.53	1.97	1.92	2.42	3.4	3.12
Gd	11.25	12.29	10.95	10.57	9.19	13.85	7.45	15.13	11.49	13.44	11.03	7.94	7.75	11.12	12.12	12.68
Tb	1.78	1.95	1.66	1.6	1.42	2.3	1.16	2.4	1.73	2.09	1.7	1.29	1.26	1.81	1.87	1.91
Dy	9.42	10.23	8.88	9.01	7.99	12.57	6.06	12.87	9.27	10.95	9.39	6.83	6.8	9.64	9.81	9.95
Ho	1.84	1.92	1.6	1.73	1.46	2.42	1.15	2.41	1.97	2.07	1.72	1.27	1.26	1.91	1.91	1.82
Er	5	5.33	4.44	5.09	4.02	6.9	3.21	6.5	5.21	5.87	4.89	3.66	3.49	5.4	5.15	5.21
Tm	0.79	0.81	0.71	0.86	0.64	1.1	0.5	0.99	0.84	0.89	0.72	0.53	0.55	0.86	0.77	0.78
Yb	4.72	4.69	4.2	5.66	3.89	6.79	3.24	5.55	5.33	5.11	4.4	3.17	3.19	4.96	4.31	4.71
Lu	0.67	0.71	0.63	0.86	0.56	0.98	0.49	0.81	0.83	0.76	0.66	0.49	0.48	0.76	0.64	0.69
Ga	18.8	19.1	18.8	18.4	17.2	18.8	18.6	18.4	21.7	18.5	18.7	20.8	17.4	17.1	16.4	17.6
Sn	2	3	3	4	2	4	2	3	3	2	3	3	3	2	2	3
W	9.5	26.6	_	_	_	_	_	0.6	0.8	45	8.3	25.3	38.2	nd	nd	42.8
Mo	0.5	1.6	2.1	1.3	2.2	1.6	2.1	9.1	2.9	2.6	1.2	1.5	1.5	6.2	6.4	2
Cu	14.8	9.7	10.9	16.4	14.5	4.5	5.9	12.1	21.1	7.8	10.4	9.3	10.5	7.5	4.7	11.4
Zn	60	58	90	79	61	77	75	80	93	64	70	63	61	65	64	78
Pb	3	2.6	6.3	3.6	4.4	9.2	7.1	4.6	3	2.9	5	4.3	3.4	4.2	2.6	4.1

Table 1 continued

Rock type	Pyroxene-free									Mafic envlaves						
	Granites									in pyroxene-bearing diorite			in pyroxene-free granodiorite			
Sample	Mat 35	Mat 43	Mat 65	Mat 32	Mat 41	Mat 23	Mat 24	Mat 20	Mat 63	Mat 47	Mat 56	Mat 61	Mat 5	Mat 6	Mat 37	Mat 40
Major elements (wt.%)																
SiO_2	76.6	76.23	74.88	74.75	74.71	74.22	73.73	73.81	73.64	55.41	63.12	58.32	61.8	63.01	60.5	65.4
TiO_2	0.26	0.04	0.35	0.29	0.31	0.38	0.47	0.37	0.37	2.26	1.51	0.9	1.63	1.41	2.29	1.26
Al_2O_3	11.86	13.24	12.81	12.85	12.93	12.93	13.01	12.78	13.31	15.87	13.92	14.44	14.24	13.96	12.29	13.79
Fe_2O_3	1.43	0.66	1.85	1.8	1.95	2.12	2.23	2.46	2.07	10	7.18	8.89	7.24	6.93	9.72	5.9
MnO	0.02	<0.01	0.03	0.03	0.03	0.02	0.03	0.03	0.03	0.09	0.1	0.13	0.09	0.09	0.15	0.08
MgO	0.18	0.06	0.41	0.3	0.35	0.45	0.55	0.5	0.42	2.56	1.99	3.51	2.07	1.86	2.9	1.17
CaO	0.65	0.7	1.11	0.82	0.99	1.09	1.35	1.18	1.03	4.35	4.43	5.63	4.4	3.75	3.71	2.61
Na_2O	3.04	3.7	3.37	3.63	3.67	3.26	3.44	3.47	3.66	4.5	3.55	3.64	3.8	3.79	2.4	3.24
K_2O	5.21	4.84	4.46	4.88	4.39	4.82	4.35	4.49	4.58	2.31	2.93	2.76	2.38	2.74	3.32	4.49
P_2O_5	0.05	0.03	0.12	0.1	0.14	0.13	0.19	0.13	0.19	1.14	0.67	0.55	0.8	0.75	0.79	0.38
Cr_2O_3	0.002	_	_	0.003	_	nd	0.007	0.006	_	_	_	_	0.01	0.006	_	_
LOI	0.5	0.4	0.4	0.4	0.4	0.4	0.4	0.5	0.5	1.2	0.2	0.7	1.1	1.2	1.4	1.2
Sum	99.8	99.94	99.78	99.85	99.87	99.82	99.76	99.75	99.83	99.7	99.61	99.52	99.56	99.55	99.5	99.54
Trace elements (ppm)																
Sc	2	nd	2	4	3	2	4	4	3	22	14	18	14	15	24	11
Ni	_	10.2	7.6	_	9.2	_	_	_	10.5	25.7	16.4	32.9	_	_	_	12.1
Co	1.7	0.8	3.7	2.7	2.9	3.4	4.4	_	3.4	21.4	15.6	23.6	17	_	21	11
V	13	15	40	23	27	24	27	27	37	130	127	156	135	109	186	96
Cs	1	0.3	0.8	5.3	2.6	1.3	1.7	2.7	1	2.4	0.5	0.4	1.4	2.3	5	1.4
Ba	1069	279	1058	667	626	803	868	522	698	499	1243	1705	978	975	693	1650
Rb	129.2	152.7	114.5	223	191.2	128	155.2	184.1	176.4	99.8	57.4	66.1	61.2	80.5	190.4	115
Sr	135.5	62.1	220.6	146.3	142.7	208.1	237.3	168.9	173.3	538.2	519.7	919.8	513.9	450.1	272.9	435.3
Nb	12.6	34.5	9.1	14.4	14	4.7	11.2	11	13.7	51.3	27.8	12.6	27.7	23.7	46.8	30
Ta	0.8	0.5	0.3	1.1	1.2	0.3	0.6	0.6	0.7	2.4	1.3	0.5	1.3	1.1	2.2	1.3
Zr	254.9	100.3	293.2	230.2	228.8	265.6	279.9	208.2	245.4	271.9	497.2	230.4	650.9	573.4	1130	825.5
Hf	7.7	5.3	7.3	7.3	7	6.8	7	6.2	6.9	6.7	11.9	5.5	15.8	14.1	30.2	20.8
Th	8.5	18.7	9.1	9.4	6.6	3.9	4.7	6.7	5.7	1.3	0.7	2.6	1.6	5.3	11.3	7
U	1	2.3	0.7	1.8	1	0.5	0.5	0.8	0.5	0.9	0.3	0.7	0.4	0.6	1.6	0.8
Y	18.5	19.8	11.8	40.5	65.1	10.6	18.6	22	23	94	65.5	38.1	68.6	41.9	152.2	67.2
La	86.2	23	65.6	48.4	58.6	67.3	37.5	50.5	44.3	55.7	78	72.8	78.1	64.4	193.7	92.4
Ce	182	51.8	132.1	121.2	122.7	114.5	92.8	106.4	92.9	157.2	194.5	169.3	221.4	162	397.1	249.3
Pr	20.09	6.06	13.95	13.66	14.93	12.69	9.09	12.5	11.06	23.7	25.45	22.54	24.39	17.22	47.31	26.29
Nd	64	22.4	49.7	49.5	62.5	41.1	31.8	43.2	41.3	108	102.1	91.9	95.7	68.3	198.3	104.6
Sm	9.7	3.99	6.28	8.67	11.05	4.9	5.48	6.46	6.49	21.88	16.82	13.36	16.84	12.24	31.8	17.53
Eu	1.18	0.55	1.32	1.15	1.18	1.35	1.26	1.02	0.91	2.76	2.99	3.1	3.28	1.64	3.81	2.65
Gd	6.38	3.66	3.84	7.14	10.1	3.16	4.25	5.06	4.84	20.39	13.08	9.41	14.33	10.58	28.3	14.39
Tb	0.9	0.73	0.51	1.21	1.71	0.42	0.67	0.82	0.79	3.15	2.09	1.32	2.25	1.57	4.47	2.28
Dy	3.98	4.53	2.42	7.03	10.65	2.06	3.68	4.23	4.42	17.32	11.47	6.91	11.89	8.44	25.08	12.49
Ho	0.72	0.96	0.43	1.43	2.07	0.35	0.66	0.78	0.85	3.32	2.25	1.29	2.36	1.57	5.02	2.39
Er	1.67	2.86	1.09	4.07	5.98	0.97	1.9	2.23	2.37	9.16	6.38	3.68	6.41	4.48	13.98	6.68
Tm	0.21	0.44	0.17	0.64	0.93	0.15	0.27	0.35	0.38	1.38	1	0.57	0.98	0.68	2.09	1.02
Yb	1.16	2.26	0.96	3.97	4.95	0.89	1.73	2.07	2.14	7.64	5.86	3.57	5.9	4.08	11.64	5.98
Lu	0.18	0.33	0.15	0.58	0.61	0.14	0.23	0.31	0.3	1.08	0.86	0.53	0.87	0.63	1.75	0.89
Ga	15.3	16.1	14.7	17	15.3	14.9	15.5	14.9	17.2	22	18.1	17.6	18.6	18.9	21	18.4
Sn	2	nd	nd	3	1	nd	1	2	2	3	3	4	3	2	5	4
W	51.7	nd	nd	26.4	nd	10.2	40	_	nd	nd	nd	nd	41.2	_	0.9	nd
Mo	1.7	7.6	5.5	1.6	8	0.4	1.2	1.4	7.8	4.9	3.3	4	2	0.9	7.1	11.9
Cu	1.9	1.4	2.4	1.9	2.9	2.6	3.5	2.1	2.2	45.1	30.2	25.8	22.5	17.6	20	10.7
Zn	31	14	30	40	43	33	37	32	29	26	61	46	102	85	154	84
Pb	3.2	7.3	7.1	3.2	3.9	2.7	2.7	5	5.2	5.7	4.9	2.8	2.5	5	4.6	5

A mild negative correlation between Al_2O_3 and SiO_2 is a feature for the Matok pluton granitoids (Fig. 11e), though there is a considerable scatter especially within the px-bearing granitoid group. Plagioclase ($CaAl_2Si_2O_8$) incorporates more Al_2O_3 into its crystal structure than alkali feldspar (Na, K)$AlSi_3O_8$. Even though mineral chemistry revealed that plagioclase is never a pure end-member but rather a solid solution of both Ca and Na, the effect of plagioclase of px-bearing granitoids being slightly more Ca-rich than that of the px-free granitoids may be held accountable for the slightly higher Al_2O_3 of px-bearing granitoids. Likewise, px-free granitoids that have higher Ca content in the plagioclase have, overall, slightly higher bulk rock Al_2O_3 like px-bearing granitoids within the similar SiO_2 range. It is also worth pointing out that a few of the px-diorites1 and px-diorites2 are at the same Al_2O_3 concentration as px-free granitoids, even when the latter are more evolved (in terms of SiO_2; Fig. 11e).

Na_2O is in the restricted range of 4.55-3.14 wt.% for all the Matok pluton granitoids, with the exception of two extreme values of 2.4 and 5.73 wt.% for a mafic enclave in px-free granodiorite and a px-granite respectively. In general, the distribution of Na_2O versus SiO_2 can be divided into three fields, whereby all the rocks with dioritic composition (both px-bearing and px-free) define a mild positive correlation with SiO_2 while granodiorites (both px-bearing and px-free) and granites with ≤71 wt.% SiO_2 show no correlation (Fig. 11f). The third field would be that defined by px-free granites with >71 wt.% SiO_2. This division of the Na_2O versus SiO_2 into three fields raises the possibility of three separate magma groups. It is however important to note that if such magma groups were present, one group would have been for all the rocks with dioritic composition (px-bearing and px-free alike) another group for all rocks with granodioritic and granitic composition with ≤71 wt. % SiO_2 and the other one for the px-free granites with >71 wt.% SiO_2.

All the rocks of the Matok pluton show an overall positive correlation between K_2O and SiO_2 (Fig. 11g). The trend crosses the three fields (medium-K calc-alkaline, high-K calc-alkaline and shoshonitic fields) defined by Peccerillo and Taylor (1976). Px-diorites1 and px-diorites2 fall within the medium-K calc-alkaline field. On contrary, px-free diorites fall within the high-K calc-alkaline field. Granodioritic rocks (both px-bearing and px-free) fall within the high-K calc-alkaline field. Contrary to the px-free granites which are high in K_2O and fall within the high-K calc-alkaline field, the px-granites have low K_2O and fall within the medium-K calc-alkaline field. A few samples; a couple mafic enclaves in px-free granodiorites and another pair of px-free granites with ≤71 wt.% SiO_2 plot 'just' in the shoshonitic field (Fig. 11g). The crossing of compositional boundaries in Figure 11g is inconsistent with fractionation (e.g. Roberts and Clemens, 1993; Ferré et al., 1998), but may suggest either some kind of mixing line and/or three separate magma groups.

All the Matok pluton granitoids with ≤71 wt.% SiO_2 are metaluminous, as classified by the A/NK versus A/CNK plot defined by Shand (1943) while both px-granites and px-free granites with >71 wt.% SiO_2 are slightly peraluminous (Fig. 11h).

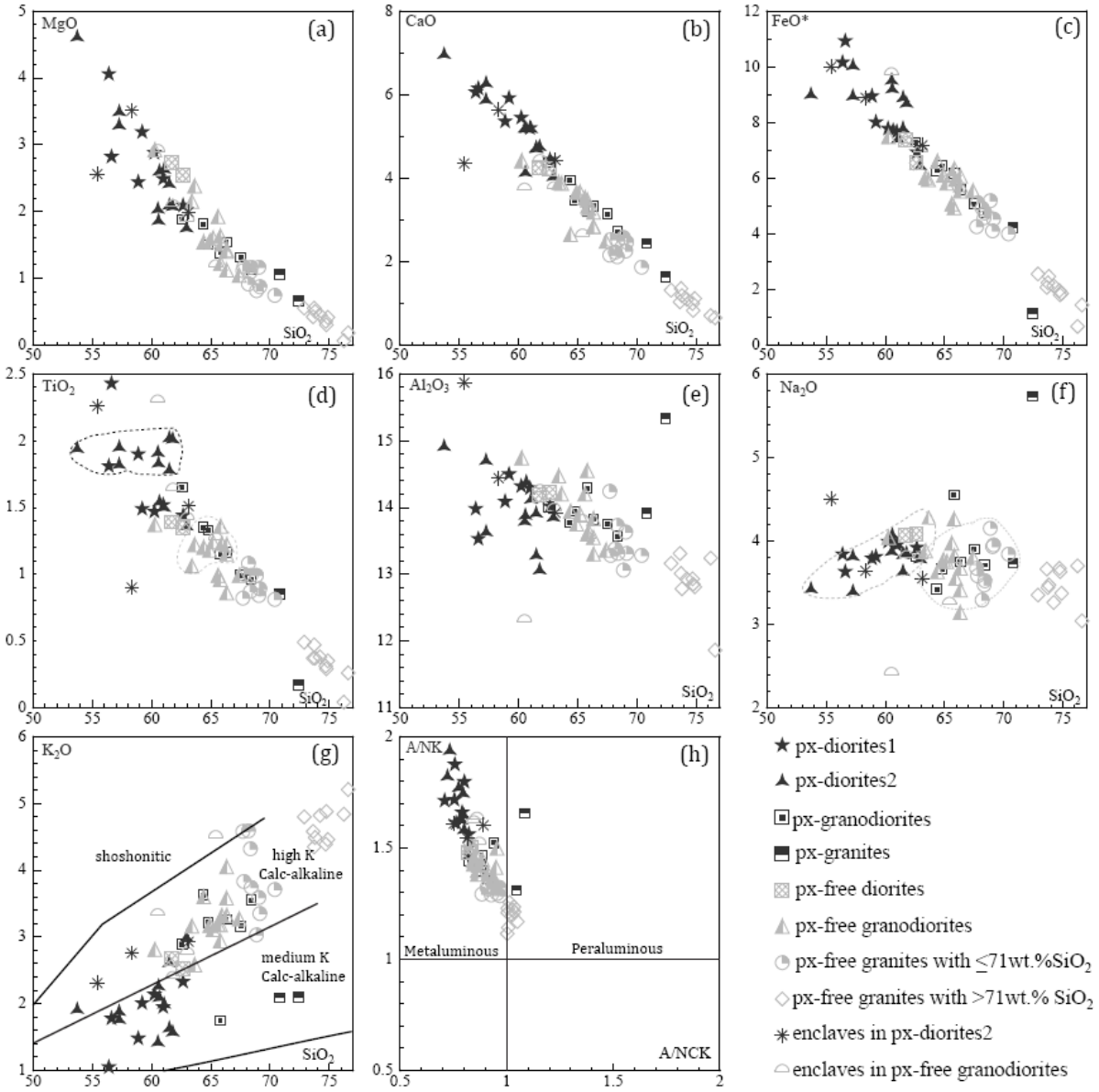

Figure 11. Variation of bulk rock major element compositions (in wt. %) and a measure of peraluminity for the rocks of the Matok pluton. All Fe is represented as Fe^{3+} in the notation FeO*. Symbols with fully dark colour or part thereof are for px-bearing granitoids while grey symbols are for px-free granitoids.

6. TRACE ELEMENT CHARACTERISTICS

Trace elements are traditionally divided into groups according to their ionic potential and behaviour in melts. This behaviour is partly governed by 'partition coefficient'(D), which is a measure of the preference of a trace element to be partitioned into either a mineral phase or a coexisting melt. $D = C_{min}/C_{mel}$, where C_{min} is the concentration of the element in the mineral and C_{mel} is the element concentration in the coexisting liquid phase. The discovery of this relationship has thus lead to division of trace elements into compatible and incompatible elements. The former are preferentially incorporated into the mineral phase (and have D value of > unity) and the latter preferentially dwell in the melt phase (and have D value of < unity).

The incompatible elements are further classified into groups according to their ionic potential (charge/radius) in melts. One group based on the element's affinity for a silicate melt is made of the large ion lithophile elements (LILE) which are characterised by large ionic radius and are thus more readily 'released' from the solid residue and preferentially dwell in the melt. Another group is that of the more incompatible high field strength elements (HFSE). When hydrous fluids are involved in partial melting (such as in subduction zones), the LILE preferentially become incorporated into the melt while the less soluble HFSE are preferentially retained in the residual solid source (e.g. Barry et al., 2006). This is because the LILE are readily fluid mobile and would thus be mobilised by fluids released from a subducting slab. This LILE-HFSE relationship consequently has the tendency to result in negative anomalies of the HFSE relative to the LILE on spidergrams (e.g. Pearce et al., 2000; Best and Christiansen, 2001; Barry et al., 2006). Another coherent group of incompatible elements is that of the rare earth elements (REE) which are considered to usually be insoluble in aqueous solutions and thus making them good indicators of magmatic processes (Best and Christiansen, 2001). Each of these groups of trace elements will be presented to analyse their characteristic behaviour in the Matok pluton granitoids.

Compatible trace elements: The relationship between SiO_2 and selected compatible trace elements in the Matok pluton granitoids is illustrated in Figure 12. A negative correlation between SiO_2 and Ni is characteristic of the Matok granitoids and Ni concentration is generally less than 50 ppm for all the granitoids (Fig. 12a). Co also shows a negative correlation with SiO_2 and is typically less than 30ppm (Fig. 12b). Both V and Sc also show compatible behaviour and demonstrate a negative correlation with SiO_2 (Fig. 12 c and d). The distribution of these compatible elements in the Matok pluton granitoids is generally compatible with the presence of pyroxene and the superior abundance of ilmenite and magnetite in the px-bearing granitoids

relative to the px-free granitoids. These elements are mostly compatible in the aforementioned minerals than in the rest of the minerals present in the Matok pluton granitoids.

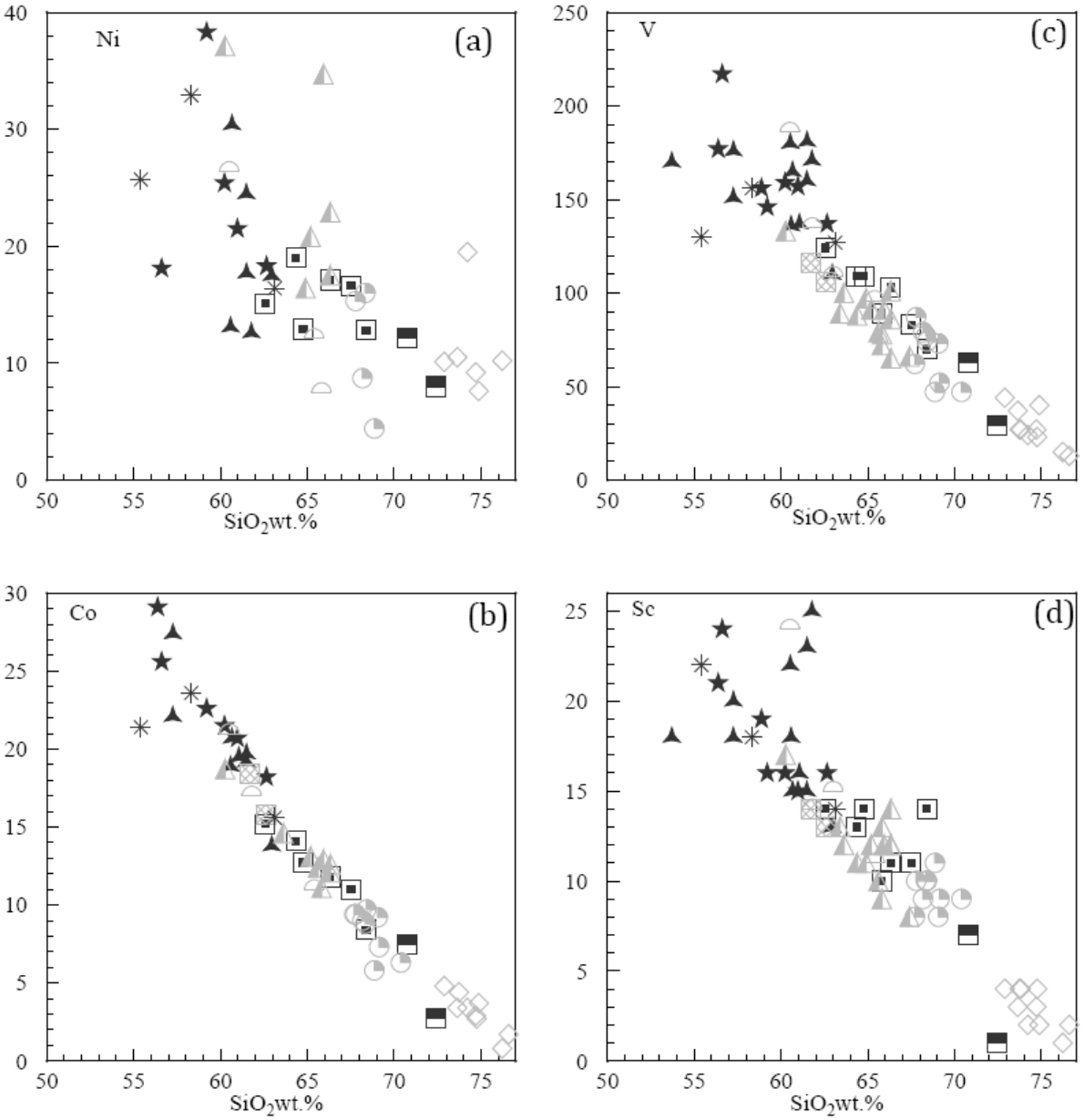

Figure 12. Variation of compatible trace elements (in ppm) with SiO_2 for the Matok pluton granitoids. Symbols are the same as in Figure 11.

HFSE: The distribution of the HFSE does not, generally, distinguish between the px-bearing and px-free granitoids. Ranges of Zr are 376.6 - 737.5, 59.7 - 529.5, 402.0 - 854.8, 453.3 - 487.5, 340.2 - 853.5, 396.3 - 995.6 and 88.5 - 293.2 ppm for px-diorites1, px-diorites2, px-granodiorites, px-free diorites, px-free granodiorites, px-free granites with ≤71 wt.% SiO_2 and the granites with >71 wt.% SiO_2 respectively. Hf concentrations on the other hand are in the ranges 9.1 – 18.0, 2.0 - 11.5, 9.1 – 18.0, 11.3 - 12.6, 9.4 - 13.9, 12.1 - 24.7, 2.4 - 11.6 ppm for px-diorites1, px-diorites2, px-granodiorites, px-free diorites, px-free granodiorites, px-free granites

with ≤71 wt.% SiO_2 and the granites with >71 wt.% SiO_2 respectively. A summary of variation of the HFSE with SiO_2 is illustrated in Figure 13. Also shown in Figure 13a is a zircon saturation curve for granitic melts at 800 and 900°C (after Watson and Harrison, 1983). It can be seen from Figure 13a and b that though majority of the Matok pluton granitoids can be classified under

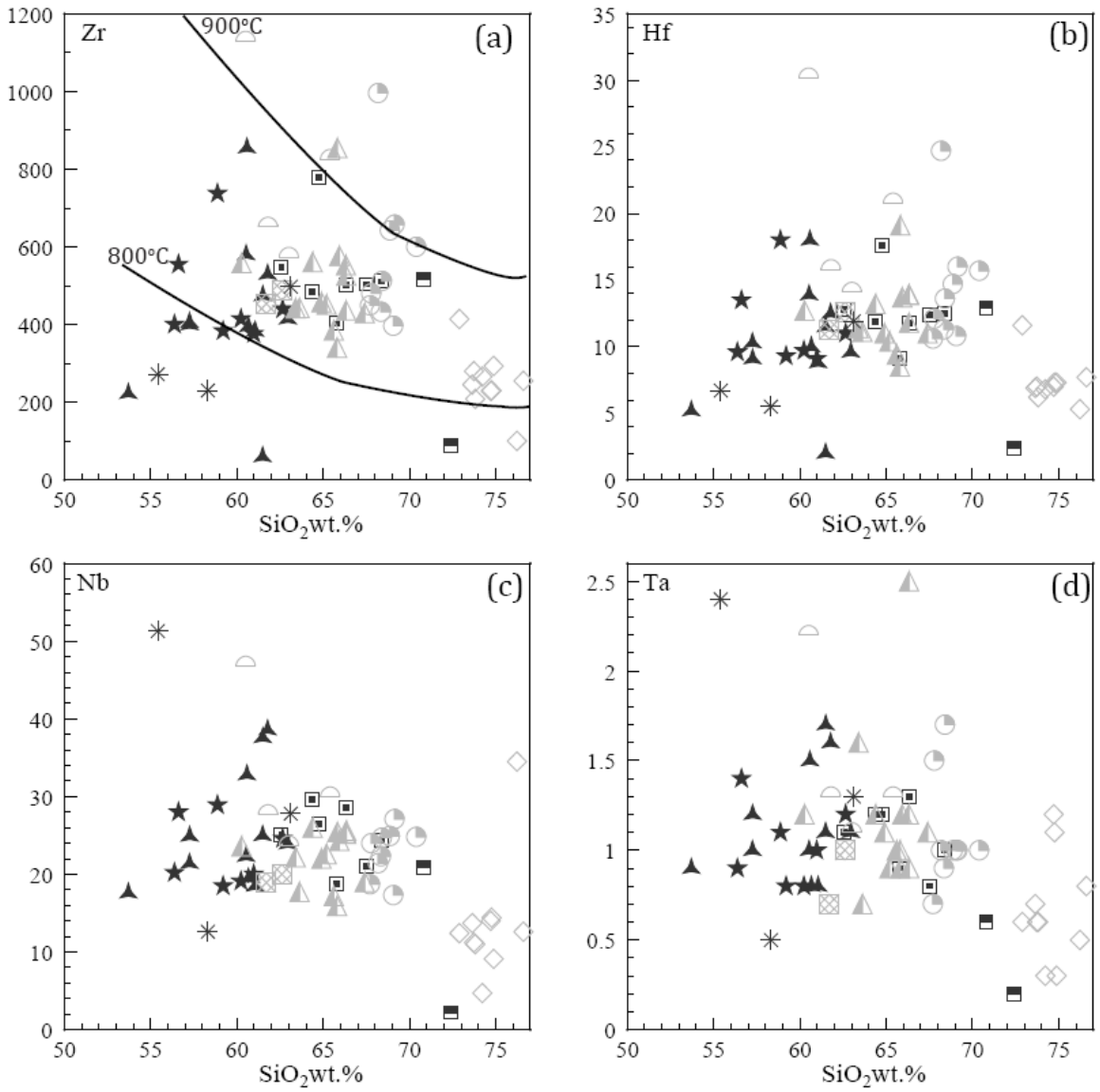

Figure 13. Variation of the HFSE (in ppm) with SiO_2 for the Matok granitoids. Symbols are the same as in Fig. 11.

restricted ranges of Zr and Hf, a considerable scatter is also present. The scatter may be due to magmatic processes, subsolidus alteration or zircon inheritance from the source. Hornblende thermometer (section 4.4) suggests hornblende to have crystallised in the temperature range of 684-757°C in all the Matok pluton granitoids. Assuming the hornblende temperatures to be correct, the fact that the majority of the Matok pluton granitoids plot above the 800°C zircon saturation curve (Fig. 13a) points to Zr oversaturation. This therefore raises the possibility of zircon inheritance from the source, though the effects of subsolidus alteration can also not be

ruled out. It will be seen later that the distributions of the Y and the HREE are not scattered across the Matok pluton granitoids. These elements (Y and HREE) are also highly compatible in zircon, and zircon inheritance would thus tend to produce non-uniform distribution of these elements.

Variation of Nb and Ta with SiO_2 also does not distinguish between px-bearing and px-free granitoids (Fig. 13c, d). This is despite titanite, the main mineral that incorporates Nb and Ta more than ilmenite and magnetite (Best and Christiansen, 2001) in the Matok granitoids, being present in the px-free granitoids and absent in px-bearing granitoids. The distribution of both Nb and Ta therefore does not raise any concept of mineral fractionation control to link the px-bearing and px-free granitoids.

LILE: The variation of selected LILE with SiO_2 is illustrated in Figure 14. Sr concentration is variable and decreases with increasing SiO_2. The highest Sr concentration is recorded by a px-granite. Px-bearing granitoids with dioritic composition have higher Sr concentrations of up to 866.4 ppm while px-free diorites have less Sr (highest is 560.3 ppm). On the other hand both granodioritic px-bearing and px-free rocks have about the same Sr concentrations. Overall, granitic rocks have the lowest Sr concentrations, especially the granites with >71 wt.% SiO_2 which on all the plots tend to define their own field away from the rest of the Matok pluton granitoids. Rb shows no correlation with SiO_2 and px-free granitoids generally have higher Rb than px-bearing granitoids at the same SiO_2 (Fig. 14b). Px-granites have (like all other px-bearing granitoids) low concentrations of Rb.

Ba concentration is largely confined to between 1000 and 1500 ppm for both px-bearing and px-free granitoids (Fig. 14c). A few outliers beyond this range are present though. While Pb does not show correlation with SiO_2 (Fig. 14d), px-diorites generally have higher Pb concentrations than all other granitoids. Notably, the px-free diorites have lower Pb concentrations, like all other px-free granitoids. At granodioritic composition however, the px-bearing granitoids have intermediate Pb concentrations which may even be lower that Pb concentrations of px-free granodiorites. Th and U do distinguish between px-bearing and px-free granitoids. Both Th and U concentrations are noticeably higher for px-free than for px-bearing granitoids (Figs. 14e, f). Even when a px-bearing granitoid is at the same SiO_2 as a px-free granitoid the latter typically has more Th and U. In a hydrous magmatic system, both Th and U readily partition into the melt than would be the case in an anhydrous system (Wood and Blundy, 2001). It is however worth highlighting that the two px-granites also have high Th and U, similar to the px-free granitoids.

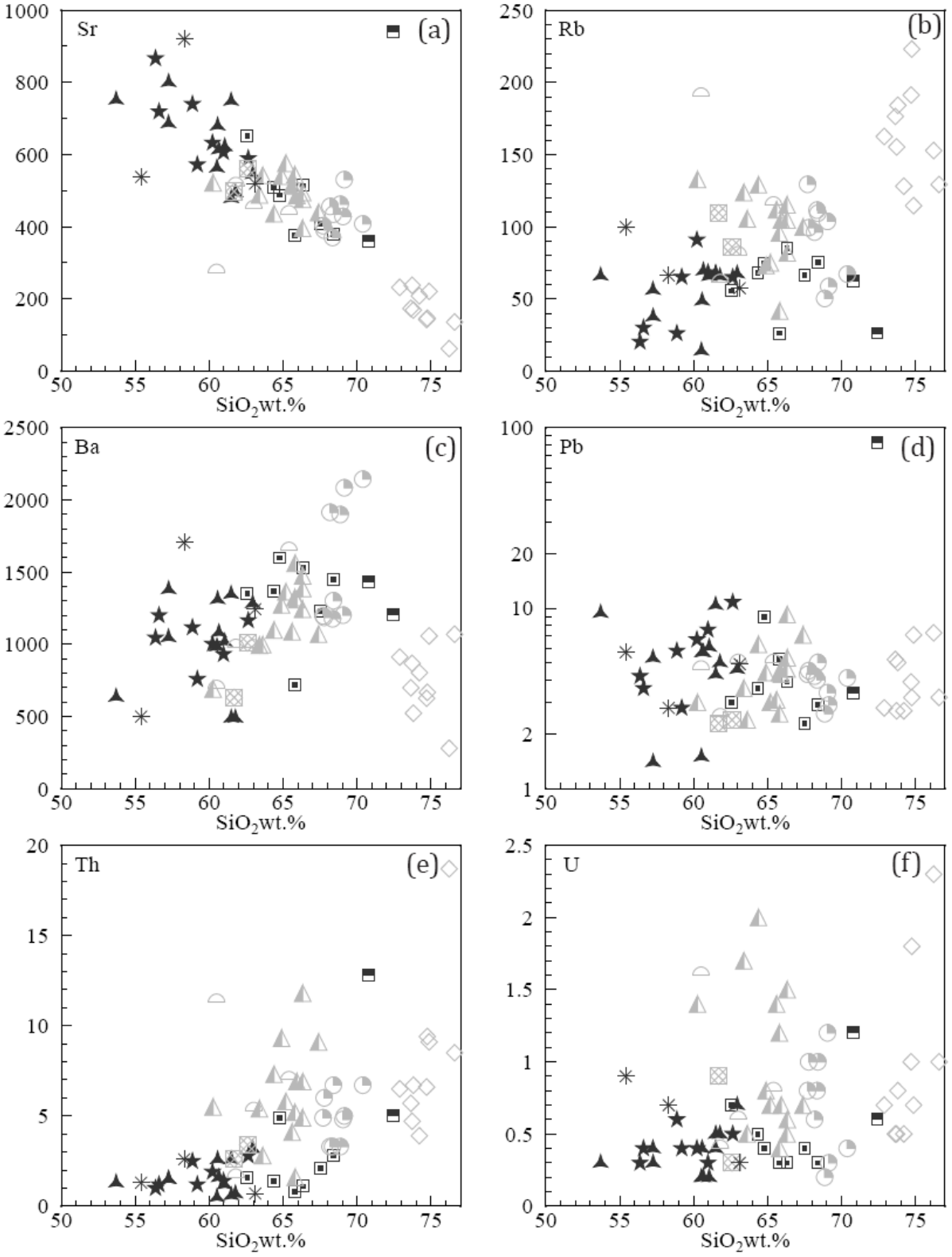

Figure 14. Variation of the LILE (in ppm) with SiO_2 for the Matok granitoids. Symbols are the same as in Fig. 11.

REE: The REE except Eu, show no systematic distinction between px-bearing and px-free granitoids. Within the rocks of dioritic composition, px-diorites1 have an average of La = 114×primitive mantle, px-diorites2 have average of 93×primitive mantle while px-free

diorites have average of 90×the primitive mantle value. Each of the granodioritic rock suites (px-bearing and px-free) have an average of about 123 La×primitive mantle. Px-free granites with ≤71 wt.% SiO_2 have an average of 120 La×primitive mantle while granites with >71 wt.% SiO_2 have an average of 71 La×primitive mantle. Thus, within the px-bearing suite px-diorites1 have intermediate La whilst px-granodiorites have La more enriched than px-diorites2. Within the px-free granitoids La enrichment increases from diorites to granodiorites but declines in granites with ≤71 wt.% SiO_2 through to granites with >71 wt.% SiO_2. The relatively more compatible Lu averages are 9.8, 9.2, 8.2, 9.7, 9.3, 8.0 and 3.9×primitive mantle for px-diorites1, px-diorites2, px-free diorites, px-granodiorites, px-free granodiorites, px-free granites with ≤ 71 wt.% SiO_2 and px-free granites with >71 wt.% SiO_2 respectively.

The Lu enrichment is generally similar for all the rock types, except for granites with >71 wt.% SiO_2. Both the light rare earth elements (LREE) and heavy rare earth elements (HREE) show no correlation when plotted against SiO_2 for all the rock types but are generally within confined ranges with the exception of the granites with >71 wt.% SiO_2. The LREE and HREE are represented respectively by La and Lu in Figure 15a and c. Eu on the other hand behaved relatively compatibly and shows a negative correlation with SiO_2 (Fig. 15b). Similar to the Sr-SiO_2 relationship, px-free diorites have lower Eu concentrations than the px-diorites while px-granodiorites and px-free granodiorites have overlapping Eu concentrations.

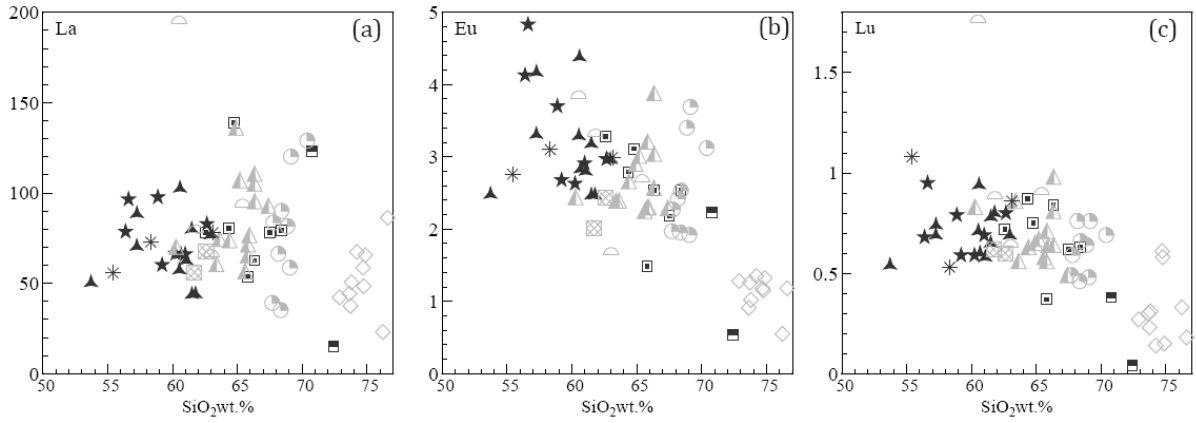

Figure 15. Variation of selected REE (in ppm) with SiO_2 for the Matok pluton granitoids. Symbols are the same as in Fig. 11.

Primitive mantle normalised REE diagrams are shown in Figure 16 and the rocks are grouped into diorites, granodiorites and granites to show that at a particular composition (e.g. granodiorites) the REE patterns and Eu anomaly are similar for all the classified rocks regardless of pyroxene presence. The px-diorites1 are plotted independent of other diorites to highlight that even though they are gneissic their REE patterns do not show evidence for alteration. The LREE show enrichment relative to the HREE. Eu shows a mild negative anomaly

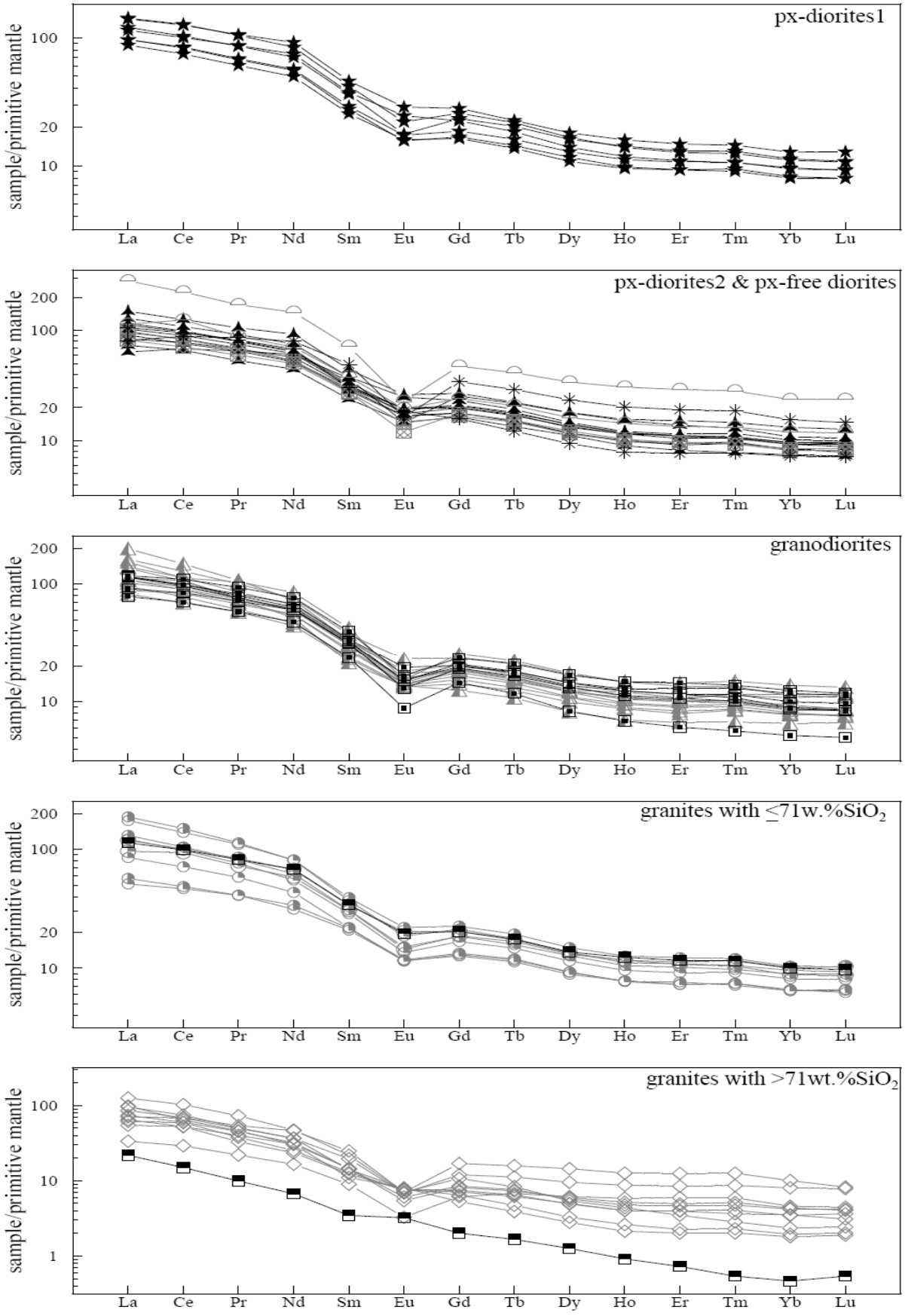

Figure 16. Primitive mantle normalised REE patterns for the Matok pluton granitoids. Normalising values are from Sun and McDonough (1989). Symbols are the same as in Fig. 11.

relative to elements with similar compatibility for all but one px-granite. Px-free granites with >71 wt.% SiO_2 have the largest negative Eu anomaly. Contrarily a px-granite with >71 wt.% SiO_2 which has the lowest concentration of Eu among all the granitoids shows a mild positive Eu anomaly relative to elements with similar compatibility. Also, this rock has concave upward HREE in addition to having the least REE enrichment among all the rocks in the Matok pluton.

Spidergrams: Extended incompatible trace elements are normalised to the primitive mantle values and shown in Figure 17. Again, to illustrate that rocks at similar SiO_2 saturation (regardless of whether they are px-bearing or not) show similar magnitude of negative anomalies, the plots are accordingly grouped into diorites, granodiorites, granites with ≤71 wt.% SiO_2 and granites with >71 wt.% SiO_2 (Fig. 17). The elements are arranged according to the order of their compatibility in basaltic melts with the most incompatible on the left and the most compatible on the far right of the diagram (Sun and McDonough, 1989). It is assumed that similar relative compatibility of the elements applies to granitoid melts. All the rocks of the Matok pluton show similar spiky-gently negative sloping primitive mantle normalised patterns.

The HFSE -Nb, Ta and Ti and the LILE -Th, U and Sr show negative anomalies relative to adjacent elements with the same compatibility (Fig. 17). Important to note however is the fact that both px- diorites-1- and 2, and px-granodiorites have a more pronounced negative Th anomaly relative to the adjacent U while the px-free diorites, px-free granodiorites and px-free granites have the reverse (Fig. 17). Mafic enclaves in px-bearing diorites2 have similar Th-U relationship as the host rocks and the mafic enclaves in px-free granitoids also have the same Th-U patterns as their host rocks. Also, px-free granitoids are slightly enriched in Cs relative to the px-bearing granitoids. The Sr negative anomaly is nearly similar among the rocks of dioritic and granodioritic composition and in granites with ≤71 wt.% SiO_2. An exception is the px-granite with >71wt.% SiO_2 which has a positive Sr anomaly. The px-diorites1, px-diorites2 and px-granodiorites have variably slightly positive to slightly negative Pb anomaly with the majority showing a mild positive anomaly. Px-free granites with >71 wt.% SiO_2 largely have no Pb anomaly while a px-granite with >71 wt.% SiO_2 has the largest positive Pb anomaly. The majority of the px-free granitoids with ≤71 wt.% SiO_2 shows a slight negative Pb anomaly and a few show minimal positive Pb anomaly. On contrary, the magnitude of negative anomalies of Nb and Ta are consistent and generally similar among all the rock types in the Matok pluton. The Ti negative anomaly slightly increases from the diorites, through granodiorites to granites. Rocks at similar SiO_2 saturation (e.g. granodiorites) have similar magnitude of Ti negative anomaly, regardless of whether they are px-bearing or not.

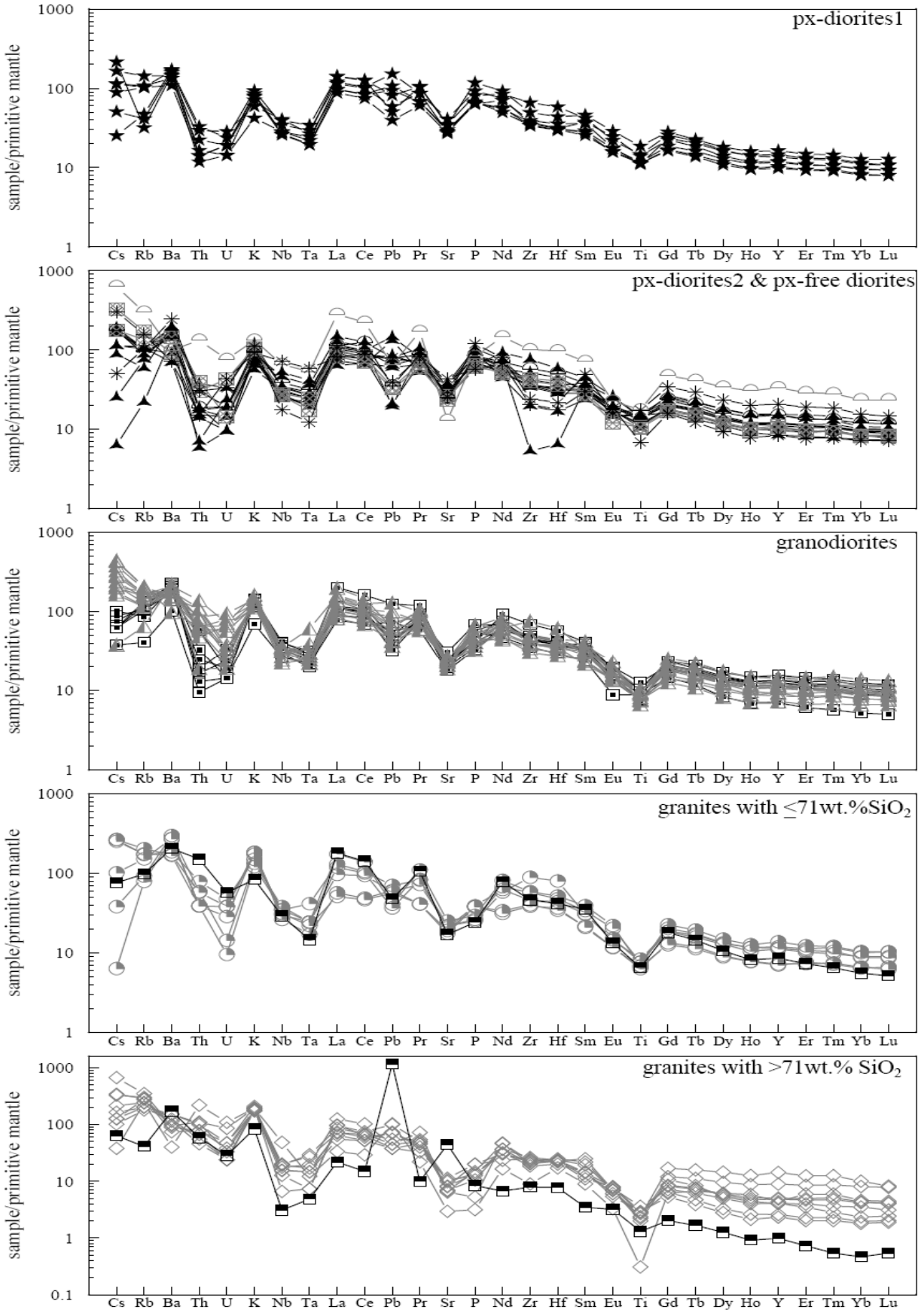

Figure 17. Primitive mantle normalised spidergrams for the incompatible trace elements of the Matok pluton granitoids. Normalising values taken from Sun and McDonough (1989). Symbols are the same as in Fig. 11.

A clearer presentation of the magnitude of the negative anomalies of the HFSE and Sr in Figure 17 is plotted against SiO_2 in Figure 18. Here, the magnitude of the anomaly expressed as X/X* is the ratio of primitive mantle normalised value for element X to that of the interpolated value (X*) obtainable if there were no anomaly relative to the two adjacent elements with similar compatibility (after le Roex et al., 2003). Because the magnitude of Ta anomaly will be affected in a similar manner to Nb, La (instead of Ta) is selected to interpolate the Nb anomaly on the more compatible side and K is selected on the more incompatible side. The magnitude of negative Nb anomaly shows a mild increase with increasing SiO_2 and is generally smaller for the px-bearing granitoids (Fig. 18a). Because the distribution of La does not systematically distinguish between px-bearing and px-free granitoids (Fig. 15), the slightly higher magnitude of negative Nb anomaly for the px-free granitoids is influenced by the higher (relative to px-bearing granitoids) K concentrations that they have.

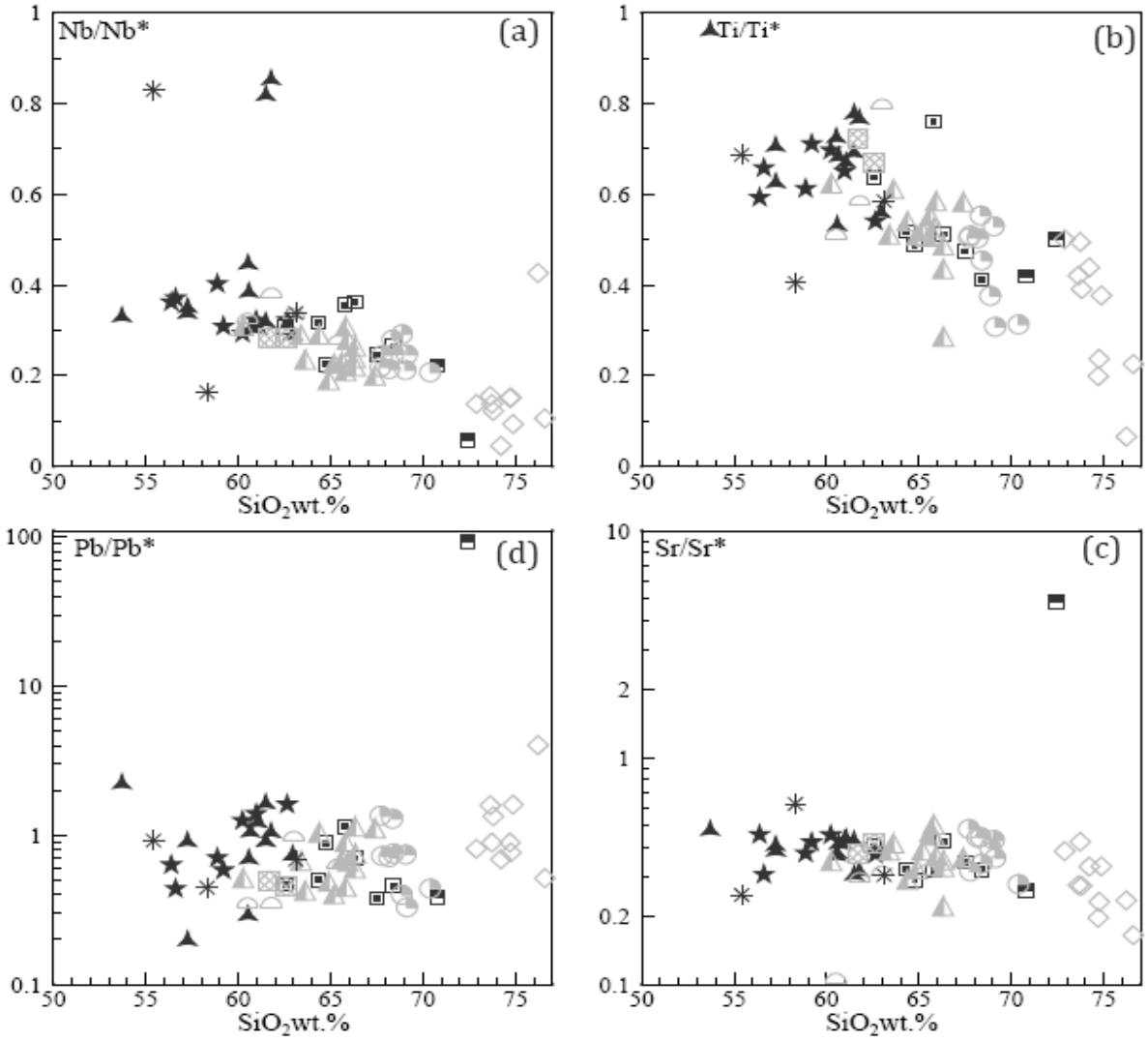

Figure 18. Variation of SiO_2 with magnitude of negative anomalies for selected trace elements of the Matok pluton granitoids. Symbols are the same as in Fig. 11.

The magnitude of the Ti negative anomaly shows a general increase with SiO_2. The px-diorites1, px-diorites2, and px-free diorites show almost similar and the smallest negative Ti anomaly. The anomaly then increases progressively through to rocks of granitic composition (Fig. 18b). To some extent the px-granodiorites and px-free granodiorites have overlapping Ti/Ti* values.

The elements chosen to interpolate the Sr* value are P and Pr. The P abundance of the Matok pluton granitoids decreases with increasing SiO_2 (like Sr) and Pr is non-correlative with SiO_2 without distinguishing between px-bearing and px-free granitoids. The use of P and Pr then yields a fairly constant Sr/Sr* with increasing SiO_2 for all the Matok pluton granitoids. The exception is a px-granite with >71 wt.% SiO_2 which has a positive Sr anomaly (Fig. 18c). Pb/Pb*also shows a confined range with increasing SiO_2 and ranges from slightly positive (Pb/Pb* >1) to slightly negative (Fig. 18d). Again, there is no systematic distinction between both px-bearing and px-free granitoids.

Inter-trace element relationships: Negative anomalies of the HFSE on primitive mantle normalised diagrams have popularly been suggested to signify subduction related magmatism because in such a setting the relatively more immobile HFSE are preferentially retained in the source while the more mobile LILE are mobilised by fluids (e.g. Pearce et al., 2000; Best and Christiansen, 2001; Martin et al., 2005; Lobach-Zhuchenko et al., 2005; Barry et al., 2006; Wen et al., 2008). If the observed negative HFSE anomalies in the Matok pluton granitoids were acquired in one petrogenetic process (e.g. were achieved at a partial melting event) then there is more chance that they (HFSE) will correlate among themselves as well as with the other incompatible trace elements. If the negative anomalies were acquired through different petrogenetic processes, there is likely to be no correlation between the concentrations of HFSE and other incompatible trace elements. In order to test for any evidence of decoupling of the HFSE from the LILE and/or REE, inter-element plots of selected HFSE, REE and the LILE are illustrated in Figures 19 and 20. Although there is a notable scatter, both Zr and Nb generally show positive correlation with La and the correlation does not necessarily distinguish between the px-bearing and px-free granitoids (Fig. 19a, b). The correlation is consistent with both La and the HFSE concentrations having been influenced by a similar petrogenetic process. Contrarily, variation of Th with La distinguishes between px-bearing and px-free granitoids. Two fields in which one is defined by px-bearing granitoids and the other by px-free granitoids can be defined. Even at the same La concentrations the px-free granitoids have higher Th concentrations than px-bearing granitoids. Both groups of granitoids however tend to define similar positively sloping fields (Fig. 19c). The px-granites are exceptions and do not fall within

the field defined by all other px-bearing granitoids because they have higher Th concentrations like the px-free granitoids.

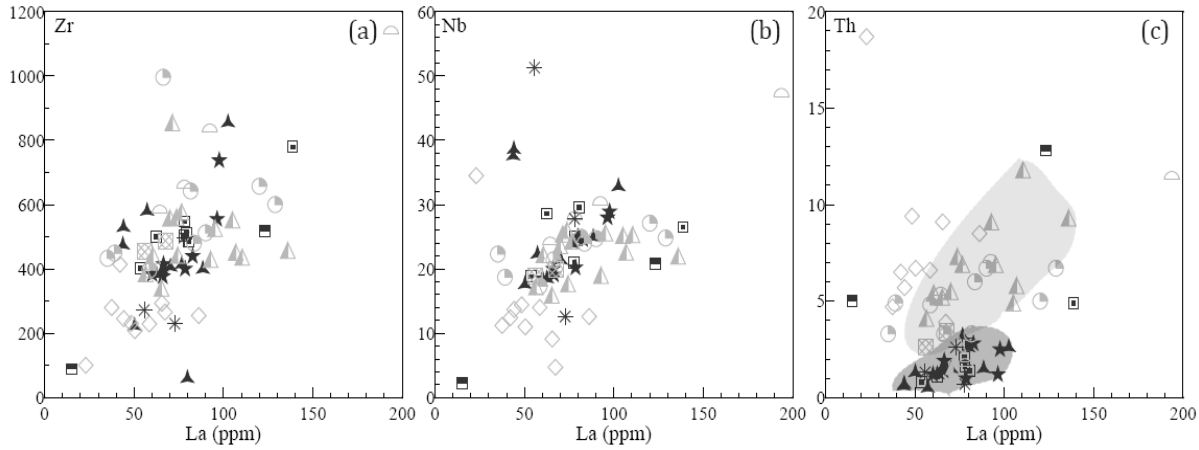

Figure 19. Variation of Zr, Nb and Th with La (in ppm) for the Matok pluton granitoids. Symbols are the same as in Fig. 11.

Px-free granitoids have higher Th and Rb concentrations (relative to the px-bearing granitoids), but there is no correlation between Th and Rb among all the Matok pluton granitoids (Fig. 20a). On the other hand, the variation of Ba with both Zr and Nb can be constrained within their respective fields without distinguishing px-free from px-bearing granitoids (Fig. 20b, c). Because Sr shows a compatible behaviour in the Matok pluton granitoids (Fig. 14a), the relationship between Sr and Nb distinguishes between px-bearing and px-free granitoids, where at similar Nb concentrations, the former have higher Sr concentrations than the latter (Fig. 20d). Similarly, due to the compatible behaviour of Sr, the relationship between Sr and La can be classified into two fields occupied each by px-bearing and px-free granitoids. The field occupied by px-bearing granitoids shows a positively correlating relationship while the px-free granitoids have confined Sr abundance with increasing La (Fig. 20e). As usual, the px-free granites with >71 wt.% SiO_2 plot off the trend of all other granitoids and define their own field.

Two trends of the negatively correlating Rb and La can be constructed where one field is defined by the px-bearing granitoids and the other by px-free granitoids. The px-free granitoids have higher Rb at a given La concentration (Fig. 20f). With the exception of a few outliers, a constrained field of positive correlation between Ba and La can be classified for the Matok pluton granitoids (Fig. 20g). There is no distinction between px-bearing and px-free granitoids in this regard. With the exception of granites with >71 wt.% SiO_2, the relation between Th and Sr shows restricted Th concentrations with increasing Sr for the px-bearing granitoids but an increasing Th at a constrained Sr concentrations for the px-free granitoids. The relative abundance of these two elements raises a question about the effect of a combined role of fractionation and assimilation (Fig. 20h).

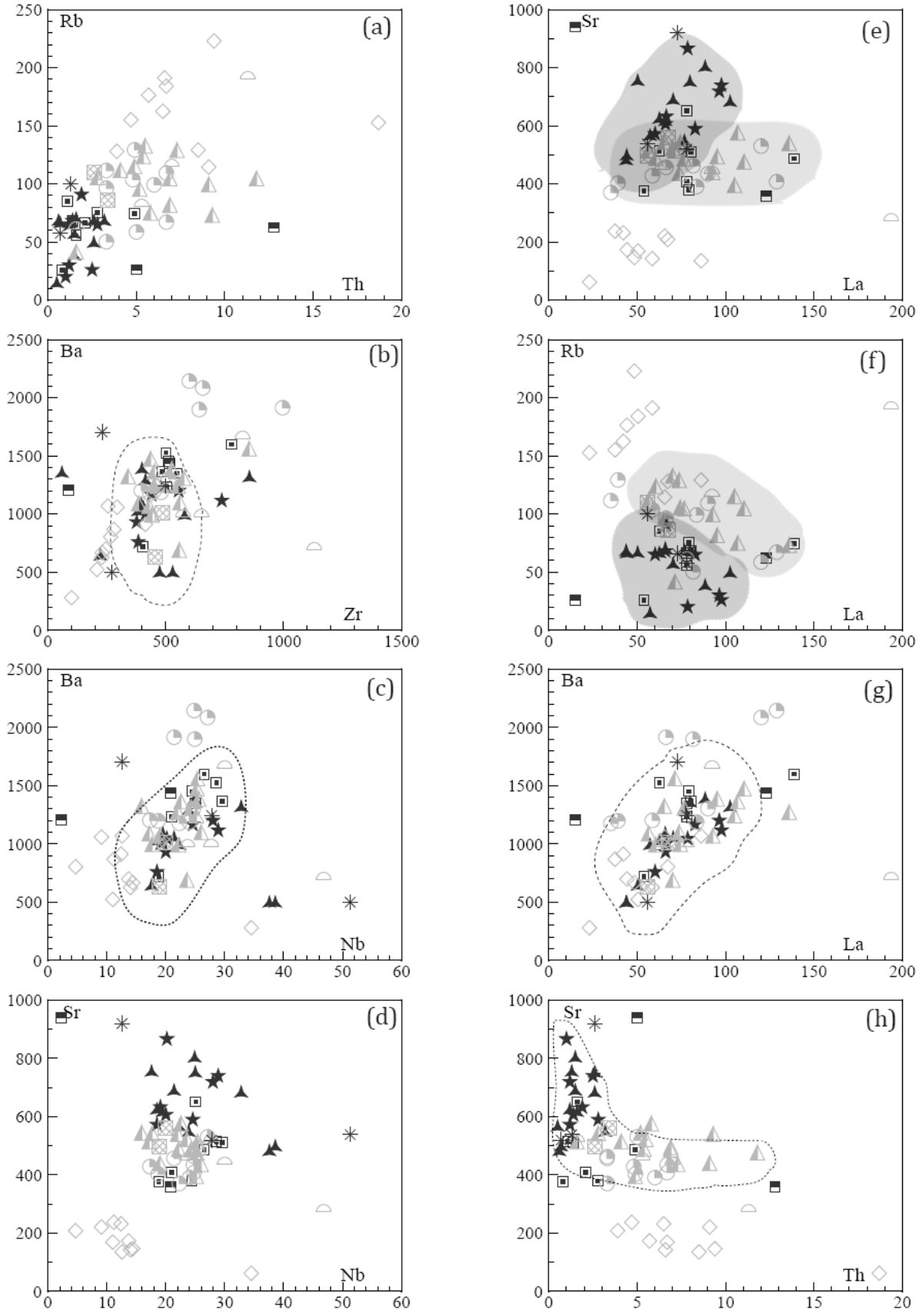

Figure 20. Variations between the selected HFSE, LILE and REE (in ppm) for the Matok pluton granitoids. Symbols are the same as in Fig. 11.

Trace element ratios: A more robust evaluation of HFSE, REE and LILE would involve their ratios because more often their ratios cannot be changed by magmatic processes (e.g. Hofmann, 1997; Condie, 2005). A further assessment of the distribution of trace elements in the Matok pluton granitoids will accordingly now be performed on the basis of trace element ratios versus SiO_2. Representatives of HREE/HREE, LREE/LREE, LREE/HREE, HFSE/HFSE, LILE/HFSE, LILE/LILE ratios will in this regard be tested to determine if there is any regular pattern with SiO_2 or similarity between px-bearing and px-free granitoids.

The Yb/Lu ratio for all the rock types, excluding granites with >71wt.% SiO_2 is restricted to 6.2 - 7.5 (Fig. 21a), suggesting a similar partial melting process for the granitoids. This is compatible with the observation that the HREE primitive mantle normalised patterns are similar for all the rock types. There is a considerable scatter in the La/Ce ratio versus SiO_2, though a positively correlating field can be defined for most of the granitoids, with both px-bearing and px-free granitoids inclusive (see field in Fig. 21b). The px-bearing granitoids in this relationship have lower La/Ce ratio. Although Ce is unlikely to exist in a tetravalent state in magmatic processes Ce^{4+} is known to occur in some rocks found in tropical weathering environments (Schreiber et al., 1980; Class and le Roex, 2005). The considerable scatter in Figure 21b may therefore be due to Ce which may have been relatively more oxided in the magmas of px-free.

The La/Yb is generally restricted to between 12 and 23 with increasing SiO_2 for many rocks excluding granites with >71 wt.% SiO_2 (Fig. 21c). Since both Yb/Lu and La/Yb ratios are broadly similar for all granitoids (except granites with >71 wt.% SiO_2), it is reiterated that the scatter in the La/Ce (Fig. 21b) has to do with Ce and not La concentrations. The broadly constant La/Yb for all the Matok pluton granitoids suggests the absence of fractionation of a mineral which would fractionate the LREE from the HREE.

The ratio of two HFSE (Zr/Nb) is generally restricted (with a couple of outliers) within a wide range of SiO_2 and does not distinguish between px-bearing and px-free granitoids, excluding granites with >71 wt.% SiO_2 (Fig. 21d). The somewhat confined Zr/Nb ratio is consistent with non-decoupling of Zr and Nb in the Matok pluton granitoids. Similarly, the Rb/Zr ratio is by far restricted for all the rock types excluding granites with >71 wt.% SiO_2 which show extreme Rb/Zr ratios (Fig. 21e). The Rb/Cs ratio (LILE/LILE) shows a mild increase with SiO_2 for the px-bearing granitoids and is generally constant for the px-free granitoids with ≤71 wt.% SiO_2 (Fig. 21e).

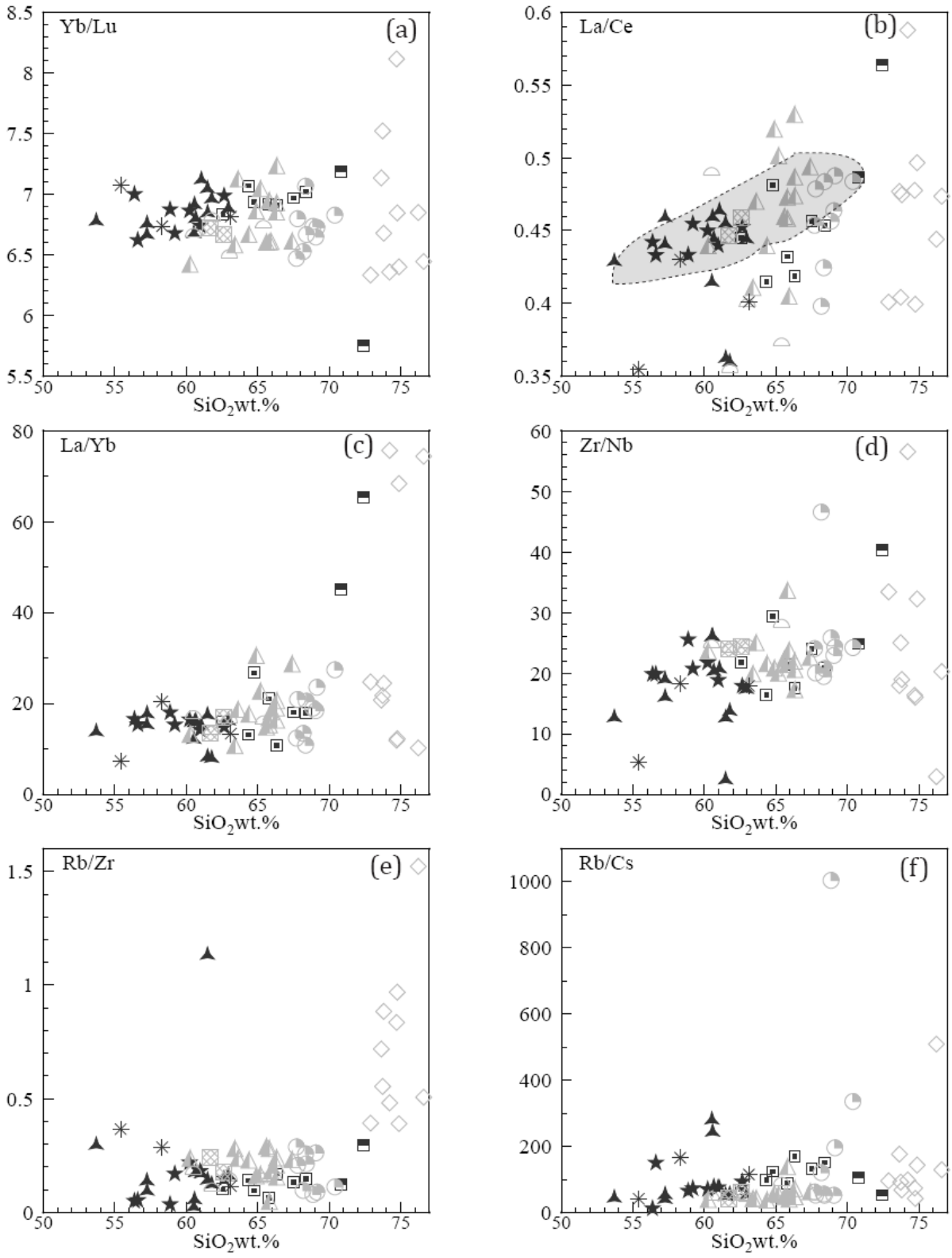

Figure 21. Selected trace element ratios variation with SiO_2 for the Matok pluton granitoids. Symbols are the same as in Fig. 11

Despite Th and U showing preferentially higher concentrations in the px-free granitoids both Th and U still show negative anomalies for px-free granitoids, on the primitive mantle normalised diagrams (Fig. 17). Nb and Ta absolute concentrations on the other hand do not

distinguish between px-bearing and px-free granitoids and they also show negative anomalies on primitive mantle normalised diagram. In order to assess if Th (and U) can be regarded to have been decoupled from Nb and Ta during magmatic evolution, ratios involving Ta (or Nb) and Th (or U) can be used to assess such a possibility, and in this case plots of two ratios will be illustrated as opposed to one ratio versus SiO_2 (Fig. 22).

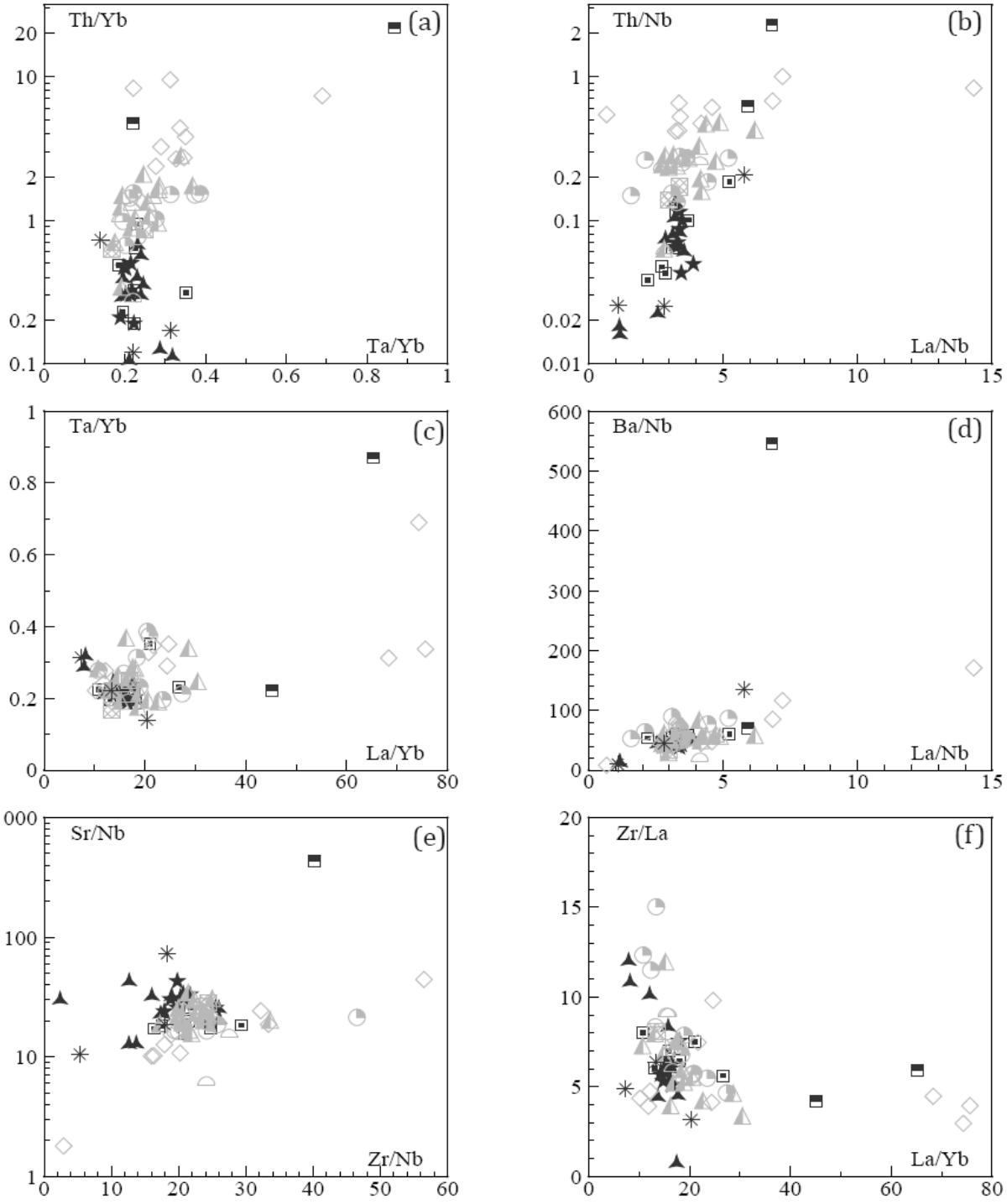

Figure 22. Variation of selected trace element ratios for the Matok pluton granitoids. Symbols are the same as in Fig. 11.

The Ta/Yb ratio is relatively constant for both px-bearing and px-free granitoids at an increasing Th/Yb ratio, with the px-free granitoids showing higher Th/Yb ratio due to their higher Th concentrations (Fig. 22a). The exceptions are the granites with >71 wt.% SiO_2 (including px-granites) which tend to have slightly higher Ta/Yb ratio and therefore plot slightly off the trend. Although the granites with >71 wt.% SiO_2 do not have the highest Th concentrations (compared to all other px-free granitoids; Fig. 14e), they have the highest Th/Yb ratio (Fig. 22a). Similar to the Ta/Yb versus Th/Yb relationship, the La/Nb versus Th/Nb relationship shows a sharp increase of the Th/Nb at a generally constrained La/Nb. However, a few px-free granitoids including the ones with ≤71 wt.% SiO_2 do plot off the defined trend (Fig. 22b). The overall consistency in the Ta/Yb versus Th/Yb and La/Nb versus Th/Nb ratio plots for the majority of the granitoids suggests that the use of the elements Ta, Yb, La and Nb in petrogenetic modelling may be reliable. This is providing the partitioning coefficients of trace elements and minerals used for petrogenetic modelling can be assumed to have been constant through out the magmatic process.

Comparison of a LREE/HREE ratio with HFSE/HREE ratio (La/Yb versus Ta/Yb) shows a tightly constricted field for all the rock types, excluding a few of granites with >71 wt.% SiO_2 (Fig. 22c). This relationship again suggests a non-decoupling behaviour between the HFSE and REE. Compatible with the restrictive La/Yb versus Ta/Yb plot is the Ba/Nb versus La/Nb relationship which also shows clustering of all the rock types (Fig. 22d). The Zr/Nb versus Sr/Nb plot also shows a restricted and clustering of nearly all the rock types (Fig. 22e). This further suggests that the relative abundances of Zr with Nb and Sr with Nb were influenced by a single petrogenetic process. Although not as tightly clustered as in Figure 22c-e, the Zr/La versus La/Yb ratio plot also shows a generally confined field for the majority of the Matok pluton granitoids (Fig. 22f). Again, supporting the fact that the ratio of incompatible trace elements in the Matok pluton granitoids (except granites with >71 wt.% SiO_2) does not, generally, distinguish between the presence of high temperature mineral assemblage and low temperature assemblages (px-bearing versus px-free granitoids).

6.1. The effects of subsolidus alteration

In the petrography section, it was stated that the epidote microlite inclusions in feldspar signify an impact of late-stage fluids associated with magmas of the px-free granitoids which were fluxed into some of the earlier crystallised px-free granitoids. The suggested influx of late stage fluids in the px-free granitoids may have effected the Sr and Eu concentrations. Baring in mind that Sr shows compatible behaviour when plotted against SiO_2 (Fig. 14a), the requirement

is that if such fluids leached away Sr, then it may be expected that the px-free granitoids show a relatively more pronounced Sr negative anomaly, providing both px-bearing and px-free rocks were cogenetic. However, when considering the fact that both the px-free and px-bearing granitoids at the same SiO_2 concentrations have similar magnitude of the Sr anomalies (Fig. 18c), it is tempting to believe that such anomalies did not result from the 'epidotisation' process, or any other subsolidus processes. And thus the establishment of the secondary epidote, as suggested, owed its existence to the fluids that were part of a partial melt that had left the source region at the same time as the bulk of the pluton which had already crystallised. Therefore the negative Sr anomaly is simply a manifestation of magmatic processes and by implication the HFSE negative anomalies are not due to subsolidus processes.

The notion that the HFSE are, relative to the LILE usually preferentially retained in the source in processes that involve fluids (e.g. Pearce et al., 2000; Best and Christiansen, 2001; Martin et al., 2005; Lobach-Zhuchenko et al., 2005; Barry et al., 2006; Wen et al., 2008) would tend to produce well correlated trends between these two groups of elements if the observed characteristics resemble that of a single process in a magmatic environment. It is rational that rocks that are related by a common source would ideally show sub-parallel normalised trace element patterns providing such rocks were 'immune' to contamination and/or subsolidus alteration processes. In the event of the normalised trace elements showing non-parallel patterns, such behaviour may be attributed to the effects of sub-solidus processes or mixing of magmas from different sources (e.g. Lahaye et al., 1995). The rocks of the Matok pluton, by far, produce sub-parallel primitive mantle normalised patterns (Figs. 16, 17).

Meteoric waters are capable of metasomatising minerals and leading to the formation of more hydrous phases (Liu, 2002). The elements Ti, Zr, Al and P are relatively immobile in greenschist facies metamorphism while Ca, Ba, Rb, Sr, Eu and Cr may be mobile (Bialek et al., 1999). In the majority of the Matok pluton granitoids with a gneiss fabric, the development of the gneiss seemingly did not alter the bulk rock composition. The geochemical analyses evidence that loss on ignition (LOI) obtained is in accord with petrographic observations whereby the most altered samples have the highest LOI. The LOI obtained ranges from 0.2 to 2.1 wt.%. Six px-bearing granitoids, three px-free granitoids, one mafic enclave in a px-granitoid and all the mafic enclaves in px-free granitoids have LOI of greater than 1 wt.% while the rest of the rocks have less than or equal to 1 wt.% LOI. In order to asses whether subsolidus processes, as based on the loss on ignition, had an impact on the trace elements, a graphic illustration of LOI versus selected trace elements is shown in Figure 23. On the left of the dotted line are granitoids which had less than 1 wt.% LOI and on the right are the granitoids which had greater than 1 wt.% LOI. From this illustration it can be seen that except for two px-diorties1 and a px-

diorite2 in which the selected trace elements correlate with LOI, all other granitoids do not show any correlation between the LOI and the trace elements. And so, if it can be assumed that LOI can be used as a measure of how geochemical characteristics of the Matok pluton granitoids were altered by subsolidus processes, it is realistic to assume that such processes did not have a significant impact on the overall geochemistry.

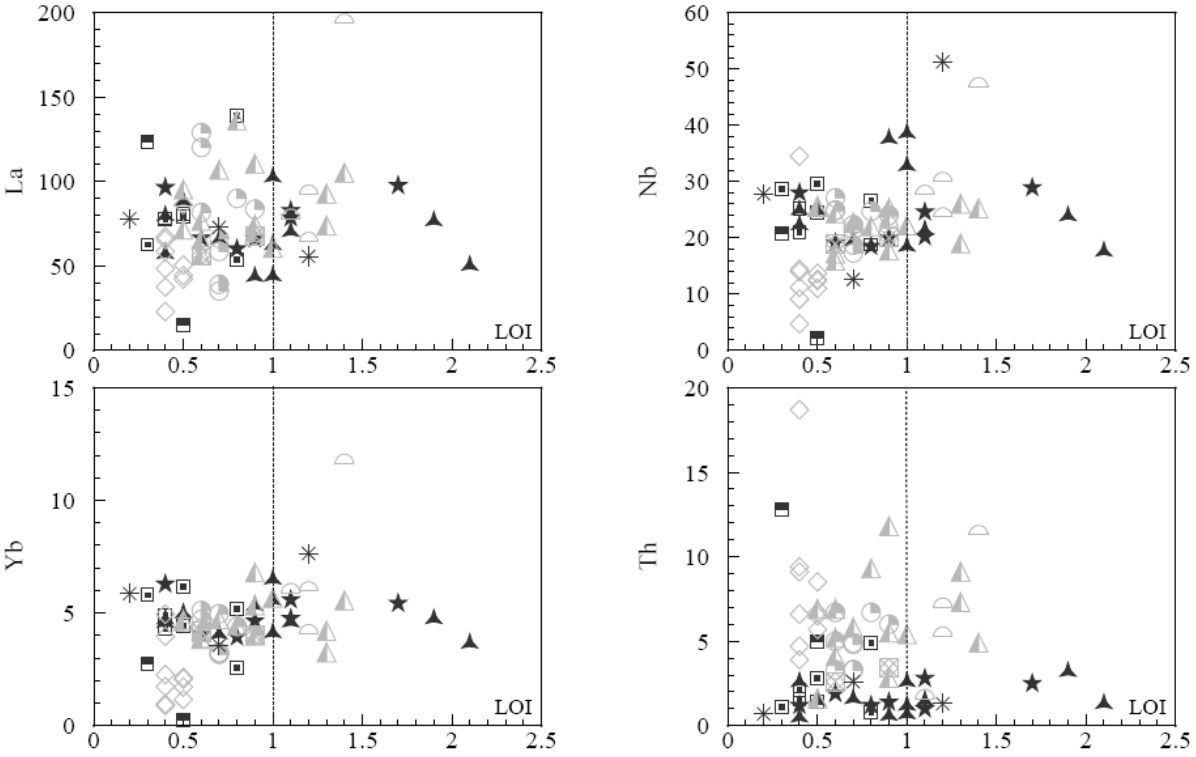

Figure 23. Variation of selected trace elements (in ppm) with loss on ignition (LOI in wt.%) for the Matok pluton granitoids. Symbols are the same as in Fig. 11.

Primitive-mantle-normalised trace element patterns for samples that show subsolidus alteration from petrographic studies and in addition have greater than 1 wt.% LOI are shown in Figure 24. One feature that would suggest the impact of subsolidus alteration is the Pb anomaly which ranges from a slight positive to a slight negative (Figs. 17, 24). However, considering the fact that, even among the unaltered rocks, the Pb anomaly ranges from slightly positive to slightly negative, it is more compelling to suggest that the Pb anomalies were not entirely due to subsolidus effects. Figure 24 also shows that, regardless of the LOI, the px-bearing granitoids still have lower negative Ti and Sr anomalies and deeper negative Th and U anomalies than the px-bearing granitoids; just as is the case with unaltered rocks. Additionally, the similar magnitudes of anomalies of Nb and Ta for both altered and unaltered granitoids support the role of magmatic processes as opposed to subsolidus processes. It is undeniable that subsolidus processes may have impacted on these anomalies, but considering the fact that such anomalies

are also characteristic of unaltered granitoids, it is compelling to suggest that the anomalies are inherent of magmatic processes.

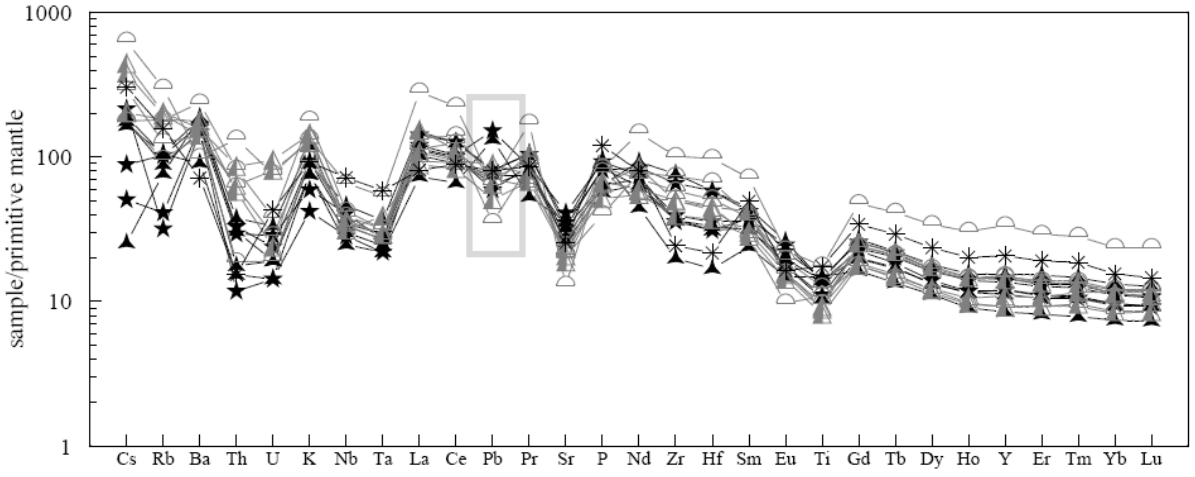

Figure 24. Primitive mantle normalised diagrams for samples with >1wt.% LOI (loss on ignition) for the Matok pluton granitoids. Normalising values taken from Sun and McDonough (1989). Symbols are the same as in Fig. 11.

7. PETROGENESIS

Field relations in the Matok pluton suggest at least two episodes of magmatic injection. The first episode comprised both px-bearing and px-free granitoids, though only px-bearing granitoids were sampled for this study. The second episode also comprised both px-bearing and px-free granitoids and representatives of each suite were sampled. Petrography reveals the existence of magmatic hornblende in both px-bearing and px-free granitoids and its abundance is not necessarily different between the px-bearing and px-free granitoids with ≤71 wt.% SiO_2. However, the px-free granites with >71 wt.% SiO_2 are virtually devoid of hornblende and magmatic epidote; raising the possibility of mineral fractionation to account for their existence. Plagioclase is more abundant and slightly calcic-rich in the px-bearing granitoids than in the px-free granitoids. Epidote and titanite which are only present in the px-free granitoids are known to be great repository minerals for incompatible trace elements (e.g. Deer et al., 1992; Lahaye et al., 1995; Best and Christiansen, 2001; Marks et al., 2008; Šarić et al., 2009), yet the distribution of the incompatible elements does not portray this feature across all the Matok pluton granitoids.

Mineral chemistry reveals the insignificance of differences in fO_2, as judged by the Fe^{3+}/Fe^{2+} ratio of ilmenite and hornblende in both px-bearing and px-free granitoids. The Ti content of biotite on the other hand clearly shows the influence of difference in temperature of crystallisation of biotite in the px-bearing versus that of px-free granitoids (section 4.3). These observations will be explained and evaluated in this chapter. This will be achieved by highlighting the geochemical similarities and differences between the px-bearing and px-free granitoids. The role of crystallisation and partial melting processes and the possibility of crustal contamination will be evaluated. Contamination in this case is viewed in the sense of country rock assimilation, as opposed to two magmas 'contaminating' each other.

7.1. Assessment of country rock assimilation

Regardless of the source, any magma ascending through the thick continental crust is likely to assimilate the crustal material through which it passes (Best and Christiansen, 2001). The resultant contamination will be a function of the rate of ascend of the magma ± temperature contrast between the magma and the country rock ± fluid budget of the intruding body itself (Best and Christiansen, 2001). Since plutonic rocks would not crystallise 'instantaneously', the extended residence time of magmas before the final stage of crystallisation may result in a

higher rate of contamination. A careful evaluation of geochemical data is thus needed to separate the effects of contamination from that of the 'true' source region.

By virtue of their high immobility, the HFSE and REE are generally immune to crustal contamination (Krzemińska, 2005). The readily mobile elements (LILE), on the other hand, are more prone to diffusion and an interchange of these elements between the Matok melts and the granulite-facies-induced melting must be considered. However, assuming an initially homogenised magma, it is unlikely that assimilation of country rock would produce uniform concentrations of contaminants in both px-bearing and px-free granitoids of the Matok pluton alike. Moreover, the fact that on primitive mantle normalised diagrams (Figs. 16, 17) both the px-bearing and px-free granitoids show similar patterns suggests that the relative abundances of LILE to HFSE and REE were not caused by assimilation of the country rock. However, the subtle differences both within and between the px-bearing and px-free granitoids, such as the observed Pb anomaly which ranges from a slight positive to a slight negative in both groups of granitoids suggests that upper crustal contamination may not be ruled out. Negative Pb anomalies on primitive mantle normalised diagrams may signify a mantle source while positive Pb anomalies are more of a crustal signature (Hoffmann, 1997). On the other hand, the continental crust is relatively enriched in Th, U and K because these elements were readily mobilised from the upper mantle as it contributed to the crustal production (Hofmann, 1997; le Roex et al., 2003; Weyer et al., 2003; Krzemińska, 2005), and, as such, the elevated concentrations of these elements in igneous rocks may indicate a continental crustal origin. The SMZ, like many other granulite terranes, is depleted in these heat producing elements (Th, U and K; Kramers et al., 2001). This depletion has, in many granulite terranes, been attributed to preferential mobilisation of these elements owing to partial melting related to the granulite facies metamorphism (Fyfe, 1973; Taylor and McLennan, 1997; Zhao, 2007). In the SMZ however, such low Th and U concentrations were not consequent upon the high grade metamorphism but are rather characteristic of the SMZ (Kramers et al., 2001).

The px-free granitoids of the Matok pluton have higher concentrations of K_2O, Th and U relative to the px-bearing granitoids. Even when the px-bearing rocks are of granitic composition, their K_2O is much lower than that of px-free granitoids and overlaps that of all other px-bearing granitoids. This therefore suggests that either the px-free granitoids come from different magmas or that the more hydrous nature of the px-free granitoids may have facilitated scavenging of K from the country rock. In order to assess whether the px-free granitoids of the Matok pluton have higher concentrations of Th, U and K, due to assimilation of country rock, concentrations of these elements in the Baviaanskloof Gneiss needs to be considered. Two samples of the Baviaanskloof Gneiss were sampled in this study. The average

Th and U concentrations of these samples are 2.3 and 0.5 ppm respectively. Kramers et al. (2001) have also obtained averages of 1.1ppm Th and 0.3ppm U for granulites of the SMZ. Considering the absolute concentrations of Th and U of the Matok pluton granitoids (Table1), assimilating nearly all of the px-bearing granitoids with 100% of the Baviaanskloof Gneiss would still produce less Th and U concentrations of these px-free granitoids. Moreover, despite having highest concentrations of Th and U, the px-free granitoids still show negative anomalies of Th and U when compared to elements with similar compatibility (Fig. 17). In a similar manner, the high K_2O concentrations of px-free granitoids cannot be explained by assimilating the Baviaanskloof Gneiss.

An alternative incorporation of the Baviaanskloof Gneiss in the Matok melts would have been in the form of partial melts derived from the gneiss itself. The partial melts should have had higher Th, U and K concentrations, relative to the unmelted gneiss. One possibility for the generally lower Th, U and K_2O concentration in the px-bearing granitoids is if they were derived by higher degrees of partial melting relative to the px-free granitoids, providing a similar source can be inferred upon. However, the higher degrees of partial melting should also manifest in the form of other incompatible trace elements (e.g. HFSE). Other than Th, U, K, Rb, Cs and Sr, absolute concentrations of all incompatible trace elements do not distinguish between px-bearing and px-free granitoids, placing much uncertainty on the concept of differing degrees of partial melting. The exceptions are, as usual, the granites with >71 wt.% SiO_2. These granites may have assimilated some country rock material.

7.2. Magmatic history

Assimilation of the Baviaanskloof Gneiss cannot account for the distinction between px-bearing and px-free granitoids in the Matok pluton. The remaining alternatives are differences in source composition ± fractional crystallisation ± variation in degrees of partial melting ± magma mixing (e.g. Barbey et al., 2008). Major element distributions of the Matok pluton granitoids have been shown to correlate well on Harker diagrams when SiO_2 is used as a differentiation index. This raises the possibility of crystal fractionation-controlled process. Also, considering the fact that some of the Matok granitoids are porphyritic while others are not, the possible role of crystal fractionation needs to be assessed.

The similarity in primitive-mantle normalised diagrams for all the rock types of the Matok pluton suggests some kinship. Even when the incompatible trace elements (except Th and U) are plotted against silica, no major difference is discernible, with the exceptions being the granites with >71 wt.% SiO_2.

7.2.1. Semi-quantitative modelling of crystal fractionation

It was stated that plagioclase is more abundant (and more calcic) in the px-bearing than in the px-free granitoids (section 4.2 and 4.3). To assess the possibility of plagioclase and pyroxene fractionation, variations of selected trace element ratios are shown in Figure 25. Mineral-melt partitioning coefficients used in the modelling are presented in Table 2. The equation used is $C_l = C_m \times F^{(D-1)}$. Where C_l is the concentration of an element in the residual melt, C_m is the concentration of the same element in the parental melt, F is melt fraction and D is the bulk distribution coefficient. The most primitive and least altered px-diorite1 sample (Mat 16) is chosen as a proxy for the composition of a parental magma. Sample Mat 28 (a px-diorite 2) is

Table 2. Partition coefficients (D) used for trace element modelling.

	Amp	Cpx	Opx	Magn	Ilmn	Tita	Zircon	Plag	Epidote	Apatite	Biotite	Rutile	Oliv	Kspar	Quartz
Cs	0.166	0.0026	0.047	0.001	0.025	0.3	4.4	0.087	0.0045	0.05	0.63	0.01	0.0001		0.22
Rb	0.055	0.01	0.047	0.001	0.025	0.5	4	0.068	0.0045	0.1	2.25	0.0076	0.0005	4.3	
Ba	0.046	0.006	0.047	0.001	0.018	1.5	4	1.016	0.408	0.45	6	0.0043	0.0005		
Th	0.055	0.104	0.13	0.02	0.09	0.16	62	0.095	156	23	0.01	0.2	0.02		
U	0.05	0.032	0.089	0.02	0.09	0.14	298	0.091	1.29	25	0.1	0.2	0.03		
K	0.333	0.0039	0.047	0.001	0.034	0.7	4	0.252	0.0045	0.2	3	0.005			
Nb	0.274	0.007	0.01	0.04	3	2.2	50	0.239	0.226	0.05	0.085	42.8	0.01		
Ta	0.477	0.028	0.126	0.04	2.7	6.55	50	0.053	0.226	0.05	0.107	68	0.02	0.03	0.04
La	0.319	0.028	0.0003	0.015	0.015	4.73	26.6	0.358	2.05	12	0.02	0.0057	0.00044	0.5	
Ce	0.56	0.059	0.0007	0.016	0.012	7.57	23.5	0.339	2.44	15	0.03	0.0065	0.0003		
Pb	0.175	0.022	0.047	0.022	0.0078	0.04	0.001	0.77	0.5	0.1	0.1	0.0154		3.76	
Pr	0.898	0.116	0.0014	0.018	0.011	9	20	0.316	2.86	17	0.008	0.0073			
Sr	0.389	0.032	0.047	0.022	0.0022	2.68	20	6.65	2	1.4	0.1	0.036	0.016		0.025
P	0.225	0.162	0.05	0.024	0.002	0.057	20	0.079	0.18	410	0.005	0.03		0.02	
Nd	1.32	0.115	0.0028	0.026	0.01	12.4	21.7	0.289	3.34	19	0.03	0.0082	0.0002		
Zr	0.417	0.125	0.031	0.12	2.3	1.92	130	0.078	0.1	16	0.023	3.7	0.003		
Hf	0.781	0.208	0.246	0.97	2.4	2.43	450	0.069	10	16	0.023	4.97	0.024	0.17	
Sm	2.09	0.259	0.0085	0.024	0.009	14	17.7	0.237	4.22	20	0.04	0.0954	0.00018	0.03	0.015
Eu	1.79	0.341	0.68	0.025	0.01	13.8	12.1	2.17	3.78	13	0.031	0.00037	0.0002	0.07	0.014
Ti	4.03	0.473	0.5	5	12.5	67	10	0.078	0.375	14	3.5	45	0.007	0.04	
Gd	2.53	0.422	0.02	0.018	0.011	11.9	15	0.192	4.67	20	0.04	0.0106	0.00025		
Tb	2.6	0.502	0.03	0.019	0.018	10	37.3	0.17	4.67	19	0.05	0.0111	0.000475	0.04	
Dy	2.55	0.57	0.043	0.018	0.02	8.27	60	0.15	4.5	18	0.06	0.0116	0.0007	0.018	0.056
Ho	2.41	0.616	0.06	0.018	0.035	5.5	120	0.132	4.18	16.8	0.08	0.0119	0.00122	2.6	
Y	2.47	0.603	0.054	0.018	0.037	5.42	80	0.138	4.3	17.5	0.07	0.0118	0.002	0.011	
Er	2.22	0.64	0.079	0.018	0.067	5.54	200	0.117	3.78	15.5	0.09	0.0122	0.00174		
Tm	2	0.644	0.101	0.018	0.102	4	300	0.104	3.36	14.2	0.1	0.0124	0.00348	0.05	
Yb	1.79	0.635	0.125	0.018	0.13	3.02	490	0.094	2.96	13	0.11	0.0126	0.00522		
Lu	1.59	0.617	0.149	0.018	0.19	2	632	0.085	2.59	10	0.12	0.0127	0.00852		

Most of the D values in this table are taken from Bédard (2006). Supplementary data are taken from Mahomed (1998) and Best and Christiansen (2001). Amp = amphibole, cpx=clinopyroxene, opx=orthopyroxene, Magn=magnetite, Ilmn-ilmenite, Tita=titanite, Plag=plagioclase, Oliv=olivine and Kspar=K feldspar.

also chosen as a representative of the second episode of intrusion to model the composition of the liquid that would descent from it.

Neither K nor Rb is compatible in plagioclase and pyroxene. A pyroxene and plagioclase fractionation-controlled process should as a result yield a near constant K/Rb ratio with increasing Rb. It is however clear that this is not the trend in the Matok pluton granitoids (Fig. 25a) and thus suggests the absence of mutual plagioclase and pyroxene fractionation. Likewise, the trajectory linking Sr and Th refute relation of the px-free granitoids to px-bearing granitoids by fractionation (Fig. 25b). A sharp decline of Sr concentrations at a confined Th for most of the px-bearing granitoids may however suggest the possibility of plagioclase fractionation among the px-bearing granitoids.

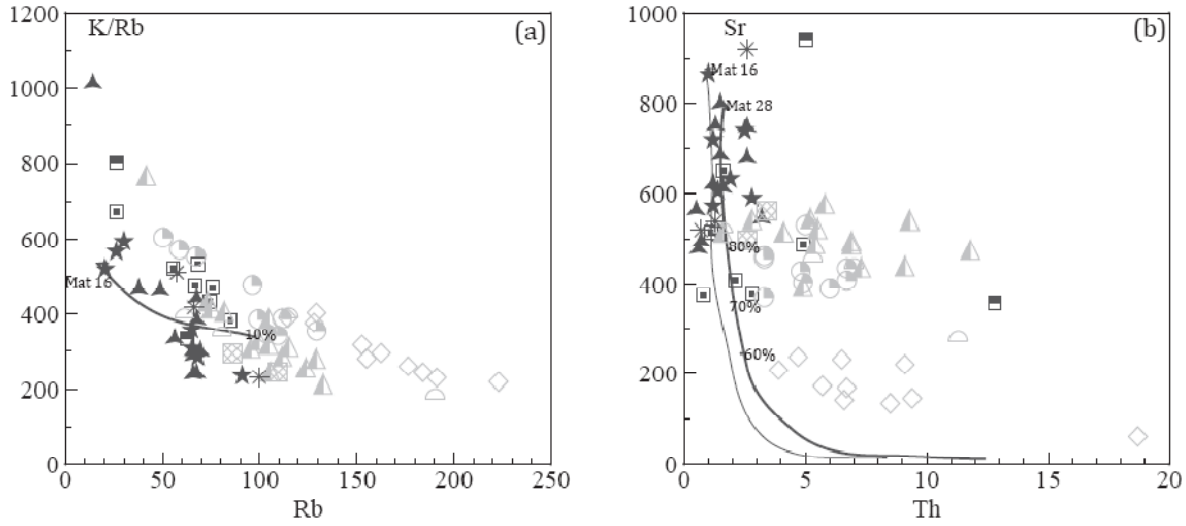

Figure 25. Variation of selected trace element ratio(s) for the Matok pluton granitoids. Fractionation trajectories that would be possible if the Matok granitoids were linked by crystal fractionation are illustrated. In (a) fractionation trajectory from the most primitive px-diorite1 (Mat 16), (b) two fractionation trajectories from the most primitive px-diorite1 (Mat 16) and the other from a px-diorite2 (Mat 28) are shown. Symbols are the same as in Fig. 11.

Yet again, if fractionation had to link the px-bearing and px-free granitoids then the normally incompatible trace elements which are compatible in pyroxene have to be higher and lower in the high temperature assemblage (px-bearing) and low temperature assemblage (px-free) respectively. The broadly similar REE (and the HFSE) concentrations between the px-bearing and px-free granitoids (excluding granites with >71wt. % SiO_2) suggests that pyroxene fractionation cannot be held accountable for the co-existence of anhydrous high temperature assemblages and hydrous low temperature assemblages (px-bearing and px-free granitoids, respectively) in the Matok pluton. Furthermore, it is well accepted that rocks related by fractional crystallisation-only process tend to produce boundary-bound parallel trends (Ferré et al., 1998). This is not the case in the medium-K calc-alkaline – High-K calc-alkaline plot (Fig. 11g).

Both magnetite and ilmenite are more abundant in the px-bearing than in the px-free granitoids (section 4.2), and the possibility of their fractionation needs to be evaluated as well.

Magnetite in the Matok pluton granitoids is Ti-poor. This implies that if fractionation could relate the px-bearing to the px-free granitoids, the only phase capable of exacerbating the observed Ti negative anomalies in the px-free granitoids (Fig. 17) is ilmenite. Titanite is unlikely to have done so, as it is found only in the px-free granitoids. However, the universal presence of Ti, Nb and Ta negative anomalies in both px-bearing and px-free granitoids (Fig. 17) suggests that such a characteristic is unlikely to relate the two rock suites by fractionation.

If it can be assumed that a hypothetical parental magma which had no Nb negative anomaly (Nb/Nb*= 1) produced the Matok pluton granitoids, the required amount of ilmenite fractionation ranges from about 30 to 40% for most of the Matok pluton granitoids (Figure 26). This required ilmenite is unreasonably high and as a result ilmenite was not a significant phase in the source nor can its fractionation link the px-bearing to px-free granitoids. By implication the negative anomalies of Nb (and Ta) were rather inherited from the source. Rutile is another mineral which may be effective in producing the negative anomalies of Nb and Ti via fractionation. However, considering the fact there generally is no rutile in the Matok pluton granitoids, it becomes rational to suggest that rutile fractionation cannot be accountable for the Nb and Ta negative anomalies.

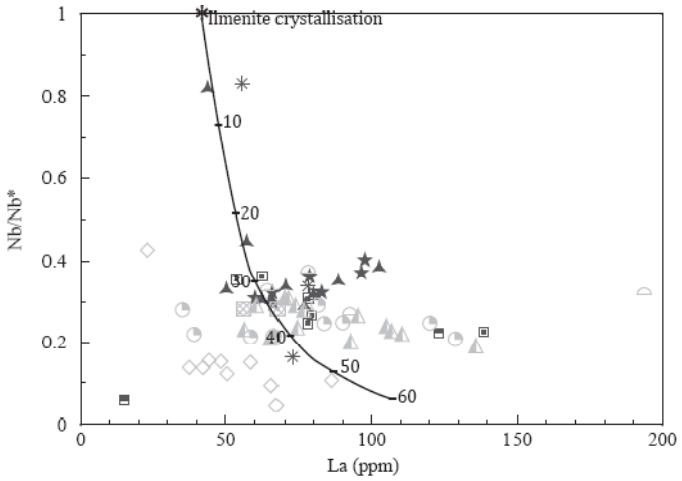

Figure 26. Variation of Nb/Nb* with La for the Matok granitoids. Also shown on the diagram is the ilmenite fractionation trajectory from a hypothetical parental magma that had no Nb anomaly relative to elements with similar compatibility. The numbers along the trajectory represent the required percentage of ilmenite fractionation in order to account for the Nb anomaly on the y axis. Symbols are the same as in Fig. 11.

Unlike Nb and Ta, the two other HFSE; Zr and Hf, do not produce negative anomalies on primitive mantle normalised diagrams (Fig. 17). Zircon is by far the major Zr and Hf hosting mineral. However, clinopyroxene has been observed to host a significant amount of these two elements as well (up to 50-90% of total Zr; Bodinier et al., 1996; Bedini and Bodinier, 1999; Kalfoun et al., 2002; Pfänder et al., 2007). The Matok pluton granitoids are oversaturated with Zr (Fig. 13), and zircon inheritance has been ruled out to account for such high Zr

concentrations (chapter 6). This suggests that a significant amount of Zr and Hf was hosted by clinopyroxene (in the source). Again, if the Matok granitoids were related by pyroxene fractionation, the Zr (and Hf) concentrations would have had to be different between the px-bearing and px-free granitoids. But from Figures 13a, 17and 19a, there is clearly no major difference between px-bearing and px-free granitoids. This again supports the proposal that the two suites of granitoids are not related by differentiation processes.

It was stated in chapter four that all the px-free granitoids with >71 wt.% SiO_2 are effectively devoid of hornblende. Hornblende is stoichometrically poor in Al_2O_3, and as such, its fractionation may promote slightly peraluminous residual melts (e.g. Cawthorn and O'Hara, 1976; Clarke 1992; Bonin et al., 1998). The px-free granitoids with >71 wt.% SiO_2 are slightly peraluminous (Fig. 11h), and whether such characteristic were achieved via hornblende fractionation need to be assessed. The HREE are more compatible in hornblende than the LREE and hornblende fractionation tends to produce concave-upward HREE on primitive mantle normalised diagrams (e.g. Best and Christiansen, 2001). Hornblende fractionation would thus produce higher LREE/HREE ratios for the most differentiated rocks relative to their parental magma(s). A plot of La versus La/Yb ratio is shown in Figure 27a.

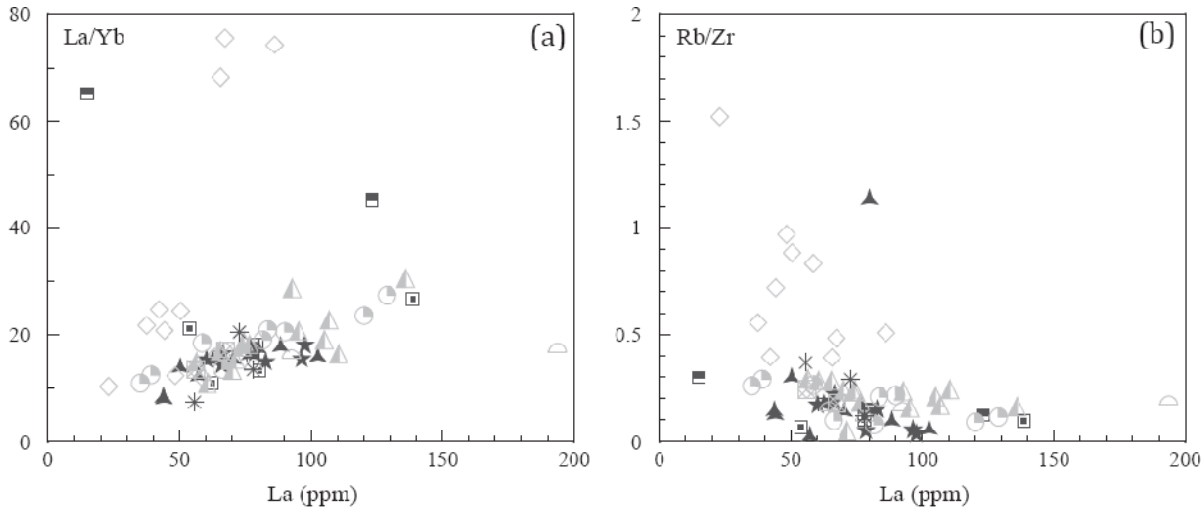

Figure 27. Variation of La with La/Yb and Rb/Zr ratios for the Matok pluton granitoids. Symbols are the same as in Fig. 11.

It is evident from Figure 27a that a couple (not all) of px-free granitoids with >71 wt.% SiO_2 do have the highest La/Yb ratio, and therefore possibly developed via hornblende fractionation. A px-granite also has one of the highest La/Yb (Fig. 27a) and concave upward HREE (Fig. 16), suggesting hornblende fractionation to its fate. This same sample however has, on primitive-mantle normalised diagram, a positive Sr anomaly (Fig. 17) unlike all other Matok pluton granitoids. This positive Sr anomaly on the other hand refutes plagioclase fractionation. Although a separate magma source for the px-free granites with >71 wt.% SiO_2 cannot be ruled

out, their existence through hornblende fractionation is also feasible. Additionally, their magmas may have been contaminated with the country rock. The possibility of contamination is suggested by their highest Rb concentrations (Fig. 14b) as well highest Rb/Zr ratios (Fig. 27b). Rb is a very mobile element compared to Zr, and therefore may have been readily scavenged from the assimilant. The higher La/Yb ratios for the px-granites (Fig. 27a) also support hornblende fractionation to their fate, but have their lowest Rb/Zr ratios (Fig. 27b) on the other hand suggests lower contamination of their magmas.

7.2.2. Evaluation of magma mixing

It is argued that the px-free granitoids (excluding granites with > 71 wt.% SiO_2) are not related to the px-bearing granitoids by fractional crystallisation. An alternative option to explain the co-existence of px-bearing and px-free granitoids in the Matok pluton is magma mixing of batches that may have different origins. There is enough field evidence in the Matok pluton to suggest magma mingling. This mingling occurred both within and between batches of each of the px-bearing and px-free granitoid suites (Fig. 3c-f). In addition, the rapakivi texture, which may be indicative magma mixing (e.g. Klimm et al., 2007) is common in some of the Matok pluton granitoids. Furthermore, the crossing of compositional boundaries such as shown in Figure 11g may perhaps be explained by the magma mixing concept. In order to evaluate the role of mixing in the Matok pluton, the magma mixing equation of Langmuir et al. (1978) has been applied. Because the granites with >71 wt.% SiO_2 may have had both contribution from partial melting of country rocks and hornblende fractionation (see above), they are not included in the mixing models as end-members.

Mixing test suggests a variety of possible mixing between different samples, and not necessarily between the most mafic px-bearing granitoid and the most evolved px-free granitoid. On the Rb/Y versus Rb mixing curve (Fig. 28a), the two samples Mat 26 (a px-diorite2) and Mat 4 (a px-free granodiorite) plot as end-members from which nearly all (excluding granites with >71 wt.% SiO_2) the granitoids plot tightly along the mixing line. The Sr/Rb versus Th mixing model plot (Fig. 28b) shows sample Mat 16 not 'connecting' with the rest of the Matok pluton granitoids, but rather sample Mat 26 (a px-diorite 2) and Mat 7 (a px-free granodiorite) (bold trajectory) producing a mixing line along which a significant number of granitoids plot. This relatively wide range of possible end-members suggests the possibility of mixing of diverse magma batches which perhaps had closely related composition.

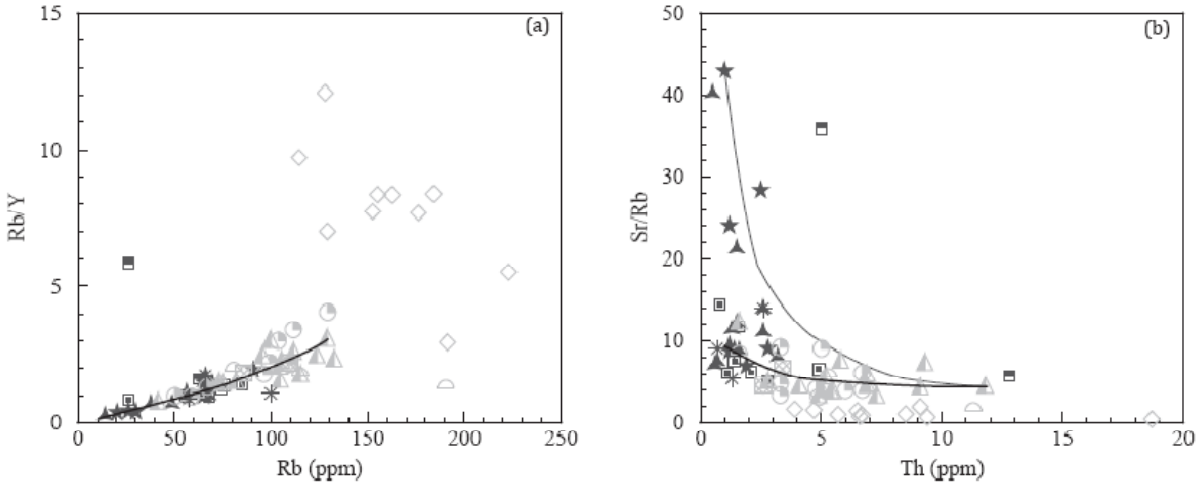

Figure 28. Variation of selected element ratio(s) from the Matok pluton granitoids. In (a) the trajectory represents a mixing curve (after Langmuir et al., 1978) obtainable if a px-diorite2 (Mat 26) mixed with a px-free granodiorite (Mat 4). Top trajectory in (b) represents the mixing line between most primitive px-diorite1 (Mat 16) with the most evolved px-free granodiorite (Mat 30), and the bottom trajectory represents the possibility of mixing a px-diorite*2* (Mat 29) with sample Mat 30.

Discussion:

Contamination of the Matok melts by the country rock (Baviaanskloof Gneiss) seems to have been negligible in all the granitoids except the granites with >71 wt.% SiO_2. The incompatible trace-element patterns refute the connection between px-bearing and px-free granitoids by crystal fractionation of both plagioclase and the mafic minerals (pyroxene, hornblende, ilmenite and magnetite). The absence of pyroxene in the px-free granitoids was therefore not due to fractionation of anhydrous mafic minerals. Plagioclase fractionation may however not be ruled out but only to link the more differentiated px-bearing granitoids with the more mafic px-bearing granitoids.

The role of magma mixing is suggested both in the field and in the geochemistry (Figs. 3, 28). Given that overall, the incompatible trace element signature does not make a distinction between the px-bearing and px-free granitoids (except for granites with >71wt.% SiO_2) the requirement is that the mixed magmas were genetically related. Because the magmas of the px-free granitoids must have been hydrous, the other requirement is that magma mixing was as inefficient process so that magmas of the px-bearing granitoids were not considerably hydrated; pyroxene would possibly have reacted to biotite and hornblende under significantly hydrous conditions. One option is that mixing occurred in the magma chamber which was compositional zoned (e.g. de Silva and Wolff, 1995). The non-distinguishing (between the px-bearing and px-free granitoids) incompatible trace-elements necessitates that such zonation should have occurred subsequent to melts segregating from the source. An alternative is that there were at

least two genetically related magma chambers; one for the px-bearing granitoids and the other for the px-free granitoid magmas and mixing occurred at the level of emplacement.

7.3. Partial melting and source characteristics

Although the incompatible trace element patterns are broadly similar in both px-bearing and px-free granitoids, the latter are generally more differentiated (high SiO_2, low MgO) than the former. One possible solution to explain the existence of the px-free granitoids is by means of differentiation from an alternative parental rock, rather than from the px-bearing granitoids. However, the similarity in the REE, HFSE and some LILE for all the Matok pluton granitoids (excluding granites with >71 wt.% SiO_2) suggests that both px-bearing and px-free granitoids are genetically related. This genetic link must apply effectively well to justify both the episodic nature of intrusions as well as px-bearing versus px-free granitoids. If the episodic nature of intrusions can be accounted for by episodic partial melting, then a difference in the concentrations of incompatible trace element may be expected in the different episodes. This is essential especially if the degree of partial melting between the episodes were different, providing a common source is inferred upon. A similar degree of partial melting in both melting events on the other hand would necessitate that the latter intrusion has relatively lower concentrations of incompatible trace elements as the first melting episode may have depleted the source in these elements. Because of the similarity in the incompatible trace elements, it is rather suggested that both episodes of intrusions in the Matok pluton are manifestation of a single partial melting event. This suggestion reconciles with the proposal by Bohlender et al. (1992) that granitoids of the second episode intruded just after the first episode. A very brief time gap between the recurring magmatic injections in turn attests to magma storage in the chamber after the first intrusion (e.g. Lobach-Zhuchenko et al., 2005; Fraga et al., 2009; Pons et al., 2006; Barbey et al., 2008). The fact that the first intrusion granitoids also have their feldspar phenocrysts aligned parallel to the trend of the Limpopo Belt support, also, a synchronous emplacement with the tectonic activity. The gneissic fabric may then have occurred shortly after emplacement due to the impact of the recurring magmatic injections (e.g. Pollard and Johnson, 1973; Pennacchioni et al., 2006; Pons et al., 2006).

The first and foremost feature of the Matok pluton granitoids that one has to consider before considering a possible source is the concentration of Ni, Cr and MgO. Absolute concentrations of these elements and oxide often provide an initial clue to the source; rocks resembling primary melts from a peridotitic mantle have ≥400 ppm Ni, ≥1000 ppm Cr and ≥8 wt.% MgO (Best and Christiansen, 2001). These values are much higher than any of the Matok

pluton granitoids have, and therefore preclude the possibility of a direct derivation from the mantle. Nonetheless, the Matok pluton granitoids can be divided into the ACG and KCG (see section 1.2), and both px-bearing and px-free granitoids are represented in the ACG group. According to the definition, the ACG necessitate a fairly large influence from mantle (DePaolo and Farmer, 1984; Barbarin, 1999).

Similarly, negative HFSE anomalies on primitive-mantle-normalised diagrams are popularly suggested to signify a subduction related magmatism (O'Brien et al., 1995; Sajona et al., 1996; Ma et al., 1998; Caprarelli and Leitch 1998; Eklund et al., 1998; Bakkali et al., 1998; Ferré et al., 1998; Ajaji et al., 1998; Barbarin, 1999; Stevenson et al., 1999; Pearce et al., 2000; Percival and Mortensen, 2002; Kalfoun et al., 2002; Tomson et al., 2006; Niu and O'Hara, 2009). In addition to the HFSE negative anomalies on primitive-mantle-normalised diagrams, the Matok pluton granitoids have negative anomalies of Sr, Eu, Th and U (Fig. 17). Because both Sr and Th are LILE, it would be expected that they behaved like other LILE in a subduction-related process, i.e. not produce negative anomalies on primitive-mantle-normalised diagram. Since it is being suggested that the Matok pluton granitoids (px-bearing and px-free) are genetically related, the use of elements that are not readily influenced by fluids (HFSE; Nb, Ta, Zr, Hf) has the potential to avoid the bias between (hydrous) magmas of px-free granitoids versus (anhydrous) magmas of px-bearing granitoids. As a result, the distribution patterns of these elements may provide a better speculation about the source composition.

7.3.1. Source composition inference on the basis of the HFSE, Th and U

Because of their generally similar chemical behaviour in fluids and melts, each of the HFSE pairs - Nb-Ta and Zr-Hf is commonly referred to as 'identical twins' (e.g. Green and Pearson 1987; Green 1995; Kalfoun et al., 2002; Weyer et al., 2003) and some workers have even suggested that their ratios (Nb/Ta, Zr/Hf) cannot be fractionated by magmatic processes (e.g. Pfänder et al., 2007). The Nb-Ta 'twins' may provide vital information about incorporating mineral phases that participated at partial melting and/or about the nature of the source with regards to the Nb-Ta budget. The term 'Nb-Ta paradox' was introduced based on the observation that, on average, both the continental crust and the depleted upper mantle have subchondritic Nb/Ta ratio (e.g. Barth et al., 2000; Rudnick et al., 2000; Schmidt et al., 2004; Xiong et al., 2005; Niu and O'Hara, 2009) and in addition to the continental crust having negative anomalies of Nb and Ta on primitive-mantle-normalised diagrams (e.g. Rudnick, 1995; Hofmann, 1997). Some researchers have suggested that the 'missing' Nb and Ta reside in the lower mantle (e.g. Klemme et al., 2002) or as deep as in the core (Wade and Wood 2001;

Schmidt et al., 2004). The high Nb/Ta ratios therefore largely resemble a mantle origin (e.g. Klemme et al., 2002; Goss and Kay, 2009). The Chondritic Nb/Ta value is ~ 17.57 while chondritic Zr/Hf value is ~36.30 (Sun and McDonough 1989).

Figure 29 illustrates the Nb/Ta versus Zr/Hf ratios for the Matok pluton granitoids. Also shown are the fields for volcanic rocks of the Barberton greenstone Belt, tonalite trondhjemite granodiorites (TTGs) and High-K- granites from the NMZ and the Ventersdorp volcanics. Shown as well are the chondritic Nb/Ta and Zr/Hf ratios (from Sun and McDonough, 1989) represented by the two corresponding lines. An attempt to find published data on the same elements for the TTGs in the SMZ was unsuccessful. The two TTG samples of the Baviaanskloof Gneiss sampled in this study give Nb/Ta values of 16 and 18.25 and Zr/Hf values of 32.74 and 35.54. These values are still much lower than that of the majority of the Matok pluton granitoids, but partly overlap with some of the px-free granites with >71 wt.% SiO_2.

One feature that stands out in Figure 29 is the fact that the Matok pluton granitoids have superchondritic Nb/Ta and Zr/Hf ratios and plot largely in the field of Ventersdorp volcanics. A significant number of the granitoids have even higher Nb/Ta ratio than the Ventersdorp volcanics. Both the Nb/Ta and Zr/Hf ratios are also higher than that of average continental rocks (10.91 and 33.24; Rudnick, 1995), the primitive mantle (17.39 and 36.25) and mid-ocean ridge basalts (17.65 and 36.1) (Sun and McDonough, 1989). This characteristic is clearly not a feature seen in the TTGs and High-K- granites of the NMZ, as they all plot well below the Nb/Ta ratio values of the Matok pluton granitoids and the Ventersdorp volcanics (Fig. 29). The analytical data is of high quality and all these elements were detected well above detection limits of the analytical instruments. Therefore the obtained Nb, Ta, Zr and Hf concentrations in the Matok pluton granitoids are representative of 'true' concentrations.

Although it is argued that mantle signature in terms of MgO, Ni and Cr is lacking in the Matok pluton granitoids, the higher Nb/Ta ratios suggest a source which had inherited these high ratios from the mantle. Because the Ventersdorp volcanics are suggested to have originated from the mantle (Crow and Condie, 1988; van der Westhuizen et al., 1991; Nelson et al., 1992; Marsh et al., 1992) and in turn their Nb/Ta versus Zr/Hf variation overlaps with that of the Matok granitoids, it is pertinent that the source to the Matok pluton granitoids has geochemical similarity with the Ventersdorp volcanics. The characteristic superchondritic Nb/Ta ratio of the Ventersdorp volcanics imply an origin in the lower mantle because the upper mantle is characterised by subchondritic Nb/Ta ratio (Barth et al., 2000; Rudnick et al., 2000; Schmidt et al., 2004; Xiong et al., 2005; Niu and O'Hara, 2009). The lower Mg, Cr and Ni

concentrations for the Matok pluton granitoids suggest that the partial melts were not derived directly from the mantle.

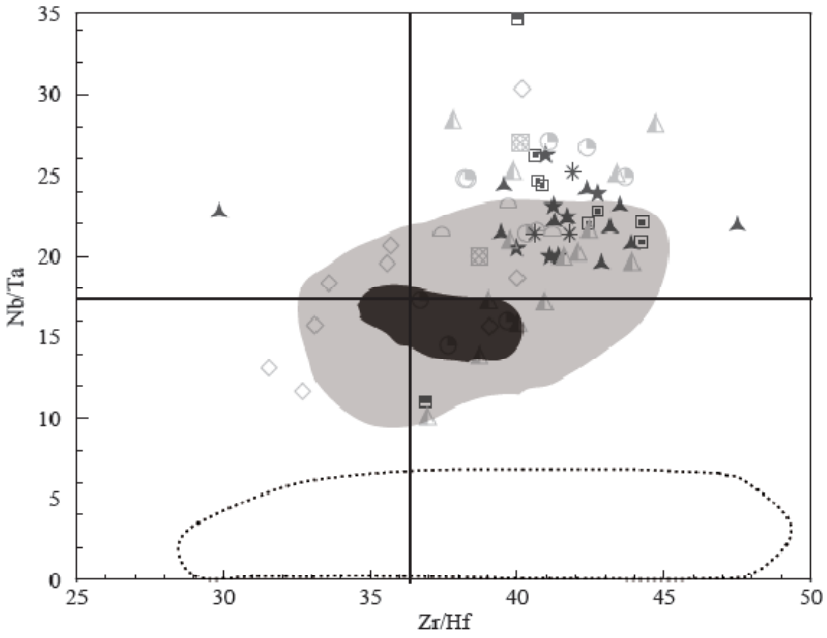

Figure 29. Variation of Nb/Ta with Zr/Hf ratios for the Matok granitoids. Dark shaded field represents volcanic rocks of the Barberton greenstone Belt (data from Parman and Shimizu, 2003), light shaded field represent the Ventersdorp volcanics (data from Crow and Condie, 1988 and Marsh et al., 1992) and the unfilled field at the bottom represents the TTGs and High-K- granites from the NMZ (data from Kampunzu et al., 2003). The two lines represent chondritic Nb/Ta and Zr/Hf ratios, from Sun and McDonough (1989).

For most of the Matok pluton granitoids (excluding granites with >71 wt.% SiO_2) both Nb/Ta and Zr/Hf ratios are generally confined with an increase in SiO_2 (Fig. 30). This HFSE ratio confinement, again, supports the absence of fractionation to account for the co-existence of px-bearing and px-free granitoids in the Matok pluton. The most viable option is therefore that the characteristic Nb/Ta and Zr/Hf ratios were acquired during partial melting and by implication are inherited from the source.

It is also argued that the characteristic negative anomalies of Nb, Ta and Ti on primitive mantle normalised diagrams for the Matok pluton granitoids do not necessarily imply a subduction-related magmatism. The relative behaviour of Nb to Ta (Nb/Ta) provides a better evaluation tool than the relative behaviour of Nb to K or Ta to La (e.g. Sims and DePaolo, 1997; see normalised patterns in Figure 17). This is because the 'twins' Nb and Ta are ideally components of similar minerals and therefore their concentrations will be governed uniformly solely by the presence of such mineral(s). The relative behaviour of both Nb and Ta to K (or La) on the other hand will depend on more variables; relative abundance of both K and La accommodating phases as well as the Nb and Ta accommodating phase(s). In this manner, the Nb/Ta ratio provides a better means of evaluating the source composition, other than

comparing the HFSE to the LILE. Therefore the Nb/Ta ratio provides a 'solid' approximation to the same ratio in the source.

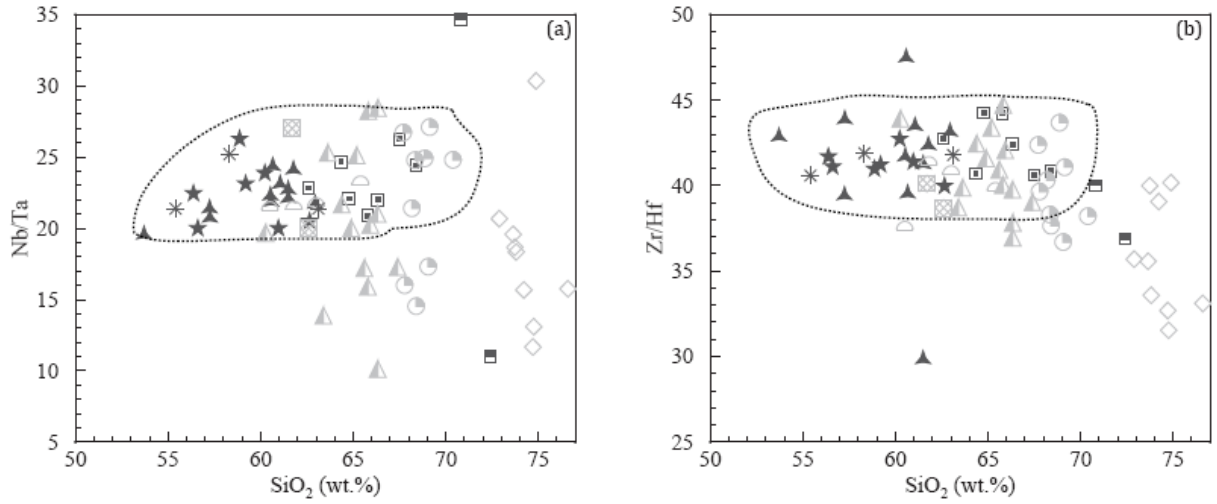

Figure 30. Variation of (a) Nb/Ta and (b) Zr/Hf ratios with SiO_2 for the Matok pluton granitoids. Illustrated fields are meant to show that these ratios are confined with increase in SiO_2.

The observation that the TTGs in the NMZ, the Ventersdorp volcanics, the Matok pluton granitoids and the Mesozoic Karoo continental flood basalts (also in the Kaapvaal Craton) all produce negative anomalies of Nb and Ta when normalised to the primitive-mantle support the argument that the negative Nb and Ta anomalies do not always imply a subduction involvement. It is unlikely that the production of all these rocks involved or had a subduction component. Moreover, both the Neoarchaean Ventersdorp volcanics and the Mesozoic Karoo continental flood basalts are argued to have originated from a mantle plume beneath the Kaapvaal Craton (Hoorwood, 1910; Crow and Condie, 1988; van der Westhuizen et al., 1991; Marsh et al., 1992; Nelson et al., 1992; Marsh et al., 2007). It is unlikely that a 'subduction component' would reside in the mantle beneath the Kaapvaal Craton for a period of two billion years without being homogenised by convection. However, since the Matok pluton granitoids and the Ventersdorp volcanics are nearly synchronous and have similar Nb/Ta ratios, it becomes realistic to infer on a genetic relationship between these two groups of rocks.

It is important to establish whether the Th and U concentrations which distinguish, clearly, between px-bearing and px-free granitoids (Fig. 14e, f), are manifestation of magmatic processes or a source characteristic. A measure of anomalies of these two elements (Th/Th* and U/U*; as described in chapter 6) is plotted against SiO_2 in Figure 31.

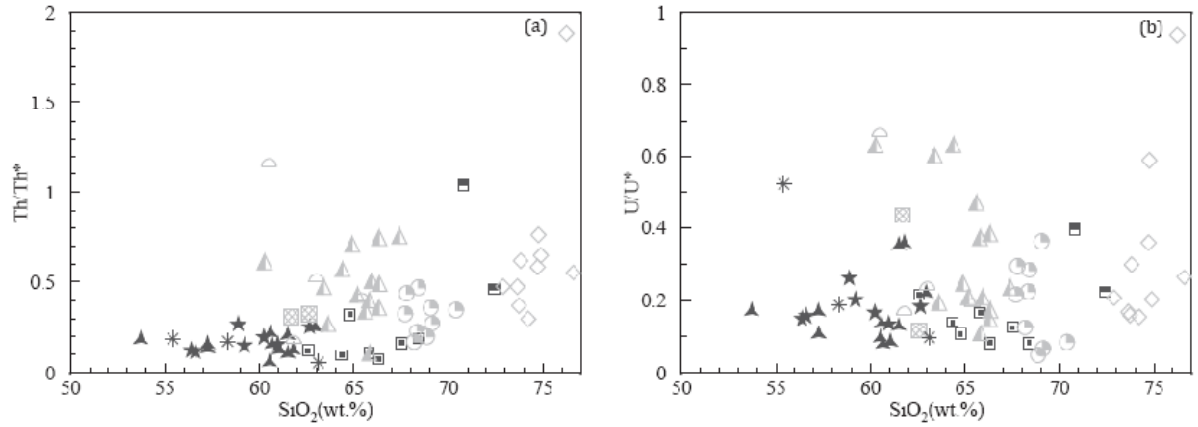

Figure 31. Variation of (a) Th/Th* and (b) U/U* with SiO_2 for the Matok pluton granitoids. Symbols are the same as in Fig. 11.

A notable difference between the px-bearing and px-free granitoids still persists in Figure 31a; px-free granitoids have, relatively, smaller magnitude of negative Th anomaly. There is a significant scatter in the U/U* versus SiO_2. However, a considerable number of rocks show less distinction between px-bearing and px-free granitoids. The average Th concentrations of the Ventersdorp volcanics from studies by Marsh et al. (1992) and Crow and Condie (1988) are 1.4 and 2.2ppm respectively, and the U average is 0.6ppm (Crow and Condie, 1988). The Ventersdorp volcanics also show negative anomalies of Th and U when normalised to the primitive mantle. This suggests that the distinction between px-bearing and px-free granitoids, in terms of Th and U absolute concentrations rather reflects on the internal processes either during the partial melting or in the magma chamber. Since the high concentrations of both Th and U in px-free granitoids (excluding granites with > 71wt.% SiO_2) are unlikely to have resulted from assimilating the SMZ country rock (section 7.1), the requirement is that these high Th and U are due to the hydrous nature of their melts/magma batches. Both Th and U are easily mobilised by fluids, (e.g. Kramers et al., 2001; Rollinson and Tarney, 2005; Barry et al., 2006). The implication is that magma batches of px-free granitoids may have been derived from a relatively hydrous source, but which had an overall geochemical similarity with that of the px-bearing granitoids. Despite having the highest Th and U concentrations, the px-free granitoids still maintain negative anomalies (Fig. 17) of these two elements relative to elements with similar compatibility. It is therefore suggested that the source also had negative Th and U anomalies, but the departure of both Th and U from the source was also governed by the fluid budget.

7.3.2. Semi-quantitative incompatible trace element modelling of the source region

The most important hint before assuming the composition of the source requires consideration of the distributions of the HFSE and REE as well as the maficity of the Matok

pluton granitoids. The non-fractionated HREE patterns of the Matok pluton granitoids (Fig. 16) require the absence of residual garnet and hornblende in the source (e.g. Farrow and Barr, 1992; Wen et al., 2008); residual garnet would have led to steep HREE while hornblende would have led to concave upward HREE patterns. Because the zircon saturation curve fails to account for the high abundance of Zr in the Matok granitoids, it is possible that residual pyroxene had significant amounts of Zr (e.g. see Bodinier et al., 1996; Bedini and Bodinier, 1999; Kalfoun et al., 2002; Pfänder et al., 2007). If it can be assumed that this was the case, then clinopyroxene may have been a significant phase in the source. The characteristically high Nb/Ta ratios of the Matok pluton granitoids refute a source in the upper crust but rather call for a mafic source which had the high Nb/Ta ratio influence from the mantle (section 7.3.1).

The partitioning coefficients used for source modelling are given in Table 2. Equilibrium (batch) melting is assumed and the equation used is $C_l = C_o/ (D+F(1-D))$ (Consolmagno and Drake, 1976). Where C_l is the concentration of an element in the partial melt, C_0 is the initial concentration of the same element in the solid source, F is fraction of the melt and D is the bulk distribution coefficient. The 'true' F is unknown and will therefore be speculated. Because the minimum melt fraction at which granitic melts may efficiently segregate from migmatites is 10% F (Clemens and Mawer, 1992), it is herein assumed that the Matok pluton granitoids segregated from their source at ≥10% F.

To support the proposal that the Matok pluton did not form by partial melting of the Baviaanskloof Gneiss, semi-quantitative geochemical modelling was carried out, with the Gneiss as the potential source. Geochemical composition of the two Baviaanskloof Gneiss samples taken for this study is presented in Table 3. Partition coefficients used are presented in Table 2.

Table 3. Major (in wt.%) and trace element (in ppm) compositions of the two Baviaanskloof Gneiss samples

	SiO_2	Al_2O_3	FeO*	MgO	CaO	Na_2O	K_2O	TiO_2	P_2O_5	MnO	Cr_2O_3	LOI	Sum
Bav 1	73.41	14.92	1.56	0.43	1.95	5.43	1.48	0.14	0.08	0.02	0.018	0.5	99.91
Bav 2	72.98	14.94	1.85	0.48	2.02	5.37	1.39	0.19	0.08	0.02	0.016	0.6	99.92

	Sc	Ni	Co	V	Cs	Nb	Ta	Zr	Hf	Ba	Rb	Sr	Th	U	Pb
Bav 1	2	9.3	3.2	19	0.6	8	0.5	88.4	2.7	526	42.5	399.5	3.3	0.6	2.1
Bav 2	3	5.5	2.4	17	0.8	7.3	0.4	138.6	3.9	302	50.8	345	4.6	0.8	3

	La	Ce	Pr	Nd	Sm	Eu	Gd	Tb	Dy	Ho	Er	Tm	Yb	Lu	Y
Bav 1	17.2	29.3	3.21	11.4	1.72	0.49	1.38	0.22	1.18	0.23	0.68	0.11	0.71	0.1	8.4
Bav 2	17.9	33	3.64	12.6	2.08	0.47	1.55	0.23	1.08	0.19	0.5	0.08	0.51	0.07	6.1

The Matok pluton granitoids are much more enriched in REE and HFSE such that even a small degree of partial melting (~5%F) of the Baviaanskloof Gneiss would not produce the characteristic concentration of these elements in the Matok pluton granitoids. Such a low

amount of partial melting would not be enough for the melts from the Baviaanskloof Gneiss to accumulate and leave their source. Also, the Gneiss is much more differentiated (>70 wt.% SiO_2 and MgO < 0.5 wt.%) and unlikely to produce mafic rocks with as low as 53% SiO_2.

If negative anomalies of Nb, Ta and Ti indeed resemble a subduction influence as popularly suggested (e.g. O'Brien et al., 1995; Sajona et al., 1996; Bakkali et al., 1998; Caprarelli and Leitch 1998; Stevenson et al., 1999; Pearce et al., 2000; Percival and Mortensen, 2002; Kalfoun et al., 2002; Tomson et al., 2006; Niu and O'Hara, 2009), another choice for source composition and mineralogy would be that of 'typical' metasomatic assemblage present during slab melting (e.g. Moyen et al., 2001). An additional feature of the Matok pluton granitoids that is absent in the so-called subduction-related magmatism is the negative anomalies of Eu and the LILE; Th, U, Sr ± Pb. If the negative HFSE, Th, U and Sr (and Eu) anomalies were formed by two different processes (subduction and the other), there is more likely to be no correlation between the magnitude of the HFSE and Th, U and Sr anomalies. If however, they were formed by a single process, some kind of correlation is likely.

Illustrated in Figure 32 is the variation of Nb/Nb* with Th/Th*, Pb/Pb* and Sr/Sr*. Even though it was shown that px-free granitoids have higher Th concentrations than px-bearing granitoids, the overall negative correlation between Th/Th* and Nb/Nb* (Fig. 32a) suggests that in both groups of granitoids the concentrations of Th and Nb were achieved during a single (partial melting) process. There is a significant scatter in the plot of magnitude of Pb anomaly and Nb/Nb*, though a generalised negative correlation can be made (Fig. 32b). Similarly, the relationship between the Nb/Nb* and Sr/Sr* is defined by a very tight field (excluding granites with > 71wt.% SiO_2; Fig. 32b) suggesting that both the negative Nb and Sr anomalies were also acquired during a single partial melting event. For this reason it is suggested that the Matok

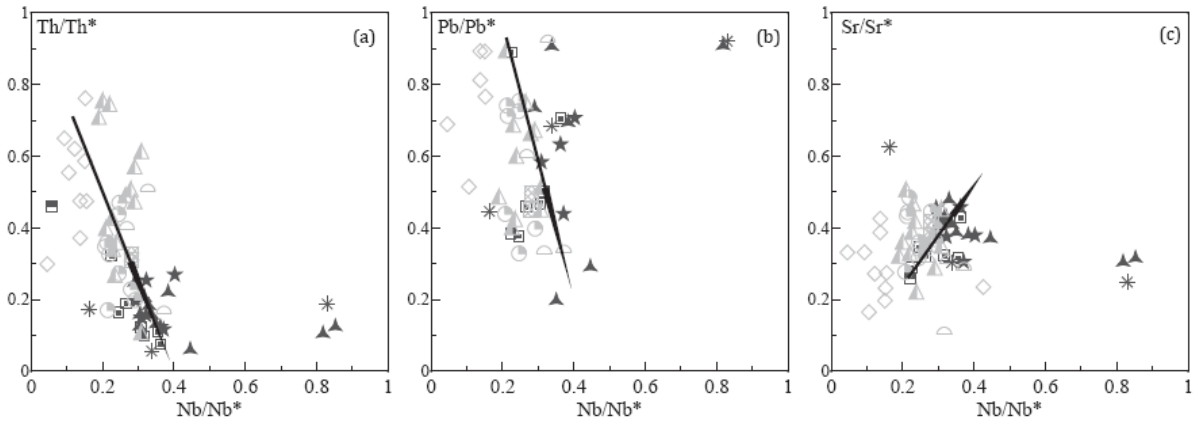

Figure 32. Variation of Nb/Nb* with (a) Th/Th*, (b) Pb/Pb* and (c) Sr/Sr* for the Matok pluton granitoids. The lines drawn in each diagram indicate the kind of correlation between the plotted variables. The magnitude of anomalies is calculated as explained in section 4.2. Symbols are the same as in Fig. 11.

pluton granitoids bear no evidence for a subduction process and therefore assemblage typical of subduction-related magmatism is discarded as a possible proxy for source mineralogy.

Because the source of the Matok pluton granitoids needs to have been a mafic crust, two more alternatives that can be considered are the mantle-derived Ventersdorp volcanics and the komatiites of the Kaapvaal Craton. Both rock types had formed prior to the Matok pluton emplacement and are equally potentially lower crust components in the vicinity of the SMZ. The primary mineralogy of the komatiites of the Barberton Greenstone Belt (in the Kaapvaal Craton) has been subjected to significant metamorphic overprinting (Parman et al., 2003). The magmatic assemblage however constituted augite, olivine, Cr-spinel ± pigeonite ± magnetite (Parman et al., 2003). Similarly, the volcanics of the Ventersdorp Supergroup are comprised of augite, olivine, magnetite, plagioclase (An_{23-63}) and orthopyroxene (Hoorwood 1910; Schweitzer and Kröner, 1985; Crow and Condie, 1988). These assemblages can therefore be used as proxy for the mineralogical composition of the lower mafic crust in the SMZ.

Figure 33 shows primitive mantle normalised diagrams for the three samples of the Matok pluton Mat 16 (px-diorite1), Mat 28 (px-diorite2) and Mat 11 (px-free diorite). The grey field shown is for the Ventersdorp volcanics. The four samples shown in green are the Ventersdorp volcanic samples of Reitgat and Goedgenoeg Formations. It is evident in Figure 33 that the Matok pluton granitoids have similar patterns as the Reitgat and Goedgenoeg samples.

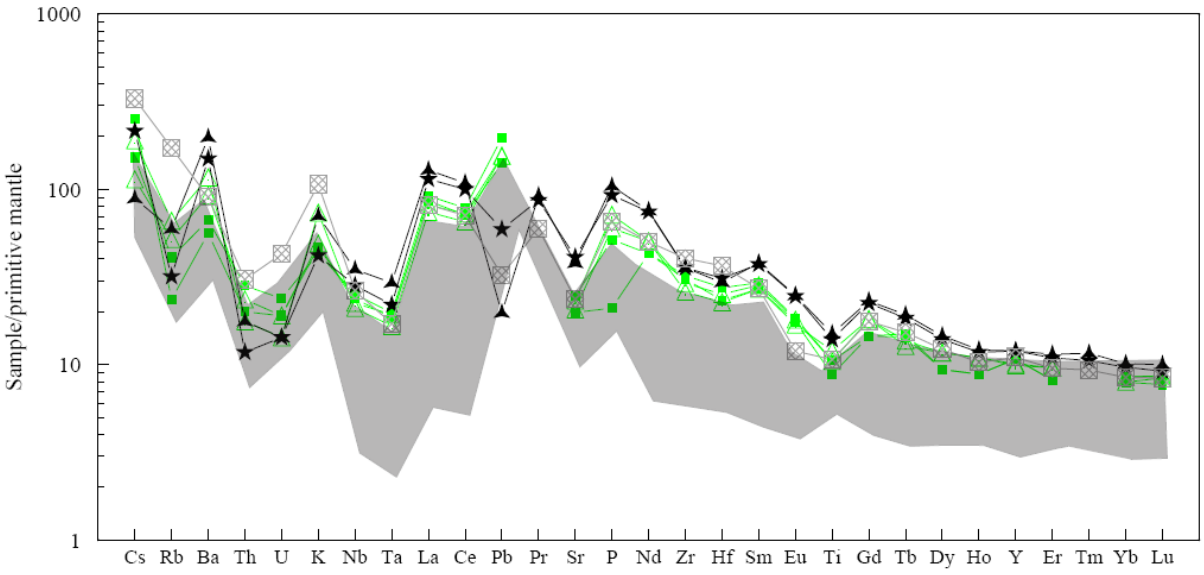

Figure 33. Primitive mantle normalised diagrams for the Ventersdorp volcanics. Data taken from Nelson et al. (1992) and Crow and Condie (1988). Shown in green are the samples of Reitgat and Goedgenoeg Formations of the Ventersdorp volcanics which show trace element patterns similar to those of the Matok pluton granitoids. The Matok pluton granitoids are shown in black and grey with symbols same as in Fig. 11.

About 80% degree of partial melting is needed to generate the Matok pluton granitoids' incompatible trace elements from both Reitgat and Goedgenoeg basaltic andesites. A smaller degree of partial melting would be required from most of the volcanics represented by the volcanics field in Figure 33. However, none of the other volcanics' Formations would produce primitive mantle normalised patterns that largely conform with the Matok pluton granitoid patterns. The patterns of both Reitgat and Goedgenoeg samples conform exclusively (Fig. 33), with the exception of Pb anomaly which is positive for the volcanics and negative for the Matok pluton granitoids.

The HFSE (Nb, Ta ± Ti) present a much decisive role in the geochemistry of the Matok pluton granitoids. The mineral assemblages of both Barberton Greenstone Belt and the Ventersdorp volcanics presented above do not include main Ti, Nb and Ta-accommodating phases. For this reason additional minerals that will be assumed to have been in the source are rutile, ilmenite and hornblende. Also, because apatite and zircon are major repositories for Th and U (Deer et al., 1992; Bédard, 2006), the presence of zircon (and apatite) in the source will also be evaluated. Since it has been argued that the stabilisation of magmatic epidote and titanite in the px-free granitoid magmas was induced by higher fO_2 (± fH_2O) towards the final stages of crystallisation (section 4.2.2 and 4.4), it seems appropriate to discard the presence of titanite and epidote in the source. The proportions of lower crust minerals have been arbitrarily inferred and each mineral assemblage will be tested according to the proportions shown in Table 4.

Illustrated in Figure 34 is the Nb/Ta versus La plot for the Matok granitoids. Also shown are the melting trajectories from a Ventersdorp volcanic sample of Goedgenoeg basaltic andesite. The main minerals that would impact on the Nb and Ta budget of melts derived from the Goedgenoeg source are rutile and amphibole. Figure 34a shows the effect of having 1% rutile, 0% amphibole in the source and Figure 34b shows the effect of having 0% rutile and 5%

Table 4. Inferred mineral proportion of the lower crust

	Mafic crust[1]	Mafic crust[2]
Olivine	15	15
Amphibole	0	5
Magnetite	2.5	2
Ilmenite	0.5	2
Zircon	0.0001	0.2
Plagioclase	26	15
Clinopyroxene	35	40
Orthopyroxene	20	18
K-feldspar	0	2.5
Apatite	0.001	0.001
Rutile	1	0

amphibole in the source (see Table 4). Regardless of rutile or amphibole in the source, the fraction of melt required to account for the Matok pluton granitoids ranges from 100 to ~40% F.

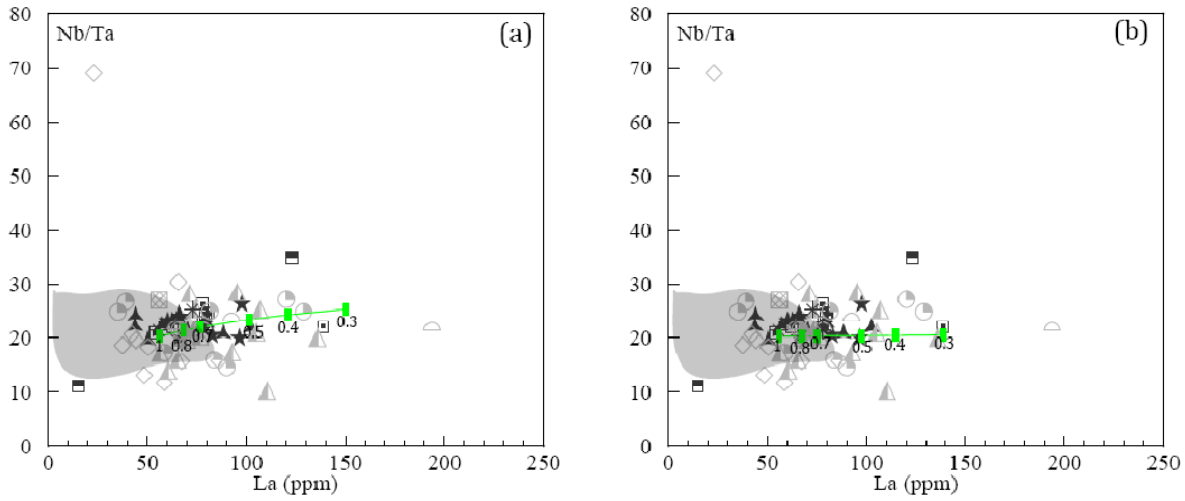

Figure 34. Nb/Ta ratio versus La for the Matok pluton granitoids. The grey fields shown represent the Ventersdorp volcanics (data taken from Nelson et al., 1992 and Crow and Condie, 1988). Green lines represent melting trajectories from the inferred Goedgenoeg parental source. (a) shows a trajectory from a source with 1% rutile, 0% amphibole and (b) shows trajectory with 5% amphibole, 0% rutile. The numbers shown along the trajectories next to the tick marks represent the fraction of the melt successively from the parental source (1) to 0.8, 0.7, 0.5, 0.4 and 0.3 out of 1. Symbols for the Matok pluton granitoids are the same as in Fig. 11.

The trajectories in Figure 35 contrast the effect of having zircon in the source. Figure 35a shows a source with 0.0001% zircon and Figure 35b shows a source with 0.2% zircon. The absence of residual zircon (0.0001%) results in a steep Zr/Nb (Fig. 35a) because Zr would behave as an incompatible element. The presence of residual zircon on the other hand would not significantly change the Zr/Nb of melts because Zr is highly compatible in zircon. On contrary, the La/Yb ratio of melts would, in the presence of residual zircon, change significantly because Yb is significantly compatible in zircon while La is not (Table 2). However, it is worth highlighting that regardless of the amount of residual zircon, the Matok pluton granitoids can be achieved by between 100 and 40% melt fraction from the Goedgenoeg sample. The distinctively higher melt fraction needed to produce the Matok pluton granitoids from the Ventersdorp volcanics is not incompatible with genesis from a 'just' underplated magma which had not yet fully solidified.

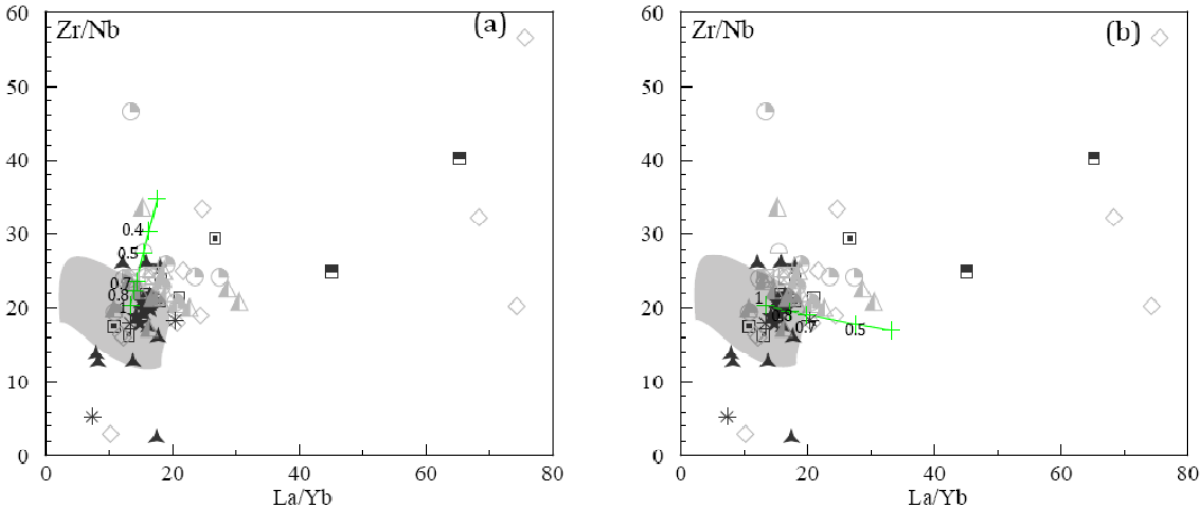

Figure 35. Zr/Nb versus La/Yb ratio for the Matok pluton granitoids. The grey fields shown represent the Ventersdorp volcanics (data taken from Nelson et al., 1992 and Crow and Condie, 1988). Green lines represent melting trajectories from the inferred sources of Ventersdorp volcanics. (a) shows a trajectory from a source with 0.0001% zircon and (b) shows trajectory with 0.2% zircon. The numbers shown along the trajectories next to the tick marks represent the fraction of the melt successively from the parental source (1) to 0.8, 0.7, 0.5 and 0.4 out of 1. Symbols for the Matok pluton granitoids are the same as in Fig. 11.

7.3.3. Implication on the presence of negative anomalies on primitive mantle normalised diagrams

Both Th and U are fluid mobile and mainly compatible in the refractory minerals (e.g. zircon and apatite; Fyfe, 1973; Taylor and McLennan, 1997; Rollinson and Tarney, 2005; Barry et al., 2006). Mobilisation of Th and U would therefore be more efficient under relatively high melting temperature conditions, which would then melt the refractory zircon and apatite (Eklund et al., 1998; Ferré at al., 1998; Barry et al., 2006). One account for the high Th and U concentrations for the px-free granitoids would thus be melting at higher temperatures, relative to the px-bearing granitoids. The observation that the px-free granitoids are enriched also in other fluid mobile elements (Cs, Rb; Figs. 14 and 17) suggests that it was not melting under higher temperature or residual mineralogy but rather partial melting under more hydrous conditions that yielded high Th and U concentrations. Furthermore, despite the px-free granitoids with ≤ 71 wt.% SiO_2 having distinctively high concentrations of Th and U relative to the px-bearing granitoids, these elements still display negative anomalies on the primitive mantle normalised diagrams (Fig. 17). The negative Th and U anomalies were therefore not induced by residual mineralogy, but more probably a feature of the source. Likewise, the presence of negative anomalies of Ti, Nb and Ta cannot be accounted for by the role of residual mineralogy during partial melting (section 7.3.2). Both titanite and rutile have the potential to have induced the observed Nb and Ta negative anomalies, but these minerals are argued to have

been absent in the source (section 7.3.2). And again, the negative anomaly of these elements is a feature inherited from the source rather than partial melting -induced.

Concentrations of Sr and Eu distinguish between px-bearing and px-free granitoids; px-bearing granitoids have higher Sr and Eu. On the one hand, the magnitude of Sr anomaly (Sr/Sr*) does not, generally, distinguish between px-bearing and px-free granitoids (Fig. 36a). On the other hand the magnitude of Eu negative anomaly does; it increases with SiO_2 for the px-bearing granitoids and decreases with increasing SiO_2 for px-free granitoids (Fig. 36b). The similarity in Sr/Sr* among both suites of granitoids implies that the Sr departure from the source were more likely influenced by one factor; the residual mineralogy (plagioclase). This might have been the case with Eu. However, the oxidation state of Eu typically changes with magmatic oxidation state and it exists in the Eu^{2+} under reducing conditions and Eu^{3+} state under oxidising conditions (Hess, 1989). Because magmas of the px-free granitoids evolved into higher fO_2, these conditions must have been conducive to Eu changing the oxidation state. This contrast between Sr/Sr* and Eu/Eu* with increasing SiO_2 (Fig. 36) therefore is only a manifestation of magmatic internal process subsequent to segregating from the source. Otherwise both Sr and Eu negative anomalies in the Matok pluton granitoids were produced due to residual plagioclase holding back Sr and Eu in the basaltic source.

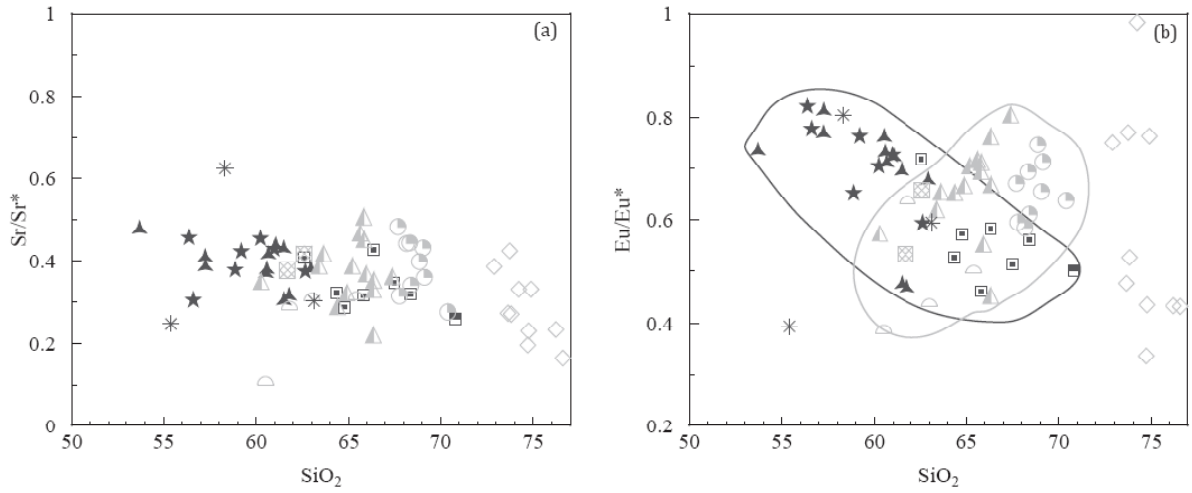

Figure 36. Variation of Sr/Sr* and Eu/Eu* with SiO_2 for the Matok pluton granitoids. Symbols are the same as in Fig. 11.

7.3.4. Magmatic evolution

It is suggested that the episodic nature of the intrusions in the Matok pluton was achieved owing to magma storage in the chamber(s) and that both episodes were separated by an insignificant time gap as suggested by the ENE-WSW magmatic mineral foliation in both episodes. The gneissic development in the earlier granitoids was probably due to the intrusive impact of successive intrusions. The indistinguishable REE and HFSE characteristics between

the px-diorites1 and the rest of the Matok pluton granitoids negates the role of different sources and differing degree of partial melting and therefore supports magma storage, following segregation of the first intrusion. It is also argued that neither the first intrusion versus the second intrusion nor the px-bearing versus px-free granitoids can be linked by fractional crystallisation (or by fractional melting at the source region). The difference in temperature alone cannot be accountable for the division of the Matok pluton granitoids into px-bearing and px-free granitoids. A combination of chemical composition, temperature, fH_2O and fO_2 plays a significant role in influencing which mineral phases are stabilised to the solidus (Borg and Clynne, 1998; Holtz et al., 2001; Pons et al., 2006). The requirement for the fate of pyroxene in the px-bearing granitoids requires that a thermal boundary layer between their magma batches and magma batches of the px-free granitoids was minimally or absolutely not crossed (e.g. Pons et al., 2006). This would have prevented hydration of the px-bearing granitoid magma batches because hydration would have led pyroxene reacting with the melt before the subsolidus temperature. There are at least two possible solutions to the coexistence of px-bearing and px-free granitoids in the Matok pluton, and both will be discussed:

(1) It is possible that there were at least two magma chambers. In this scenario one magma chamber must have been that of px-bearing granitoids (anhydrous) and the other must have been that of px-free granitoids (hydrous). Both chambers must have formed from a related source to account for the similar REE and HFSE in the px-bearing and px-free granitoids. However, the partial melts of the px-free granitoids must have been generated under hydrous conditions, relative to those of px-bearing granitoids. Partial melting under hydrous conditions would explain the higher Th, U, K_2O, Cs and Rb concentrations of the px-free granitoids. Although the magmas were in two separate chambers, there was only one focal point to which magma batches were, subsequent to leaving their chambers, destined for - the Matok pluton. This concept of two magma chambers-one destination is better explained by the proposition that the construction of a pluton is a consequence of amalgamation of magma batches by means of feeder dikes, rather than a diapiric rise (e.g. Clemens and Mawer, 1992; Archanjo et al., 1998; Pons et al., 2006; Barbey et al., 2008). The feeder dikes from the respective magma chambers must have been, for most time, isolated to avoid hydration of px-bearing granitoid magmas.

(2) It is also possible that there was only one magma chamber. A development of hydrodynamic sorting in single magma chamber may have led to magma zonation into batches which had slight difference in temperature, fH_2O ± different level of polymerisation. All the 'zones' that ultimately gave rise to the different phases of the px-free granitoids (Fig. 2) were mostly at similar temperature and fH_2O but at slightly different level of polymerisation. It was the difference in the budget of major element proportions (level of polymerisation) that in turn

led to the difference in proportions of minerals when yet the overall textures were similar in all the phases of the px-free granitoids. Similarly, each of the zones of the px-bearing granitoid magmas had a slight difference in level of polymerisation, but all the batches were at similar temperature and fH_2O conditions. The main difference between the 'zones' of px-bearing granitoid magmas versus that of px-free granitoid magmas was fH_2O which progressively induced also a difference in temperature. A crucial requirement is that this magma zonation occurred in the magma chamber to account for the similarity in the REE and HFSE in both px-bearing and px-free granitoids. However, Th, U, Cs and K were rather preferentially incorporated into the more hydrous magma zones. Because some time is needed to establish this hydrodynamic sorting, it is possible that the magma had ponded for a while before it intruded. Although it is not implied that a single mineral crystal would be zoned into areas with different temperatures, the sector zoning in minerals best clarifies how the suggested magma zoning occurred in the magma chamber of the Matok pluton. It is also not implied that the zoning was achieved by growth (additions of more partial melts), as it would be the case in mineral zonation; zoning must have been established internally after melt accumulation.

Even in the case of one magma chamber the requirement is still that magma batches left the chamber in the form of feeder dikes. It is imperative that the feeder dikes mimicked the zoning in the chamber; it must have been relatively easier to establish a feeder dike out of an intact unit/zone, than out of two adjacent zones with different level of polymerisation (± slight difference in viscosity). It has been suggested that the mineralogy of px-bearing and px-free granitoids may have initially been similar (section 4.2.2). To account for the destruction of pyroxene before the solidus, the px-free granitoid magma must have had a relatively prolonged molten state, requiring that the feeder dikes of the px-free granitoids evolved differently from those of px-bearing granitoids. The higher proportions of oxides of readily volatile elements (H, K) in the px-free granitoid magmas must have contributed to the prolonged history of molten state (e.g. Holtz et al., 2001; Kuritani 2004). The prolonged molten state in turn enabled crystallisation parameters to be conducive to replacement of pyroxene by biotite and/ hornblende as well as the formation of epidote and titanite at the expense of clinopyroxene, hornblende, ilmenite and magnetite. This prolonged history is compatible with the 'just before the solidus' formation of the magmatic epidote in the Matok pluton px-free granitoids.

Whichever mechanism was responsible for the co-magmatism of px-bearing and px-free granitoids, the HRSZ may have facilitated magma departure from the source. The magma must have formed slightly earlier, ponded and then intruded when the shear zone was well established to effectively facilitate such a process. The important point here is that even the

processes happening in the upper crust also played a significant role in encouraging magma departure from its source.

8. GEODYNAMIC IMPLICATIONS

Magmatic mineral foliation in the Matok pluton is aligned roughly ENE-WSW (parallel to the Limpopo Belt trend) pointing to a syntectonic emplacement. The intrusion of Matok magma was possibly achieved owing to establishment of HRSZ which may have facilitated magma segregation from the source (e.g. see Bonin et al., 1998; Archanjo et al., 1998; Rajesh 2008; Konopelko et al., 2009). The two episodes of intrusion are characterised by porphyritic rocks. Even the granitoids of the first intrusion (px-diorites1) do have feldspar phenocrysts aligned ENE-WSW. This means that the petrogenetic model presented above can be used to infer on the geodynamic setting of the SMZ, and by implication of the Limpopo Belt. Because the Matok pluton is one of the many plutons that intruded in the Kalahari Craton during the time 2.7-2.5 Ga, which in turn coincided with the regional high grade metamorphism in the Limpopo Belt (Tankard et al., 1982; McCourt and Vearncombe, 1992; Kamber and Biino, 1995; Berger and Rollinson 1997; Hickman, 1978; Holzer et al., 1999; Frei et al., 1999; Vinyu et al., 2001; Blenkinsop et al., 2004; Rigby et al., 2008) the inference is that the cause for this regional event can be explained from this study.

Many studies of plutons emplaced during the Phanerozoic and Proterozoic have been proposed to evidence a subduction-related magmatism based mainly on the negative anomalies of Nb, Ta and Ti on primitive mantle normalised diagrams (e.g. Sajona et al., 1996; Pearce et al., 2000; O'Brien et al., 1995; Percival and Mortensen, 2002; Tomson et al., 2006; Goss and Kay, 2009). It is popularly suggested that the 'subduction signature' is accomplished as fluids emanating from a dehydrating slab preferentially release the LILE, while the HFSE are retained in the slab (e.g. Ferré et al., 1998; Barry et al., 2006). The inferred subduction-related igneous intrusions are typically found within terranes with ample evidence for tectonic activity (e.g. Ajaji et al., 1998; Bakkali et al., 1998; Bonin et al., 1998; Grigoriev and Pshenichny 1998; Küster and Harms 1998; Ma et al., 1998; Glebovitsky et al., 2001). When the so-called 'subduction signature' is found in intrusions which clearly 'post-date collision', it is usually suggested that the source of the magmas had been generated during the preceding subduction (e.g. Liégeois, 1998).

In the southern African context, the negative HFSE (Nb and Ta in particular) anomalies are also found in kimberlites, Ventersdorp and Karoo continental flood basalts- all of which outcrop in the Kaapvaal Craton (Becker and le Roex, 2006; Crow and Condie, 1988; Marsh et al., 1992; Nelson et al., 1992; Marsh et al., 2007). The line of reasoning for such signature in these basalts and kimberlites of the Kaapvaal Craton is that the source had a subduction component

(e.g. Becker and le Roex, 2006; Marsh et al., 2007). The Ventersdorp volcanics and Karoo basalts have an age difference of more than two billion years. It is therefore unlikely that a subduction component could have resided in the mantle below the Kaapvaal Craton for such a long period without being homogenised by convection. Likewise, the fact that primitive mantle normalised patterns for the TTGs in the Limpopo Belt, and the Matok pluton granitoids show negative anomalies of Nb and Ta does not imply all these rocks have a subduction component. On these grounds, negative anomalies of the HFSE do not always imply a subduction, and the Matok pluton is possibly just one of those rocks with no subduction component.

Both crustal thickening and magmatic underplating have the potential to induce granulite-facies metamorphism and melting of the middle to lower crust (Guffanti et al., 1996; Kramers et al., 2001; Sizova et al., 2010; Bédard, 2006; Bonin et al., 1998). Kramers et al. (2001) have investigated the heat producing elements (Th, U and K) in the SMZ and deduced that the observed peak metamorphic conditions are much higher than the geothermal gradient that prevailed at the time of granulite facies metamorphism. Based on these observations, it can then be speculated that the single P-T loop observed in the SMZ (Stevens and van Reenen, 1992a) was accomplished owing to the underplated mafic magmas which were simulated by the Ventersdorp mantle plume. The similarity in Nb/Ta ratios of the Matok pluton and the Ventersdorp volcanics, together with the near synchronous age of the (~2.7 Ga) Ventersdorp volcanics, (~2.69 Ga) granulite facies metamorphism and (~2.67 Ga) emplacement of the Matok pluton corroborate on this relationship. This connection suggests that the Matok pluton formed from the then just underplated magmas, explaining why the Matok granitoids record a mantle oxygen isotope signature (Vennemann and Smith 1992; Hoernes and van Reenen, 1992). Mantle-sourced young underplated basaltic magmas are isotopically similar to their source (Liégeois, 1998).

Because there is no evidence of the existence of the Ventersdorp volcanics right within the Limpopo Belt, a possibility holds that the Ventersdorp mantle plume magmas were stalled and impeded underneath the Limpopo Belt (e.g. Hatton, 1995). A plume activity may be observed within a couple of hundreds of kilometres away from the plume centre but the horizontal extent may be even larger (Lubnina et al., 2010). This implies that the axis of the Ventersdorp mantle plume must have been to the south and southwest of the Limpopo Belt where the Ventersdorp volcanics outcrop (see Fig. 1a) but the horizontal extent must have been larger and extended as far as the Limpopo Belt where the plume magmas were impeded from extruding but rather underplated.

The climax of the plume impact which presumably generated the largest volume of underplated mafic magmas must have coincided with peak metamorphic conditions in the SMZ and in the Limpopo Belt as a whole to account for the observed regional high grade metamorphism (during the Neoarchaean) and subsequent wide spread magmatic intrusions. As the plume impact waned (and so was the amount of heat emanating from the underplated magmas), only retrograde metamorphism was feasible in the context of the SMZ, thus accounting for the characteristic single P-T loop (see Stevens and van Reenen, 1992a). This plume-induced metamorphism model is in accord with the observation of Smit et al. (1992) and Stevens and van Reenen (1992a, b) that retrograde path in the SMZ occurred under isobaric conditions.

The additional granulite facies metamorphism observed in the NMZ and CZ (see section 2.1) is the potential objection to the suggested plume-induced metamorphism. However, the observation that both zones had high enough geothermal gradients to have induced such metamorphism (Berger and Rollinson, 1997; Kramers et al., 2001) suggests that localised *in situ* radiogenic heat generated from within the crust played a role as well. Thus, while the plume is accountable for the regional (in the whole Limpopo Belt) high-grade metamorphism, the other high-grade metamorphism events unique to each of the NMZ and CZ were potentially accomplished via *in situ* radiogenic heat. Since it is unlikely that the *in situ* radiogenic heat would produce multiple granulite facies metamorphism in period of a few million years at a particular area, the observation that for instance the 2.0 Ga granulite-facies metamorphism was rather widespread than regional within the CZ (Buick et al., 2007; Millonig et al., 2008) resolves this issue. Short scale (localised) metamorphism is a consequence of an *in situ* radiogenic heat built-up generated from within the crust while large scale regional metamorphism is more likely a consequence of a plume impact (e.g. Guillou-Frottier, 1995; Burov et al., 1998; Jaupart and Mareschal, 1999; Perry et al., 2006; Michaut, 2009).

Although the cause of high-grade metamorphism in the Limpopo Belt is as argued above, the deformation which occurred jointly with metamorphism demands an explanation as well. Neither the Neoarchaean (Barton and van Reenen, 1992; de Wit et al., 1992; McCourt and Vearncombe, 1992; Smit et al., 1992) nor the Proterozoic collision model (~2.0 Ga; Kamber et al., 1995; Holzer et al., 1998, 1999; Schaller et al., 1999; Kreissig et al., 2001) resolve the architectural structure of the Limpopo Belt. The Neoarchaean collision which is based upon an inferred subduction (de Wit et al., 1992) fails to account for the inward dipping North Limpopo Thrust zone and the HRSZ (de Beer and Stettler, 1992; McCourt and Vearncombe, 1992) as well as the Proterozoic granulite-facies metamorphism observed in the CZ but absent in the marginal zones. The 2.0 Ga collision model which suggests the CZ as an exotic block does not account for

why the general trend in the CZ and magmatic foliation in the plutons therein (McCourt and Armstrong, 1998; Millonig et al., 2008) is similar to that observed in the two marginal zones. Moreover, the Proterozoic collision would imply that the amalgamation occurred at least six hundred million years after the Matok pluton emplacement. Then again, the ENE-WSW trending magmatic mineral foliation in the Neoarchaean Matok pluton, which points to a syn-kinematic emplacement, would not just be a coincidence. Moreover, collision at 2.0 Ga should have induced metamorphism in the Matok pluton.

In view of these controversies, what comes into ones mind is, does the Limpopo Belt truly represent a collision between Kaapvaal and Zimbabwe Cratons and/or between the CZ and Kaapvaal and Zimbabwe Cratons? Answering this question is best viewed in the context of a model which suggests that a linear zone of weakness within a big craton may form due to a mantle plume impact (Kröner, 1977) and/or in response to far field forces occurring at the margins of a craton (e.g. Guillou-Frottier, 1995; Burov et al., 1998; Jaupart and Mareschal, 1999; Perry et al., 2006; Michaut, 2009). Though the cause of this weakness localisation is unknown it is likely that the forces, either from the mantle plume or the craton margins, may not be strong enough to rapture/rift the crust. Failure to rapture may simply lead to a linear zone of weakness (Kröner, 1977) which then becomes more vulnerable to deformation and metamorphism. Deformation will then manifest in the form of ductile behaviour at lower crustal levels while in the upper crust is brittle (Perry et al., 2006).

The more feasible solution to the Limpopo Belt therefore is that the belt represents an intracratonic 'weak zone' which formed due to a positive feedback between the Ventersdorp mantle plume and stresses occurring at the margins of a Kalahari Craton, during the Neoarchaean. The ~2.7 Ga extrusion of the Ventersdorp volcanics and the regional Neoarchaean tectonothermal events along the northern margin of Zimbabwe Craton (Vinyu et al., 2001) and in the south-eastern Kaapvaal Craton (Elworthy et al., 2000) must have been instrumental in the establishment of the Limpopo Belt. The Neoarchaean activity on the margins of the Kaapvaal Craton may have been widespread and obliterated subsequently by the establishment of the Proterozoic Namaqua-Natal Mobile Belt. The observation that the SMZ rocks are equivalent to those in the Kaapvaal Craton (as is the case with the NMZ and Zimbabwe Craton) and the gradational contact between the Kaapvaal Craton and the SMZ (Mason, 1973) point to confinement of deformation and metamorphism within one Province; the Kalahari Craton.

The Proterozoic high grade metamorphism observed in the CZ but absent in the marginal zones and the reactivation of shear zones in the NMZ (Kamber et al., 1995a, b) correspond well with the establishment of the ~2.0 Ga Kheiss, Magondi and Okwa Belts that

surround Kaapvaal and Zimbabwe Cratons (see Fig. 1; James et al., 2003). The *in situ* radiogenic heat may have been responsible, without the requirement of a plume impact. It is nonetheless also possible that the mantle sourced ~ 2.0 Ga Bushveld Igneous Complex (see Fig. 1a) which was emplaced to the south of the Limpopo Belt (Lubnina et al., 2010; Olsson et al., 2010) points to another plume influence. It can be argued that the axial plane of the plume had shifted and was less intense at ~2.0 Ga. In this case it can be argued that the focus of the weakest zone within the Kalahari Craton had 'shrinked' and was confined only to the CZ, which was inherently more vulnerable. Because the CZ comprises the oldest rocks in the Kalahari Craton (Griffin et al., 2003), it must have been easier to localise strain around it in response to the tectonic activity on the margins of the Kalahari Craton or even a minor plume impact, or it could have just been a coincidence.

9. SUMMARY AND CONCLUSIONS

Petrography and geochemical characteristics of the Matok pluton granitoids were studied with the intention of proposing a petrogenetic model. The petrography of the different granitoids was described and distinction between magmatic and subsolidus minerals was made. Preservation of magmatic minerals and textures in the px-diorites1 which field evidence suggests they were subjected to deformation prior to intrusion of the second episode of magmatic injection implies that no major geochemical alteration was accomplished in those rocks. This is further corroborated by no major differences in the geochemistry of both intrusion phases. Geochemical data was further used to suggest how one pluton can comprise granitoids of anhydrous high temperature mineral assemblage (px-bearing) as well as those of hydrous low temperature mineral assemblages (px-free).

9.1. Field, petrography and mineral chemistry perspective

The establishment of fracture zones (e.g. the HRSZ) in the SMZ assisted and facilitated the ascend of the Matok melt from the lower crust. Although the reactivation of the HRSZ, as suggested by Smit et al. (1992) could have been instrumental in the episodic nature of the Matok pluton, the reactivation is not necessarily a requirement since it can be fairly concluded that the intrusion episodes were broadly synchronous. The ductile deformation which had led to the development of gneissocity in the px-diorites1 and px-free granodiorite gneiss (G5; Fig. 2) of the Matok pluton does not necessitate to have happened long after these rocks were emplaced. These rocks, like all other rocks in the Matok pluton preserve the ENE-WSW magmatic foliation that parallels the Limpopo Belt trend, attesting to a syntectonic emplacement.

Although not always present in the px-bearing granitoids, orthopyroxene is a high temperature mineral which its presence resembles a magma that crystallised under relatively anhydrous and high temperature conditions. The dominance of clinopyroxene over orthopyroxene alludes to the calc-alkaline nature of the Matok pluton. The px-free granitoids on the other hand are, in addition to hornblende and biotite, characterised by magmatic titanite and epidote as the mafic minerals. The incompatibility of magmatic titanite and epidote with pyroxene as well as a decline in modal abundances of ilmenite and magnetite with titanite and epidote in the Matok pluton granitoids affirms to the slightly different evolution, subsequent to segregating from the magma chamber(s). Likewise, the similarity in mineral assemblages and

textures, but difference in mineral modal abundances within the px-free granitoids is suggestive of magma batches which had only a slight difference in chemical composition, rather than fO_2 and fH_2O. A group of granitoids (px-free granites with > 71 wt.% SiO_2) lack hornblende and epidote. These rocks evolved, possibly, via combined processes of hornblende fractionation and assimilation of country rocks.

Geothermobarometric calculations reveal no significant difference in recorded temperatures (and pressure) of magmatic hornblende of px-bearing and px-free granitoids. In addition, the Fe^{3+}/Fe^{2+} ratio of both hornblende and ilmenite of px-bearing and px-free granitoids is similar, suggesting both suites to have had, initially, similar fO_2 conditions. Ilmenite is one of the earliest phases to have crystallised in both px-bearing and px-free granitoids. The evolution of the px-free granitoid magmas rather progressed into higher fO_2 conditions which led to the establishment of magmatic epidote and titanite. It was during the protracted molten state of px-free granitoid magmas that the initially crystallised pyroxene reacted with the melt and therefore did not survive to the subsolidus.

9.2. Geochemical perspective

Major element data illustrate that the px-bearing granitoids are mainly of dioritic and granodioritic composition while px-free granitoids are dominated by rocks of granodioritic and granitic composition. The similarity in the incompatible trace elements between the px-bearing and px-free granitoids rather calls for a common source. This means that the dominance of dioritic and granodioritic composition in the px-bearing granitoids could have been a coincidence, or can be attributed to magma zonation (a process analogous to sector zoning in minerals) most probably while in the magma chamber. The magma zonation impacted on the degree of silica saturation and associated level of polymerisation (relative abundances of major element oxides), but ensured a homogenised level of incompatible trace element (excluding highly fluid mobile Th, U, Cs, Rb and K) saturation in all the 'zones'. Alternatively, each of the px-bearing and px-free granitoid suites had a separate magma chamber but the sources of which were genetically related, to account for the similarity in HFSE and REE distributions. In this scenario partial melts of px-free granitoids were generated under relatively hydrous conditions to account for the higher abundances of fluid mobile elements (Th, U, Cs, Rb and K).

The refractory trace elements (Nb and Ta) provide invaluable information regarding the source of the Matok pluton. The continental crust is notoriously known for its subchondritic Nb/Ta ratio. The Matok pluton granitoids have superchondritic Nb/Ta ratio that plot in the field of (and above) the Ventersdorp volcanics. It is widely accepted that superchondritic Nb/Ta ratio

signifies a source in the lower mantle. The lack of MgO, Ni and Cr mantle signature in the Matok pluton granitoids suggests a source not in the mantle, but in the crust. It is therefore proposed that the Matok pluton owes its existence to a source with composition similar to that of Ventersdorp volcanics via partial melting of ~80% F. The Matok melts were generated from a juvenile crust that had formed from 'just' underplated magmas owing to the Ventersdorp mantle plume. The requirement is that the underplates had not yet endured any enrichment (metasomatism) or depletion events so that no other differentiation processes would have obliterated such signature in the Matok incompatible trace elements. The source discrepancy between the Nb/Ta ratio (mantle) and Cr and Ni (just underplated crust) in the Matok pluton granitoids lies in the fact that both Cr and Ni are compatible elements and their compatibility depended on the presence of accommodating residual phases while the incompatible trace elements (Nb and Ta) concentrations were governed largely by their partitioning coefficient in the melt.

Negative anomalies of Nb, Ta and Ti on primitive mantle normalised diagrams are popularly suggested to signify a subduction component. In addition to these anomalies, the Matok granitoids have negative Th, U, Sr and Eu anomalies, which are not related to subduction, and all these anomalies have been a product of a single process in the Matok melts. It is therefore concluded that negative anomalies of Nb, Ta and Ti on primitive mantle normalised diagrams do not always imply a subduction. This argument is supported by the observation that the plume-sourced Neoarchaean Ventersdorp volcanics and the Mesozoic Karoo continental flood basalts also have negative Nb and Ta anomalies on primitive mantle normalised diagrams. It is highly unlikely that a subduction component would reside in the mantle underneath the Kaapvaal Craton for a period of two billion years without being homogenised by convection.

The syntectonic emplacement of the Matok pluton and all other plutons of similar age in the Limpopo Belt as well as the concurrent regional granulite facies metamorphism suggest that the regional high grade metamorphism experienced across the Limpopo Belt was due to magma underplating that was formed by the Ventersdorp mantle plume. Since the SMZ has been suggested to have undergone a single regional P-T loop in the Neoarchaean, it can fairly be proposed that it was the underplated mafic magmas that provided heat to induce metamorphism in the SMZ. The climax of magmatic underplating at the lower crust coincided with peak metamorphic conditions while the decline (due to the waning plume activity) in underplates generation ensured the isobaric cooling experienced in the SMZ.

REFERENCES:

Ajaji, T., Weis, D., Giret, A., Bouabdellah, M., 1998. Coeval potassic and sodic calc-alkaline series in the post-collisional Hercynian Tanncherfi intrusive complex, northeastern Morocco: geochemical, isotopic and geochronological evidence. Lithos 45, 371-393.

Anderson, J.L., Smith, D.R., 1995. The effects of temperature and fO_2 on the Al-in hornblende barometer. American Mineralogist 80, 549-559.

Archanjo, C.J., Macedo, J.W.P., Galindo, A.C., Araújo, M.G.S., 1998. Brasiliano crustal extension and emplacement fabrics of the mangerite-charnockite pluton of Umarizal, north-east Brazil. Precambrian Research 87, 19-32.

Arculus, R. J., 2003. Use and abuse of the terms calc-alkaline and calcalkalic. Journal of Petrology 44(5), 929-935.

Armstrong, R.A., Compston, W., de Wit, M. J., Williams, I. S., 1990. The stratigraphy of the 3.5-3.2 Ga Barberton Greenstone Belt revisited: a single zircon ion microprobe study. Earth and Planetary Science Letters 101, 90-106.

Bakkali, S.E., Gourgaud, A., Bourdier, J-L., Bellon, H., Gundogdu, N., 1998. Post-collision neogene volcanism of the Eastern Rif (Morocco): magmatic evolution through time. Lithos 45, 523-543.

Baker, J., van Reenen, D.D., van Schalkwyk, J.F., Newton, R.C., 1992. Constraints on the composition of fluids involved in retrograde anthophyllite formation in the Limpopo Belt, South Africa. Precambrian Research 55, 327-336.

Barbarin, B., 1999. A review of the relationships between granitoid types, their origins and their geodynamic environments. Lithos 46, 605-626.

Barbey, P., Gasquet, D., Pin, C., Bourgeix, A.L., 2008. Igneous banding, schlieren and mafic enclaves in calc-alkaline granites: the Budduso pluton (Sardinia). Lithos 104(1-4), 147-163.

Barry, T.L., Pearce, J.A., Leat, P.T., Millar, I.L., le Roex, A.P., 2006. Hf isotope evidence for selective mobility of high-field-strength elements in a subduction setting: South Sandwich Islands. Earth and Planetary Science Letters 252, 223-244.

Barth, M.G., McDonough, W.F., Rudnick, R.L., 2000. Tracking the budget of Nb and Ta in the continental crust. Chemical Geology 165 (3–4), 197–213.

Barton Jr., J.M., van Reenen, D.D., 1992. When was the Limpopo Orogeny? Precambrian Research 55, 7-16.

Barton Jr., J.M., Doig, R., Smith, C.B., Bohlender, F., van Reenen, D.D., 1992. Isotopic and REE characteristics of the intrusive charnoenderbite and enderbite geographically associated with the Matok pluton, Limpopo Belt, southern Africa. Precambrian Research 55, 451 - 467.

Becker, M., le Roex, A.P., 2006. Geochemistry of South African on- and off-craton, Group I and Group II kimberlites: Petrogenesis and source region evolution. Journal of Petrology 47, 673-703.

Bédard, J.H, 2006. A catalytic delamination-driven model for coupled genesis of Archaean crust and sub-continental lithospheric mantle. Geochimica et Cosmochimica Acta 70, 1188–1214.

Bedini, R.M., Bodinier, J.-L., 1999. Distribution of incompatible trace elements between the constituents of spinel peridotite xenoliths: ICP-MS data from the East African rift, Geochimica et Cosmochimica Acta 63, 3883-3900.

Berger, M., Kramers, J.D., Nägler, T.F., 1995. Geochemistry and geochronology of charnoenderbites in the Northern Marginal Zone of the Limpopo Belt, southern Africa, and genetic models. Schweizer Mineralogisch Petrographische Mitteilungen 75, 17–42.

Berger, M., Rollinson, H., 1997. Isotopic and geochemical evidence for crust-mantle interaction during late Archaean crustal growth. Geochimica et Cosmochimica Acta 61(22), 4809-4829.

Best, M.G., Christiansen, E.H., 2001. Igneous petrology, 458pp. Massachusetts, Blackwell Science.

Bialek, D., 1999. Chemical changes associated with deformation of granites under greenschist facies conditions: the example of the Zawidów granodiorite (SE Lusatian granodiorite Complex, Poland). Tectonophysics 303, 251-261.

Blenkinsop, T.G., Mkweli, S., Rollinson, H.R., Fedo, C.M., Paya, B.K., Kamber, B.S., Kramers, J.D., Berger, M., 1995. The Limpopo Thrust Zone (NLTZ): The northern boundary of the Limpopo Belt in Zimbabwe and Botswana. In: Barton Jr., J. M., Copperthwaite, Y. E., (eds.), Extended Abstracts. Centennial Geocongress 1995, volume 1, Geological Society of South Africa, Johannesburg, South Africa, pp. 174-177.

Blenkinsop, T. G., Kroner, A., Chiwara, V., 2004. Single stage, late Archaean exhumation of granulites in the Northern Marginal Zone, Limpopo Belt, Zimbabwe, and relevance to gold mineralization. South African Journal of Geology 107 (3), 377-396.

Bodinier, J.-L. Merlet, C., Bedini, R.M. Simien, F. Remaidi, M. Garrido, C.J., 1996. Distribution of niobium, tantalum, and other highly incompatible trace elements in the lithospheric mantle: the spinel paradox, Geochimica et Cosmochimica Acta 60, 545-550.

Bohlender, F., van Reenen, D.D., Barton Jr., J.M., 1992. Evidence for metamorphic and igneous charnockites in the southern marginal zone of the Limpopo Belt. Precambrian Research 55, 429-449.

Bohlender, F., 1992. Igneous and metamorphic charnockitic rocks in the southern marginal zone of the Limpopo Belt with special emphasis on the Matok enderbitic -granitic suite. Ph.D. thesis (Unpublished), Rand Afrikaans University-Johannesburg.

Bonin, B., Azzouni-Sekkal, A., Bussy, F., Ferrag, S., 1998. Alkali-calcic and alkaline post-orogenic (PO) granite magmatism: petrologic constraints and geodynamic settings. Lithos 45, 45-70.

Borg, L.E., Clynne, M.A., 1998. The Petrogenesis of felsic Calc-alkaline magmas from the Southernmost Cascades, California: origin by partial melting of basaltic lower crust. Journal of Petrology 39(6), 1197-1222.

Boshoff, R., Van Reenen, D.D., Smit, C.A., Perchuk L.L., Kramers J.D., Armstrong, R. 2006. Geologic history of the Central Zone of the Limpopo Complex: the West Alldays Area. Journal of Geology 114, 699-716.

Bowen, N.L., 1928. The evolution of igneous rocks. Princeton, N. J., Princeton University Press.

Brandon, A.D., Creaser, R.A., Chacko, T., 1996. Constraints on rates of granitic magma transport from epidote dissolution kinetics. Science 271, 1845–1848.

Broska, I., Harlov, D., Tropper, P., Siman, P., 2007. Formation of magmatic titanite and titanite–ilmenite phase relations during granite alteration in the Tribeč Mountains, Western Carpathians, Slovakia. Lithos 95, 58-71.

Buick, I. S., Hermann, J., Williams, I. S., Gibson, R. L., Rubatto, D., 2006. A SHRIMP U–Pb and LA-ICP-MS trace element study of the petrogenesis of garnet–cordierite–orthoamphibole gneisses from the Central Zone of the Limpopo Belt, South Africa. Lithos 88, 150–172.

Buick, I. S., Hermann, J., Maas, R., Gibson, R. L., 2007. The timing of sub-solidus hydrothermal alteration in the Central Zone, Limpopo Belt (South Africa): Constraints from titanite U-Pb geochronology and REE partitioning. Lithos 98, 97–117.

Burov, E., Jaupart, C., Mareschal, J.C. 1998. Large-scale crustal heterogeneities and lithospheric strength in cratons. Earth and Planetary Science Letters 164, 205–219.

Caprarelli, G., Leitch, E.C., 1998. Magmatic changes during the stabilisation of a cordilleran fold belt: the Late Carboniferous–Triassic igneous history of eastern New South Wales, Australia. Lithos 45, 413-430.

Cawthorn, R. G., O'Hara, M. J., 1976. Amphibole fractionation in calc-alkaline magma genesis. American Journal of Science 276, 309–329.

Chappell, B.W., White, A.J.R., 1992. I- and S-type granites in the Lachlan Fold Belt. Transactions of Royal Society of Edinburgh: Earth Science 83, 1–26.

Chappell, B.W., White, A.J.R., Wyborn, D., 1987. The importance of residual source material (restite) in granite petrogenesis. Journal of Petrology 28, 1111–1138.

Class, C., le Roex, A.P., 2008. Ce anomalies in Gough Island lavas-Trace element characteristics of a recycled sediment component. Earth and Planetary Science Letters 265, 475–486

Clarke, D.B., 1992. Granitoids Rocks. Topics in the Earth Sciences, London, Chapman and Hall, Volume 7, 283 pp.

Clemens, J.D., Mawer, C.K., 1992. Granitic magma transport by fracture propagation. Tectonophysics 204, 339– 360.

Clemens, J.D., Droop G.T.R., 1998. Fluids, P–T paths and the fates of anatectic melts in the Earth's crust. Lithos 44, 21-36.

Clemens, J.D., 2005. Granites and granitic magmas: strange phenomena and new perspectives on some old problems. Proceedings of the Geologists ' Association 116, 9-16.

Clemens, J.D., Darbyshire, D.P.F., Flinders, J., 2009. Sources of post-orogenic calc-alkaline magmas: The Arrochar and Garabal Hill–Glen Fyne complexes, Scotland. Lithos 112, 524-542.

Condie, K.C., 2005. High field strength element ratios in Archean basalts: a window to evolving sources of mantle plumes? Lithos 79, 491-504.

Consolmango, G.J., Drake, M.J., 1976. Equivalence of equations describing trace element distribution during equilibrium partial melting. Geochimica et Cosmochimica Acta 40, 1421-1422.

Coward, M.P., James, P.R., Wright, L., 1976. Northern margin of the Limpopo mobile belt, southern Africa. Geological Society of America Bulletin 87, 601-611.

Cox, K.G., Johnson, R.L., Monkman, L.J., Stillman, C.J., Vail, J.R., Wood, D.N., 1965. The geology of the Nuanetsi igneous province. Philosophical Transactions Royal Society of London, A 257, 71-218.

Cox, K.G., Bell, J. D., Pankhurst, R. J., 1979. The interpretation of igneous rocks, 450pp. London Boston G. Allen & Unwin.

Crow, C., Condie, K.C., 1988. Geochemistry and origin of late Archean volcanics from the Ventersdorp Supergroup, South Africa. Precambrian Research 42(1-2), 19-37.

de Beer, J.H., Stettler, E.H., 1992. The deep structure of the Limpopo Belt from geophysical studies. Precambrian Research 55, 173-186.

Deer, W.A., Howie, R.A., Zussman, J., 1992. An introduction to the rock forming minerals, 696 pp. England, Pearson Prentice Hall.

Deer, W.A., Howie, R.A., Zussman, J., 1963. Rock-forming minerals. Volume 2-chain silicates. Great Britain, Longman.

DePaolo, D.J., Farmer, G.L., 1984. Isotopic data bearing on the origin of Mesozoic and Tertiary granitic rocks in the western United States. Philosophical Transactions of the Royal Society of London, A 310, 743–753.

de Silva, S.L., Wolff, J.A., 1995. Zoned magma chambers: the influence of magma chamber geometry on sidewall convective fractionation. Journal of Volcanology and Geothermal Research 65, 111-118.

de Wit, M.J., Roering, C., Hart, R.J., Armstrong, R.A., de Ronde, C.E.J., Green, R.W.E., Tredoux, M., Peberdy, E., Hart, R.A., 1992. Formation of an Archean continent. Nature 357, 553– 562.

Droop, G.T.R., 1987. A general equation for estimating Fe^{3+} concentrations in ferromagnesian silicates and oxides from microprobe analyses, using stoichiometric criteria. Mineralogical Magazine 51, 431-435.

Duchesne, J-C., Wilmart, E., 1997. Igneous charnockites and related rocks from the Bjerkreim-Sokndal layered intrusion (south west Norway): a jotunite Hypersthene monzodiorite)-derived A-type granitoid suite. Journal of Petrology 38(3), 337-369.

Durrheim, R.J., Barker, W.H., Green, R.W.E, 1992. Seismic studies in the Limpopo Belt. Precambrian Research 55, 187-200.

du Toit, M.C., van Reenen, D.D., Roering, C., 1983. Some aspects of the geology, structure and metamorphism of the Southern Marginal Zone of the Limpopo metamorphic Complex. Special Publication, Geological Society of South Africa 8, 121-142.

Eglington, B.M., Armstrong, R.A., 2004. The Kaapvaal Craton and adjacent orogens, southern Africa: a geochronological database and overview of the geological development of the craton. South African Journal of Geology 107 (1-2), 13-32.

Eklund, O., Konopelko, D., Rutanen, H., Fröjdö, S., Shebanov, A.D., 1998. 1.8 Ga Svecofennian post-collisional shoshonitic magmatism in the Fennoscandian shield. Lithos 45, 87-108.

El Aouli, E.H., Gasquet, D., Cheilletz, A., 2010. Lower Cryogenian calc-alkaline mafic rocks of the Western Anti-Atlas (Morocco): An example of orogenic-like magmatism in an extensional setting. Journal of African Earth Sciences 58, 81–88.

Elworthy, T., Eglington, B. M., Armstrong, R.A., Moyes, A.B., 2000. Rb-Sr isotope constraints on the timing of late to post-Archaean tectonometamorphism affecting the southeastern Kaapvaal Craton. Journal of African Earth Sciences 30(3), 641-650.

Eriksson, P.G., Altermann, W., Catuneanu, O., van der Merwe, R., Bumby, A.J., 2002. Major influences on the evolution of the 2.67-2.1 Ga Transvaal basin, Kaapvaal Craton. Sedimentary Geology 141-142, 205-231.

Eriksson, P.G., Condie, K.C., van der Westhuizen, W., van der Merwe, R., de Bruiyn, H., Nelson, D.R., Altermann, W., Catuneanu, O., Bumby, A.J., Lindsay, J., Cunningham, M.J., 2002. Late Archaean superplume events: a Kaapvaal–Pilbara perspective. Journal of Geodynamics 34, 207–247.

Evans, B.W., Vance, J.A., 1987. Epidote phenocrysts in dacitic dikes, Boulder county, Colorado. Contribution to Mineralogy and Petrology 96, 178-185.

Eyal, M., Litvinovsky, B.A., Katzir, Y., Zanvilevich, A. N., 2004. The Pan-African high-K calc-alkaline peraluminous Elat granite from southern Israel: geology, geochemistry and petrogenesis. Journal of African Earth Sciences 40, 115–136.

Farrow, C.E.G., Barr, S.M., 1992. Petrology of high-Al-hornblende- and magmatic-epidote-bearing plutons in the southeastern Cape Breton Highlands, Nova Scotia. Canadian Mineralogist 30, 377-392.

Ferré, E.C., Caby, R., Peucat, J. J., Capdevila, R., Monie, P., 1998. Pan-African, post-collisional, ferro-potassic granite and quartz–monzonite plutons of Eastern Nigeria. Lithos 45, 255-279.

Fraga, D.M., Buenano Macambira, M.J., Dall'Agnol, R., Sena Costa, O.B., 2009. 1.94-1.93 Ga charnockitic magmatism from the central part of the Guyana Shield, Roraima, Brazil: single zircon evaporation data and tectonic implications. Journal of South American Earth Sciences 27(4), 247-257.

Frei, R., Blenkinsop, T.G., Schonberg, R., 1999. Geochronology of the Late Archaean Razi and Chilimanzi suites of granites in Zimbabwe: Implications for the Late Archaean tectonics of the Limpopo Belt and Zimbabwe Craton. South African Journal Geology 102, 55-63.

Frost, B.R., Lindsley, D.H., 1992. Equilibria among Fe–Ti oxides, pyroxenes, olivine, and quartz: Part II. Application. American Mineralogist 77, 1004–1020.

Frost, B.R., Frost, C.D., 2008. On charnockites. Gondwana Research 13, 30 – 44.

Frost, B.R., Frost, C.D., Hulsebosch, T.P., Swapp, S.M., 2000. Origin of the charnockites of the Louis Lake batholith, Wind River range, Wyoming. Journal of Petrology 41, 1759–1776.

Fyfe, W.S., 1973. The granulite-facies, partial melting and the Archaean crust. Philosophical Transaction of Royal Society of London A 273, 457–462.

Gerdes, A., Zeh, A., 2009. Zircon formation versus zircon alteration - New insights from combined U–Pb and Lu–Hf in-situ LA-ICP-MS analyses, and consequences for the

interpretation of Archean zircon from the Central Zone of the Limpopo Belt. Chemical Geology 261 (3-4), 230-243.

Glebovitsky, V., Marker, M., Alexejev, N., Bridgwater, D., Sedova, I., Salnikova, E., Berezhnaya, N., 2001. Age, evolution and regional setting of the Palaeoproterozoic Umba igneous suite in the Kolvitsa–Umba zone, Kola Peninsula: constraints from new geological, geochemical and U–Pb zircon data. Precambrian Research 105, 247–267.

Goss A.R., Kay, S.M., 2009. Extreme high field strength element (HFSE) depletion and near-chondritic Nb/Ta ratios in Central Andean adakite-like lavas (~28°S, ~68°W). Earth and Planetary Science Letters 279, 97-109.

Grantham, G. H., Allen, A. R. Cornell, D. H. Harris, C. 1996. Geology of Nicholson's Point granite, Natal Metamorphic Province, South Africa: the chemistry of charnockitic alteration and origin of the granite. Journal of African Earth Sciences 23(3), 465-484.

Green, T.H., Pearson, N.J., 1987. An experimental study of Nb and Ta partitioning between Ti-rich melts and silicate liquids at high pressure and temperature. Geochimica et Cosmochimica Acta 51, 55-62.

Green, T.H., 1995. Significance of Nb/Ta as an indicator of geochemical processes in the crust-mantle system. Chemical Geology 120, 347-359.

Cribb, I. W., Barton, M., 1997. Significance of crustal and source region processes on the evolution of compositionally similar calc-alkaline lavas, Mt. Hood, Oregon. Journal of Volcanology and Geothermal Research 76, 229-249

Griffin W.L., O'Reilly, S.Y., Natapov, L.M., Ryan, C.G. 2003. The evolution of lithospheric mantle beneath the Kalahari Craton and its margins. Lithos 71, 215-241.

Grigoriev, S.I., Pshenichny, C.A., 1998. Late Mesozoic post-collisional intermediate to silicic magmatism in the Badjal area, Far East of Russia. Lithos 45, 457-468.

Guffanti, M., Clynne, M. A., Muffler, L. J. P., 1996. Thermal and mass implications of magmatic evolution in the Lassen volcanic region, California, and constraints on basalt influx to the lower crust. Journal of Geophysical Research 101**,** 3001–3013.

Guillou-Frottier, L., Mareschal, J.C., Jaupart, C., Gariépy, C., Lapointe, R., Bienfait, G., 1995. Heat flow variations in the Grenville Province, Canada. Earth and Planetary Science Letters 136, 447-460.

Halla, J., 2005. Late Archean high-Mg granitoids (sanukitoids) in the southern Karelian domain, eastern Finland: Pb and Nd isotopic constraints on crust-mantle interactions. Lithos 79, 161-178.

Hammarstrom, J.M., Zen, E-an., 1986. Aluminum-in-hornblende: an empirical igneous geobarometer. American Mineralogist 71, 1297– 1313.

Hatton, C. J., 1995. Mantle plume origin for the Bushveld and Ventersdorp magmatic provinces. Journal of African Earth Science 21(4), 571-577.

Hess, P.C., 1989. Origins of igneous rocks, 336 pp. Massachusetts, Harvard College.

Hickman M.H., 1978. Isotopic evidence for crustal reworking in the Rhodesian Archaean Craton, southern Africa. Geology 6, 214-216.

Hin, R.C., Morel, M.L.A., Nebel, O., Mason, P.R.D., van Westrenen, W., Davies, G.R., 2009. Formation and temporal evolution of the Kalahari sub-cratonic lithospheric mantle: constraints from Venetia xenoliths, South Africa. Lithos 112S, 1069–1082.

Hoernes, S., van Reenen, D.D., 1992. The oxygen-isotopic composition of granulites and retrogressed granulites from the Limpopo Belt as a minor fluid-rock interaction. Precambrian Research 55, 353-364.

Hofmann, A.W., 1997. Mantle geochemistry: the message from oceanic volcanism. Nature 385, 219-229.

Holland, T., Blundy, J., 1994. Non-ideal interactions in calcic amphiboles and their bearing on amphibole-plagioclase thermometry. Contributions to Mineralogy and Petrology 116, 433–447.

Hollister, L.S., Grissom, G.C., Peters, E.K., Stowell, H.H., Sisson, V.B., 1987. Confirmation of the empirical correlation of Al in hornblende with pressure of solidification of calc-alkaline plutons. American Mineralogist 72, 231-239.

Holtz, F., Johannes, W., Tamic, N., Behrens, H., 2001. Maximum and minimum water contents of granitic melts generated in the crust: a reevaluation and implications. Lithos 56, 1-14.

Holzer, L., Frei, R., Barton Jr., J.M., Kramers, J.D., 1998. Unravelling the record of successive high grade events in the Central Zone of the Limpopo belt using Pb single phase dating of metamorphic minerals. Precambrian Research 87, 87–115.

Holzer, L., Barton Jr., J.M., Paya, B.K., Kramers, J.D., 1999. Tectonothermal history in the western part of the Limpopo belt: Test of the tectonic models and new perspectives. Journal of African Earth Sciences 28, 383–402.

Hoorwood, C.B., 1910. Notes and analyses of typical Transvaal rocks. Transactions of the Geological Society of South Africa 13, 29-55.

Jackson, M.D., Gallagher, K., Petford, N., Cheadle, M.J., 2005. Towards a coupled physical and chemical model for tonalite–trondhjemite–granodiorite magma formation. Lithos 79, 43-60.

James, D.E., Niu, F., Rokosky, J., 2003. Crustal structure of the Kaapvaal craton and its significance for early crustal evolution. Lithos 71, 413– 429.

Jaupart, C., Mareschal, J.C., 1999. The thermal structure and thickness of continental roots. Lithos 48, 93-114.

Johannes, W., Holtz, F., 1990. Formation and composition of H_2O-saturated granite melts. In: Ashworth, J. R., Brown, M., (eds.). High-temperature metamorphism and crustal anatexis. London, Unwin Hyman pp. 87-104.

Kalfoun, F., Ionov, D., Merlet, C., 2002. HFSE residence and Nb/Ta ratios in metasomatised, rutile-bearing mantle peridotites. Earth and Planetary Science Letters 199, 49-65.

Kamber, B.S., Kramers, J.D., Napier, R., Cliff, R.A., Rollinson, H.R., 1995a. The Triangle shear zone, Zimbabwe, revisited: new data document an important event at 2.0 Ga in the Limpopo belt. Precambrian Research 70, 191–213.

Kamber, B.S., Blenkinsop, T.G., Villa, I.M., Dahl, P.S., 1995b. Proterozoic transpressive deformation in the Northern Marginal Zone, Limpopo Belt, Zimbabwe. Journal of Geology 103, 493–508.

Kamber, B.S., Biino, G.G., 1995. The evolution of high T–low P granulites in the Northern Marginal Zone sensu stricto, Limpopo Belt, Zimbabwe-the case for petrography. Schweizerische Mineralogische und Petrographische Mitteilungen 75, 427–454.

Kampunzu, A.B., Tombale, A.R., Zhai, M., Bagai, Z., Majaule, T., Modisi, M.P., 2003. Major and trace element geochemistry of plutonic rocks from Francistown, NE Botswana: evidence for a Neoarchaean continental active margin in the Zimbabwe craton. Lithos 71, 431-460.

Keane, S., Morrison, J., 1997. Distinguishing magmatic from subsolidus epidote: laser probe oxygen isotope compositions. Contributions to Mineralogy and Petrology 126, 265-274.

Key, R.M., Hutton, S.M., 1976. The western extremity of the Limpopo mobile belt, Precambrian Research 3, 79-90.

Klemme, S., Blundy, J.D., Wood, B.J., 2002. Experimental constraints on major and trace element partitioning during partial melting of eclogite. Geochimica et Cosmochimica Acta 66, 3109– 3123.

Klimm, K., Holtz, H., King, P.L., 2008. Fractionation vs. magma mixing in the Wangrah Suite A-type granites, Lachlan Fold Belt, Australia: experimental constraints. Lithos 102(3-4), 415-434.

Konopelko, D., Seltmann, R., Biske, G., Lepekhina, E., 2009. Possible source dichotomy of contemporaneous post-collisional barren I-type versus tin-bearing A-type granites, lying on opposite sides of the South Tien Shan suture. Ore Geology Reviews, 35(2), 206-216.

Kovalenko, A., Clemens, J.D., Savatenkov, V., 2005. Petrogenetic constraints for the genesis of Archaean sanukitoid suites: geochemistry and isotopic evidence from Karelia, Baltic Shield. Lithos 79, 147– 160.

Kramers, J.D., Kreissig, K., Jones, M.Q.W., 2001. Crustal heat production and style of metamorphism: A comparison between two Archean high grade provinces in the Limpopo Belt, southern Africa. Precambrian Research 112, 149-163.

Kreissig, K., Nägler, T.F., Kramers, J.D., van Reenen, D.D., Smit, C.A., 2000. An isotopic and geochemical study of the northern Kaapvaal Craton and the Southern Marginal Zone of the Limpopo Belt: Are they juxtaposed terranes? Lithos 50, 1-25.

Kreissig, K., Holzer, L., Frei, R., Villa, I.M., Kramers, J.D., Kröner, A., Smit, C.A., van Reenen D.D., 2001. Geochronology of the Hout River Shear Zone and the metamorphism in the Southern Marginal Zone of the Limpopo Belt, Southern Africa. Precambrian Research 109, 145-173.

Kröner, A., 1977. Precambrian mobile belts of southern and eastern Africa-ancient sutures or sites of ensialic mobility? A case for crustal evolution towards plate tectonics. Tectonophysics, 40, 101-135.

Kröner, A., Tegtmeyer, A., 1994. Gneiss-greenstone relationships in the Ancient Gneiss Complex of southwestern Swaziland, southern Africa, and implications for early crustal evolution. Precambrian Research 67, 109-139.

Kröner, A., Jaecke, P., Brandl, G., Nemchin, A.A., Pidgeon, R.T., 1999. Single zircon ages for granitoid gneisses in the Central Zone of the Limpopo Belt, Southern Africa and geodynamic significance. Precambrian Research 93, 299–337.

Krzemińska, E., 2005. The outline of geochemical features of the late Neoproterozoic volcanic activity in the Lublin-Podlasie Basin, eastern Poland**.** Mineralogical Society of Poland – special papers 26, 47-51.

Kuno, H., 1968. Differentiation of basalt magmas. In: Hess, H. H., Poldervaart, A. A. (eds.), Basalts: The Poldervaart treatise on rocks of basaltic composition, 2. New York, Interscience, pp. 623-688.

Kuritani, T., 2004. Magmatic differentiation examined with a numerical model considering multicomponent thermodynamics and momentum, energy and species transport. Lithos 74, 117-130.

Küster, D., Harms, U., 1998. Post-collisional potassic granitoids from the southern and northwestern parts of the Late Neoproterozoic East African Orogen: A review. Lithos 45, 177-195.

Lahaye, Y., Arndt, N., Byerly, G., Chauvel, C., Fourcade. S., Gruau, G., 1995. The influence of alteration on the trace-element and Nd isotopic compositions of komatiites. Chemical Geology 126, 43-64.

Langmuir, C.H., Vocke, R.D., Hanson, G.N., Hart, S.R. 1978. A general mixing equation with applications to Icelandic basalts. Earth and Planetary Science Letters 37, 380-392.

le Roex, A.P., Bell, D.R., Davis, P., 2003. Petrogenesis of Group I Kimberlites from Kimberley, South Africa: Evidence from Bulk-rock Geochemistry. Journal of Petrology 44 (12), 2261-2286.

Liang, J.L., Ding, X., Sun, X.M., Zhang, Z.M., Zhang, H., Sun, W.D., 2009. Nb/Ta fractionation observed in eclogites from the Chinese Continental Scientific Drilling Project. Chemical Geology 268, 27-40.

Liégeois, J._P., 1998. Preface - Some words on the post-collisional magmatism. Lithos 45, xv-xvii.

Liu, W., 2002. Fluid–rock interaction during subsolidus microtextural development of alkali granite as exemplified by the Saertielieke pluton, Ulungur of the northern Xinjiang, China. Chemical Geology 182, 473-482.

Lobach-Zhuchenko, S.B., Rollinson, H.R., Chekulaev, V.P., Arestova, N.A., Kovalenko, A.V., Ivanikov, V.V., Guseva, N.S., Sergeev, S.A., Matukov, D.I., Jarvis, K.E., 2005. The Archaean sanukitoid series of the Baltic Shield: geological setting, geochemical characteristics and implications for their origin. Lithos 79, 107-128.

Long, L.E., Castellana, H.C., Sial, A.N., 2005. Age, origin and cooling history of the Coronel João pluton, Bahia, northeastern Brazil. Journal of Petrology 46 (2), 255–273.

Lubnina, N., Ernst, R., Klausen, M., Söderlund, U., 2010. Paleomagnetic study of Neoarchaean–Paleoproterozoic dykes in the Kaapvaal Craton. Precambrian Research 183(3), 523-552.

Ma, C., Li, Z., Ehlers, C., Yang, K., Wang, R., 1998. A post-collisional magmatic plumbing system: Mesozoic granitoid plutons from the Dabieshan high-pressure and ultrahigh-pressure metamorphic zone, east-central China. Lithos 45, 431-456.

Marks, M. A. W., Coulson, I. M., Schilling, J. S., Jacob, D. E., Schmitt, A. K., Markl, G., 2008. The effect of titanite and other HFSE-rich mineral (Ti-bearing andradite, zircon, eudialyte) fractionation on the geochemical evolution of silicate melts. Chemical Geology 257, 153–172.

Marsh, J.S., Bowen, M.P., Rogers, N.W., Bowen, T.B., 1992. Petrogenesis of late Archaean flood-type basic lavas from the Klipriviersberg Group, Ventersdorp Supergroup, South Africa. Journal of Petrology 33, 817 - 847.

Marsh, J.S., Hooper, P.R., Rehacek, J., Duncan, R.A., Duncan A.R., 1997. Stratigraphy and age of Karoo basalts of the Lesotho and implications for correlations within the Karoo Igneous Province. In: Mahoney, J.J., Coffin, M.R. (eds.), Large Igneous Provinces: Continental, Oceanic and Planetary Flood Volcanism. American Geophysical Union, Washington D.C. 100, 247-272.

Martin, H., Smithies, R.H., Rapp, R., Moyen, J.-F., Champion, D., 2005. An overview of adakite, tonalite-trondhjemite-granodiorite (TTG) and sanukitoid: relationships and some implications for crustal evolution. Lithos 79, 1-24.

Marzouki, F., Kerrich, R., Fyfe, W.S., 1979. Epidotisation of diorite at Hadah, Saudi Arabia: Fluid influx into cooling pluton. Contributions to Mineralogy and Petrology 68, 281-284.

Mason, R., 1973. The Limpopo mobile Belt-southern Africa. Philosophical Transactions Royal Society of London A 273,463-485.

McCourt, S., Vearncombe, J.R., 1987. Shear zones bounding the central zone of the Limpopo mobile belt, southern Africa. Journal of Structural Geology 9, 127–137.

McCourt, S., Vearncombe, J.R., 1992. Shear zones of the Limpopo Belt and adjacent granitoid-greenstone terranes: Implication for late Archaean collision tectonics in southern Africa. Precambrian Research 55, 553-570.

McCourt, S., Armstrong, R.A., 1998. SHRIMP U-Pb zircon geochronology of granites from the central zone, Limpopo Belt, southern Africa: Implications for the age of the Limpopo Orogeny. South African Journal of Geology 101(4) 329, 338.

Michaut, C., Jaupart, C., Mareschal, J.C., 2009. Thermal evolution of cratonic roots. Lithos 109, 47-60.

Millonig, L., Zeh, A., Gerdes, A., Klemd, R., 2008. Neoarchaean high-grade metamorphism in the Central Zone of the Limpopo Belt (South Africa): Combined petrological and geochronological evidence from the Bulai pluton. Lithos 103, 333-351.

Mišković, A., Francis, D. 2006. Interaction between mantle-derived and crustal calc-alkaline magmas in the petrogenesis of the Paleocene Sifton Range volcanic complex, Yukon, Canada. Lithos 87, 104–134.

Miyashiro, A., 1974. Volcanic rocks in island arc and active continental margins. American Journal of Science 274, 321-355.

Mkweli, S., Kamber, B., Berger, M., 1995. Westward continuation of the Craton–Limpopo belt tectonic break in Zimbabwe and new age constraints on the timing of the thrusting. Journal of the Geological Society London 152, 77–83.

Mouri, H., Brandl, G., Whitehouse, M., de Waal, S., Guiraud, M., 2008. CL-imaging and ion microprobe dating of single zircons from a high-grade rock from the Central Zone, Limpopo Belt, South Africa: Evidence for a single metamorphic event at ~2.0 Ga. Journal of African Earth Sciences 50, 111–119.

Moyen, J.-F., Martin, H., Jayananda, M., 2001. Multi-element geochemical modelling of crust-mantle interactions during late-Archaean crustal growth: the Closepet granite (South India). Precambrian Research 112, 87-105.

Nachit, H., Ibhi, A., Abia, E-H., Ohoud, M. B., 2005. Discrimination between primary magmatic biotites, reequilibrated biotites and neoformed biotites. Comptes Rendus Geosciences 337, 1415–1420.

Nakada S., 1991. Magmatic processes in titanite-bearing dacites, central Andes of Chile and Bolivia. American Mineralogist 76, 548-560.

Nany, M.T., 1983. Phase equilibria of rock-forming ferromagnesian silicates in granitic systems. American Journal of Science 283, 993–1033.

Nelson, D.R. Trendall, A.F. de Laeter, J.R. Grobler, N.J. Fletcher, I.R. 1992. A comparative study of the geochemical and isotopic systematics of late Archaean basalts from the Pilbara and Kaapvaal Cratons. Precambrian Research 54 (2-4), 231-256.

Newton, R.C., 1992. An overview of charnockite. Precambrian Research 55, 399-405.

Niu, Y., O'Hara, M.J., 2009. MORB mantle hosts the missing Eu (Sr, Nb, Ta and Ti) in the continental crust: New perspectives on crustal growth, crust–mantle differentiation and chemical structure of oceanic upper mantle. Lithos 112, 1-17.

Oberthür, T., Davis, D.W., Blenkinsop, T.G., Höhndorf, A., 2002. Precise U–Pb mineral ages, Rb–Sr and Sm–Nd systematic for the Great Dyke, Zimbabwe - constraints on late Archean events in the Zimbabwe Craton and Limpopo Belt. Precambrian Research 113, 293-305.

O'Brien, H.E., Irving, A.J., McCallum, I.S., Thirlwall, M.F., 1995. Strontium, neodymium, and lead isotopic evidence for the interaction of post-subduction asthenospheric potassic mafic

magmas of the Highwood Mountains, Montana, USA, with ancient Wyoming craton lithospheric mantle. Geochimica et Cosmochimica Acta 59(21), 4539-4556.

Parman, S.W., Shimizu, N., Grove, T.L., Dann, J.C., 2003. Constraints on the pre-metamorphic trace element composition of Barberton komatiites from ion probe analyses of preserved clinopyroxene. Contributions to Mineralogy and Petrology 144, 383-396.

Pearce, J., Kempton, P., Nowell, G., 2000. The origin of HFSE anomalies in subduction zone Magmas: Evidence from Hf-Nd isotope and element covariations. Journal of Conference Abstracts 5(2), 775.

Peccerillo, A., Taylor S.R., 1976. Rare earth elements in East Carpathian volcanic rocks. Earth and Planetary Science Letters 32 (2), 121-126.

Pennacchioni, G. Di Toro, G., Brack, P., Menegon, L., Villa, I.M., 2006. Brittle–ductile–brittle deformation during cooling of tonalite (Adamello, Southern Italian Alps). Tectonophysics 427, 171-197.

Perchuk, L.L., Gerya, T.V., van Reenen, D.D., Krotov, A.V., Safonov, O.G., Smit, C.A., Shur, M. Yu., 2000a. Comparative petrology and metamorphic evolution of the Limpopo (South Africa) and Lapland (Fennoscandia) high-grade terrains. Mineralogy and Petrology 69, 69-107.

Perchuk, L.L., Gerya, T.V., van Reenen, D.D., Smit, C.A., Krotov, A.V., 2000b. P-T paths and tectonic evolution of shear zones separating high-grade terrains from cratons: examples from Kola Peninsula (Russia) and Limpopo Region (South Africa). Mineralogy and Petrology 69, 109-142.

Percival, J.A., Mortensen, J.K., 2002. Water-deficient calc-alkaline plutonic rocks of northeastern Superior Province, Canada: Significance of charnockitic magmatism. Journal of Petrology 43 (9), 1617-1650.

Perry, H.K.C., Mareschal, J.-C., Jaupart, C., 2006. Variations of strength and localized deformation in cratons: The 1.9 Ga Kapuskasing uplift, Superior Province, Canada. Earth and Planetary Science Letters 249, 216–228.

Pfänder, J.A., Münker, C., Stracke, A., Mezger, K., 2007. Nb/Ta and Zr/Hf in ocean island basalts-implications for crust–mantle differentiation and the fate of Niobium. Earth and Planetary Science Letters 254, 158–172.

Phaup, A. E., 1973. The granitic rocks of the Rhodesian Craton. In: Lister, L. A., (ed.), Symposium on granites, gneisses and related rocks. Geological Society of South Africa, Johannesburg, South Africa. Special Publication number 3, 59-67.

Pollard, D.D., Johnson, A.M., 1973. Mechanics of growth of some laccolithic intrusions in the Henry Mountains, Utah, II: bending and failure of overburden layers and sill formation. Tectonophysics 18, 311 –354.

Pons, J., Barbey, P., Nachit, H., Burg, J.-P., 2006. Development of igneous layering during growth of pluton: The Tarçouate Laccolith (Morocco). Tectonophysics 413, 271-286.

Rajesh, H.M., 2007. The petrogenetic characterization of intermediate and silicic charnockites in high-grade terrains: a case study from southern India. Contributions to Mineralogy and Petrology 154, 591-606.

Rajesh, H.M., 2008. Petrogenesis of two granites from the Nilgiri and Madurai blocks, southwestern India: implications for charnockite–calc-alkaline granite and charnockite–alkali (A-type) granite link in high-grade terrains. Precambrian Research 162, 180-197.

René, M., Holtz, F., Luo, C., Oliver, B, O., Stelling, J., 2008. Biotite stability in peraluminous granitic melts: Compositional dependence and application to the generation of two-mica granites in the South Bohemian batholith (Bohemian Massif, Czech Republic). Lithos 102, 538-553.

Retief, E.A., Compston, W., Amstrong, R.A., Williams, I.S., 1990. Characteristics and preliminary U-Pb ages of zircon from Limpopo Belt lithologies. Extended Abstracts, Limpopo workshop, Rand Afrikaans University, Johannesburg, pp. 95-99.

Rigby, M., Mouri, H., Brandl, G., 2008. A review of pressure - temperature- time evolution of the Limpopo Belt: constraints for a tectonic model. Journal of African Earth Sciences 50, 120-132.

Roberts, M.P., Clemens, J.D., 1993. Origin of high-potassium, talc-alkaline, I-type granitoids Geology 21(9), 825-828.

Roering, C., van Reenen D.D., Smit, C.A., Barton, J.M., Jr., de Beer, J.H., de Wit, M.J., Stettler, E.H., van Schalkwyk, J.F., Stevens, G., Pretorius, S., 1992a. Tectonic model for the evolution of the Limpopo Belt. Precambrian Research 55, 539-552

Roering, C., van Reenen, D.D., de Wit, M.J., Smit, C.A., de Beer, J.H., van Schalkwyk, J.F., 1992b. Structural geological and metamorphic significance of the Kaapvaal Craton-Limpopo Belt contact. Precambrian Research 55, 69-80.

Rollinson H.R., 1993. A terrane interpretation of the Archean Limpopo Belt. Geological Magazine 130, 755-765.

Rollinson, H. R., Tarney, J., 2005. Adakites - the key to understanding LILE depletion in granulites. Lithos 79, 61– 81.

Rudnick, R. L., 1995. Making continental crust. Nature 378, 571-578.

Sajona, F.G., Maurv, R.C., Bellon, H., Cotten, J., Defant, M., 1996. High field strength element enrichment of Pliocene-Pleistocene island arc basalts, Zamboanga Peninsula, western Mindanao (Philippines). Journal of Petrology 37(3), 693-726.

Šarić, K., Cvetković, V., Romer, R.L., Christofides, G., Koroneos, A., 2009. Granitoids associated with East Vardar ophiolites (Serbia, F.Y.R. of Macedonia and northern Greece): origin, evolution and geodynamic significance inferred from major and trace element data and Sr–Nd–Pb isotopes. Lithos 108, 131–150.

Scarrow, J.H., Molina, J.F., Bea, F., Montero, P., 2009. Within-plate calc-alkaline rocks: Insights from alkaline mafic magma-peraluminous crustal melt hybrid appinites of the Central Iberian Variscan continental collision. Lithos 110, 50–64.

Schaller, M., Steiner, O., Studer, I., Holzer, L., Herwegh, M., Kramers, J.D., 1999. The Palala Shear Zone, Transvaal: Exhumation of the Limpopo Central Zone granulites and continent-scale transcurrent movement at 2.0 Ga. Precambrian Research 96, 263–288.

Schmidt, M.W., Thomson, A.B., 1996. Epidote in calc-alkaline magmas: an experimental study of stability, phase relationships and the role of magmatic epidote in magmatic evolution. American Mineralogist 81, 462-474.

Schmidt, M.W., Dardon, A., Chazot, G., Vannucci, R., 2004. The dependence of Nb and Ta rutile-melt partitioning on melt composition and Nb/Ta fractionation during subduction processes. Earth and Planetary Science Letters 226 (3–4), 415–432.

Schreiber, H.D., Lauer, H.V., Thitinant, T., 1980. The redox state of cerium in basaltic magmas: an experimental study of iron–cerium interactions in silicate melts. Geochimica et Cosmochimica Acta 44, 1599–1612.

Sial A.N., Toselli A.J., Saavedra J., Parada M.A., Ferreira V.P., 1999. Emplacement, petrological and magnetic susceptibility characteristics of diverse magmatic epidote-bearing granitoid rocks in Brazil, Argentina and Chile. Lithos 46, 367-392.

Sial, A. N., Vasconcelos, P.M., Ferreira V.P., Pessoa, R.R., Brasilino, R.G., Morais Neto, J.M., 2008. Geochronological and mineralogical constraints on depth of emplacement and ascension rates of epidote-bearing magmas from northeastern Brazil. Lithos 105, 225-238.

Silver, P.G., Fouch, M. J., Gao, S. S., Schmitz, M., 2004. Seismic anisotropy, mantle fabric and the magmatic evolution of Precambrian southern Africa. South African Journal of Geology 107, 45-58.

Sizova, E., Gerya, T., Brown, M., Perchuk, L.L., 2010. Subduction styles in the Precambrian: insight from numerical experiments. Lithos 116(3-4), 209-229.

Smit, C.A., Roering, C., van Reenen, D.D., 1992. The structural framework of the southern margin of the Limpopo Belt, South Africa. Precambrian Research 55, 51-67.

Smit, A., van Reenen, D.D., 1997. Deep crustal shear zones, high-grade tectonites and associated metasomatic alteration in the Limpopo Belt, South Africa: Implications for deep crustal processes. The Journal of Geology 105, 37-57.

Steenfelt, A., Garde, A.A., Moyen, J.-F., 2005. Mantle wedge involvement in the petrogenesis of Archaean grey gneisses in West Greenland. Lithos 79, 207-228.

Stern, R.A., Hanson, G.H., Shirey, S.B., 1989. Petrogenesis of mantle-derived, LILE-enriched Archean monzodiorites and trachyandesites (sanukitoids) in southwestern Superior Province. Canadian Journal of Earth Sciences 26, 1688-1712.

Stevens, G., van Reenen, D.D., 1992a. Constraints on the form of the P-T loop in the Southern Marginal Zone of the Limpopo Belt, South Africa. Precambrian Research 55, 279-296.

Stevens, G., van Reenen, D.D., 1992b. Partial melting and the origin of metapelitic granulites in the Southern Marginal Zone of the Limpopo Belt, South Africa. Precambrian Research 55, 303-319.

Stevenson, R., Henry, P., Gariépy, C., 1999. Assimilation-fractional crystallisation of origin of Archean sanukitoid suites: western Superior Province, Canada. Precambrian Research 96, 83-99.

Stiefenhofer, J., Viljoen, K.S., Tainton, K.M., Dobbe, R., Hannweg, G.W., 1999. The petrology of a mantle xenolith suite from Venetia, South Africa. In Gurney, J.J., Gurney, M.D., Pascoe, M.D., Richardson, S.H., (eds.), Proceedings of the VIIth international kimberlite conference (v2). Red Roof Design, Cape Town.

Stormer, J.C., Whitney, J.A., 1977. Two-feldspar geothermometry in granulite facies metamorphic rocks. Contributions to Mineralogy and Petrology 65,123-33.

Strik, G., de Wit, M.J., Langereis, C.G., 2007. Palaeomagnetism of the Neoarchaean Pongola and Ventersdorp Supergroups and an appraisal of the 3.0–1.9 Ga apparent polar wander path of the Kaapvaal Craton, Southern Africa. Precambrian Research 153, 96–115.

Stuart, G.W., Zengeni, T.G., 1987. Seismic crustal structure of the Limpopo mobile belt, Zimbabwe. Tectonophysics 144, 323-335.

Sun, S.S., McDonough, W.F., 1989. Chemical and isotopic systematics of oceanic basalts: implications for mantle composition and processes. In: Saunders, A.D., Norry, M.J. (eds.),

Magmatism in the Ocean Basins. Special Publication, Geological Society, London 42, 313–345.

Tankard, A.J., Jackson, M.P.A., Erikson, K.A., Hobday, D.K., Hunter, D.R., Minter, W.E.L., 1982. Crustal evolution of southern Africa: 3.8 billion years of earth history. Springer-Verlag, New York, 523 pp.

Tatsumi, Y., Ishizaka, K., 1982. Origin of high-magnesian andesites in the Setouchi volcanic belt, southwest Japan, I. Petrographical and chemical characteristics. Earth and Planetary Earth Sciences 60, 293-304.

Tomson, J.K., Bhaskar Rao, Y.J., Vijaya Kumar, T., Mallikharjuna Rao, J. 2006. Charnockite genesis across the Archaean–Proterozoic terrane boundary in the South Indian Granulite Terrain: Constraints from major-trace element geochemistry and Sr–Nd isotopic systematics. Gondwana Research 10, 115-127.

Tulloch, A. 1979. Secondary Ca-Al silicates as low-grade alteration products of granitoid biotite. Contribution to Mineralogy and Petrology 69, 105-117.

van der Westhuizen, W.A. de Bruiyn, H. Meintjes, P.G., 1991. The Ventersdorp Supergroup: an overview. Journal of African Earth Sciences, 13(1), 83-105.

van Reenen, D.D., 1983. Cordierite + garnet + hypersthene + biotite-bearing assemblages as a function of changing metamorphic conditions in the Southern Marginal Zone of the Limpopo Belt. In: van Biljon, W.J., Legg, J.H. (eds.), Geological Society of South Africa, Special Publication 8,143-167.

van Reenen, D.D., 1986. Hydration of cordierite and hypersthene and a description of the retrograde orthoamphibole isograd in the Limpopo Belt, South Africa. American Mineralogist 71, 900-915.

van Reenen, D.D., Roering, C., Smit, C.A., Van Schalkwyk, J.F., Barton Jr., J.M., 1988. Evolution of the northern high-grade margin of the Kaapvaal Craton. South African Journal of Geology 96, 549–560.

van Reenen, D., Roering, C., Ashwal, L.D., de Wit, M. J., 1992. Regional geological setting of the Limpopo Belt. Precambrian Research 55, 1-5.

van Schalkwyk, J.F., van Reenen, D.D., 1992. High-temperature hydration of ultramafic granulites from the Southern Marginal Zone of the Limpopo Belt by infiltration of CO_2-rich fluid. Precambrian Research 55, 337-352.

Vennemann, T.W., Smith, H.S., 1992. Stable isotope profile across the orthoamphibole isograd in the Southern Marginal Zone of the Limpopo Belt, South Africa. Precambrian Research 55, 365-397.

Vinyu, M.L., Hanson, R.E., Martin, M.W., Bowring, S.A., Jelsma, H.A., Dirks, P.H.G.M., 2001. U-Pb zircon ages from a craton-margin Archaean erogenic belt in northern Zimbabwe. Journal of African Earth Sciences 32 (1), 103-l 14.

Wade, J., Wood, B.J., 2001. The Earth's 'missing' niobium may be in the core, Nature 409, 75–78.

Watson, E. B., Harrison, T.M., 1983. Zircon saturation revisited: temperature and composition effects in a variety of crustal magma types. Earth and Planetary Science Letters 64(2), 295-304.

Wen, D-R., Chung, S-L., Song, B., Iizuka, Y., Yang, H-J., Ji, J., Liu, D., Gallet, S., 2008. Late Cretaceous Gangdese intrusions of adakitic geochemical characteristics, SE Tibet: petrogenesis and tectonic implications. Lithos 105, 1-11.

Weyer, S., Münker, C., Klaus Mezger, K., 2003. Nb/Ta, Zr/Hf and REE in the depleted mantle: implications for the differentiation history of the crust-mantle system. Earth and Planetary Science Letters 205, 309-324.

Wingate, M.T.D., 2000. Ion microprobe U–Pb zircon and baddeleyite ages from the Great Dyke and its satellite dykes, Zimbabwe. South African Journal of Geology 103, 74– 80.

Wintsch, R.P., Yi, K., 2002. Dissolution and replacement creep: a significant deformation mechanism in mid-crustal rocks. Journal of Structural Geology 24, 1179-1193.

Wones, D., 1989. The petrologic significance of the assemblage titanite + magnetite + quartz in granitic rocks. American Mineralogist 74, 744-749.

Wood, B.J., Blundy, J.D., 2001. The effect of crystal cation charge on crystal-melt partitioning of trace elements. Earth and Planetary Science Letters 188, 59-71.

Xiong, X.L., Adam, T.J., Green, T.H., 2005. Rutile stability and rutile/melt HFSE partitioning during partial melting of hydrous basalt: implications for TTG genesis. Chemical Geology 218, 339– 359.

Xirouchakis, D., Lindsley, D.H, Anderson, D.J., 2001. Assemblages with titanite ($CaTiOSiO_4$), Ca-Mg-Fe olivine and pyroxenes, Fe-Mg-Ti oxides, and quartz: Part I. Theory. American Mineralogist 86, 247-253.

Zeh, A., Gerdes, A., Klemd, R., Barton Jr., J.M., 2007. Archean to Proterozoic crustal evolution in the Central Zone of the Limpopo Belt (South Africa–Botswana): constraints from

combined U–Pb and Lu–Hf isotope analyses of zircon. Journal of Petrology 48, 1605–1639.

Zeh, A., Klemd, R., Buhlmann, S., Barton Jr., J.M., 2004. Pro- and retrograde P–T evolution of granulites of the Beit Bridge Complex (Limpopo belt, South Africa); constraints from quantitative phase diagrams and geotectonic implications. Journal of Metamorphic Geology 22, 79–95.

Zen, E-an., Hammarstrom, J.M., 1984. Magmatic epidote and its petrologic significance. Geology 12, 515-518.

Zen, E-an. 1985. Implications of magmatic epidote-bearing plutons on crustal evolution in the accreted terranes of northwestern North America. Geology 13, 266-269.

Zhao, Z-F., Zheng, Y-F., Chen, R-X., Xia, Q-X., Wu, Y.B., 2007. Element mobility in mafic and felsic ultrahigh-pressure metamorphic rocks during continental collision. Geochimica et Cosmochimica Acta 71, 5244–5266.

APPENDICES:

A. Petrographic descriptions for individual samples

Petrographic studies were carried on polished thin sections. Characteristic features such as crystal habit, size, zoning, presence of inclusions and overall inter-mineral textural relationships were the main focus. In the following descriptions the percentages given in brackets after the minerals' names represent modal abundances of that particular mineral in the rock being described. The percentages were estimated by visual observation.

Mat 16 (px-diorite1)

This is a very fine-grained rock with occasional subhedral plagioclase phenocrysts that range up to 4mm. The phenocrysts host minute inclusions of orthopyroxene, green biotite and opaque minerals. Minute magnetite crystals occur as inclusions in the green biotite or as interstitial between the tiny felsic minerals. The rock is traversed by micro-veinlets which are filled mostly with quartz, brown biotite and rarely with green biotite. The green biotite is interpreted as of magmatic origin while the brown biotite is metamorphic. The rock has suffered a low-grade metamorphism, as suggested by the veinlets; otherwise the overall magmatic texture is evident.

Mat 19 (px-diorite1)

This is a severely altered fine to medium grained rock. Plagioclase (70%) has subhedral to anhedral grains and is severely sericitised with both epidote and muscovite being the results of sericitisation. The plagioclase phenocrysts range from ~1 to 3.5mm. A myrmekitic intergrowth with quartz is also present. Some plagioclase grains exhibit deformational twinning. The presence of orthopyroxene is evidenced by minute relics which occur rarely in subsolidus biotite. Hornblende (2%) occurs as subhedral grains with an average size of 1.5mm. Ilmenite (3%) is anhedral and is nearly always rimmed by thin slices of subsolidus titanite. It in turn hosts inclusions of very tiny chalcopyrite. Apatite (traces) occurs mostly as perfectly hexagonal inclusions in plagioclase and hornblende.

Quartz (17%) occurs both as large grains (up to 1.5mm) and smaller (recrystallised) grains. The smallest (recrystallised) quartz grains together with chlorite, an opaque mineral ± biotite ± titanite typically occupy alteration veinlets. The alteration phases; biotite, chlorite, titanite, epidote and muscovite are completely anhedral. Chlorite is pseudomorph after biotite

while titanite occurs mostly as a thin slice around ilmenite or rarely nearly completely having replaced ilmenite.

Mat 44 (px-diorite1)

The overall mineralogy texture suggests igneous origin. Hornblende (35%) is anhedral and has a variable size ranging from <0.4mm to ~2mm. The average size is ~0.9mm. Most grains are seemingly 'autorecrystallisation' products after clinopyroxene. A few grains are prismatic. Rarely, smaller grains occur as inclusions in plagioclase. A significant number of grains have biotite along their edges suggesting biotite to have formed at the expense of magmatic hornblende, at subsolidus conditions. A group of hornblende grains has inclusions of small plagioclase grains, reiterating on the autorecrystallisation of clinopyroxene to hornblende. Infrequent relics of clinopyroxene in hornblende grains are supportive of hornblende having replaced clinopyroxene.

Biotite (4%) is typically <1mm and commonly occurs as prismatic and/or fragmentary grains intergrown with quartz, suggestively at the expense of orthopyroxene. It is interpreted as magmatic, but was subsequently subjected to alteration. Ilmenite (1%) occurs as small grains (typically <1.5mm) and is occasionally rimmed by a thin slice of titanite and/ or apatite. It in turn occurs as an inclusion in plagioclase and hornblende. Even when it hosts inclusions of ilmenite which in turn is rimmed by apatite or titanite, plagioclase has albite twinning preserved.

Plagioclase (40%) forms subhedral to anhedral grains, majority of which are anhedral and sparingly sericitised. Some grains are preferentially sericitised at the core. It exhibits undulose extinction. Twinning is present in the majority of the grains. Alkali feldspar is present in minor amounts. Quartz (19%) is commonly ≤ 1mm and typically has developed subgrains. It is fresh relative to all other minerals.

Mat 45 (px-diorite1)

Hornblende (37%) is anhedral and typically less than 0.5mm in size. Some grains are fragmentary owing to their replacement by subsolidus biotite. A small number of grains have minute relics of clinopyroxene suggesting hornblende to have replaced clinopyroxene presumably at subsolidus conditions. Most of the hornblende defines the gneissocity. The grains that have survived the gneissocity are interstitial between the felsic minerals. Although most of hornblende in this rock is metamorphic, a few grains (e.g. ones being replaced by biotite) are interpreted as of igneous origin.

Biotite (2%) forms anhedral grains which are typically less than 1mm. Majority of biotite defines the gneissocity in this rock. A yet another group of biotite constitutes interstitial grains, which are suggestive of igneous origin. Opaque minerals (2%) occur commonly as microlite inclusions in all other minerals. A significant number of grains are equigranular at ~ 0.2mm. The minimal gneissocity preserved in this rock is defined by mafic minerals.

Plagioclase (42%) forms subhedral to anhedral grains than range from micron scale to up to ~ 1cm phenocrysts. Subhedral grains typically have well developed albite twinning. Myrmekitic intergrowth with quartz is present. Alkali feldspar (microcline; 2%) is typically anhedral and has phenocrysts that may range up to ~1mm. Quartz (15%) forms anhedral grains typically < 0.5mm and rarely up to 1mm. Development of subgrains is common.

Mat 50 (px-diorite1)

Hornblende (22%) shows equigranular (average 0.15mm) subhedral to anhedral grains and occurs mostly interstitial between the felsic minerals. The interstitial hornblende is interpreted to have formed at the expense of pyroxene, as judged by a few px-granitoids (e.g. sample Mat 26) in which pyroxene is preserved and is interstitial between felsic minerals. This replacement suggests an 'autorecrystallisation' of the former clinopyroxene. Very tiny hornblende microlites are inclusions in feldspar and quartz, possibly suggesting their late crystallisation in a magmatic environment. In a few number of grains, a micron-scale relics of pyroxene are preserved within a hornblende grain suggesting the latter to have replaced the former, at subsolidus conditions.

Biotite (2%) is anhedral and averages 0.5mm. It is randomly oriented and most of the grains seemingly formed at the expense of orthopyroxene, at subsolidus conditions. An intergrowth with quartz is also common. Some grains host inclusions of ilmenite and rarely of quartz. The biotite that is intergrown with quartz and one that has inclusions of ilmenite are inferred to be magmatic. Both magnetite and ilmenite (2%) occur as inclusions in all other minerals except quartz and are generally <0.1mm.

Plagioclase (50%) is anhedral and generally equigranular (~0.1mm). It occurs rarely as an inclusion in microcline as well as intergrown with other alkali feldspar. Very few grains show albite twinning. Even when twinning is present it is irregular within the grain, possibly suggesting subsolidus alteration. Both sericitisation and undulose extinction are also another subsolidus alteration features in plagioclase. Even the grains that are inclusions in alkali feldspar are sericitised. Microcline (4%) occurs as anhedral smaller grains and has phenocryst that may range up to 2.5cm. It is also heavily sericitised. Quartz (20%) is anhedral, free of

inclusions and generally <0.15mm. This rock has suffered a low grade metamorphism but the overall igneous texture can be seen as typified by the porphyritic nature where feldspars being the phenocrysts are in a matrix of nearly equigranular other minerals.

Mat 60 (px-diorite1)

The overall texture of the rock is porphyritic with feldspar phenocrysts being set in a matrix of the rest of the minerals. The smaller grained minerals are fairly equigranular. Orthopyroxene (5%) and clinopyroxene (7%) display anhedral grains that average 0.2mm with occasional size of up to 0.9mm. Both minerals occur as inclusions in plagioclase. Biotite (15%) ranges from subhedral to anhedral grains, with the majority being anhedral. The grains are generally equigranular at about 0.3mm. It is elongated in a common direction and is nearly always intergrown with quartz, suggesting formation at the expense of orthopyroxene in a magmatic environment. Magnetite and ilmenite (1%) are typically < 0.005mm in size and commonly occur as inclusions in pyroxene and plagioclase.

Plagioclase (47%) is subhedral to anhedral and typically exhibit albite twinning. Some grains are heavily sericitised and these grains have in turn been overgrown by thin slice of non-sericitised plagioclase. Other than the rare phenocryst of up to 2mm, the grain size of plagioclase is on average <0.3mm. Microcline (5%) is present and exhibit anhedral grains that are generally <1mm. Quartz (16%) is typically < 0.1mm, free of inclusions and most commonly intergrown with biotite. A large number of grains show subgrain development.

Mat 67 (px-diorite1)

This is a very fine-grained rock with mafic minerals (except opaque minerals) being generally equigranular). Both biotite (7%) and hornblende (30%) occur as anhedral (and rarely subhedral) grains that are rarely up to 1mm. The typical relics of clinopyroxene found in parts of hornblende grains suggest that most hornblende replaced clinopyroxene. Biotite grains are commonly either fragmentary or intergrown with quartz. The fragmentary grains are interpreted as subsolidus replacement of pyroxene and occasionally of hornblende and the grains intergrown with quartz are interpreted as of magmatic origin. The hornblende replaced by biotite with no indication of clinopyroxene around it is interpreted as of magmatic origin. Fragmentary orthopyroxene grains ranging up to 0.9mm and now almost wholly replaced by biotite attest to a prior presence of orthopyroxene. Opaque minerals (3%) and apatite (traces) are the tiniest minerals, generally <0.1mm and occur as inclusions in plagioclase, hornblende, quartz and biotite.

Plagioclase (35%) forms euhedral, subhedral and anhedral grains that range from a few mm to up to phenocrysts of about 2.5cm. The bigger grains are preferentially anhedral while smaller grains (<0.3mm) tend to be euhedral. The bigger grains tend to be sericitised preferentially at the core but a small number of small ones are also sericitised. Many grains preserve well developed albite twinning. Quartz (25%) forms small grains typically 0.3< mm.

Mat 28 (px-diorite2)

Orthopyroxene and clinopyroxene (15%) range from euhedral, subhedral to anhedral prismatic and 'equant' grains, with no indication of subsolidus alteration. Biotite (6%) is generally anhedral and has a variety of both well developed grains and symplectitic grains both of which are intergrown with quartz and mostly interstitial between the feldspars. All this biotite is interpreted as of magmatic origin, possibly through the reaction of orthopyroxene with melt. The grains are mainly <1mm, but a few that range up to 2mm exist. Magnetite (3%) and chalcopyrite (traces) occur mainly as interstitial phases with the grain size ranging from <0.1mm to ~1mm. Chalcopyrite also occurs as an inclusion in plagioclase and pyroxene.

Plagioclase (47%) has grains that range from anhedral to euhedral. Most of plagioclase grains are less than 1mm, but a few may range up to 7mm. A few grains show albite twinning. Minimal sericitisation is present. Alkali feldspar (7%) has subhedral to anhedral grains that typically lack twinning. Quartz (23%) has most commonly developed subgrains and rarely recrystallised with majority of the grains being less than 0.5mm.

Mat 29 (px-diorite2)

Clinopyroxene (10%) has subhedral to anhedral grains and is almost equigranular (~0.5mm). It occurs mainly as an interstitial phase but a few grains are inclusions in plagioclase. Magnetite (2%) is typically smaller than 0.1mm. Majority of the grains are interstitial, but the smallest of the grains are inclusions in clinopyroxene and feldspar. Biotite (5%) is anhedral and mostly fragmentary and averages 2mm in size. A few grains have minute (< 0.2mm) plagioclase inclusions. It is more commonly found around areas where plagioclase is sericitised and suggests an intergrowth with plagioclase. It is seemingly magmatic but was subjected to subsolidus alteration.

Plagioclase (64%) is characterised by anhedral grains that are on average 1.5mm in size. Some grains are completely sericitised while others show preferential sericitisation at the core. Quartz (19%) is typically less than 0.4mm, free of inclusions and has most commonly developed subgrains.

Mat 17 (px-diorite2)

This rock is severely altered such that the only evidence for prior existence of pyroxene is fragmentary biotite grains which, as judged by comparison with other rocks in which biotite had formed at the expense of pyroxene at subsolidus conditions (e.g. sample Mat 67), is subsolidus. Biotite (31%) can be classified into two distinctive populations; one comprises the heavily deformed grains which are now essentially chlorite pseudomorph after biotite and the other comprises fairly subhedral to anhedral grains. While a few grains up to 4mm exist, the average grain size is 2mm. The smallest of the grains (<0.3mm) occur as inclusions in plagioclase, and are possibly subsolidus.

Plagioclase (64%) grains are anhedral, severely sericitised and commonly exhibit undulose extinction. Grain size averages between 2mm and 4mm. Rarely (in less altered grains), remnants of crystal faces can be traced, suggesting a former subhedral habit. Patchy zoning can be traced in some grains and is commonly accompanied by sericitisation that occurs in distinct zones within a grain. Muscovite is the product of sericitisation and typically appears as small 'scattered flakes' within a feldspar grain. Some muscovite has completely replaced feldspar. Inclusions of perfectly hexagonal apatite and minute opaque minerals are present in plagioclase. A few microcline microcrystals exist. Opaque minerals (5%) appear either mantled by a rim of biotite or on 'chloritised' zones. The ones found on chloritised zones are probably subsolidus, but the ones rimmed by biotite are probably magmatic.

Mat 18 (px-diorite2)

Orthopyroxene (traces) has anhedral grains most of which have altered to biotite and only a fraction of the pyroxene remaining. A lamellar intergrowth of probably two pyroxenes with different composition was observed. Biotite (13%) can be divided into two varieties; the brown and the green grains. Both have anhedral grains. The green variety is nearly always intergrown with quartz and probably formed by the reaction of pyroxene with melt in a magmatic environment. The brown variety is the most fragmentary, not always intergrown with quartz and hosts tiny plagioclase grains. It is interpreted to be subsolidus. The grain size of biotite is generally less than 0.1mm.

Plagioclase (70%) is anhedral and significantly sericitised to muscovite. A few grains are prismatic. Opaque minerals, magnetite (2%), ilmenite (traces) and chalcopyrite (traces) occur as very tiny (<0.001mm) interstitial phases. They in addition occur as inclusions in quartz. Quartz (14%) is relatively fresh and has mostly developed subgrains.

Mat 26 (px-diorite2)

Orthopyroxene (15%) and clinopyroxene (5%) occur commonly as interstitial pristine anhedral grains with both equant and prismatic habit. An occasional alteration of clinopyroxene to hornblende is present. Biotite (1%) is anhedral and only appears as secondary alteration product of pyroxene. In cases where it does not appear in well developed morphology, it appears along grain boundaries and along cracks within the pyroxene. The grains are typically less than 0.7mm. Opaque minerals; chalcopyrite, ilmenite and magnetite (1%) occur as tiny grains ranging up to ~ 0.8mm but mostly ≤0.1mm. The smaller grains are the most dominant and occur mainly as interstitial phases between felsic phases or as inclusions in both pyroxene and feldspar.

Plagioclase (40%) is fairly euhedral. A few grains may range up to 3mm but majority are less than 0.8mm. Many grains developed intergrown boundaries with other plagioclase grains or with quartz. A significant amount of grains are sericitised. Patches of more Ca-rich plagioclase occur occasionally within bigger albitic host. Apatite (traces) is very tiny (less than 0.0001mm) and occurs as inclusions in plagioclase. Quartz (22%) is typically less than 0.8mm, relatively fresh compared to all other minerals and has more commonly developed subgrains.

Mat 46 (px-diorite2)

Orthopyroxene and clinopyroxene (traces) exhibit anhedral grains that average ~1.5mm in size. Smaller (~0.5mm) grains are common but majority have now been replaced by biotite. Biotite (11%) is anhedral and shows fragmented grains that may range up to 2mm. An intergrowth with quartz is common. Minute relics of hornblende around some biotite grains suggest that biotite had replaced hornblende. In many cases biotite is seemingly interstitial, supposedly having replaced the former interstitial pyroxene and/or hornblende. Hornblende (10%) has anhedral grains most of which are fragmentary. A rare occurrence of pyroxene relics within hornblende grains is found. Inclusions of smaller pyroxene, opaque minerals, biotite, and apatite are common in hornblende. The grain size is variable between ~ 0.4mm and 3mm. Opaque minerals (4%), zircon and apatite (traces) are typically < 0.05mm and occur as inclusions in clinopyroxene, plagioclase, biotite and hornblende. Magnetite is also commonly an interstitial phase.

Plagioclase (40%) is anhedral to subhedral and shows limited twinning. Grain size may range up to 2.5mm but smaller grains (<0.1mm) are more common. An overgrowth of one plagioclase by another as well as myrmekitic intergrowth is present. Undulose extinction is common. Sericitisation is variably manifested preferentially at the core with relatively fresh

rims or in sectors within a grain. Some grains which are preferentially sericitised at core exhibit twinning which is continuous between the sericitised core and the fresh rim. Alkali feldspar (7%) is anhedral and typically lacks twinning. Grain size may range up to 1.6mm. Quartz (22%) shows 0.5 -1mm anhedral grains which are typically fresh and free of inclusions.

Mat 51 (px-diorite2)

Pyroxene (traces) occurs only as relics in hornblende and/or biotite, suggesting transformation of pyroxene into the hydrous minerals. Biotite (5%) shows anhedral grains that are generally <1mm and rarely range up to 3mm in size. It occurs mainly either intergrown with quartz or as an interstitial phase. The biotite intergrown with quartz is interpreted to be of magmatic origin and the interstitial biotite is interpreted to be subsolidus conditions. Biotite occurs rarely around the hornblende and is seemingly a subsolidus replacement of the hornblende. Hornblende (30%) is commonly anhedral and rarely subhedral and commonly hosts inclusions of opaque minerals. A significant number of grains suggest formation at the expense of pyroxene, as evidenced by sparse relics of pyroxene within hornblende grains. Magnetite, ilmenite (2%) and apatite (traces) occur as tiny inclusions in hornblende and plagioclase.

Plagioclase (45%) and alkali feldspar (3%) show anhedral grains. Plagioclase grains are generally equigranular with about 1mm diameter while alkali feldspar grains are generally smaller (<0.5mm). A few plagioclase grains exhibit albite twining but the majority shows no twinning. Myrmekitic texture is rare. Undulose extinction and sericitisation in both feldspars are common. Sericitisation is commonly severe at the core and decreases in magnitude toward the rim. Quartz (15%) shows anhedral grains largely <0.5mm and rarely up to >2mm in size. It is free of inclusions.

Mat 52 (px-diorite2)

Orthopyroxene (traces) is anhedral and averages 1.5mm. It is found only as small relics in the biotite grains. Biotite (2%) is nearly always intimately associated with hornblende and/or severely altered orthopyroxene grains. It is more commonly skeletal suggesting its formation at the expense of hornblende and/ or orthopyroxene, at subsolidus conditions. Grain size may occasionally range up to 1.5mm but is mainly less than 1mm. Hornblende (24%) exhibit mainly anhedral grains and a few subhedral ones both with average size of 1mm. It hosts inclusions of ilmenite, magnetite and quartz. The texture suggests that hornblende was at equilibrium with orthopyroxene and therefore magmatic. Zircon, apatite and ilmenite (traces) are poikilitically

enclosed in orthopyroxene. Ilmenite has minute biotite and plagioclase inclusions. Rare cases where ilmenite is rimmed by a thin slice of titanite and/ or apatite were found.

Plagioclase (50%) is dominantly anhedral and shows albite twinning. It hosts inclusions of apatite needles and hornblende. Some grains show undulose extinction. Alkali feldspar (5%) is anhedral and generally 1 to 1.5mm in size. Twinning is uncommon. Sericitisation is preferentially incurred by plagioclase as opposed to alkali feldspar. Quartz (20%) is anhedral and may range up to 1.5mm but majority of the grains are < 0.5mm. It is relatively fresh and free of inclusions. The rare allanite that is found in this rock has quartz inclusions.

Mat 66 (px-diorite2)

Orthopyroxene (1%) and clinopyroxene (2%) exhibit mostly anhedral and rarely subhedral grains that average 0.5mm in size. The grains are moderately to severely deformed. A significant proportion of the grains occur only as severely deformed crystals on hornblende grains, suggesting the latter to have formed at the expense of the former at subsolidus conditions. Hornblende (14%) is anhedral and generally equigranular (~1.5mm). Although the majority probably formed due to alteration of pyroxene, some grains are intergrown with plagioclase while others host copious numbers of opaque minerals inclusions, suggesting a magmatic origin. Biotite and chlorite (traces) form minute anhedral gains that are suggestive of formation at the expense of pyroxene and hornblende at subsolidus conditions. Magnetite, ilmenite (2%) and apatite (traces) are typically less than 0.5mm. Both magnetite and ilmenite are generally equigranular. They occur as inclusions in all the minerals except in quartz. A rare thin slice of apatite around ilmenite that in turn is an inclusion in plagioclase was found. A rare allanite found in this rock has apatite inclusions.

Plagioclase (70%) has anhedral to subhedral grains that average 2mm and rarely up to 4mm in size. A minimal myrmekitic texture is present. Sericitisation ranges from moderate to severe. A significant number of grains are preferentially sericitised at the core but fresh on the rim. Twinning is common even in the severely sericitised grains. Some grains exhibit undulose extinction due to deformation. Quartz (10%) is anhedral and free of inclusions.

Mat 27 (px-granodiorite)

Orthopyroxene (8%) and clinopyroxene (5%) exhibit anhedral grains that occur mainly as interstitial between the felsic minerals. Grain size is variable between micron scale to ~3.5mm. Inclusions of smaller plagioclase grains in both pyroxenes are present. Biotite (1%) is anhedral and mainly occurs in close proximity with pyroxene, commonly intergrown with quartz and seemingly in equilibrium with pyroxene. It has average grain size of ~1.5mm. The

smallest biotite grains (less than 0.005mm) occur as relative euhedral inclusions in feldspar. Opaque minerals; chalcopyrite and magnetite (1%) are present commonly with a size range of ~0.4 to 0.8mm. The largest grains are interstitial and agglomerate with pyroxene while the smallest grains (typically < 0.01mm) occur also as inclusions in plagioclase and pyroxene. Trace amounts of apatite occur as inclusions in the opaque minerals.

Plagioclase (75%) is euhedral and may range to 4mm in size. A significant number of grains are sericitised and replaced by muscovite. Some grains are preferentially sericitised at the core while others have patchy sericitisation scattered across the whole plagioclase grain. Quartz (10%) is relatively fresh, free of inclusions and may range up to 4mm.

Mat 57 (px-granodiorite)

The rock has suffered a significant amount of recrystallisation of biotite, quartz and hornblende. Tiny veinlets filled with sericite are also present. The pristine biotite (4%) forms anhedral grains either intergrown with quartz or interstitial between felsic phases. Majority of the grains are < 0.5mm but the size may range up to 1mm. The smallest (<0.1mm) biotite grains occur as inclusions in feldspar. Some biotite grains are seemingly replacement of hornblende, at subsolidus conditions. Hornblende (9%) forms anhedral (and very rarely subhedral) grains predominantly in the size range of 0.2-1mm but rarely up to 2.5mm. Owing to the rarely found tiny grains of clinopyroxene in hornblende most of the hornblende probably owes its existence to clinopyroxene. The larger hornblende grains host apatite and opaque mineral inclusions. These larger hornblende grains are interpreted to be magmatic. Minute hornblende grains occur as inclusions in feldspar and are also magmatic. Opaque minerals (1%), zircon and apatite are typically < 0.1mm and occur as inclusions in hornblende, biotite and feldspar.

Plagioclase (38%) and alkali feldspar (18%) form euhedral, subhedral and anhedral grains generally in the size range of 0.2mm - 1.6mm, except in minor cases where they have recrystallised. Some plagioclase grains are perfectly euhedral and preserve albite twinning. Twinning is not always present though. Myrmekitic, granophyric and antiperthitic textures are all present. Alkali feldspar phenocrysts up to 1cm are present and typically preserve calsbard twinning. Some grains show undulose extinction while others are sericitised. Quartz (30%) is anhedral and has both bigger and the smaller (recrystallised) grains. The bigger grains may range up to 1.75mm.

Mat 58 (px-granodiorite)

Biotite (1%) occurs as anhedral crystals with an average grain size of 0.5mm and mostly associated with hornblende. It seemingly formed at the expense of hornblende. A few grains

that are not associated with hornblende are intergrown with quartz and presumably attest to magmatic origin. Hornblende (7%) forms anhedral grains which are commonly interstitial between the felsic minerals. The grains are nearly equigranular (average 0.7mm). Most of these grains are probably magmatic as there is no indication of clinopyroxene around them. Relics of clinopyroxene (traces) grains are however rarely found at the core or on edges of a few hornblende grains. This was possibly a magmatic hornblende-pyroxene replacement. Rare tiny clinopyroxene grains are inclusions in plagioclase. Ilmenite, magnetite (1%) and apatite (traces) form the smallest grains (and rarely up to 0.5mm) that occur chiefly as inclusions in all other minerals. Rarely, ilmenite forms an alteration rim around tiny hornblende grains - possibly a subsolidus alteration.

Plagioclase (40%) and alkali feldspar (15%) occur rarely as subhedral and more commonly as anhedral grains with average size of 1.5mm. Phenocrysts of up to 6 mm are rare. Perthitic and antiperthitic textures as well as sericitisation are present. Twinning is not always present. Quartz (35%) forms subhedral to anhedral grains that range up to 0.5mm.

Mat 59 (px-granodiorite)

Biotite (2%) forms anhedral grains a large number of which are interstitial between the felsic minerals. An intergrowth with quartz is also common as well as a rare embayment onto plagioclase. A significant number of biotite grains are associated with hornblende, suggesting formation at the expense of hornblende. The interstitial biotite is optically similar to the biotite in samples Mat 53, 54 and 55 and interpreted to be subsolidus replacement of pyroxene. The biotite intergrown with hornblende is also interpreted to be subsolidus. The biotite intergrown with quartz and the one embayed onto plagioclase are interpreted to be magmatic. Grain size is generally in the size range 0.3-0.7mm but a few grains up to 1.8mm are present. Smaller grains are mostly the subsolidus biotite while the larger ones are the magmatic variety. Hornblende (9%) ranges from euhedral, subhedral to anhedral grains. Perfectly euhedral grains are inclusions in plagioclase. The only indication of a prior existence of clinopyroxene is suggested by a rare presence of tiny relics within hornblende grains. This was possibly a hornblende-clinopyroxene magmatic replacement.

Plagioclase (59%) and alkali feldspar (18%) form subhedral to anhedral grains which are typically <1mm. Phenocrysts of ~2.5mm are also present. Small (~0.4mm) plagioclase grains are inclusions in the bigger plagioclase grains of slightly different composition as well as in alkali feldspar. Myrmekite texture is present. Minimal microgranophyric texture is present and commonly manifests itself on the grain boundaries of bigger quartz or plagioclase grains. Zircon, apatite, ilmenite and magnetite (traces) are typically <0.1mm and form the smallest

grains that are chiefly poikilitically enclosed in hornblende, plagioclase and biotite. Quartz (10%) forms anhedral grains with mainly <0.5mm and rarely up to 2.5mm in size. It is free of inclusions and fresh relative to other minerals, though some grains have recrystallised.

Mat 62 (px-granodiorite)

Clinopyroxene (traces) forms anhedral grains which are mainly found within hornblende grains, suggesting that the latter formed at the expense of the former. Hornblende (9%) is anhedral to subhedral with the average grain size of ~1mm. Rarely, grains are ~2.5mm in size. More commonly hornblende occurs as an interstitial phase between the felsic minerals. Smaller hornblende grains (<0.5mm) occur as inclusions in plagioclase, pointing to a magmatic origin. Biotite (5%) forms anhedral grains typically < 0.5mm but rarely up to 1mm in size. The bigger grains seemingly replaced hornblende, at subsolidus conditions. Biotite-quartz intergrowth is common, suggesting pyroxene reaction with the melt to liberate biotite and quartz. Opaque minerals (1%) and apatite form the smallest grains and rarely range up to 0.5mm. The smallest grains are inclusions in all other minerals while the bigger grains generally participate in the glomeropophyritic texture defined with other mafic minerals.

Plagioclase (44%) and alkali feldspar (10%) form subhedral to anhedral grains ranging in size from micron scale to phenocrysts with ~1cm. Minimal myrmekitic and perthitic textures are present. Alkali feldspar rarely shows calsbard twinning, but majority of both feldspars do not show twinning. A few grains are preferentially sericitised at the core and fresher on the rims. Both undulose extinction and recrystallisation along grain boundaries are common. Quartz (30%) forms relatively fresh grains.

Mat 68 (px-granodiorite)

Biotite (2%) forms anhedral grains that occur either intergrown with quartz or interstitial between the felsic minerals. A few grains have relics of pyroxene, suggesting pyroxene to have been present at the solidus. Both the biotite intergrown with quarts and the interstitial grains are probably magmatic. A small population formed at subsolidus conditions at the expense of hornblende. Hornblende (9%) forms subhedral to anhedral grains that range from about 0.3 to 1mm in size. A few grains of hornblende are embayed onto plagioclase. Majority of hornblende occurs either as the bigger symplectitic (with quartz) variety or as the smaller grains which formed seemingly due to hydration of clinopyroxene. Both varieties of hornblende are largely interstitial between felsic minerals and are interpreted to be magmatic. Rare cases of a thin slice of magnetite rimming hornblende as well as bigger magnetite grains

hosting minute hornblende inclusions are found. Opaque (1%) minerals and apatite form the smallest of all the minerals and are inclusions in all other minerals.

Plagioclase (48%) and alkali feldspar (16%) form rarely subhedral and more commonly anhedral grains. The grain size is in the range 0.2 – 1.6mm, but overall alkali feldspar is generally smaller than plagioclase. Plagioclase phenocrysts up to 6mm are present. Both myrmekitic and minimal graphic texture are present. Twinning is not always present. Many grains have preferentially incurred sericitisation at the core and relatively fresh on the rim. Some grains show undulose extinction. Quartz (23%) forms rare subhedral and more commonly anhedral grains. The majority of the grains have size of 0.2 -1.2mm. A minimal recrystallisation around grain boundaries is present.

Mat 53 (px-granodiorite)

Hornblende (9%) forms anhedral to subhedral grains which are mainly between 0.5-1.2mm in size. Nearly all the grains are interstitial between felsic minerals. A very small number of hornblende grains have relics of clinopyroxene either at the core or as a tiny bit on the edges. Symplectitic hornblende is also present. Rarely, hornblende occurs as minute inclusions in alkali feldspar. Hornblende in turn has tiny inclusions of plagioclase, apatite and opaque minerals. Biotite (1%) forms anhedral grains which are typically <0.5mm. It occurs in most cases associated with hornblende both being interstitial between the felsic minerals. Where it occurs away from hornblende it is typically intergrown with quartz forming skeletal grains. Ilmenite, magnetite (1%), pyrite, zircon and apatite (traces) occur as minute inclusions in all other minerals including quartz.

Plagioclase (48%) forms subhedral to anhedral grains that are mainly < 1mm. A large number of grains do not have twinning. Sericitisation is commonly incurred at the core while the rims are relatively fresh. Some grains do show undulose extinction. Alkali feldspar (20%) has euhedral to anhedral grains mainly <1mm but with a few phenocrysts up to ~7mm in size. Some grains display calsbard twinning attesting to an igneous origin. A rare graphic texture is also present. Quartz (20%) forms anhedral grains most of which are <0.5mm in diameter.

Mat 54 (px-granite)

Biotite (1%) occurs only as a pseudomorph after orthopyroxene and is almost always interstitial between the felsic minerals. The grains are generally equigranular (~0.6mm). It has that dark-brown to maroon colour which is characteristic of formation at the expense of orthopyroxene, as suggested by other rocks in which a positive proof of pyroxene's presence was made. Inclusions of quartz in biotite are rare. Hornblende (traces) forms anhedral grains

most of which are probably subsolidus alteration of pyroxene. Magnetite and ilmenite (traces) occur as tiny inclusions mainly in biotite and hornblende.

Plagioclase (62%) is all albite and displays perfect albite twins and forms euhedral to subhedral grains. The grains are on average about 2mm and rarely range up to 4mm in diameter. A minimal subsolidus alteration has also contorted the twinning in a few of plagioclase grains. Alkali feldspar (1%) forms anhedral grains and typically lacks twinning. Quartz (35%) forms anhedral grains and has an average grain size of 2.5mm.

Mat 55 (px-granite)

Biotite (8%) occurs only as an anhedral interstitial pseudomorph after orthopyroxene. Except for the very tiny crystals which occur as inclusions in quartz and albite, the size of interstitial grains is essentially equigranular (~0.55mm). The transformation from pyroxene to biotite occurred at subsolidus conditions. Very tiny relics of orthopyroxene (traces) are typically present within the biotite grains. Magnetite and ilmenite (traces) also occur as tiny interstitial grains and always found around where biotite is.

Plagioclase (62%) ranges from euhedral-subhedral to anhedral, with the grain size predominantly being in the range 0.1-2.2mm. Myrmekite texture is common. Majority of the grains do not have twinning but a minimal albite twinning is present. Traces of apatite inclusions are present in plagioclase. Alkali feldspar (2%) shows anhedral grains and is less commonly enclosed in albite. Quartz (29%) forms subhedral to anhedral fresh grains which are mainly in the size range of 0.5-1.7mm.

Mat 10 (px-free diorite)

Biotite (8%) exhibits anhedral grains which range from less than 0.1mm to 1mm. Most grains are at micron scale. An intergrowth with quartz and/ or feldspar is very common. In a few cases biotite is either embayed onto titanite or has inclusions of tiny titanite. Ilmenite (traces) is always associated with biotite and in many cases mantled by thin slice of subsolidus titanite. More commonly, a tiny grain of ilmenite within a titanite grain is all that remains. Titanite (1%) occurs chiefly as an alteration product of ilmenite and rarely as small inclusions in feldspar. The overall size of titanite is ≤ 0.2mm. Both apatite and epidote (1%) occur as prismatic tiny inclusions in the feldspar, with no preferred orientation. The aspect ratio of the grains is ~200.

Both plagioclase (35%) and alkali feldspar (30%) form subhedral to anhedral grains that are on average ~0.7mm but rarely have grown to ~6mm. Twinning is commonly

preserved. Even when the whole grain has been 'invaded' by microlite inclusions of epidote and apatite, the outline of twins can be traced. The 'invasion' by epidote and apatite is nearly always accompanied by sericitisation of the feldspars. Both undulose extinction and subgrains development are common. Quartz (22%) exhibit anhedral grains most of which have developed subgrains. In few cases it has inclusions of alkali feldspar. Chlorite (traces) occurs as a minor subsolidus phase after the alteration of biotite ±feldspar

Mat 11 (px-free diorite)

Biotite (15%) has grains that range from anhedral through subhedral to euhedral. The grains are predominantly prismatic with no preferred orientation. Most grains are intergrown with quartz possibly implying pyroxene reaction with melt to liberate biotite and quartz, in a magmatic environment. There is no proof of pyroxene presence in this rock. When intergrown with feldspar, biotite abuts onto the shape of the feldspar grain, suggesting crystallisation after the feldspar. Some grains in turn have inclusions of plagioclase. Hornblende (1%) forms subhedral to anhedral grains ranging up to ~2mm in size. A rare symplectitic hornblende is present.

Ilmenite (traces) forms grains ranging up to 0.2mm. It is commonly rimmed by subsolidus titanite. Titanite (1%) exhibit anhedral grains which have a size of up to 2mm. Most grains have equant shape and are devoid of ilmenite inclusions. Judging by titanite grains that rim ilmenite, these equant titanite grains are also subsolidus. A few grains however preserve the typical diamond shape of titanite and have inclusions of apatite and alkali feldspar. These are presumably magmatic titanite grains. Epidote (1%) occurs both as hundreds of microlite inclusions in feldspar as well as up to 1.5 mm symplectitic grains. The symplectitic epidote together with biotite, hornblende, ilmenite and titanite are typically glomeropophyritic.

Plagioclase (35%) and alkali feldspar (30%) range from subhedral to anhedral grains with an average size up ~ 0.4mm. The grain size is rarely up to 3mm. Twinning is common. A few grains have suffered sericitisation producing muscovite, in addition to hosting the epidote microlites. Quartz (10%) is free of inclusions and has commonly developed subgrains.

Mat 3 (px-free granodiorite)

Biotite (11%) exhibits anhedral grains that are more commonly intergrown with quartz, suggesting pyroxene reaction with the melt to liberate these two minerals. Most grains are ≤ 1mm and a few are up to 2mm in diameter. A significant number of the grains are prismatic with no preferred orientation. A possible biotite formation at the expense of hornblende is suggested by rare cases where a pseudo120^{o} cleavage intersection is apparent in the biotite

grains. Hornblende (5%) exhibits anhedral grains with a size ranging from micron scale to up to ~2.5mm. It rarely has inclusions of prismatic biotite and apatite. Ilmenite (traces) is typically < 0.1mm and occurs as an inclusion phase in biotite and hornblende. Ilmenite is commonly rimmed by a thin slice of titanite and/or apatite, even when it is an inclusion in hornblende. Titanite (2%) forms both wedge-shaped grains and anhedral grains most of which are between 0.2mm and 0.5mm and rarely ~1mm. The anhedral titanite grains are mainly due to subsolidus replacement of ilmenite while the wedge-shaped grains are magmatic. Titanite also occurs as an inclusion in feldspar and biotite.

Epidote (3%) occurs both as symplectitic non-inclusion grains and as hundreds of microlite inclusions in feldspar and rarely in biotite. Both epidote varieties are optically zoned. The symplectitic grains are magmatic while the microlite inclusions are secondary. The grain size of the symplectitic variety ranges up to 1.5mm. The microlite inclusions commonly form trails within the feldspar host and formed at the same time as the titanite rimming ilmenite. The symplectitic epidote rarely shows a 120^{o} cleavage intersection typical of hornblende. This possibly suggests a 'quick' transformation of hornblende chemistry to that of epidote (possibly just before the subsolidus conditions). Intergrowth of symplectitic epidote and biotite is present.

Plagioclase (35%) and alkali feldspar (20%) form anhedral to subhedral grains that range up to 3mm. Both graphic and myrmekitic textures are present. Twinning is less common but a few grains do have twinning. Even the alkali feldspar that has calsbard twinning hosts hundreds of epidote microlite inclusions. Quartz (25%) forms grain size that range up to 4mm, is relatively fresh, free of inclusions and has commonly developed subgrains.

Mat 8 (px-free granodiorite)

Biotite (12%) forms anhedral (and seldom subhedral) grains which are mostly less than 0.4mm and rarely up to 3mm. Intergrowth with quartz is common as well as embayment onto feldspar and titanite. All this biotite is interpreted to be magmatic. A subordinate biotite population occurs as inclusion feldspar and tends to be elongated parallel to cleavage the host feldspar- this biotite is subsolidus. Ilmenite (traces) forms smaller grains ranging up to 0.4mm. Many ilmenite grains have a rim of titanite around them, suggesting a subsolidus formation of the latter at the expense of the former. Titanite (3%) forms largely anhedral grains which may be as big as 4mm. A few grains, most of which are inclusions in biotite and feldspar are less than 0.2mm. Twinning in titanite is common. Zircon inclusions in titanite grains are present. Most titanite does not seem to be in equilibrium with all other minerals and is therefore subsolidus.

Epidote (1%) occurs both as bigger symplectitic to well developed euhedral grains as well as hundreds of microlite inclusions in plagioclase, alkali feldspar, biotite and titanite. The symplectitic/well developed epidote grains have a variety of shapes ranging from prismatic to equant, are ≤ 0.2mm and commonly define glomeropophyritic texture with other mafic minerals. Both epidote varieties are optically zoned. The symplectitic/well developed epidote is magmatic and the microlite inclusion in feldspar is secondary.

Plagioclase (17%) and alkali feldspar (52%) form predominantly anhedral and rarely subhedral grains with size most commonly between ~0.3mm and 1mm. Phenocrysts up to ~1cm are present. Both myrmekitic and perthitic textures are present. Apatite inclusions in both plagioclase and alkali feldspar are present. A few feldspar grains are significantly sericitised. Quartz (18%) forms anhedral to subhedral grains that are relatively fresh, free of inclusions and more commonly have developed subgrains.

Mat 9 (px-free granodiorite)

Biotite (10%) forms anhedral, subhedral and euhedral magmatic grains that are generally free of inclusions. Majority of the grains are less than 0.8mm, but a few ranging up to 2mm are present. Smaller grains are commonly intergrown with quartz while the bigger grains are intergrown with titanite and epidote ± opaque minerals. There is minimal evidence for a prior existence of hornblende the alteration product of which is now biotite. Epidote (3%) occurs both as hundreds of microlite secondary inclusions in feldspar as well as magmatic symplectitic to well formed non-inclusion grains. The grain size of the latter may range up to 0.8mm. Zoning is always present in both epidote varieties. Titanite (2%) forms anhedral, subhedral and euhedral grains that are typically <1mm in size. The smallest titanite grains are inclusions in feldspar and in biotite. Both magmatic and subsolidus titanite varieties are present. Subsolidus titanite is texturally not in equilibrium with all other minerals while magmatic titanite is in equilibrium and typically intergrown with biotite and symplectitic epidote.

Plagioclase (22%) and alkali feldspar (45%) form anhedral to subhedral grains that range from ~0.1mm to 2mm. Alkali feldspar tend to form relatively bigger grains than plagioclase. Relics of hornblende grains, traces of chalcopyrite and apatite are inclusions in feldspar. Quartz (18%) forms anhedral grains that are free of inclusions and typically have developed sub-grains.

Mat 12 (px-free granodiorite)

Biotite (15%) has both euhedral and anhedral grains with a grain size ranging up to 2mm. Anhedral grains occasionally have inclusions of smaller euhedral biotite grains. An intergrowth with titanite and epidote is common for both anhedral and euhedral grains, suggesting both varieties are of magmatic origin. Titanite (1%) forms anhedral grains which occasionally show twinning. The grain size ranges between 0.08mm and 1.7mm. Apatite (traces) forms minute grains which occur as inclusions in biotite and titanite. Epidote (1%) occurs both as microlite inclusions in feldspar (and rarely in titanite) as well as symplectitic to well developed grains that are typically intergrown with titanite and biotite. Both epidote varieties are optically zoned. The microlite inclusions are secondary while the symplectitic grains are magmatic.

Plagioclase (38%) and alkali feldspar (35%) form anhedral to subhedral grains. Minimal myrmekitic texture is present. It is common for one feldspar to host another of a different composition. Twinning is generally absent. Sericitisation is minimal. Quartz (10%) shows anhedral grains that range up to 2mm and has more commonly developed sub-grains.

Mat 21(px-free granodiorite)

Biotite (5%) forms anhedral grains which commonly define a glomeropophyritic texture with titanite, epidote, hornblende ± ilmenite. When not in the glomeropophyritic intergrowth, biotite is intergrown with quartz. A rare biotite embayment onto the feldspar is present. There is some evidence for the presence of a 'dirty biotite' being secondary alteration product of titanite. This 'dirty biotite' is subsolidus but the rest is magmatic. Ilmenite and apatite (traces) form the smallest grains that are typically found as inclusions in hornblende, feldspar and biotite. Ilmenite is more commonly rimmed by thin slice of titanite. Titanite (1%) forms mainly anhedral grains ranging up to 0.8mm and is commonly found as an inclusion in hornblende and in biotite. Hornblende (3%) forms subhedral to anhedral grains and has an overall grain size being <0.5mm. Inclusions of minute apatite grains are present in hornblende. Epidote (traces) is very rarely found as a secondary inclusion in feldspar. A few grains are however found as symplectitic to well developed euhedral grains. Both epidote varieties are always zoned.

Plagioclase (45%) and alkali feldspar (17%) form anhedral to subhedral grains with a grain size ranging up to 5mm. A more calcic plagioclase inclusion in a more albitic plagioclase as well as in alkali feldspar is common. Perthitic texture is present. Albite and calsbard twinning, microcline as well as sericitisation are rare. Sericitisation is occasionally incurred preferentially at the core while the rim is fresh. Microcline is more commonly recrystallised along grain boundaries while albite is relatively fresh. Quartz (23%) has both the recrystallised smaller

grains and the non-recrystallised variety both of which are free of inclusions. The larger quartz grains (the non-recrystallised grains) are relatively equigranular (~ 1.5mm).

Mat 22 (px-free granodiorite)

Biotite (4%) forms both well formed prismatic grains as well as symplectitic grains. An intergrowth with quartz and hornblende is common. Biotite alteration to chlorite is also present. Hornblende (10%) has subhedral to anhedral grains with an average grain size of 1mm. A fair number of hornblende grains are symplectitic, suggesting either reaction of the hornblende with the melt, or reaction of clinopyroxene with melt to liberate hornblende and quartz. Magnetite and ilmenite (3%) form grains that range up to 1mm while apatite, chalcopyrite and zircon (traces) form generally <0.4mm grains. Ilmenite is more commonly rimmed by thin 'slice' of titanite. Titanite (1%) occurs as anhedral to euhedral grains and is more commonly intergrown with biotite, hornblende and a rare epidote. The titanite that rims ilmenite is probably subsolidus, but the well formed euhedral to anhedral grains that typically agglomerate with other mafic minerals are interpreted to be magmatic.

Plagioclase (62%) and alkali feldspar (5%) have anhedral to subhedral grains. The average grain size is 0.5mm but up to 1mm grains are present. Myrmekitic, granophyric and perthitic textures are present. Albite twinning in plagioclase and calsbard twinning in alkali feldspar are common. Many grains are commonly 'corroded' along the edges. There is a minimal sericitisation, as well as undulose extinction. Quartz (15%) preserves fairly equigranular grains and has commonly developed subgrains.

Mat 4 (px-free granodiorite)

Biotite (7%) forms subhedral to euhedral grains most of which are less than 0.8mm and rarely have grown up to ~4mm. Both biotite intergrowth with quartz and embayment onto plagioclase are common. Bigger biotite grains commonly ‘mimic’ the edge of plagioclase grain onto which they share a common boundary, suggesting that the biotite crystallised after plagioclase. There are also biotite grains poikilitically enclosed in plagioclase while in turn plagioclase is an inclusion phase in biotite. Orientation of biotite grains in plagioclase is commonly random. Ilmenite (traces) forms minute grains that are mostly rimmed by titanite. Titanite (2%) forms anhedral to euhedral grains up to 2.5mm. Euhedral grains commonly preserve the perfect diamond shape that is typical of titanite. More commonly when titanite preserves the diamond shape, it has no bit of ilmenite within and is therefore interpreted to be magmatic. The grains that rim ilmenite are subsolidus. Epidote (4%) occurs both as symplectitic

to well developed non-inclusion grains as well as typically prismatic hundreds of microlite inclusions in feldspar. The non-inclusion grains may range up to 0.4mm. Both epidote varieties are optically zoned.

Plagioclase (45%) and alkali feldspar (18%) form anhedral to subhedral grains most of which are in the range of 1mm to 2mm and rarely form phenocrysts of ~5mm. Both albite twinning in plagioclase and calsbard twinning alkali feldspar are common. Myrmekitic, granophyric and perthitic textures are present. Apatite (traces) is an inclusion phase in both plagioclase and alkali feldspar. Quartz (23%) is anhedral with a grain size ranging up to 3mm. It is relatively fresh, free of inclusions, commonly developed subgrains and rarely recrystallised. It tends to 'mimic' the shape of the feldspar grain it is in contact with.

Mat 13 (px-free granodiorite)

Biotite (13%) forms anhedral and rarely euhedral grains with the grain size of up to 3mm. An intergrowth with quartz as well as an embayment onto plagioclase is common. A significant number of grains are elongated and are roughly oriented in the same direction. A number of grains seemingly formed owing to the alteration of titanite. Titanite (traces) grains range from prismatic to non-prismatic grains with a size ranging up to 2mm. It hosts plagioclase inclusions and in turn titanite is an inclusion phase in plagioclase. Except for the titanite that rims a rare ilmenite in this rock all titanite is magmatic. Chalcopyrite, magnetite and ilmenite (traces) form very small (< 0.1mm) grains. Epidote (3%) occurs both as symplectitic to well developed euhedral to subhedral non-inclusion grains as well as prismatic hundreds of microlite inclusions in feldspar (and subordinately in biotite). The size of non-inclusion grains ranges up to 0.5mm. Both epidote varieties are optically zoned.

Plagioclase (47%) and alkali feldspar (15%) form anhedral to subhedral grains that are overall < 2mm and rarely form up to 6mm as phenocrysts. Alkali feldspar is dominated by microcline. Myrmekitic, granophyric and perthitic textures are all present. Smaller (<0.7mm) plagioclase grains are inclusions in titanite and biotite. Quartz (21%) forms ~ 1mm relatively fresh anhedral grains which are free of inclusions and typically have developed sub-grains.

Mat 14 (px-free granodiorite)

Biotite (18%) forms subhedral to anhedral grains which range from micron scale to up to 2mm. Intergrowth with quartz, embayment onto feldspar as well as a glomeropophyritic intergrowth with titanite and epidote are typical. Microlite inclusions of both epidote and titanite are present in biotite. The smallest biotite grains occur as inclusions in plagioclase and have presumably formed at the same time as the secondary epidote. Titanite (3%) forms

anhedral to subhedral and rarely euhedral grains that commonly range up to 2mm in diameter. Titanite occurs as an inclusion phase in plagioclase and in turn poikilitically enclose smaller plagioclase grains. Titanite inclusions in plagioclase are typically <0.2mm Plagioclase inclusions in titanite may be sericitised while the mantleling titanite grain may be fresh and euhedral.

Epidote (6%) occurs both as non-inclusion symplectitic to well-developed euhedral and subhedral grains as well as microlite inclusions in feldspar. The non-inclusion epidote typical has grain size that range up to 1mm while the microlite inclusions are <0.01mm. Due to severe resorption of some symplectitic grains, a fallacious impression of plagioclase and biotite being inclusions in epidote is implied. Countless epidote microlite grains form along the edges of feldspar grains. Epidote on the edges of feldspar as well as the microlite inclusions in the feldspar is secondary while the symplectitic to well-developed epidote is magmatic.

Plagioclase (46%) and alkali feldspar (12%) form anhedral to subhedral grains with a grain size from <1mm to up to ~2mm. Rare phenocrysts of ~4mm are present. Smaller feldspar grains (<0.1mm) are rare and occur as inclusions in biotite. Antiperthitic, perthitic and myrmekitic textures are present. Alkali feldspar is dominated by microcline. A significant number of grains show undulose extinction and a few grains have developed subgrains. Twinning is common. Even alkali feldspar grains that have epidote microlite inclusions preserve calsbard twinning. Quartz (15%) forms anhedral grains most of which are between 0.1 and 1mm, fresh and free of inclusions. Subgrain development is also common.

Mat 30 (px-free granodiorite)

Biotite (23%) forms anhedral elongated grains which are more commonly glomeropophyritic with titanite, epidote and ilmenite and less commonly intergrown with quartz. The grain size of the biotite mainly ranges up to 2mm and rarely up to 4mm. About half of biotite is characterised by grains that are less than 1mm and the other half by grains > 1mm. Biotite is rarely embayed on to hornblende. A texture where fragmentary biotite is pseudo-embayed into feldspar is present, but this is suggestively a subsolidus intergrowth. Some biotite (nearly opaque) seemingly formed from titanite alteration, presumably at subsolidus conditions. Hornblende (1%) forms anhedral grains that range up to 4mm.

Ilmenite (traces) forms micron-scale grains that commonly occur as inclusions in hornblende and in feldspar. Thin slice of titanite along the edges of ilmenite are common, even when ilmenite is an inclusion in hornblende and feldspar. Titanite (traces) forms anhedral to subhedral grains and rarely occurs as an inclusion in feldspar and epidote. The inclusion titanite is typically equant and < 0.3mm. A significant number of titanite grains retain a perfect diamond

shape but in turn show a dark brown coloured core which is almost opaque throughout the rotation of microscope stage. These grains suggest a preferential alteration of titanite at the core and are different from ilmenite that is rimmed by titanite which is always perfectly black under the microscope. Epidote (3%) occurs both as non-inclusion symplectitic to well-developed grains and as hundreds of microlite inclusions in feldspar (and subordinately in biotite). Both epidote varieties are anhedral and rarely subhedral. The grain size of non-inclusion grains is up to 1.5mm. Apatite (traces) forms perfectly euhedral grains that are inclusions in the feldspars and the mafic minerals.

Plagioclase (39%) and alkali feldspar (25%) form anhedral grains. The grain size of plagioclase is generally equigranular (~1.2mm) while alkali feldspar is relatively bigger and has phenocrysts of about 6mm. Myrmekitic, perthitic and antiperthitic textures are present. Albite twinning in plagioclase and calsbard twining in alkali feldspar are present. Both plagioclase and alkali feldspar do occur as inclusions in biotite and plagioclase is also an inclusion in titanite. Sericitisation of both feldspars is rare. Quartz (25%) is free of inclusions, forms relatively fresh anhedral grains, has more commonly developed subgrains and less commonly recrystallised. The grain size of the non-recrystallised quartz ranges up to 3mm.

Mat 34 (px-free granodiorite)

This is a fine to medium grained rock with the average grains size of mafic minerals being less than 4mm while the felsic minerals are bigger. The assemblage consists of biotite, plagioclase, alkali feldspar, epidote, titanite, quartz and accessory phases of magnetite, ilmenite, apatite and zircon. Biotite (6%) is defined largely by anhedral and less commonly subhedral grains with the average size of ~0.4mm. A biotite-quartz intergrowth is common. Biotite is rarely embayed onto hornblende and occasionally forms fragmentary grains that are, starting from the outside of the feldspar, penetrative into feldspar grains. The fragmented bits of biotite are commonly parallel to twining in the feldspar into which it 'invades'. Except for the biotite strewn into feldspar, all the biotite in this rock is interpreted as of magmatic origin. A small population of biotite has seemingly formed at the expense of hornblende at magmatic condition. This biotite is typically symplectitic with relics of hornblende found in close proximity. Hornblende (%1) occurs as subhedral to euhedral grains with an overall size of <0.3mm.

Epidote (3%) occurs both as non-inclusion symplectitic to well-developed grains and as hundreds of microlite inclusions in feldspar. Less commonly, epidote is found along grain boundaries of mafic minerals. Both the non-inclusion and inclusion epidote grains are mostly euhedral and exhibit optical zoning. The grain size of non-inclusion epidote grains ranges up to 0.3mm. The epidote found along the edges of other mafic minerals and the microlite inclusions

in feldspar are subsolidus; the non-inclusion variety is magmatic. The anhedral to perfectly euhedral titanite (2%) grains are generally <0.5mm in diameter and rarely range up to 1mm. Plagioclase inclusions in titanite are present while in turn titanite is an inclusion in plagioclase. When an inclusion in plagioclase, titanite may either be perfectly euhedral (showing the perfect diamond shape) or anhedral. In turn the plagioclase may be inclusion in a perfectly euhedral wedge-shaped titanite. Traces of magnetite, ilmenite, apatite and zircon occur as inclusions in feldspar and titanite.

Plagioclase (41%) and alkali feldspar (17%) are anhedral to subhedral and generally > 5mm in diameter. Phenocrysts ranging up to 35mm are present. Alkali feldspar typically shows no twinning while plagioclase is more commonly twinned. Even the plagioclase inclusion in titanite has well developed albite twinning while at the same time is sericitised and hosts minute inclusions of epidote microcrystallites. Alkali feldspar is also commonly minimally sericitised. Subgrain development is rare in plagioclase. The anhedral quartz (29%) shows more commonly a development of subgrains and recrystallisation. The recrystallised grains are typically < 0.01mm in diameter while the non -recrystallised grains are fairly equigranular (~3.5mm).

Mat 38 (px-free granodiorite)

This is a fine-grained rock with the average grain size of 1mm. The assemblage comprises biotite, plagioclase, alkali feldspar, epidote, titanite and traces of ilmenite. Biotite (8%) is generally anhedral with the grain size of < 0.2mm and rarely ranging up to 1mm. A biotite–quartz intergrowth is common. Opaques minerals are the smallest grains more commonly found as inclusions in other minerals (except quartz). Ilmenite forms small grains which are more commonly rimmed by titanite. Titanite (1%) occurs seemingly as a subsolidus phase owing to the alteration of ilmenite. Rarely, titanite grains are inclusions in feldspar. Epidote (1%) occurs as non-inclusion symplectitic to well-developed grains, hundreds of microlite inclusions in feldspar as well as anhedral grains along the grain boundaries of mafic minerals. Only the non-inclusion symplectitic to well-developed grains are magmatic. The proportion of magmatic to subsolidus epidote is ~ 50:50.

The subhedral to anhedral plagioclase (40%) and alkali feldspar (20%) make up the bigger grain size in this rock with an average size of 1.7mm. Microcline dominates alkali feldspar. Twinning is commonly present in both plagioclase and alkali feldspar. Some grains do show undulose extinction. Quartz (29%) forms anhedral grains, is fresh and free of inclusion.

Mat 70 (px-free granodiorite)

This is medium to coarse-grained porphyritic rock consisting of biotite, plagioclase, alkali feldspar, titanite, epidote and quartz. Biotite (30%) is anhedral and averages 0.3mm in size. It is rarely observed as an inclusion in the feldspar. Titanite (1%) forms anhedral to perfectly euhedral grains with the average size of ~2mm. Minute grains occur as inclusions in plagioclase. In turn, titanite hosts smaller plagioclase inclusions. The tiny titanite inclusions in plagioclase are interpreted to be subsolidus, while the rest are interpreted as of magmatic origin. Epidote (1%) occurs either as microlite inclusions in both plagioclase and alkali feldspar (and rarely in biotite) as well as a larger (up to 0.3mm) symplectitic to well-developed non-inclusion grains. The epidote microlites are subsolidus and the symplectitic to well-developed epidote is magmatic. All epidote is optically zoned.

Plagioclase (40%) and alkali feldspar (9%) form subhedral to anhedral grains with the majority of the grains being ~5mm. Phenocrysts of ~10mm are more common. These phenocrysts rarely have inclusions of smaller myrmekitic plagioclase. Twinning is present but not always in both plagioclase and alkali feldspar. Some grains are preferentially sericitised at the core and fresh on the rims. Quartz (19%) forms the freshest of all minerals with grain size of up to 4mm. It is free of inclusions.

Mat 1 (px-free granite with ≤71 wt.% SiO_2)

This is a medium grained porphyritic rock comprising the assemblage biotite, plagioclase, alkali feldspar, quartz, titanite and accessory phases of ilmenite and chalcopyrite. The euhedral to anhedral biotite (20%) is typically elongated with no preferred orientation and has the grain size of about 2.5mm. Biotite embayment onto hornblende is present. There is subsolidus biotite which seemingly formed from alteration of titanite. Hornblende (7%) forms generally equigranular (~1.5mm) subhedral to anhedral grains. Ilmenite occurs also fairly as equigranular grains (0.7mm) which are commonly rimmed by thin slice of titanite. Titanite (1%) forms anhedral grains with an average grain size of ~ 1.5mm. Most commonly, the bigger titanite grains with no core of ilmenite are glomeropophyritic with ilmenite, hornblende and biotite. The titanite 'rimming' ilmenite is subsolidus but the titanite in the glomeropophyritic intergrowth is interpreted to be magmatic. Titanite subsolidus alteration to leucoxene is common.

Plagioclase (32%) and alkali feldspar (20%) form anhedral grains with the majority being <5mm. The phenocrysts of ~20mm are both of alkali feldspar and plagioclase. Inclusions of smaller (<0.2mm) biotite, chalcopyrite and apatite grains are present. Granophyric texture is present. Sericitisation is minor. Quartz (20%) forms anhedral grains which are generally <2.5mm and is more commonly recrystallised.

Mat 7 (px-free granite with ≤71 wt.% SiO_2)

The assemblage biotite, plagioclase, alkali feldspar, quartz, epidote and titanite define this porphyritic medium to coarse grained rock. The mafic minerals are generally ≤2mm while the felsic minerals are bigger. Biotite (8%) forms mainly anhedral grains which are more commonly intergrowth with quartz. There is fragmented biotite which commonly extends from the outside of feldspar into the inside of 'the host' feldspar. The 'outside' portion is well developed while the part in the feldspar is well fragmented. This biotite is probably subsolidus but the one intergrown with quartz is magmatic. Traces of small hornblende grains which in turn host minute apatite inclusions are present in this rock. Ilmenite (traces) is typically on micron scale and more commonly rimmed by thin slice of titanite. Titanite (3%) forms anhedral to euhedral grains of up to 2mm and is nearly always associated with biotite, hornblende ± ilmenite. There are titanite inclusions in plagioclase and in symplectitic epidote. Epidote (2%) occurs both as non-inclusion symplectitic to well–developed grains and as hundreds of microlite inclusions in feldspar. The non-inclusion epidote grains may range up to 0.5mm while the inclusion grains are < 0.01mm in diameter.

Plagioclase (42%) and alkali feldspar (20%) form anhedral to subhedral grains with the most common grain size being ~5mm. Phenocryst of both alkali feldspar and plagioclase are most commonly ~10mm but up to 55mm are rare. Alkali feldspar is dominated by microcline. Undulose extinction is common. Even the feldspar that preserves twinning has inclusions of titanite, biotite, apatite and epidote. Quartz (24%) forms anhedral grains which typically have developed subgrains. It is relatively fresh.

Mat 31 (px-free granite with ≤71 wt.% SiO_2)

This is a porphyritic leucocratic rock with mineral assemblage that constitutes biotite, hornblende, plagioclase, alkali feldspar, quartz, titanite, epidote and traces of ilmenite. Veinlets occupied by mafic minerals are present. Recrystallisation of feldspar and quartz is also widely spread. In addition, a large proportion of epidote is subsolidus and is a consequence of metamorphism. An overall igneous texture suggests anhedral to subhedral biotite (20%) with the average grain size of ~2mm. The bigger well-developed biotite grains are commonly intergrown with quartz, possibly suggesting the reaction of pyroxene with melt to liberate biotite and quartz. More commonly biotite grains are skeletal and penetrative into feldspar. This skeletal biotite is subsolidus. Ilmenite (traces) forms grains that are <0.2mm and is nearly always rimmed by titanite. Titanite (1%) exhibit anhedral grains which are typically 0.4 to 3mm

in diameter. Anhedral micro titanite grains are also inclusions in feldspar and in turn have a core of ilmenite. Titanite alteration to leucoxene is more prevalent. The titanite rimming ilmenite is subsolidus, even when it occurs in feldspar. The one that is typically altered to leucoxene is interpreted to be magmatic, but were subjected to subsolidus alteration.

Plagioclase (29%) and alkali feldspar (25%) form anhedral grains that are more commonly 'sinuous' due to the low grade metamorphism. Phenocrysts of ~ 20m diameter are present. Myrmekitic texture is present and is probably magmatic. Sericitisation and perthitic texture (which is probably subsolidus) are common. Epidote (2%) occurs both as a subsolidus and magmatic phase. The subsolidus grains are more dominant to magmatic ones. The former occur as hundreds of microlite inclusions in the feldspar (and subordinately in biotite) and the latter occur as symplectitic to well-developed grains with an average grain size of 0.4mm. Both epidote varieties are zoned. Quartz (23%) shows anhedral grains that have more commonly developed subgrains or recrystallised.

Mat 33 (px-free granite with ≤71 wt.% SiO_2)

This is a fine to medium grained porphyritic rock with the mineral assemblage biotite, plagioclase, alkali feldspar, quartz, titanite, epidote and traces of ilmenite. Biotite (7%) has both bigger (up to 1.7mm) and smaller (< 0.2mm) grains that are commonly elongated with no preferred orientation. Smaller grains are typically intergrown with quartz and are interpreted to be magmatic. The larger (and the more dominant) grains are mostly skeletal and more commonly 'penetrative' into feldspar. This is a subsolidus biotite. A few biotite grains seem to have formed from a contribution of titanite also at subsolidus conditions. Ilmenite (traces) forms micron scale grains which are more commonly rimmed by subsolidus titanite. Titanite (1%) is anhedral with the average grain size of ~0.25mm. Alteration of magmatic titanite to leucoxene is common. Epidote (2%) occurs both as magmatic non-inclusion symplectitic to well-developed grains and as secondary hundreds of microlite inclusion in feldspars. The grain size of the magmatic epidote is about 0.4mm.

Plagioclase (40%) and alkali feldspar (19%) form anhedral grains most of which are ~ 3mm in diameter. Apatite occurs as inclusions in feldspar. Alkali feldspar has a significant microcline component. Myrmekitic and perthitic textures are present. It is common to find a myrmekitic plagioclase as an inclusion in a perthite. Sericitisation is common. Quartz (30%) forms anhedral grains most of which have developed subgrains. It has inclusions of minute biotite grains that have formed from titanite alteration.

Mat 36 (px-free granite with ≤71 wt.% SiO_2)

This is a medium grained rock with an average grain size of 3mm. Biotite (3%) forms anhedral grains of up to 1.7mm and occurs either as an interstitial phase or intimately associated with titanite ± ilmenite. In minor cases biotite is poikilitically enclosed in alkali feldspar. Both the biotite inclusion in feldspar and biotite intergrown with quartz are magmatic while the one associated with titanite is subsolidus. Ilmenite (2%) forms grains with an average size of 1mm. It is commonly rimmed by titanite. Titanite (5%) exhibit anhedral to euhedral grains with an average size of ~1mm. Euhedral grains show a perfect diamond shape and occur mainly where there is no ilmenite. This titanite is interpreted as of magmatic origin. Epidote forms minute anhedral grains found in close proximity with ilmenite and titanite. This is seemingly subsolidus epidote. Zircon and apatite are accessory phases.

Plagioclase (24%) and alkali feldspar (40%) form subhedral to euhedral grains with an average grain size of ~ 3.5mm in diameter. Alkali feldspar is dominated by microcline. Minimal sericitisation is present. Quartz (26%) forms anhedral grains most of which are recrystallised. It is free of inclusions.

Mat 39 (px-free granite with ≤71 wt.% SiO_2)

This is a very fine-grained equigranular (~0.1mm) rock with mineral assemblage biotite, plagioclase, alkali feldspar, quartz and accessory phases of ilmenite, titanite and epidote. Biotite (5%) occurs as a magmatic phase with anhedral grains and commonly occurs in places where hornblende is present. Hornblende (27%) is anhedral and also magmatic, though it is now very altered. More commonly, hornblende has subsolidus epidote along the edges. Ilmenite (traces) occurs as minute grains which are nearly always rimmed by titanite. Titanite (traces) forms anhedral grains which formed at the expense of ilmenite at subsolidus conditions. Epidote (traces) occurs as anhedral grains either as tiny microlite grains around hornblende grains or as inclusions in the feldspar. Both these epidote varieties are subsolidus. Plagioclase (35%) and alkali feldspar (microcline; 25%) form anhedral grains more commonly <1mm. Phenocrysts of ~25mm are present. While other minerals are heavily altered, quartz (22%) is relatively fresh but has commonly developed subgrains.

Mat 42 (px-free granite with ≤ 71wt.% SiO_2)

Biotite (3%) forms anhedral grains which are mostly < 1.5mm and rarely ~ 1.5mm in diameter. It is commonly symplectitic and nearly always intergrown with quartz, suggesting reaction of hornblende with melt to liberate biotite and quartz. Hornblende (7%) exhibits anhedral grains that are also commonly skeletal and range up to 2mm. Hornblende is an inclusion phase in plagioclase. Magnetite, ilmenite (1%) and apatite occur as tiny inclusions in

plagioclase, hornblende and biotite. Apatite is in turn an inclusion in both magnetite and ilmenite. Ilmenite is rarely rimmed by a thin slice of titanite, even when it is an inclusion in plagioclase or hornblende. Accessory zircon is available as anhedral to subhedral grains and mostly as inclusion in the feldspar.

Plagioclase (45%) and alkali feldspar (15%) form anhedral and rarely subhedral grains that may range up to 3mm in diameter. A few grains are zoned. Albite twinning is commonly present in the plagioclase. However the twinning is commonly contorted and accompanied by undulose extinction. Smaller grains of one plagioclase (<0.05mm) are present as inclusions in the bigger plagioclase of slightly different composition. Where sericitisation has occurred, both muscovite and biotite are the byproducts, but the latter is more well develop into grains which may occasionally be subhedral. Perthitic texture, which is probably subsolidus, is present. Quartz (29%) is anhedral and free of inclusions.

Mat 23 (px-free granite with >71 wt.% SiO_2)

This is porphyritic leucocratic rock defined by the assemblage biotite, plagioclase, alkali feldspar, magnetite, quartz and accessory phases of ilmenite, zircon and titanite. Biotite (4%) forms anhedral to subhedral grains that can be divided into two distinct populations. One population is made of subhedral prismatic (with no preferred orientation) grains which are nearly always intergrown with quartz, suggesting the reaction of pyroxene and/or hornblende with melt to liberate biotite and quartz. More frequently these grains are interstitial. The second generation of biotite appears to be 'pseudomorph' after an altered titanite, and is interpreted to be subsolidus. Ilmenite occurs as smaller grains (typically <0.1mm) which are more commonly rimmed by titanite. Titanite forms anhedral to euhedral grains that are also typically <0.1mm in diameter. Nearly all the titanite grains have at least some bit of ilmenite relics on them, testifying to the replacement of the latter by the former, presumably at subsolidus conditions. Plagioclase (29%) and alkali feldspar (35%) exhibit subhedral to anhedral grains most of which are~2mm. Phenocrysts of ~10mm in diameter are present. Myrmekitic and perthitic textures are common. Zircon is an inclusion phase in plagioclase. Quartz (31%) forms fresh anhedral grains, generally <1mm in diameter.

Mat 24 (px-free granite with >71 wt.% SiO_2)

This is a medium grained porphyritic rock with mineral assemblage biotite, plagioclase, alkali feldspar, quartz and accessory ilmenite and titanite. Mafic minerals are generally <2mm while felsic minerals are bigger. Biotite (4%) forms anhedral grains that are commonly intergrown with quartz. Small biotite grains (not intergrown with quartz) are inclusions in

plagioclase. Traces of ilmenite are also found as inclusions in the feldspar. Titanite (traces) is generally less than 0.2mm and frequently occurs rimming ilmenite. Even the ilmenite that is an inclusion in feldspar has a titanite rim.

Plagioclase (31%) and alkali feldspar (28%) exhibit anhedral grains mainly about 5mm in diameter. Phenocryst of both alkali feldspar and plagioclase are present and are ~ 25mm. Myrmekitic and perthitic textures are present as well as subgrain development for both feldspars. There is also minimal sericitisation. Quartz (35%) forms anhedral grains that are on average 3mm. Development of subgrains is common. Both feldspars and quartz have been subjected to minimal recrystallisation. The recrystallised grains typically accumulate on the grain boundaries of or are interstitial between the bigger grains of both feldspars and quartz.

Mat 32 (px-free granite with >71 wt.% SiO_2)

This is a porphyritic medium grained rock with an average grain size of ~1mm for mafic minerals and quartz and relatively larger feldspar crystals. Biotite (12%) forms anhedral grains that are overall <1.5mm. Plagioclase (24%) and alkali feldspar (35%) form anhedral grains that are generally bigger than 2mm. Phenocrysts of both feldspars are on average ~10mm in diameter. Quartz (38%) forms anhedral grains which are generally < 1mm and in addition have developed subgrains. Recrystallisation of both feldspar and quartz is common.

Mat 35 (px-free granite with >71 wt.% SiO_2)

This is a fine to medium grained porphyritic rock that had suffered moderate recrystallisation of the felsic minerals. Biotite (11%) forms anhedral grains with an average grain size of 1mm. A very small number of biotite grains are intergrown with quartz, possibly suggesting a magmatic origin. A large proportion of biotite is associated with titanite, suggesting a subsolidus origin at the expense of titanite. Biotite replacement by subsolidus muscovite is common. Ilmenite (traces) commonly occurs as minute crystal rimmed by secondary titanite. Titanite (1%) forms subhedral to anhedral grains which more commonly < 0.3mm. Anhedral titanite grains are always associated with biotite and have evidence of minute (and rarely bigger) ilmenite which they replaced. This titanite is subsolidus and has in turn altered to form biotite. The subhedral titanite grains are also associated with biotite which in turn is intergrown with quartz, but ilmenite is absent in the neighbourhood- this is possibly magmatic titanite.

Plagioclase (18%) and alkali feldspar (30) form anhedral grains most of which are ~4mm in diameter. Phenocrysts of both plagioclase and alkali feldspar are present with an average of ~20mm in diameter. Alkali feldspar is dominated by microcline. Granophyric texture is common. Apatite (traces) is typically less than 0.02mm and occurs as an inclusion in the

feldspars. Quartz (40%) forms anhedral grains that have commonly developed subgrains as well as recrystallisation. The non-recrystallised grains may be as big as 1.7mm.

Mat 41 (px-free granite with SiO_2 >71 wt.%)

This is a fine to medium grained porphyritic rock. Biotite (1%) exhibits anhedral grains which are commonly skeletal/fragmentary suggesting formation at the expense of either hornblende or pyroxene. An intergrowth with alkali feldspar is common. Biotite grain size is generally at micron scale but up to 1.5mm grains rarely occur. Hornblende (traces) occurs only as very tiny (micron scale) 'remnant' around where biotite is or at the core of a biotite grain. It is therefore more probable that hornblende reacted out with the melt to produce biotite. Ilmenite (1%) occurs as minute grains (< 0.3mm) which are nearly always rimmed by a thin slice of titanite. Ilmenite in turn has inclusions of small biotite grains. Titanite (traces) forms anhedral grains which are typically < 0.5mm and had formed as a subsolidus phase at the expense of mostly ilmenite ± biotite. Accessory apatite and zircon occur as inclusions in the feldspars.

Plagioclase (23%) and alkali feldspar (40%) form anhedral grains that are dominantly <4mm in diameter. Phenocrysts up to ~10mm are common. Alkali feldspar is dominated by microcline. Myrmekitic texture is present. The myrmekitic plagioclase is in turn an inclusion in microcline. Twinning is nearly always present in both alkali feldspar and plagioclase. Quartz (33%) forms anhedral grains most of which are ~3mm in diameter and has commonly developed subgrains. There are zircon inclusions in quartz.

Mat 20 (px-free granite with SiO_2 >71 wt.%)

This is a generally medium grained (average 2mm) porphyritic rock with moderate recrystallisation of felsic minerals. Biotite (6%) forms anhedral grains which can texturally be classified into two generations. The dominant generation is that of subsolidus biotite which commonly occurs in clusters with secondary titanite ± altered ilmenite. This biotite had formed at the expense of both titanite and ilmenite. The other generation consists of biotite which in a few cases is poikilitically enclosed in plagioclase and more commonly intergrown with quartz. This biotite is interpreted to be magmatic. Ilmenite (traces) forms minute grains which are more commonly rimmed by subsolidus titanite.

Plagioclase (34%) and alkali feldspar (30%) form euhedral to anhedral grains majority of which are ~5mm. Phenocryst of both alkali feldspar and plagioclase are present and about 10mm in diameter. Zircon and apatite are accessory phases occurring as inclusions in the feldspars. Quartz (29%) forms anhedral grains which are moderately recrystallised.

Mat 43 (px-free granite with SiO_2 >71 wt.%)

This is a very fine to fine grained rock in which none of the minerals present shows distinct shapes. Biotite (traces) forms anhedral grains that are commonly less than 0.005mm. It is intergrown with quartz and/ or microcline. Opaque minerals (traces) occur as minute grains that are either interstitial or inclusions in the feldspars. Plagioclase (5%) and alkali feldspar (59%) form anhedral grains which are generally < 0.6mm in diameter. Plagioclase commonly has albite twinning. Alkali feldspar is dominated by microcline. Minute apatite inclusions are present both feldspars. Quartz (35%) forms anhedral grains which are typically < 0.5mm.

Mat 63 (px-free granite with SiO_2 >71 wt.%)

This is a generally fine-gained porphyritic rock with the average size of smaller grains being equigranular (0.2~mm). Overall texture of the rock suggests subsolidus re-equilibration which has by large caused most of the microcline to have twinning that suggests such re-equilibration. Recrystallisation of quartz and microcline is relatively abundant especially along boundaries of bigger grains. Biotite (4%) forms anhedral grains most of which are < 0.2mm and commonly intergrown with quartz. In fresher parts of the thin section, biotite, ilmenite and epidote tend to form a distinct glomeropophyritic texture. Ilmenite (traces) forms micron scale grains. Epidote (traces) forms anhedral grains which are typically 0.2mm and have seemingly pseudomorphed hornblende. There is however no evidence of hornblende in this rock.

Plagioclase (12%) and alkali feldspar (43%) form anhedral grains ranging from micron scale to phenocrysts which may be as big as 6mm in diameter. The phenocrysts are only of alkali feldspar composition. Myrmekitic texture is present and the myrmekitic plagioclase is commonly poikilitically enclosed in alkali feldspar. Minute apatite inclusions are present in both plagioclase and alkali feldspar. Both feldspars exhibit undulose extinction. Quartz (40%) forms anhedral grains which are fresh relative to all other minerals, free of inclusions and have commonly developed subgrains.

Mat 65 (px-free granite with SiO_2 >71 wt.%)

This is a fine to medium grained rock with occasional alkali feldspar phenocrysts that may range up to 10mm. Recrystallisation of plagioclase, alkali feldspar and quartz along boundaries of bigger grains is common. Rarely, biotite and opaque mineral(s) are found along the edges of feldspar. Sericitisation of plagioclase is common, but is not accompanied by epidote inclusions. Biotite (5%) forms subhedral to anhedral grains which are mostly < 3mm in diameter. Ilmenite (traces) forms smaller grains which occur around 'spots' where biotite also occur as well as around 'zones' of recrystallised quartz and feldspar. Titanite (traces) forms very

small grains (micron scale) typically where biotite and ilmenite occur and is suggestively not a replacement of ilmenite- it is most probably magmatic.

Plagioclase (5%) and alkali feldspar (44%) form subhedral to anhedral grains which are mainly smaller than 1mm. Phenocrysts of alkali feldspar of up to 10mm show calsbard twinning. A rare alkali feldspar overgrowth on myrmekitic plagioclase is present, possibly due to a subsolidus process. Microcline indicates subsolidus re-equilibration. Undulose extinction and sericitisation of both feldspars are common. Tiny apatite inclusions are present in both plagioclase and alkali feldspar. Quartz (45%) has anhedral grains that vary from micron scale to ~ 0.5mm. Majority of quartz grains have developed subgrains. There are minute zircon inclusions in quartz.

Mat 5 (enclave in px-free granodiorite)

Biotite (15%) ranges from euhedral to anhedral with most grains being is less than 1mm, though a few grains of ~1mm do exist. It commonly forms 'clusters' with titanite. Some non-pleochroic biotite grains form part of titanite grains and seemingly formed from the altered titanite, at subsolidus conditions. Inclusions of apatite are present in biotite. Titanite (2%) forms anhedral grains with average size of ~0.2mm. It most commonly has tiny 'inclusions' of ilmenite grains, presumably the only relic left after transformation to titanite. This ilmenite-titanite transformation occurred at subsolidus conditions. Titanite is rarely an inclusion in alkali feldspar, possibly also having replaced ilmenite which was an inclusion in the feldspar.

Plagioclase (60%) and alkali feldspar (2%) show anhedral to subhedral grains that are mostly <2mm but rarely range up to 3.5mm. A significant number of grains are prismatic. Twinning is very limited in both plagioclase and alkali feldspar. Sericitisation is pervasive and where more intense, relatively bigger epidote grains occur (together with the smaller ones) in the feldspars. This bigger epidote grains are misleadingly suggesting epidote to be a magmatic inclusion in the feldspar. Although most of the epidote in this rock is subsolidus, a few magmatic grains do exist as ~0.4mm symplectitic to well-developed euhedral grains that commonly occur in a matrix of smaller biotite and felsic minerals. Both subsolidus and magmatic epidotes are optically zoned. Quartz (20%) exhibit anhedral grains and is most commonly recrystallised.

Mat 6 (enclave in px-free granodiorite)

Biotite (20%) exhibits euhedral grains which are typically <1mm and prismatic with no preferred orientation. In a few cases it is intergrown with quartz, suggesting a magmatic origin where pyroxene or hornblende reacted with the melt to produce biotite and quartz. Ilmenite (traces) forms smaller grains that are rarely ~ 0.6mm. Most commonly, ilmenite has a titanite

rim around it. Titanite (traces) occurs as an anhedral grains, typically <0.7mm and most probably all subsolidus owing to ilmenite alteration.

Plagioclase (25%) and alkali feldspar (40%) form anhedral to subhedral grains which commonly show no twinning. Grain size is mainly <1mm but grains up to 4mm do exist. Myrmekitic texture is present and it is common to find a myrmekitic plagioclase inclusion in alkali feldspar. Perthitic texture and sericitisation are frequently accompanied by epidote microlite inclusions in the feldspars. Epidote (1%) occurs both as magmatic and subsolidus phase. The subsolidus epidote is typically on micron scale and occurs as microlite inclusion in the feldspar (rarely in biotite) while magmatic epidote occurs as symplectitic grains which are not inclusions. The size of magmatic epidote may range up to ~1mm in diameter. Quartz (13%) forms relatively fresh grains which in most cases have developed sub-grains and less commonly recrystallised.

Mat 37 (enclave in px-free granodiorite)

Biotite (50%) forms anhedral grains which are generally <1mm and commonly associated with hornblende. Some grains are suggestively subsolidus due to hornblende alteration. Hornblende (27%) forms anhedral grains which in most cases have been subjected to subsolidus deformation. Grain size is generally <2mm. Ilmenite (1%) forms minute grains which are nearly always rimmed by titanite. Titanite (2%) is anhedral and typically < 1mm and is most probably all subsolidus and formed owing to ilmenite alteration. Accessory zircon occurs as an inclusion in biotite and feldspar.

Plagioclase (5%) and alkali feldspar (2%) exhibit subhedral to anhedral grains. Twinning in both plagioclase and alkali feldspar is limited. Alkali feldspar is dominated by microcline and sericitisation is significant. Epidote (3%) shows anhedral grains all of which are presumably subsolidus. Bigger grains are nearly always associated with hornblende ± titanite mostly forming along the edges of both hornblende and titanite. Smaller grains which are commonly inclusions in feldspar are also subsolidus. Quartz (10%) forms relatively fresh and inclusion-free grains, a significant number of which have developed subgrains.

Mat 40 (enclave in px-free granodiorite)

This is a fine grained rock with the assemblage that suggests both igneous and low grade metamorphic minerals to coexist. Biotite (10%) is anhedral and generally less than 0.2mm, but a few grains up to 1mm occur. An intergrowth with quartz is common suggesting formation at the expense of hornblende (or pyroxene), possibly in a magmatic environment. Opaque minerals (traces) form very small grains which are commonly inclusions in feldspars and mafic

minerals. Titanite (2%) exhibits generally equigranular (~0.8mm) anhedral grains which have mostly weathered to leucoxene. No ilmenite core has been found in any titanite grain; titanite is possibly magmatic. Inclusions of epidotes and plagioclase (~0.2mm) are present in titanite. Epidote (1%) occurs both as magmatic and subsolidus phase. Magmatic epidote occurs as anhedral (commonly symplectitic) grains, of about 0.2mm, which are nearly always glomeropophyritic with biotite and titanite. Subsolidus epidote occurs as microlite inclusion in both plagioclase and alkali feldspar. Both epidote varieties are optically zoned. The symplectitic epidote suggests resorption in a magmatic environment.

Plagioclase (10%) and alkali feldspar (50%) form anhedral and rarely subhedral grains with a size ranging from a few microns up to 0.7mm. Plagioclase typically shows well developed albite twinning and alkali feldspar is dominated by microcline. Some grains show marked undulose extinction. Quartz (23%) is anhedral, relatively fresh and has significantly developed subgrains.

Mat 47- (enclave in px-diorite2)

Biotite (30%) forms anhedral grains that are more commonly between 1.5mm to 3mm and rarely up to 6mm in diameter. An intergrowth with quartz is common, probably suggesting a magmatic origin. Some grains are typically 'skeletal', seemingly subsolidus by-product of pyroxene and hornblende alteration. Hornblende (3%) forms anhedral grains that are on average 2mm in diameter. Majority of the grains seemingly formed at the expense of pyroxene at subsolidus conditions. Replacement of pyroxene is testified by the presence of heavily deformed skeletal pyroxene grains where hornblende occurs. Some grains of hornblende seemingly formed in equilibrium with orthopyroxene though.

Magnetite (2%), ilmenite and chalcopyrite (traces) occur as interstitial phases, as inclusions in apatite, plagioclase and pyroxene relics as well as inclusions in the skeletal hornblende and biotite that formed at the expense of pyroxene. Accessory apatite also occurs as an inclusion in hornblende and in the heavily altered pyroxene. The grain size of apatite may range up to ~0.4mm. Anhedral epidote (traces) with grain size of about 0.2mm occurs typically where biotite is present. When it is an inclusion in albite, it occurs in the vicinity of ilmenite. Epidote is a subsolidus phase in this rock.

Plagioclase (60%) and alkali feldspar (2%) form subhedral to anhedral grains with size mostly between 0.7 – 2mm. Plagioclase occurs as an inclusion in biotite. A few grains show albite twinning but twinning is generally absent. Most grains are heavily sericitised, the by-

product of which is muscovite. Quartz (5%) is anhedral and has inclusions of small magnetite and hornblende grains.

Mat 56 (enclave in px-diorite2)

Biotite (9%) forms anhedral to subhedral grains that occur either intergrown with quartz or more commonly as a replacement of hornblende. In the latter case it is nearly always skeletal and in the former case it is fairly subhedral and probably formed due to replacement of pyroxene in the magmatic environment. The grain size is generally less than 0.4mm but on rare occasions may range up to 0.9mm. Hornblende (13%) forms anhedral grains most of which are smaller than 0.9mm. Hornblende suggestively formed at the expense of pyroxene as shown by rare clinopyroxene cores in the interior of a few hornblende grains. Both biotite and hornblende also define the minor schistocity seen in this rock and are elongated in a common direction. Pyroxene grains up to ~0.2mm are occasionally preserved, even though they are severely deformed. Magnetite, ilmenite (~1 %) and apatite (traces) form anhedral grains with less than 0.3mm in diameter and most commonly agglomerate where hornblende and biotite are found and rarely as inclusions in the hornblende.

Plagioclase (50%) is anhedral and may occasionally range up to 2mm, but on average is 1mm. Twinning is rare. Myrmekitic texture is occasionally present. Deformational twinning, undulose extinction and sericitisation are infrequently present. Where present, sericitisation is not as severe as it is in the px-free granitoids. In the sericitised grains, both biotite and hornblende are occasionally inclusions in the plagioclase. Quartz (27%) forms ≤ 0.1mm anhedral grains which are free of inclusions.

Mat 61 (enclave in px-diorite2)

This is a fairly equigranular rock with the assemblage that attests to magmatic origin. Biotite (9%) forms anhedral grains with an average of ~0.4mm in diameter. A fair number of grains intergrown with quartz are prismatic, well developed and randomly oriented, suggesting a magmatic origin. Some biotite grains are interstitial while others are embayed onto hornblende, suggesting magmatic origin of both minerals. Hornblende (26%) ranges from euhedral through subhedral to anhedral, but the majority being subhedral. The average grain size is ~0.4mm and the smallest grains occur as inclusions in plagioclase. Opaque minerals (1%) and apatite (traces) form micron scale grains which are inclusions in the feldspars and in hornblende.

Plagioclase (45%) and alkali feldspar (3%) exhibit anhedral to subhedral grains which are more commonly ~ 0.4mm and rarely ~ 0.9mm in diameter. Myrmekitic texture is rare.

Many grains do not show twinning. A few grains show undulose extinction. Quartz (15%) forms ~3mm subhedral to anhedral grains that typically have developed subgrains.

B. Bulk rock and mineral chemistry analyses

B.1. Rock powder preparation:

Preparation of bulk rock powders involved the cutting of samples with a diamond cutter to break into smaller chips. The chips were crushed with a jaw crusher and afterwards ground with either agate, tungsten or steel mill. Prior to grinding, the samples ground with the agate mill were also subjected to a smaller jaw crusher to make even smaller chips which would suit the size of the agate mill. Milling time was 40 minutes for each addition in the agate mill and samples ground with tungsten or steel mill were done so for three minutes per addition.

B.2. Bulk rock major and trace element analyses

Bulk rock major and trace element analyses of the rock powders were performed at ACME laboratories in Vancouver, Canada. For major element compositions a 0.1g of each sample was fused with lithium metaborate/tetraborate, digested in nitric acid and ignited at 1000^{o}C. Major element analyses were carried out by inductively coupled plasma (ICP)-emission spectrometry technique. The same sample preparation was followed for trace elements but analyses were run by the inductively coupled plasma-mass spectrometry (ICP-MS) method. The exceptions were Ni and Pb which were analysed from a 0.5g sample which was digested in Aqua Regia at 95^{o}C and analysed by the ICP-MS. Multiple analyses of the DS7 standard for Ni and Pb and the SO-18 standard for major and all other trace elements gave agreeing results at better than 95% confidence level. Generally, all concentrations used in this project were obtained well above detection limits of the instruments. Duplicates for selected samples were analysed and it was discovered that rock powders milled with the tungsten mill were severely contaminated with W and Co while samples milled with steel mill were contaminated with Cr. The samples that were subjected to a smaller jaw crusher (for agate mill) were contaminated with Ni. All other elements and oxides not affected by this contamination matched within >95% confidence level. For these reasons the concentrations of contaminated elements are not included in this project.

B.3. Mineral chemistry

Mineral chemistry analyses were performed on a scanning electron microscope (SEM) LEO® 1430VP instrument at the University of Stellenbosch. Concentrations of major element oxides for minerals were analysed on a ~0.03mm polished thin sections. The analytical set up conditions were a working distance of 13mm, a 30µm hole and 30g aperture, 30^{o} angle of detector, a beam current of 20nA, acceleration voltage of 20kv, spot size in the range -3.92 to -4A and 50 seconds per background counting time. The reported oxide proportions were standardised against Astimex mineral standards. All Fe (FeO*) was reported as Fe^{2+}.

Minerals with vacancies in their crystal structures pose a notable thread to determining the theoretical Fe^{3+}/Fe^{2+} ratio because the true cationic total is unknown. A published hornblende analytical and associated cationic data has been used as a reference standard to weigh up the precision of the theoretical Fe^{3+}/Fe^{2+} ratio of hornblende analyses in this project. The following tables present the magnesio-hornblende analysis (number 26) taken from page 245 of Deer et al. (1963). The equation of Droop (1987) for calculating the Fe^{3+} and Fe^{2+} for amphibole has been adopted to calculate the cation totals for this magnesio-hornblende. The results are compared with the published cation totals and it can be seen that there is not much difference between the 'published' and the 'herein' cations in the tables below. For this reason, the Fe^{3+}/Fe^{2+} ratio for hornblende of the Matok pluton granitoids in this study (used in section 4.3) are reasonably reliable.

Magnesio-hornblende analysis (number 26):

SiO_2	Al_2O_3	TiO_2	MgO	FeO	MnO	CaO	Na_2O	K_2O
45.69	8.43	1.06	11.64	17.23	0.42	12.11	0.51	0.71

Cations:

Cations	Si	Al	Ti	Fe^{3+}	Mg	Fe^{2+}	Mn	Ca	Na	K
published	6.709	1.291	0.117	0.801	2.547	1.315	0.052	1.905	0.095	0.133
herein	6.857	1.491	0.120	0.802	2.604	1.351	0.053	1.947	0.148	0.136

The mineral chemical compositions and associated cations for the Matok pluton granitoids are presented in the tables below. nd stands for not detected. All the analyses are presented as obtained from the electron microscope. Cations of pyroxene have also been 'corrected' according to the formula of Droop (1987) to account for both Fe^{3+} and Fe^{2+}, and hence the cation total is always 4. $_r$ stands for rim and $_c$ stands for core, i.e. analyses taken at the rim and core respectively.

Table C1. Clinopyroxene composition for the rocks of the Matok pluton.

Rock type	px-diorites1									px-diorites2								
Sample	Mat 60c	Mat 60$_r$	Mat 60	Mat 60c	Mat 60$_r$	Mat 60	Mat 60	Mat 60	Mat 60	Mat 26	Mat 26	Mat 26	Mat 29c	Mat 29$_r$	Mat 29$_r$	Mat 29c	Mat 29c	Mat 29$_r$
SiO_2	51.64	52.09	52.16	52.12	52.19	52.10	52.29	52.74	51.57	51.60	53.31	51.28	51.69	53.10	51.62	52.34	51.93	52.46
TiO_2	nd	nd	nd	nd	nd	nd	nd	nd	nd	0.14	nd	0.18	0.24	0.20	0.31	0.17	0.15	0.20
Al_2O_3	1.68	1.36	1.19	1.38	1.34	1.52	1.59	1.45	1.39	1.42	2.48	1.36	1.61	1.37	1.35	1.24	1.24	1.29
FeO*	12.57	12.41	11.50	12.48	12.94	12.71	12.83	12.83	12.56	12.40	13.59	13.29	12.38	12.11	12.15	12.06	12.22	11.79
MnO	0.98	1.19	1.03	1.11	1.21	1.06	0.95	1.20	1.03	0.39	0.28	0.39	0.52	0.61	0.57	0.68	0.58	0.62
MgO	11.54	11.94	12.15	11.76	11.62	11.77	11.68	11.86	11.59	12.06	11.78	11.92	11.71	11.97	11.64	11.88	11.90	12.01
CaO	21.42	21.49	21.76	21.67	21.29	21.35	21.66	21.41	21.22	20.64	18.78	20.35	21.03	21.90	21.46	21.69	21.57	21.75
Na_2O	0.62	0.61	0.51	0.49	0.57	0.56	0.59	0.51	0.66	0.60	0.53	0.66	0.74	0.71	0.62	0.67	0.57	0.62
Total	98.83	99.94	99.45	100.25	99.95	99.79	100.51	100.36	99.22	99.25	100.75	99.43	100.00	101.94	99.69	100.76	100.32	100.74
Number of ions on the basis of 6 oxygen atoms:																		
Si^{4+}	1.943	1.946	1.960	1.952	1.954	1.949	1.946	1.957	1.948	1.959	2.002	1.948	1.951	1.963	1.955	1.960	1.957	1.963
Al^{3+}	0.074	0.060	0.053	0.061	0.059	0.067	0.070	0.063	0.062	0.063	0.110	0.061	0.071	0.060	0.060	0.055	0.055	0.057
Fe^{3+}	0.085	0.092	0.064	0.071	0.074	0.074	0.080	0.059	0.089	0.053	0.000	0.082	0.068	0.053	0.058	0.064	0.064	0.051
Cr^{3+}	0.000	0.000	0.000	0.000	0.000	0.000	0.000	0.000	0.000	0.002	0.000	0.000	0.000	0.000	0.000	0.000	0.000	0.000
Ti^{4+}	0.000	0.000	0.000	0.000	0.000	0.000	0.000	0.000	0.000	0.004	0.000	0.005	0.007	0.005	0.009	0.005	0.004	0.006
Mg^{2+}	0.647	0.665	0.680	0.657	0.648	0.656	0.648	0.656	0.653	0.683	0.659	0.675	0.659	0.660	0.657	0.663	0.668	0.670
Fe^{2+}	0.310	0.295	0.298	0.320	0.331	0.323	0.320	0.339	0.308	0.341	0.427	0.340	0.323	0.321	0.327	0.313	0.321	0.317
Mn^{2+}	0.031	0.038	0.033	0.035	0.038	0.034	0.030	0.038	0.033	0.012	0.009	0.013	0.017	0.019	0.018	0.022	0.019	0.020
Ca^{2+}	0.863	0.860	0.876	0.870	0.854	0.856	0.864	0.851	0.859	0.839	0.756	0.828	0.850	0.868	0.871	0.870	0.871	0.872
Na^{+}	0.046	0.044	0.037	0.036	0.042	0.040	0.043	0.036	0.048	0.044	0.039	0.049	0.054	0.051	0.046	0.048	0.042	0.045
Cation total	4.000	4.000	4.000	4.000	4.000	4.000	4.000	4.000	4.000	4.000	4.000	4.000	4.000	4.000	4.000	4.000	4.000	4.000
En	0.355	0.365	0.367	0.356	0.354	0.358	0.354	0.355	0.359	0.366	0.358	0.366	0.360	0.357	0.354	0.359	0.359	0.360
Fer	0.170	0.162	0.161	0.173	0.181	0.176	0.175	0.184	0.169	0.183	0.232	0.185	0.176	0.174	0.176	0.170	0.172	0.171
Wo	0.474	0.472	0.472	0.471	0.466	0.466	0.472	0.461	0.472	0.451	0.410	0.449	0.464	0.469	0.470	0.471	0.468	0.469

Table C1 (*continued*)

Rock type	px-diorites2													px-granodiorites			
Sample	Mat 29_r	Mat 29c	Mat 29	Mat 29c	Mat 29_r	Mat 66	Mat 66	Mat 66	Mat 66	Mat 66	Mat 66	Mat 66	Mat 66	Mat 27	Mat 27	Mat 62	Mat 62
SiO_2	52.45	52.33	52.01	51.26	51.68	54.05	52.20	52.85	53.74	53.20	54.07	54.21	51.91	51.85	52.90	52.29	52.37
TiO_2	0.26	0.19	0.19	0.19	0.24	nd	nd	nd	nd	nd	nd	nd	nd	0.15	0.11	nd	nd
Al_2O_3	1.22	0.93	0.87	1.25	1.27	2.11	2.20	1.34	1.35	0.93	1.14	0.94	2.76	1.05	1.06	1.30	1.22
FeO*	11.54	11.05	11.21	11.87	11.87	20.89	20.88	18.53	18.80	17.36	19.15	17.43	21.54	13.18	12.63	13.57	13.55
MnO	0.60	0.50	0.70	0.58	0.54	0.38	0.32	0.22	0.26	0.36	0.32	0.48	0.33	0.35	0.33	1.20	1.17
MgO	12.15	12.24	11.98	11.63	11.79	12.59	12.30	12.32	12.40	12.64	12.36	13.31	10.73	11.36	11.69	10.83	10.85
CaO	21.97	22.54	21.97	21.45	21.86	11.48	11.17	12.39	12.55	14.49	12.27	12.52	11.00	19.94	21.19	21.82	22.11
Na_2O	0.58	0.49	0.58	0.63	0.62	0.49	0.52	0.41	0.42	0.34	0.40	0.35	0.47	0.60	0.66	0.76	0.80
Total	100.74	100.25	99.52	98.82	99.84	101.47	99.46	98.10	99.58	98.52	99.93	99.22	96.83	98.62	100.57	100.41	100.60
Number of ions on the basis of 6 oxygen atoms:																	
Si^{4+}	1.961	1.964	1.969	1.956	1.952	2.033	2.011	2.062	2.067	2.043	2.078	2.080	2.033	1.994	1.987	1.951	1.948
Al^{3+}	0.054	0.041	0.039	0.056	0.056	0.093	0.100	0.061	0.061	0.042	0.052	0.043	0.128	0.047	0.047	0.057	0.054
Fe^{3+}	0.052	0.055	0.054	0.068	0.071	0.000	0.000	0.000	0.000	0.000	0.000	0.000	0.000	0.000	0.020	0.094	0.108
Cr^{3+}	0.000	0.000	0.000	0.000	0.000	0.000	0.000	0.000	0.000	0.000	0.000	0.000	0.000	0.000	0.000	0.000	0.000
Ti^{4+}	0.007	0.005	0.005	0.005	0.007	0.000	0.000	0.000	0.000	0.000	0.000	0.000	0.000	0.004	0.003	0.000	0.000
Mg^{2+}	0.677	0.685	0.676	0.662	0.664	0.706	0.706	0.716	0.711	0.724	0.709	0.761	0.626	0.652	0.655	0.603	0.602
Fe^{2+}	0.309	0.292	0.301	0.311	0.303	0.657	0.673	0.604	0.604	0.558	0.616	0.559	0.705	0.424	0.377	0.330	0.313
Mn^{2+}	0.019	0.016	0.022	0.019	0.017	0.012	0.010	0.007	0.008	0.012	0.010	0.016	0.011	0.012	0.011	0.038	0.037
Ca^{2+}	0.880	0.906	0.891	0.877	0.884	0.463	0.461	0.518	0.517	0.596	0.505	0.515	0.461	0.822	0.853	0.873	0.881
Na^{+}	0.042	0.036	0.042	0.047	0.045	0.036	0.039	0.031	0.032	0.025	0.030	0.026	0.036	0.045	0.048	0.055	0.058
Cation total	4.000	4.000	4.000	4.000	4.000	4.000	4.000	4.000	4.000	4.000	4.000	4.000	4.000	4.000	4.000	4.000	4.000
En	0.363	0.364	0.362	0.358	0.358	0.362	0.367	0.359	0.356	0.365	0.352	0.378	0.321	0.341	0.345	0.334	0.335
Fer	0.166	0.155	0.161	0.168	0.164	0.401	0.393	0.381	0.385	0.334	0.396	0.366	0.443	0.228	0.205	0.183	0.174
Wo	0.472	0.481	0.477	0.474	0.478	0.237	0.240	0.260	0.259	0.301	0.251	0.256	0.236	0.430	0.450	0.483	0.491

Table C2. Orthopyroxene composition for the rocks of the Matok pluton.

	px-diorites1		px-diorites2									
Sample	Mat 60	Mat 60	Mat 26	Mat 26	Mat 26	Mat 26	Mat 26	Mat 26	Mat 26	Mat 26	Mat 26	Mat 26
SiO_2	49.97	50.08	50.12	49.63	49.93	50.48	51.00	50.05	50.61	50.94	50.31	50.70
TiO_2	nd	nd	0.05	0.11	0.05	nd	nd	nd	nd	0.15	0.06	0.05
Al_2O_3	0.69	1.14	0.76	0.69	0.68	0.73	0.61	0.73	0.73	0.58	0.63	0.70
Cr_2O_3	nd	nd	nd	0.01	0.07	nd	nd	nd	0.04	0.23	0.01	nd
FeO*	30.36	31.45	30.03	30.27	30.28	30.98	30.48	30.11	30.53	30.14	30.51	30.44
MnO	2.77	2.77	1.00	0.88	0.97	1.03	0.97	0.98	0.94	1.02	0.88	0.96
MgO	15.63	15.59	16.71	16.96	16.83	16.90	17.12	16.85	17.11	17.10	16.70	17.31
CaO	0.80	0.69	0.77	0.46	0.48	0.39	0.57	0.54	0.58	0.58	0.88	0.49
Na_2O	0.27	0.21	0.15	0.18	0.32	0.29	0.24	nd	0.27	0.20	0.21	0.22
K_2O	nd	nd	nd	0.01	0.01	nd	0.02	nd	nd	0.02	nd	nd
Total	99.93	101.50	99.60	99.20	99.62	100.80	101.01	99.25	100.81	100.95	100.19	100.86
Number of ions on the basis of 6 oxygen atoms:												
Si^{4+}	1.937	1.918	1.946	1.933	1.935	1.936	1.949	1.951	1.938	1.950	1.942	1.939
Al^{3+}	0.032	0.051	0.035	0.031	0.031	0.033	0.028	0.033	0.033	0.026	0.028	0.031
Fe^{3+}	0.114	0.127	0.081	0.110	0.117	0.115	0.091	0.064	0.109	0.074	0.098	0.103
Cr^{3+}	0.000	0.000	0.000	0.000	0.002	0.000	0.000	0.000	0.001	0.007	0.000	0.000
Ti^{4+}	0.000	0.000	0.002	0.003	0.001	0.000	0.000	0.000	0.000	0.004	0.002	0.001
Mg^{2+}	0.903	0.890	0.967	0.985	0.972	0.966	0.976	0.979	0.977	0.976	0.961	0.987
Fe^{2+}	0.870	0.880	0.893	0.876	0.864	0.879	0.883	0.918	0.869	0.891	0.887	0.871
Mn^{2+}	0.091	0.090	0.033	0.029	0.032	0.033	0.031	0.032	0.031	0.033	0.029	0.031
Ca^{2+}	0.033	0.028	0.032	0.019	0.020	0.016	0.023	0.023	0.024	0.024	0.036	0.020
Na^{+}	0.020	0.015	0.011	0.014	0.024	0.021	0.017	0.000	0.020	0.015	0.016	0.016
K^{+}	0.000	0.000	0.000	0.000	0.000	0.000	0.001	0.000	0.000	0.001	0.000	0.000
Cation total	4.000	4.000	4.000	4.000	4.000	4.000	4.000	4.000	4.000	4.000	4.000	4.000
En	0.476	0.471	0.502	0.516	0.515	0.510	0.510	0.502	0.514	0.507	0.502	0.517
Fer	0.507	0.514	0.481	0.474	0.475	0.481	0.478	0.487	0.473	0.480	0.478	0.472
Wo	0.017	0.015	0.017	0.010	0.011	0.008	0.012	0.012	0.012	0.012	0.019	0.011

Table C2. (*continued*)

Rock type	**px-diorites2**		**px-granodiorites**								
Sample	Mat 66	Mat 66	Mat 27	Mat 27	Mat 27	Mat 27	Mat 27	Mat 27	Mat 27	Mat 27	Mat 27
SiO_2	53.10	49.62	50.12	50.85	50.97	51.48	50.82	50.74	50.46	51.12	51.54
TiO_2	nd	0.14	0.05	0.07	0.05	0.02	nd	0.17	0.10	0.08	0.18
Al_2O_3	0.94	1.37	0.72	0.61	0.65	0.61	0.55	0.55	0.59	0.69	0.70
Cr_2O_3	nd	nd	nd	nd	nd	nd	nd	nd	nd	nd	nd
FeO*	24.09	26.75	31.93	31.89	31.88	32.20	31.79	31.88	30.39	30.65	30.88
MnO	3.85	2.75	0.74	0.82	0.89	0.98	0.88	0.87	0.58	0.62	0.72
MgO	15.77	13.88	15.44	14.98	15.03	14.95	14.86	14.95	15.75	15.76	16.11
CaO	2.54	3.34	0.67	0.68	0.67	0.38	0.71	0.57	0.81	0.80	0.64
Na_2O	0.44	0.32	0.37	0.27	0.21	0.27	0.30	0.31	0.22	0.29	0.22
K_2O	nd	nd	nd	nd	nd	nd	nd	nd	nd	nd	nd
Total	99.92	98.26	100.04	100.17	100.36	100.90	99.89	100.02	99.05	100.00	100.98
Number of ions on the basis of 6 oxygen atoms:											
Si^{4+}	2.029	1.966	1.951	1.983	1.985	1.995	1.988	1.982	1.981	1.984	1.982
Al^{3+}	0.042	0.064	0.033	0.028	0.030	0.028	0.025	0.025	0.027	0.032	0.032
Fe^{3+}	0.000	0.019	0.090	0.022	0.014	0.001	0.022	0.023	0.023	0.017	0.011
Cr^{3+}	0.000	0.000	0.000	0.000	0.000	0.000	0.000	0.000	0.000	0.000	0.000
Ti^{4+}	0.000	0.004	0.002	0.002	0.001	0.001	0.000	0.005	0.003	0.002	0.005
Mg^{2+}	0.898	0.820	0.896	0.871	0.873	0.864	0.867	0.870	0.922	0.912	0.923
Fe^{2+}	0.838	0.867	0.949	1.018	1.024	1.043	1.018	1.018	0.975	0.978	0.982
Mn^{2+}	0.125	0.092	0.024	0.027	0.029	0.032	0.029	0.029	0.019	0.020	0.024
Ca^{2+}	0.104	0.142	0.028	0.029	0.028	0.016	0.030	0.024	0.034	0.033	0.026
Na^{+}	0.032	0.025	0.028	0.020	0.016	0.021	0.022	0.023	0.017	0.022	0.016
K^{+}	0.000	0.000	0.000	0.000	0.000	0.000	0.000	0.000	0.000	0.000	0.000
Cation total	4.000	4.000	4.000	4.000	4.000	4.000	4.000	4.000	4.000	4.000	4.000
En	0.457	0.427	0.472	0.448	0.447	0.442	0.446	0.448	0.473	0.469	0.472
Fer	0.490	0.499	0.513	0.537	0.539	0.550	0.539	0.539	0.510	0.514	0.514
Wo	0.053	0.074	0.015	0.015	0.014	0.008	0.015	0.012	0.017	0.017	0.013

Table C3. Hornblende composition for the rocks of the Matok pluton

Rock type	Pyroxene-bearing																			
	diorites1																		diorites2	
Sample	Mat 44	Mat 44	Mat 44	Mat 44	Mat 44	Mat 44_r	Mat 44_c	Mat 44	Mat 45	Mat 45	Mat 50	Mat 67_c	Mat 67_r	Mat 67_c	Mat 67_r	Mat 67_c	Mat 67_r	Mat 67_c	Mat 29	Mat 29
SiO_2	43.21	42.46	41.61	41.59	42.07	42.22	40.03	42.75	43.62	42.77	41.80	43.83	44.32	43.74	44.08	43.72	45.41	47.79	39.57	40.56
TiO_2	1.31	1.44	1.21	1.27	1.35	1.22	1.04	1.12	1.08	1.21	0.76	1.55	1.09	1.80	1.23	1.26	0.86	0.68	0.09	0.05
Al_2O_3	9.57	9.48	11.25	9.00	9.60	9.30	12.04	10.12	9.01	9.34	9.02	9.25	10.15	9.18	9.21	9.48	9.14	6.87	13.75	14.02
Cr_2O_3	0.02	nd	nd	nd	nd	0.04	0.04	nd	nd	nd	0.07	0.05	nd	0.08	nd	nd	nd	nd	nd	nd
FeO*	20.26	20.97	17.90	20.25	20.40	20.04	21.51	20.29	19.67	19.91	19.02	20.66	19.97	20.96	20.90	20.59	19.55	18.63	18.55	18.94
MnO	0.32	0.39	0.33	0.36	0.27	0.34	0.34	0.28	0.36	0.39	0.30	0.37	0.34	0.33	0.33	0.36	0.40	0.39	0.18	0.33
MgO	9.34	9.16	9.30	8.66	8.97	9.14	7.61	9.26	9.72	9.31	9.36	8.93	8.94	9.12	9.27	9.15	9.59	11.05	8.79	8.81
CaO	12.01	11.81	11.34	11.47	11.65	11.76	11.58	11.89	11.60	11.52	11.33	11.60	11.73	11.64	11.44	11.69	11.58	11.51	11.74	12.01
Na_2O	1.61	1.61	1.70	1.49	1.61	1.57	1.66	1.69	1.41	1.68	1.39	1.69	1.43	1.73	1.47	1.59	1.42	1.25	1.16	1.18
K_2O	1.44	1.42	1.42	1.43	1.46	1.42	1.94	1.53	1.28	1.38	1.44	1.35	1.37	1.39	1.38	1.46	1.12	0.76	2.37	2.35
Total	99.13	98.72	96.05	95.51	97.37	97.11	97.86	98.93	97.75	97.52	94.47	99.27	99.32	99.97	99.30	99.29	99.07	98.92	96.20	98.25
Number of ions on the basis of 23 oxygen atoms:																				
Si^{4+}	6.421	6.349	6.323	6.436	6.369	6.408	6.047	6.350	6.567	6.450	6.498	6.524	6.583	6.467	6.561	6.495	6.751	7.097	5.994	6.022
$Al^{3+}{}_{total}$	1.675	1.670	6.323	1.641	1.714	1.663	2.143	1.772	1.599	1.660	1.653	1.623	1.776	1.599	1.615	1.660	1.602	1.202	2.454	2.453
sum T	8.000	8.000	6.323	8.000	8.000	8.000	8.000	8.000	8.000	8.000	8.000	8.000	8.000	8.000	8.000	8.000	8.000	8.000	8.000	8.000
Al^{3+}	0.096	0.018	6.323	0.077	0.083	0.071	0.189	0.122	0.166	0.110	0.151	0.148	0.359	0.066	0.176	0.155	0.353	0.299	0.448	0.475
Ti^{4+}	0.146	0.162	6.323	0.148	0.153	0.139	0.118	0.125	0.122	0.137	0.089	0.173	0.122	0.200	0.138	0.140	0.096	0.076	0.010	0.006
Fe^{3+}	0.436	0.632	6.323	0.494	0.525	0.481	0.595	0.498	0.610	0.536	0.585	0.421	0.386	0.489	0.673	0.501	0.474	0.559	0.657	0.626
Mg^{2+}	2.070	2.042	6.323	1.997	2.024	2.068	1.713	2.050	2.181	2.093	2.169	1.982	1.980	2.010	2.056	2.027	2.125	2.446	1.986	1.951
Fe^{2+}	2.131	2.048	6.323	2.178	2.112	2.115	2.203	2.079	1.901	2.024	1.933	2.190	2.118	2.147	1.963	2.100	1.971	1.751	1.760	1.791
Mn^{2+}	0.040	0.049	6.323	0.048	0.035	0.044	0.044	0.035	0.046	0.050	0.040	0.046	0.042	0.042	0.042	0.045	0.050	0.049	0.023	0.042
sum C	4.919	4.952	6.323	4.941	4.932	4.918	4.863	4.910	5.026	4.950	4.968	4.959	5.008	4.954	5.048	4.968	5.069	5.179	4.885	4.890
Sum C-5									0.026				0.008		0.048		0.069	0.179		
Ca^{2+}	1.911	1.891	1.846	1.902	1.889	1.913	1.874	1.892	1.871	1.862	1.887	1.849	1.866	1.844	1.823	1.861	1.845	1.832	1.904	1.910
Na^{+}	0.464	0.465	0.500	0.446	0.472	0.461	0.486	0.485	0.412	0.492	0.418	0.488	0.411	0.495	0.423	0.458	0.409	0.361	0.341	0.341
sum B	2.000	2.000	2.000	2.000	2.000	2.000	2.000	2.000	2.000	2.000	2.000	2.000	2.000	2.000	2.000	2.000	2.000	2.000	2.000	2.000
Na^{+}	0.375	0.356	0.346	0.349	0.361	0.374	0.360	0.377	0.284	0.354	0.305	0.338	0.277	0.340	0.247	0.319	0.254	0.192	0.246	0.250
K^{+}	0.274	0.270	0.275	0.281	0.282	0.276	0.373	0.290	0.245	0.265	0.285	0.257	0.260	0.262	0.262	0.276	0.212	0.144	0.458	0.444
sum A	0.648	0.627	0.621	0.630	0.643	0.650	0.734	0.667	0.529	0.619	0.589	0.594	0.537	0.602	0.509	0.595	0.466	0.337	0.704	0.695
Cation total	15.567	15.579	15.560	15.571	15.575	15.568	15.596	15.577	15.555	15.569	15.557	15.553	15.544	15.555	15.556	15.563	15.535	15.516	15.588	15.585
Fe^{3+}/Fe^{2+}	0.205	0.309	0.237	0.227	0.248	0.228	0.270	0.240	0.321	0.265	0.303	0.192	0.182	0.228	0.343	0.239	0.240	0.319	0.373	0.350
Mg#	0.493	0.499	0.530	0.478	0.489	0.494	0.437	0.496	0.534	0.508	0.529	0.475	0.483	0.484	0.511	0.491	0.519	0.583	0.530	0.521

Table C3. (*Continued*)

Rock type	Pyroxene-bearing																			
	diorites2																granodiorites			
Sample	Mat 52_r	Mat 52_c	Mat 52_c	Mat 52_r	Mat 52	Mat 52	Mat 52	Mat 52	Mat 66_c	Mat 66_r	Mat 66_c	Mat 66_r	Mat 66_c	Mat 66_r	Mat 66_c	Mat 66_r	Mat 62	Mat 62	Mat 62	Mat 57
SiO_2	42.74	42.25	42.94	42.72	42.56	40.05	42.07	42.99	42.30	43.18	43.40	43.98	42.97	43.00	43.09	42.07	43.13	42.89	43.37	41.99
TiO_2	1.07	1.17	1.53	1.39	1.04	0.82	1.10	1.36	1.59	0.75	1.65	1.62	1.97	2.16	1.91	2.13	1.19	1.14	0.24	1.66
Al_2O_3	9.58	9.39	8.97	9.50	10.01	11.52	9.76	8.94	8.79	9.97	9.92	9.62	8.48	8.89	9.02	9.16	9.37	10.29	9.91	9.86
Cr_2O_3	nd	nd	nd	nd	nd	0.04	nd	nd	nd	nd	nd	nd	nd	nd	nd	nd	nd	nd	nd	nd
FeO*	22.28	21.71	22.47	22.70	21.78	23.04	21.88	22.27	21.35	20.86	20.81	20.75	20.93	20.33	20.58	19.97	19.53	18.74	18.72	22.87
MnO	0.34	0.40	0.36	0.40	0.32	0.31	0.40	0.32	0.30	0.41	0.28	0.30	0.35	0.29	0.34	0.29	0.44	0.35	0.53	0.31
MgO	8.08	8.54	8.28	8.11	8.30	7.20	8.34	8.51	9.32	8.75	8.76	9.04	9.20	9.04	8.87	8.81	9.73	9.92	10.19	7.73
CaO	11.38	11.58	11.70	11.68	11.56	11.61	11.42	11.66	10.51	11.05	11.55	11.50	11.05	11.36	11.18	11.17	11.52	11.63	11.64	11.86
Na_2O	1.82	1.93	1.88	1.92	1.66	1.76	1.65	1.74	1.68	1.37	1.66	1.55	1.81	1.82	1.75	1.88	1.77	1.72	1.59	1.75
K_2O	1.49	1.55	1.48	1.49	1.60	2.04	1.58	1.46	1.19	1.41	1.35	1.27	1.43	1.44	1.40	1.44	1.53	1.70	1.52	1.71
Total	98.76	98.51	99.60	99.91	98.83	98.38	98.20	99.25	97.02	97.76	99.38	99.64	98.18	98.31	98.14	96.93	98.21	98.39	97.71	99.75
Number of ions on the basis of 23 oxygen atoms:																				
Si^{4+}	6.415	6.333	6.399	6.345	6.374	6.036	6.345	6.425	6.443	6.529	6.455	6.527	6.468	6.458	6.490	6.400	6.437	6.363	6.471	6.263
$Al^{3+}{}_{total}$	1.695	1.659	1.575	1.662	1.767	2.047	1.734	1.574	1.578	1.776	1.739	1.683	1.505	1.574	1.602	1.643	1.648	1.800	1.743	1.733
sum T	8.000	8.000	8.000	8.000	8.000	8.000	8.000	8.000	8.000	8.000	8.000	8.000	8.000	8.000	8.000	8.000	8.000	8.000	8.000	8.000
Al^{3+}	0.110			0.007	0.140	0.083	0.078		0.021	0.305	0.194	0.210		0.032	0.092	0.043	0.085	0.163	0.214	
Ti^{4+}	0.121	0.132	0.171	0.156	0.117	0.093	0.125	0.153	0.182	0.086	0.185	0.181	0.223	0.243	0.217	0.244	0.133	0.127	0.027	0.187
Fe^{3+}	0.580	0.542	0.468	0.525	0.575	0.652	0.684	0.559	1.129	0.818	0.481	0.561	0.656	0.398	0.499	0.386	0.536	0.487	0.658	0.434
Mg^{2+}	1.808	1.908	1.839	1.795	1.854	1.617	1.875	1.896	2.116	1.973	1.943	2.000	2.064	2.023	1.991	1.998	2.163	2.195	2.268	1.719
Fe^{2+}	2.278	2.254	2.398	2.365	2.212	2.354	2.141	2.286	1.643	1.857	2.146	2.045	2.029	2.200	2.135	2.204	1.954	1.890	1.728	2.492
Mn^{2+}	0.043	0.051	0.045	0.050	0.040	0.039	0.050	0.040	0.039	0.053	0.035	0.038	0.044	0.037	0.043	0.037	0.055	0.044	0.066	0.039
sum C	4.941	4.887	4.921	4.898	4.939	4.838	4.954	4.933	5.130	5.091	4.983	5.035	5.016	4.933	4.977	4.913	4.927	4.906	4.961	4.867
Sum C-5									0.130	0.091		0.035	0.016							
Ca^{2+}	1.829	1.859	1.868	1.858	1.854	1.874	1.845	1.867	1.715	1.791	1.841	1.829	1.782	1.827	1.805	1.821	1.841	1.849	1.860	1.895
Na^{+}	0.528	0.561	0.542	0.553	0.482	0.513	0.483	0.505	0.496	0.403	0.478	0.447	0.527	0.528	0.512	0.555	0.513	0.496	0.461	0.506
sum B	2.000	2.000	2.000	2.000	2.000	2.000	2.000	2.000	2.000	2.000	2.000	2.000	2.000	2.000	2.000	2.000	2.000	2.000	2.000	2.000
Na^{+}	0.357	0.420	0.410	0.411	0.336	0.388	0.328	0.372	0.211	0.194	0.320	0.276	0.309	0.356	0.316	0.376	0.354	0.344	0.321	0.401
K^{+}	0.285	0.296	0.281	0.282	0.305	0.391	0.304	0.278	0.231	0.272	0.256	0.240	0.274	0.275	0.268	0.280	0.292	0.321	0.288	0.326
sum A	0.642	0.716	0.691	0.693	0.641	0.779	0.632	0.650	0.442	0.466	0.576	0.516	0.583	0.631	0.584	0.656	0.646	0.665	0.609	0.727
Cation total	15.583	15.595	15.587	15.591	15.581	15.617	15.586	15.583	15.572	15.557	15.559	15.551	15.571	15.564	15.561	15.569	15.573	15.571	15.570	15.594
Fe^{3+}/Fe^{2+}	0.255	0.240	0.195	0.222	0.260	0.277	0.320	0.245	0.687	0.440	0.224	0.274	0.323	0.181	0.234	0.175	0.274	0.258	0.381	0.174
Mg#	0.442	0.458	0.434	0.431	0.456	0.407	0.467	0.453	0.563	0.515	0.475	0.494	0.504	0.479	0.483	0.476	0.525	0.537	0.568	0.408

Table C3. (*Continued*)

Rock type	Pyroxene-bearing granodiorites																	Pyroxene-free granodiorites		
Sample	Mat 57$_c$	Mat 57$_r$	Mat 57$_c$	Mat 57$_r$	Mat 58$_c$	Mat 58$_r$	Mat 58$_c$	Mat 58$_r$	Mat 59r	Mat 59$_c$	Mat 59r	Mat 59$_c$	Mat 59r	Mat 59$_c$	Mat 59r	Mat 68$_c$	Mat 68$_r$	Mat 3	Mat 3	Mat 3
SiO_2	42.42	42.55	41.91	40.57	41.82	42.20	42.21	42.69	43.59	43.52	41.64	41.62	43.07	42.99	43.10	42.24	41.90	38.26	39.16	42.40
TiO_2	1.67	1.49	1.57	1.30	1.85	1.53	1.71	1.18	1.85	1.66	1.34	1.56	1.53	1.72	1.74	1.32	1.25	0.42	0.45	0.96
Al_2O_3	9.74	9.70	9.64	10.47	8.95	9.39	8.51	9.51	9.11	8.69	10.46	8.70	9.31	8.91	9.76	9.02	9.84	11.61	11.71	8.93
Cr_2O_3	nd	nd	nd	nd	nd	nd	nd	nd	nd	nd	0.08		nd	nd	nd	nd	nd	nd	nd	nd
FeO*	22.48	22.38	22.96	23.29	19.56	19.62	20.24	19.72	21.12	21.17	21.10	22.98	20.70	20.79	20.16	20.52	20.69	25.93	26.94	25.38
MnO	0.33	0.29	0.38	0.38	0.34	0.46	0.51	0.34	0.38	0.53	0.36	0.45	0.44	0.43	0.44	0.41	0.35	0.53	0.49	0.60
MgO	8.16	8.08	7.90	7.92	8.96	9.17	9.15	9.54	9.16	9.35	8.76	9.12	9.38	9.06	9.12	8.84	8.44	5.16	5.18	6.67
CaO	11.67	11.72	11.66	10.83	11.45	11.22	11.31	11.34	11.31	11.58	11.71	10.82	11.57	11.64	11.53	11.29	11.45	11.14	11.26	11.22
Na_2O	1.76	1.67	1.62	1.63	1.70	1.61	1.87	1.78	1.86	1.91	1.70	1.76	1.80	1.81	1.75	1.74	1.55	1.45	1.54	1.67
K_2O	1.59	1.63	1.73	1.54	1.41	1.50	1.43	1.42	1.51	1.43	1.82	1.41	1.49	1.55	1.58	1.37	1.50	2.04	2.04	1.52
Total	99.82	99.51	99.36	97.94	96.02	96.69	96.96	97.52	99.88	99.84	99.05	98.43	99.27	98.90	99.16	96.75	96.98	96.56	98.76	99.35
Number of ions on the basis of 23 oxygen atoms:																				
Si^{4+}	6.310	6.352	6.279	6.160	6.420	6.425	6.416	6.421	6.443	6.430	6.201	6.269	6.389	6.416	6.402	6.442	6.388	5.971	5.981	6.419
$Al^{3+}{}_{total}$	1.707	1.706	1.703	1.874	1.619	1.685	1.525	1.686	1.586	1.512	1.837	1.545	1.627	1.567	1.709	1.622	1.768	2.136	2.107	1.593
sum T	8.000	8.000	8.000	8.000	8.000	8.000	8.000	8.000	8.000	8.000	8.000	8.000	8.000	8.000	8.000	8.000	8.000	8.000	8.000	8.000
Al^{3+}	0.018	0.057		0.034	0.038	0.110		0.107	0.029		0.038		0.016		0.111	0.064	0.155	0.107	0.089	0.012
Ti^{4+}	0.186	0.168	0.177	0.148	0.213	0.175	0.196	0.133	0.205	0.185	0.150	0.177	0.170	0.193	0.194	0.151	0.144	0.049	0.052	0.109
Fe^{3+}	0.547	0.496	0.612	1.179	0.354	0.578	0.512	0.615	0.582	0.581	0.605	1.271	0.602	0.434	0.452	0.563	0.528	0.975	1.032	0.804
Mg^{2+}	1.810	1.799	1.764	1.793	2.052	2.082	2.074	2.139	2.018	2.060	1.946	2.047	2.073	2.015	2.019	2.010	1.917	1.201	1.180	1.505
Fe^{2+}	2.315	2.360	2.338	1.859	2.203	1.966	2.120	1.918	2.081	2.096	2.096	1.708	2.024	2.218	2.100	2.107	2.161	2.533	2.536	2.487
Mn^{2+}	0.042	0.036	0.048	0.049	0.044	0.060	0.066	0.044	0.047	0.066	0.046	0.057	0.055	0.054	0.055	0.053	0.046	0.070	0.063	0.077
sum C	4.918	4.916	4.938	5.062	4.905	4.971	4.967	4.955	4.962	4.987	4.880	5.260	4.940	4.915	4.931	4.949	4.951	4.935	4.952	4.995
Sum C-5				0.062								0.260								
Ca^{2+}	1.860	1.874	1.872	1.762	1.883	1.830	1.842	1.827	1.791	1.832	1.868	1.746	1.839	1.862	1.834	1.845	1.869	1.863	1.842	1.820
Na^{+}	0.506	0.482	0.471	0.479	0.505	0.474	0.552	0.518	0.534	0.547	0.492	0.514	0.517	0.523	0.503	0.514	0.459	0.439	0.456	0.490
sum B	2.000	2.000	2.000	2.000	2.000	2.000	2.000	2.000	2.000	2.000	2.000	2.000	2.000	2.000	2.000	2.000	2.000	2.000	2.000	2.000
Na^{+}	0.366	0.356	0.343	0.241	0.387	0.304	0.393	0.346	0.325	0.380	0.359	0.261	0.356	0.385	0.337	0.359	0.329	0.302	0.298	0.310
K^{+}	0.302	0.310	0.330	0.299	0.275	0.292	0.278	0.272	0.285	0.270	0.345	0.271	0.282	0.295	0.300	0.267	0.292	0.406	0.398	0.294
sum A	0.669	0.666	0.673	0.540	0.663	0.595	0.671	0.618	0.610	0.650	0.705	0.531	0.638	0.680	0.637	0.625	0.621	0.709	0.696	0.603
Cation total	15.586	15.583	15.594	15.602	15.568	15.566	15.580	15.573	15.572	15.580	15.584	15.605	15.578	15.577	15.568	15.574	15.572	15.644	15.647	15.598
Fe^{3+}/Fe^{2+}	0.236	0.210	0.262	0.634	0.161	0.294	0.241	0.320	0.280	0.277	0.289	0.744	0.297	0.196	0.215	0.267	0.244	0.385	0.407	0.323
Mg#	0.439	0.432	0.430	0.491	0.482	0.514	0.495	0.527	0.492	0.496	0.481	0.545	0.506	0.476	0.490	0.488	0.470	0.322	0.317	0.377

Table C3. (*Continued*)

Rock type	Pyroxene-free														Enclave in px-diorites2					
	granodiorites												granites with ≤71 wt. % SiO_2		diorites					
Sample	Mat 3	Mat 22	Mat 22	Mat 22	Mat 22	Mat 22	Mat 22	Mat 22	Mat 30	Mat 30	Mat 30	Mat 30	Mat 42	Mat 42	Mat 61_c	Mat 61_r	Mat 61_c	Mat 61_r	Mat 61_c	Mat 61_r
SiO_2	43.66	44.71	42.62	41.32	42.11	41.12	42.72	43.77	41.53	41.27	39.69	39.04	40.66	42.61	43.35	43.50	43.10	43.58	43.55	43.01
TiO_2	0.72	0.60	1.01	0.75	0.73	1.16	0.87	1.08	0.51	0.45	0.46	0.65	0.73	1.25	1.53	1.65	1.71	1.47	1.44	1.35
Al_2O_3	8.11	7.35	10.08	10.58	10.30	8.33	9.65	8.70	9.72	9.96	10.91	10.55	10.02	7.88	10.00	9.88	9.79	9.81	9.54	10.02
Cr_2O_3	nd	nd	nd	nd	nd	nd	nd	nd	nd	0.10	nd	nd	nd	nd	nd	nd	nd	nd	nd	nd
FeO*	24.37	24.12	21.99	23.14	22.93	27.05	23.32	22.81	27.34	27.35	27.48	26.75	27.38	26.63	19.21	18.96	19.20	19.45	19.00	19.04
MnO	0.65	0.27	0.32	0.36	0.41	0.27	0.44	0.43	0.61	0.54	0.54	0.59	0.48	0.48	0.39	0.39	0.37	0.45	0.41	0.49
MgO	7.12	8.41	8.36	7.43	7.72	8.58	7.68	8.36	5.26	5.16	4.85	4.92	5.14	6.04	9.99	9.86	9.91	9.84	10.08	9.79
CaO	11.35	8.77	11.85	11.51	11.54	10.61	11.73	11.53	11.20	11.16	10.72	11.15	11.26	11.10	11.76	11.79	11.82	11.81	11.82	11.62
Na_2O	1.51	1.97	1.75	1.51	1.73	1.61	1.70	1.77	1.79	1.67	1.69	1.55	1.61	1.86	1.77	1.74	1.79	1.76	1.65	1.65
K_2O	1.23	1.08	1.54	1.79	1.59	1.24	1.58	1.33	1.45	1.50	1.88	1.84	1.66	1.29	1.68	1.61	1.59	1.60	1.61	1.70
Total	98.71	97.29	99.53	98.39	99.05	99.97	99.69	99.80	99.40	99.16	98.21	97.04	98.93	99.12	99.68	99.38	99.29	99.77	99.11	98.67
Number of ions on the basis of 23 oxygen atoms:																				
Si^{4+}	6.646	6.846	6.334	6.249	6.311	6.165	6.378	6.517	6.325	6.308	6.117	6.092	6.231	6.506	6.362	6.409	6.357	6.402	6.434	6.382
$Al^{3+}{}_{total}$	1.455	1.326	1.765	1.886	1.819	1.471	1.698	1.526	1.745	1.794	1.981	1.941	1.809	1.418	1.730	1.716	1.702	1.699	1.661	1.753
sum T	8.000	8.000	8.000	8.000	8.000	8.000	8.000	8.000	8.000	8.000	8.000	8.000	8.000	8.000	8.000	8.000	8.000	8.000	8.000	8.000
Al^{3+}	0.101	0.172	0.100	0.135	0.129		0.076	0.044	0.070	0.102	0.098	0.032	0.041		0.092	0.125	0.059	0.101	0.095	0.135
Ti^{4+}	0.082	0.069	0.113	0.085	0.083	0.130	0.097	0.121	0.058	0.052	0.054	0.076	0.085	0.143	0.169	0.183	0.190	0.163	0.160	0.151
Fe^{3+}	0.677	1.570	0.529	0.733	0.677	1.975	0.581	0.628	0.854	0.898	1.085	0.896	0.868	0.709	0.470	0.365	0.418	0.448	0.446	0.506
Mg^{2+}	1.616	1.920	1.852	1.676	1.725	1.917	1.709	1.856	1.195	1.177	1.113	1.144	1.173	1.374	2.185	2.166	2.178	2.154	2.220	2.167
Fe^{2+}	2.475	1.558	2.271	2.270	2.271	1.538	2.402	2.271	2.725	2.693	2.576	2.713	2.745	2.771	1.940	2.015	2.000	1.991	1.947	1.905
Mn^{2+}	0.083	0.035	0.040	0.046	0.051	0.035	0.056	0.055	0.079	0.070	0.071	0.078	0.062	0.063	0.048	0.049	0.047	0.055	0.052	0.062
sum C	5.034	5.324	4.905	4.946	4.936	5.596	4.922	4.974	4.982	4.990	4.997	4.940	4.973	5.059	4.904	4.903	4.892	4.911	4.921	4.926
Sum C-5	0.034	0.324				0.596								0.059						
Ca^{2+}	1.852	1.439	1.887	1.864	1.853	1.705	1.876	1.840	1.827	1.826	1.771	1.865	1.848	1.815	1.850	1.860	1.868	1.858	1.870	1.847
Na^{+}	0.446	0.586	0.503	0.443	0.501	0.469	0.493	0.511	0.528	0.495	0.504	0.468	0.477	0.551	0.504	0.498	0.512	0.500	0.471	0.475
sum B	2.000	2.000	2.000	2.000	2.000	2.000	2.000	2.000	2.000	2.000	2.000	2.000	2.000	2.000	2.000	2.000	2.000	2.000	2.000	2.000
Na^{+}	0.297	0.025	0.391	0.307	0.355	0.174	0.369	0.351	0.355	0.321	0.274	0.332	0.325	0.367	0.354	0.358	0.380	0.359	0.342	0.322
K^{+}	0.239	0.211	0.291	0.345	0.304	0.237	0.302	0.253	0.282	0.292	0.369	0.366	0.325	0.250	0.314	0.303	0.299	0.299	0.304	0.321
sum A	0.536	0.236	0.682	0.652	0.659	0.410	0.670	0.604	0.636	0.613	0.643	0.699	0.650	0.617	0.668	0.661	0.679	0.658	0.646	0.643
Cation total	15.570	15.561	15.587	15.598	15.594	15.643	15.592	15.578	15.618	15.603	15.640	15.639	15.624	15.599	15.572	15.565	15.571	15.569	15.566	15.569
Fe^{3+}/Fe^{2+}	0.274	1.008	0.233	0.323	0.298	1.284	0.242	0.276	0.313	0.333	0.421	0.330	0.316	0.256	0.242	0.181	0.209	0.225	0.229	0.266
Mg#	0.395	0.552	0.449	0.425	0.432	0.555	0.416	0.450	0.305	0.304	0.302	0.297	0.299	0.331	0.530	0.518	0.521	0.520	0.533	0.532

Table C4. Biotite composition for the rocks of the Matok pluton.

Rock type	Pyroxene-bearing																				
	diorites1									diorites2		granodiorites									
Sample	Mat 44_c	Mat 44_r	Mat 44_r	Mat 44	Mat 60	Mat 67_r	Mat 67_c	Mat 67_c	Mat 67_c	Mat 52	Mat 52	Mat 57	Mat 57	Mat 57	Mat 58	Mat 58	Mat $59_®$	Mat 59_c	Mat 59_r	Mat 68_c	Mat 68_r
SiO_2	35.93	37.35	37.10	37.67	36.43	36.06	36.53	36.45	36.99	36.87	36.48	36.20	36.33	36.23	35.03	35.49	37.42	37.30	36.99	36.07	36.09
TiO_2	3.62	3.66	3.94	3.93	5.32	4.54	4.78	4.77	4.58	3.81	4.00	4.53	4.59	4.16	5.21	4.95	5.70	4.34	4.74	4.16	4.09
Al_2O_3	14.09	14.54	15.03	14.65	13.19	13.50	13.25	13.49	14.08	14.36	13.94	13.60	13.30	13.56	13.16	13.09	13.59	13.26	13.05	13.09	13.37
Cr_2O_3	nd	0.02	0.04	nd	nd	nd	nd	nd	nd	nd	nd	nd	nd	nd	nd	nd	nd	nd	nd	nd	nd
FeO*	21.32	20.06	20.23	22.11	20.47	22.82	22.80	22.77	21.11	23.49	23.87	23.16	24.29	24.02	22.56	20.78	20.68	22.47	21.96	22.49	22.80
MnO	0.11	0.17	0.12	0.11	0.08	0.15	0.09	0.17	0.18	0.20	0.10	0.10	0.18	0.19	0.18	0.24	0.20	0.13	0.15	0.17	0.26
MgO	10.29	10.32	10.39	10.54	10.98	10.02	9.95	9.86	10.10	9.57	9.38	9.97	9.30	9.57	9.14	10.57	10.57	10.83	10.75	9.91	9.69
CaO	nd	0.48	nd	nd	0.06	nd	nd	nd	nd	0.03	nd	nd	nd	nd	nd	nd	nd	0.02	nd	nd	0.05
Na_2O	0.20	0.58	0.20	0.25	0.25	0.27	0.25	0.25	0.29	0.27	0.25	0.22	0.23	0.24	0.14	0.23	0.23	0.28	0.26	nd	nd
K_2O	9.70	9.40	9.86	9.92	9.81	9.70	9.74	9.72	9.66	9.92	9.87	10.01	9.83	9.70	9.57	10.20	9.93	9.56	9.85	9.57	9.40
P_2O_5	nd	nd	nd	nd	nd	nd	nd	nd	nd	nd	nd	nd	nd	nd	nd	nd	nd	nd	nd	nd	nd
BaO	0.27	nd	0.29	0.19	nd	nd	nd	nd	nd	nd	nd	nd	nd	nd	nd	nd	nd	nd	nd	0.41	0.34
Total	95.54	96.59	97.20	99.37	96.58	97.05	97.38	97.47	97.00	98.52	97.90	97.78	98.03	97.67	94.99	95.53	98.31	98.19	97.75	95.86	96.08
Number of ions on the basis of 22 oxygen atoms:																					
Si^{4+}	5.573	5.655	5.602	5.600	5.555	5.665	5.532	5.577	5.560	5.572	5.566	5.525	5.555	5.550	5.503	5.514	5.593	5.620	5.604	5.614	5.602
Al^{3+}	2.576	2.594	2.673	2.565	2.370	2.330	2.441	2.383	2.424	2.558	2.507	2.445	2.397	2.447	2.437	2.396	2.393	2.355	2.330	2.400	2.446
Ti^{4+}	0.422	0.417	0.447	0.440	0.610	0.517	0.524	0.549	0.547	0.433	0.458	0.520	0.527	0.479	0.616	0.578	0.640	0.492	0.540	0.487	0.477
Cr^{3+}	0.000	0.003	0.005	0.000	0.000	0.000	0.000	0.000	0.000	0.000	0.000	0.000	0.000	0.000	0.000	0.000	0.000	0.000	0.000	0.000	0.000
Fe^{2+}	2.764	2.540	2.554	2.748	2.610	2.506	2.927	2.910	2.904	2.969	3.046	2.955	3.106	3.077	2.964	2.699	2.585	2.831	2.782	2.927	2.959
Mn^{2+}	0.015	0.022	0.015	0.014	0.011	0.019	0.019	0.012	0.022	0.026	0.013	0.013	0.023	0.024	0.024	0.031	0.025	0.017	0.019	0.022	0.034
Mg^{2+}	2.378	2.330	2.337	2.336	2.495	2.640	2.292	2.265	2.241	2.156	2.133	2.268	2.119	2.186	2.140	2.447	2.355	2.433	2.427	2.299	2.242
Ca^{2+}	0.000	0.077	0.000	0.000	0.009	0.000	0.000	0.000	0.000	0.005	0.000	0.000	0.000	0.000	0.000	0.000	0.000	0.003	0.000	0.000	0.009
Na^{+}	0.061	0.169	0.059	0.071	0.075	0.060	0.081	0.075	0.073	0.078	0.075	0.065	0.068	0.072	0.041	0.070	0.065	0.081	0.078	0.000	0.000
K^{+}	1.919	1.815	1.898	1.880	1.907	1.891	1.899	1.896	1.892	1.913	1.921	1.948	1.917	1.895	1.918	2.020	1.893	1.838	1.903	1.900	1.861
Cation total	15.71	15.62	15.59	15.65	15.64	15.63	15.71	15.67	15.66	15.71	15.72	15.74	15.71	15.73	15.64	15.76	15.55	15.67	15.68	15.65	15.63
Mg#	0.538	0.522	0.522	0.541	0.511	0.487	0.561	0.562	0.564	0.579	0.588	0.566	0.594	0.585	0.581	0.524	0.523	0.538	0.534	0.560	0.569

Table C4. (*continued*)

Rock type	Pyroxene-free granodiorites																				
Sample	Mat 3	Mat 3_c	Mat 3_r	Mat 3	Mat $3_{@}$	Mat 3	Mat 9	Mat 9_c	Mat 9_r	Mat 9	Mat 9_c	Mat 9_r	Mat 14	Mat 14	Mat 14	Mat 14	Mat 14	Mat 14	Mat 14	Mat 14	Mat 14
SiO_2	34.20	36.04	35.85	35.46	35.24	42.53	37.03	36.52	36.56	41.51	36.82	35.50	36.12	36.51	36.01	36.42	36.12	38.29	36.77	36.81	38.40
TiO_2	2.58	2.01	2.05	2.09	2.08	1.47	2.05	2.03	1.89	1.67	1.78	2.11	1.83	1.93	1.94	1.74	1.51	1.83	1.71	1.86	1.88
Al_2O_3	13.15	14.15	14.24	13.66	13.94	16.83	15.07	14.44	14.54	16.41	13.97	13.90	13.95	14.20	14.14	13.95	13.48	15.33	14.50	14.74	14.90
Cr_2O_3	nd	nd	nd	nd	nd	nd	nd	nd	nd	nd	nd	nd	nd	0.31	0.37	0.34	0.56	nd	nd	nd	nd
FeO*	25.38	26.20	26.15	25.69	26.99	20.59	21.40	21.76	21.59	17.64	22.64	22.73	22.13	21.49	20.81	21.17	20.21	22.55	22.69	22.52	22.59
MnO	0.31	0.34	0.41	0.40	0.40	0.29	0.28	0.22	0.23	0.21	0.30	0.26	0.35	0.31	0.21	0.35	0.34	0.30	0.30	0.26	0.36
MgO	7.93	8.42	8.40	7.86	7.75	5.67	10.55	10.39	10.44	7.89	10.68	9.99	10.13	10.10	9.75	10.09	9.82	10.81	10.21	10.12	10.59
CaO	nd	nd	nd	0.06	nd	0.22	0.04	nd	nd	0.49	0.08	0.37	nd	nd	nd	nd	nd	nd	nd	nd	nd
Na_2O	0.20	0.10	0.12	0.21	0.17	3.50	0.16	0.17	0.21	2.40	0.22	0.11	0.33	0.20	0.24	0.16	0.34	0.40	nd	nd	0.23
K_2O	9.50	9.70	9.74	9.43	9.66	6.61	9.81	9.82	9.86	8.06	9.48	9.31	9.50	9.63	9.41	9.41	8.75	9.83	9.77	9.82	10.00
P_2O_5	nd	nd	nd	nd	nd	nd	nd	nd	nd	nd	nd	nd	nd	nd	nd	nd	nd	nd	nd	nd	nd
BaO	nd	nd	nd	nd	nd	nd	0.24	0.22	0.30	nd	0.16	0.29	nd	nd	nd	nd	nd	nd	nd	nd	nd
Total	93.25	96.95	96.96	94.87	96.24	97.72	96.63	95.55	95.62	96.28	96.12	94.58	94.34	94.68	92.89	93.61	91.12	99.32	95.93	96.13	98.94
Number of ions on the basis of 22 oxygen atoms:																					
Si^{4+}	5.570	5.617	5.593	5.652	5.576	6.206	5.653	5.662	5.665	6.120	5.686	5.606	5.678	5.696	5.710	5.736	5.812	5.680	5.681	5.668	5.726
Al^{3+}	2.523	2.599	2.617	2.566	2.599	2.894	2.712	2.638	2.656	2.851	2.543	2.587	2.584	2.610	2.643	2.588	2.556	2.680	2.640	2.675	2.618
Ti^{4+}	0.317	0.236	0.240	0.251	0.248	0.162	0.236	0.236	0.221	0.186	0.207	0.251	0.216	0.227	0.232	0.206	0.182	0.204	0.198	0.216	0.211
Cr^{3+}	0.000	0.000	0.000	0.000	0.000	0.000	0.000	0.000	0.000	0.000	0.000	0.000	0.000	0.038	0.046	0.042	0.071	0.000	0.000	0.000	0.000
Fe^{2+}	3.456	3.415	3.412	3.424	3.571	2.512	2.732	2.821	2.798	2.174	2.924	3.002	2.909	2.804	2.759	2.787	2.720	2.797	2.930	2.900	2.816
Mn^{2+}	0.043	0.045	0.054	0.053	0.053	0.036	0.036	0.028	0.030	0.027	0.039	0.035	0.046	0.041	0.028	0.047	0.046	0.037	0.039	0.034	0.046
Mg^{2+}	1.926	1.957	1.955	1.867	1.829	1.232	2.402	2.401	2.411	1.733	2.459	2.352	2.375	2.348	2.305	2.368	2.355	2.390	2.351	2.322	2.354
Ca^{2+}	0.000	0.000	0.000	0.011	0.000	0.034	0.006	0.000	0.000	0.077	0.013	0.062	0.000	0.000	0.000	0.000	0.000	0.000	0.000	0.000	0.000
Na^{+}	0.062	0.030	0.036	0.063	0.053	0.990	0.048	0.050	0.062	0.687	0.065	0.033	0.101	0.060	0.073	0.049	0.105	0.115	0.000	0.000	0.067
K^{+}	1.973	1.928	1.938	1.917	1.950	1.231	1.910	1.943	1.950	1.515	1.867	1.875	1.906	1.917	1.904	1.891	1.796	1.859	1.925	1.929	1.901
Cation total	15.87	15.83	15.84	15.80	15.88	15.30	15.73	15.78	15.79	15.37	15.80	15.80	15.82	15.74	15.70	15.71	15.64	15.76	15.76	15.74	15.74
Mg#	0.642	0.636	0.636	0.647	0.661	0.671	0.532	0.540	0.537	0.556	0.543	0.561	0.551	0.544	0.545	0.541	0.536	0.539	0.555	0.555	0.545

Table C4. (*continued*)

Rock type	Pyroxene-free granodiorites																				
Sample	Mat 14	Mat 14	Mat 14	Mat 14	Mat 14	Mat 14	Mat 14	Mat 14	Mat 14	Mat 14	Mat 14	Mat 14	Mat 22	Mat 22	Mat 22	Mat 22	Mat 22	Mat 30	Mat 30	Mat 30	Mat 30
SiO_2	37.29	37.39	36.77	36.19	36.57	34.54	36.12	36.22	35.73	34.22	37.12	36.93	35.80	36.87	37.65	37.20	36.08	35.96	34.89	36.12	36.03
TiO_2	2.05	1.87	2.03	1.82	1.87	1.64	1.83	1.90	1.83	1.62	1.95	1.88	3.87	3.29	3.54	3.44	3.71	1.74	3.43	2.34	2.19
Al_2O_3	14.48	14.62	14.18	14.06	14.43	13.38	13.95	13.91	13.74	12.97	15.27	14.72	13.82	13.97	14.43	14.07	13.79	13.88	18.93	14.81	14.69
Cr_2O_3	nd	nd	nd	nd	nd	nd	nd	nd	nd	nd	nd	nd	nd	0.05	nd	nd	nd	nd	nd	nd	nd
FeO*	22.98	22.87	22.78	22.28	22.20	20.97	22.13	22.16	22.23	20.66	22.77	22.91	24.09	24.22	24.29	23.89	24.65	28.62	22.80	26.94	26.22
MnO	0.29	0.35	0.34	0.28	0.29	0.30	0.35	0.26	0.28	0.28	0.26	0.25	0.18	0.16	0.23	0.19	0.22	0.41	nd	0.41	0.37
MgO	10.42	9.95	10.00	9.83	10.38	9.77	10.13	10.16	9.95	9.54	9.83	9.82	8.91	9.97	10.09	10.09	9.28	7.19	7.48	7.87	7.73
CaO	nd	nd	nd	nd	nd	nd	nd	nd	nd	nd	nd	nd	nd	nd	nd	nd	nd	nd	nd	nd	nd
Na_2O	0.28	0.18		0.27	0.23	0.41	0.33	0.37	0.19	0.40	0.19	0.27	0.21	0.19	nd	0.22	0.22	nd	0.21	0.24	0.27
K_2O	10.04	9.94	9.63	9.62	9.79	8.93	9.50	9.42	9.47	8.70	9.78	9.72	9.86	10.00	10.21	10.09	9.91	9.20	9.86	9.94	9.58
P_2O_5	nd	nd	nd	nd	nd	nd	nd	nd	nd	nd	nd	nd	nd	nd	nd	nd	nd	nd	nd	nd	nd
BaO	nd	nd	nd	nd	nd	nd	nd	nd	nd	nd	nd	nd	nd	nd	nd	nd	nd	nd	nd	nd	nd
Total	97.83	97.16	95.72	94.35	95.76	89.93	94.34	94.39	93.42	88.39	97.17	96.50	96.74	98.71	100.43	99.19	97.86	97.01	97.62	98.67	97.09
Number of ions on the basis of 22 oxygen atoms:																					
Si^{4+}	5.661	5.704	5.695	5.691	5.657	5.686	5.678	5.686	5.680	5.726	5.651	5.674	5.549	5.585	5.589	5.596	5.540	5.653	5.289	5.553	5.603
Al^{3+}	2.591	2.628	2.588	2.606	2.631	2.596	2.584	2.573	2.574	2.557	2.740	2.666	2.525	2.493	2.525	2.494	2.495	2.572	3.382	2.683	2.692
Ti^{4+}	0.234	0.214	0.236	0.215	0.217	0.203	0.216	0.224	0.219	0.204	0.224	0.217	0.452	0.374	0.396	0.389	0.428	0.206	0.391	0.271	0.256
Cr^{3+}	0.000	0.000	0.000	0.000	0.000	0.000	0.000	0.000	0.000	0.000	0.000	0.000	0.000	0.006	0.000	0.000	0.000	0.000	0.000	0.000	0.000
Fe^{2+}	2.916	2.917	2.950	2.930	2.872	2.886	2.909	2.908	2.955	2.890	2.899	2.944	3.123	3.068	3.016	3.005	3.165	3.762	2.890	3.462	3.410
Mn^{2+}	0.037	0.045	0.044	0.037	0.037	0.042	0.046	0.034	0.038	0.040	0.034	0.033	0.024	0.020	0.029	0.024	0.029	0.054	0.000	0.054	0.049
Mg^{2+}	2.358	2.263	2.310	2.305	2.395	2.398	2.375	2.377	2.359	2.379	2.230	2.249	2.058	2.251	2.232	2.262	2.124	1.685	1.691	1.803	1.793
Ca^{2+}	0.000	0.000	0.000	0.000	0.000	0.000	0.000	0.000	0.000	0.000	0.000	0.000	0.000	0.000	0.000	0.000	0.000	0.000	0.000	0.000	0.000
Na^{+}	0.081	0.054	0.000	0.083	0.069	0.130	0.101	0.111	0.059	0.131	0.057	0.081	0.063	0.056	0.000	0.065	0.066	0.000	0.063	0.071	0.083
K^{+}	1.943	1.935	1.902	1.929	1.932	1.876	1.906	1.886	1.921	1.858	1.899	1.906	1.950	1.931	1.933	1.936	1.940	1.845	1.906	1.950	1.899
Cation total	15.82	15.76	15.73	15.80	15.81	15.82	15.82	15.80	15.81	15.79	15.73	15.77	15.74	15.78	15.72	15.77	15.79	15.78	15.61	15.85	15.79
Mg#	0.553	0.563	0.561	0.560	0.545	0.546	0.551	0.550	0.556	0.548	0.565	0.567	0.603	0.577	0.575	0.571	0.598	0.691	0.631	0.657	0.655

Table C4. (*continued*)

Rock type	Pyroxene-free																			
	granodiorites														granites with ≤71 wt.% SiO_2					
Sample	Mat 30	Mat 30	Mat 30	Mat 34	Mat 34	Mat 34	Mat 34	Mat 34	Mat 34	Mat 34	Mat 34	Mat 34	Mat 70_r	Mat 70	Mat 7	Mat 7	Mat 7	Mat 7	Mat 7	Mat 31
SiO_2	35.44	35.80	34.44	36.10	35.71	35.70	35.90	35.83	34.82	32.98	33.69	36.54	38.32	36.05	35.66	34.96	34.48	35.98	35.89	36.15
TiO_2	1.24	2.01	0.47	1.84	1.73	2.02	2.08	2.10	2.04	2.24	2.30	2.14	1.25	2.59	1.92	2.04	2.07	2.05	2.10	2.06
Al_2O_3	14.13	14.32	13.79	14.57	14.21	15.64	14.78	14.27	14.17	13.24	13.73	14.51	14.87	15.96	13.90	15.06	14.71	14.71	14.80	15.60
Cr_2O_3	nd	nd	nd	nd	nd	nd	nd	nd	nd	nd	nd	nd	nd	nd	nd	nd	nd	nd	nd	nd
FeO*	28.71	27.76	27.46	27.06	27.27	28.46	27.55	29.17	28.74	27.88	28.80	29.28	24.31	20.46	25.45	23.43	23.61	25.77	25.59	25.08
MnO	0.22	0.38	0.34	0.25	0.37	0.37	0.34	0.37	0.35	0.34	0.31	0.37	0.32	0.18	0.34	0.29	0.22	0.31	0.31	0.34
MgO	7.09	7.16	6.65	7.38	7.38	6.71	7.18	6.46	6.18	5.50	5.78	6.66	10.62	8.53	7.77	7.43	7.42	7.90	7.47	7.81
CaO	0.04	nd	0.20	0.04	nd	nd	nd	nd	nd	nd	nd	nd	nd	nd	0.02	0.13	nd	nd	0.04	nd
Na_2O	0.26	nd	0.22	0.26	0.21	0.30	0.16	0.31	0.23	0.30	0.31	0.24	0.13	0.33	0.19	0.31	0.45	0.11	0.17	nd
K_2O	7.74	9.60	8.26	9.65	9.52	9.62	9.84	9.56	9.48	9.04	9.38	9.88	9.95	9.67	9.51	9.38	9.33	9.53	9.72	9.88
P_2O_5	nd	nd	nd	nd	nd	nd	nd	nd	nd	nd	nd	nd	0.12	nd	nd	nd	nd	nd	nd	nd
BaO	nd	nd	nd	nd	nd	nd	nd	nd	nd	nd	nd	nd	0.03	nd	0.17	0.16	0.24	0.28	0.24	nd
Total	94.87	97.02	91.83	97.17	96.40	98.83	97.82	98.06	96.02	91.51	94.29	99.62	99.92	93.77	94.92	93.19	92.51	96.64	96.32	96.92
Number of ions on the basis of 22 oxygen atoms:																				
Si^{4+}	5.661	5.615	5.704	5.632	5.630	5.506	5.581	5.599	5.567	5.556	5.517	5.614	5.708	5.638	5.677	5.617	5.601	5.621	5.628	5.594
Al^{3+}	2.660	2.647	2.693	2.678	2.640	2.843	2.709	2.628	2.670	2.629	2.651	2.627	2.610	2.942	2.608	2.852	2.816	2.709	2.735	2.845
Ti^{4+}	0.149	0.237	0.058	0.216	0.205	0.235	0.243	0.246	0.246	0.284	0.283	0.247	0.139	0.304	0.230	0.246	0.252	0.241	0.248	0.240
Cr^{3+}	0.000	0.000	0.000	0.000	0.000	0.000	0.000	0.000	0.000	0.000	0.000	0.000	0.000	0.000	0.000	0.000	0.000	0.000	0.000	0.000
Fe^{2+}	3.835	3.641	3.803	3.530	3.596	3.671	3.582	3.813	3.844	3.928	3.943	3.761	3.028	2.676	3.387	3.147	3.206	3.366	3.356	3.244
Mn^{2+}	0.030	0.050	0.048	0.034	0.050	0.048	0.045	0.049	0.048	0.049	0.044	0.048	0.040	0.023	0.046	0.040	0.030	0.040	0.041	0.045
Mg^{2+}	1.689	1.675	1.641	1.717	1.735	1.543	1.663	1.505	1.474	1.381	1.411	1.525	2.358	1.989	1.843	1.779	1.798	1.839	1.746	1.802
Ca^{2+}	0.007	0.000	0.036	0.007	0.000	0.000	0.000	0.000	0.000	0.000	0.000	0.000	0.000	0.000	0.003	0.022	0.000	0.000	0.006	0.000
Na^{+}	0.080	0.000	0.072	0.079	0.064	0.090	0.047	0.093	0.073	0.097	0.097	0.071	0.038	0.101	0.058	0.095	0.140	0.035	0.050	0.000
K^{+}	1.577	1.921	1.745	1.921	1.916	1.892	1.952	1.906	1.935	1.943	1.959	1.936	1.890	1.929	1.932	1.922	1.932	1.898	1.945	1.950
Cation total	15.69	15.79	15.80	15.81	15.84	15.83	15.82	15.84	15.86	15.87	15.90	15.83	15.81	15.60	15.78	15.72	15.78	15.75	15.75	15.72
Mg#	0.694	0.685	0.699	0.673	0.675	0.704	0.683	0.717	0.723	0.740	0.737	0.712	0.562	0.574	0.648	0.639	0.641	0.647	0.658	0.643

Table C4. (*continued*)

Rock type	Pyroxene-free																				
	granites with ≤71 wt.% SiO_2											granites with >71 wt.% SiO_2									
Sample	Mat 31	Mat 31	Mat 31	Mat 31	Mat 31	Mat 31	Mat 31	Mat 31	Mat 42	Mat 42	Mat 42	Mat 23	Mat 23	Mat 23	Mat 23	Mat 23	Mat 23	Mat 23	Mat 24	Mat 24	Mat 24
SiO_2	37.26	35.92	36.70	36.32	36.74	36.98	37.13	37.45	35.30	35.28	35.59	36.96	35.73	35.68	36.18	35.23	37.06	37.36	35.78	36.32	37.46
TiO_2	2.04	2.22	2.23	2.23	2.01	2.27	2.06	2.04	3.47	3.35	3.55	3.80	3.66	3.75	3.59	3.28	3.65	3.94	3.35	3.69	3.65
Al_2O_3	15.21	14.89	14.94	15.12	15.30	15.35	15.20	15.13	13.65	13.70	13.71	14.44	13.97	14.05	14.38	13.96	14.11	15.00	13.57	13.84	13.80
Cr_2O_3	nd	nd	nd	nd	nd	nd	nd	nd	nd	nd	nd	0.02	0.02	0.04	0.03	nd	nd	nd	0.02	nd	nd
FeO*	25.62	26.19	27.05	25.93	26.72	26.37	26.47	26.63	28.34	28.44	29.06	23.93	23.45	22.64	22.29	24.47	24.40	24.44	22.30	22.80	23.35
MnO	0.31	0.30	0.25	0.23	0.32	0.28	0.36	0.35	0.20	0.30	0.26	0.24	0.20	0.17	0.13	0.17	0.21	0.13	0.25	0.24	0.35
MgO	8.31	7.72	7.86	7.81	7.94	8.17	8.08	8.10	6.84	6.86	6.67	8.65	8.53	8.38	8.73	8.22	9.04	8.71	9.22	9.26	9.77
CaO	nd	nd	nd	nd	nd	nd	nd	nd	nd	nd	nd	0.01	0.02	nd	nd	nd	0.02	nd	nd	nd	nd
Na_2O	0.20	0.27	0.16		0.28	0.18	0.22	0.17	0.23	0.31	0.25	0.13	0.22	0.28	0.14	0.24	0.08	0.27	0.21	0.11	0.12
K_2O	9.90	9.86	9.51	9.82	9.76	10.16	9.96	10.07	9.51	9.41	9.78	9.90	9.55	9.62	9.56	9.35	9.94	9.76	9.72	9.64	10.15
P_2O_5	nd	nd	nd	nd	nd	nd	nd	nd	nd	nd	nd	nd	nd	nd	nd	nd	nd	nd	nd	nd	nd
BaO	nd	nd	nd	nd	nd	nd	nd	nd	nd	nd	nd	nd	nd	nd	nd	nd	nd	nd	nd	nd	nd
Total	98.85	97.37	98.70	97.48	99.06	99.74	99.46	99.94	97.55	97.65	98.87	98.08	95.35	94.60	95.03	94.93	98.51	99.59	94.41	95.89	98.65
Number of ions on the basis of 22 oxygen atoms:																					
Si^{4+}	5.651	5.576	5.610	5.607	5.594	5.587	5.623	5.645	5.534	5.529	5.526	5.618	5.594	5.613	5.636	5.570	5.621	5.585	5.638	5.627	5.653
Al^{3+}	2.719	2.724	2.691	2.751	2.745	2.733	2.712	2.688	2.523	2.531	2.508	2.586	2.579	2.605	2.640	2.602	2.522	2.642	2.521	2.528	2.454
Ti^{4+}	0.233	0.259	0.256	0.259	0.231	0.257	0.234	0.232	0.410	0.395	0.415	0.434	0.430	0.443	0.421	0.390	0.416	0.443	0.396	0.430	0.415
Cr^{3+}	0.000	0.000	0.000	0.000	0.000	0.000	0.000	0.000	0.000	0.000	0.000	0.002	0.003	0.005	0.004	0.000	0.000	0.000	0.002	0.000	0.000
Fe^{2+}	3.249	3.399	3.458	3.347	3.402	3.331	3.352	3.356	3.716	3.727	3.772	3.042	3.070	2.978	2.903	3.236	3.094	3.055	2.939	2.955	2.947
Mn^{2+}	0.039	0.040	0.033	0.030	0.041	0.036	0.046	0.045	0.027	0.040	0.034	0.031	0.027	0.022	0.017	0.022	0.027	0.016	0.033	0.031	0.044
Mg^{2+}	1.880	1.787	1.790	1.798	1.801	1.840	1.824	1.820	1.599	1.602	1.545	1.959	1.990	1.965	2.028	1.938	2.044	1.941	2.167	2.139	2.198
Ca^{2+}	0.000	0.000	0.000	0.000	0.000	0.000	0.000	0.000	0.000	0.000	0.000	0.001	0.004	0.000	0.000	0.000	0.003	0.000	0.000	0.000	0.000
Na^{+}	0.058	0.081	0.048	0.000	0.082	0.052	0.064	0.049	0.070	0.094	0.074	0.039	0.067	0.084	0.043	0.074	0.023	0.079	0.064	0.032	0.036
K^{+}	1.916	1.953	1.854	1.933	1.895	1.957	1.923	1.936	1.903	1.881	1.937	1.919	1.907	1.931	1.899	1.886	1.923	1.861	1.954	1.905	1.953
Cation total	15.74	15.82	15.74	15.73	15.79	15.79	15.78	15.77	15.78	15.80	15.81	15.63	15.67	15.65	15.59	15.72	15.67	15.62	15.71	15.65	15.70
Mg#	0.634	0.655	0.659	0.651	0.654	0.644	0.648	0.648	0.699	0.699	0.709	0.608	0.607	0.603	0.589	0.625	0.602	0.612	0.576	0.580	0.573

Table C4. (*continued*)

Rock type	Pyroxene-free granites with >71 wt.% SiO_2					
Sample	Mat 24	Mat 35	Mat 35	Mat 35	Mat 35	Mat 35
SiO_2	37.19	36.68	37.46	34.75	36.31	36.47
TiO_2	3.58	2.90	3.06	3.04	2.86	2.88
Al_2O_3	13.51	15.46	16.14	15.27	15.53	15.10
Cr_2O_3	0.10	nd	nd	nd	nd	nd
FeO*	23.77	24.19	24.04	24.05	25.32	23.92
MnO	0.27	0.38	0.37	0.30	0.33	0.21
MgO	9.65	7.41	7.47	6.32	7.80	8.16
CaO	nd	nd	nd	nd	nd	nd
Na_2O	0.27	0.36	0.42	0.25	0.36	0.34
K_2O	9.87	9.69	9.96	9.60	9.41	9.60
P_2O_5	nd	nd	nd	nd	nd	nd
BaO	nd	nd	nd	nd	nd	nd
Total	98.21	97.08	98.91	93.57	97.93	96.68
Number of ions on the basis of 22 oxygen atoms:						
Si^{4+}	5.650	5.636	5.630	5.571	5.554	5.620
Al^{3+}	2.419	2.799	2.860	2.885	2.800	2.742
Ti^{4+}	0.409	0.336	0.346	0.367	0.329	0.334
Cr^{3+}	0.012	0.000	0.000	0.000	0.000	0.000
Fe^{2+}	3.020	3.108	3.022	3.224	3.239	3.083
Mn^{2+}	0.035	0.049	0.047	0.040	0.043	0.028
Mg^{2+}	2.186	1.698	1.674	1.511	1.779	1.875
Ca^{2+}	0.000	0.000	0.000	0.000	0.000	0.000
Na^{+}	0.079	0.108	0.122	0.076	0.108	0.102
K^{+}	1.912	1.899	1.909	1.963	1.836	1.887
Cation total	15.72	15.63	15.61	15.64	15.69	15.67
Mg#	0.580	0.647	0.644	0.681	0.645	0.622

Table C5. Plagioclase composition for the rocks of the Matok pluton.

Rock type	Pyroxene-bearing																			
	diorites1											diorites2								
Sample	Mat 44	Mat 44	Mat 60_r	Mat 60_c	Mat 60_c	Mat 60_r	Mat 60	Mat 60	Mat 60_r	Mat 67_c	Mat 67_r	Mat 29_c	Mat 29_r	Mat 66_c	Mat 66_r	Mat 66_c	Mat 66_r	Mat 66	Mat 52_c	Mat 52_r
SiO_2	62.63	62.23	61.86	62.17	62.01	61.55	61.71	61.24	61.23	62.02	63.45	62.82	61.98	62.34	62.24	62.46	62.36	61.63	62.90	62.85
TiO_2	0.05	0.05	nd	nd	nd	nd	nd	nd	0.05	0.06	0.08	0.03	0.08	0.19	nd	0.19	nd	0.05	nd	nd
Al_2O_3	23.37	23.30	23.56	24.03	24.01	24.22	23.94	23.98	24.18	23.27	22.90	23.70	23.78	23.65	23.62	23.74	23.71	23.38	22.94	22.81
FeO*	0.14	0.08	0.08	0.02	0.06	0.14	nd	0.13	0.33	0.19	0.32	0.10	0.03	0.14	nd	0.14	nd	0.21	0.11	0.02
MnO	nd	nd	nd	nd	nd	nd	nd	nd	nd	nd	0.01	0.03	nd	0.02	nd	nd	nd	nd	0.01	nd
MgO	0.05	0.06	0.03	0.11	0.16	0.09	0.06	0.04	0.14	0.07	0.09	0.08	0.13	0.05	nd	0.05	nd	0.18	0.26	0.09
CaO	4.95	4.96	5.52	5.46	5.54	5.83	5.60	5.77	5.68	4.93	5.13	5.22	5.38	5.22	5.19	5.22	5.19	5.20	4.53	4.40
Na_2O	9.14	9.02	8.49	8.71	8.66	8.54	8.49	8.44	8.53	8.92	8.67	8.41	8.15	8.43	8.25	8.96	8.77	8.81	9.24	9.25
K_2O	0.11	0.23	0.33	0.30	0.20	0.20	0.32	0.26	0.30	0.06	0.08	0.17	0.22	0.09	0.16	0.09	0.16	0.15	0.24	0.14
Total	100.43	99.93	99.87	100.79	100.64	100.58	100.04	99.90	100.43	99.53	100.72	100.55	99.74	100.12	99.41	100.85	100.18	99.59	100.23	99.56
Number of ions on the basis of 8 oxygen atoms:																				
Si^{4+}	2.766	2.764	2.752	2.741	2.737	2.722	2.739	2.728	2.715	2.763	2.790	2.766	2.752	2.758	2.769	2.749	2.760	2.749	2.783	2.794
Al^{3+}	1.217	1.220	1.235	1.248	1.249	1.263	1.252	1.259	1.264	1.222	1.186	1.230	1.244	1.233	1.238	1.232	1.236	1.229	1.196	1.195
Fe^{3+}	0.005	0.003	0.003	0.001	0.002	0.005	0.000	0.004	0.011	0.006	0.010	0.003	0.001	0.005	0.000	0.005	0.000	0.007	0.004	0.001
Ti^{4+}	0.001	0.002	0.000	0.000	0.000	0.000	0.000	0.000	0.002	0.002	0.003	0.001	0.003	0.006	0.000	0.006	0.000	0.002	0.000	0.000
Mn^{2+}	0.000	0.000	0.000	0.000	0.000	0.000	0.000	0.000	0.000	0.000	0.000	0.001	0.000	0.001	0.000	0.000	0.000	0.000	0.000	0.000
Mg^{2+}	0.003	0.004	0.002	0.007	0.010	0.006	0.004	0.002	0.009	0.005	0.006	0.006	0.009	0.003	0.000	0.003	0.000	0.012	0.017	0.006
Na^{+}	0.783	0.777	0.732	0.744	0.741	0.733	0.730	0.728	0.733	0.771	0.739	0.718	0.702	0.723	0.711	0.765	0.752	0.762	0.792	0.797
Ca^{2+}	0.234	0.236	0.263	0.258	0.262	0.276	0.266	0.275	0.270	0.235	0.242	0.246	0.256	0.247	0.247	0.246	0.246	0.248	0.215	0.209
K^{+}	0.006	0.013	0.019	0.017	0.011	0.011	0.018	0.015	0.017	0.003	0.004	0.010	0.013	0.005	0.009	0.005	0.009	0.008	0.014	0.008
Cation total	5.016	5.018	5.005	5.015	5.013	5.016	5.009	5.012	5.021	5.008	4.981	4.980	4.980	4.981	4.973	5.011	5.003	5.017	5.021	5.011
An	0.229	0.230	0.260	0.253	0.258	0.271	0.263	0.270	0.265	0.233	0.245	0.253	0.264	0.254	0.256	0.242	0.244	0.244	0.210	0.206
Ab	0.765	0.757	0.722	0.730	0.730	0.718	0.720	0.715	0.718	0.764	0.750	0.737	0.723	0.741	0.735	0.753	0.747	0.748	0.776	0.786
Or	0.006	0.012	0.019	0.017	0.011	0.011	0.018	0.015	0.017	0.003	0.004	0.010	0.013	0.005	0.009	0.005	0.009	0.008	0.013	0.008

Table C5. (*continued*)

Rock type	Pyroxene-bearing																		
	diorites2			granodiorites															
Sample	Mat 52	Mat 52_c	Mat 52_r	Mat 27	Mat 27	Mat 27	Mat 27	Mat 27	Mat 27	Mat 57_c	Mat 57_r	Mat 57_c	Mat 57_r	Mat 57_c	Mat 57_r	Mat 59_c	Mat 59_r	Mat 59_c	Mat 59_r	Mat 59_c
SiO_2	62.59	63.29	63.18	63.55	64.40	67.16	63.78	63.81	63.97	62.70	62.88	62.85	63.01	62.98	62.49	62.86	63.19	63.62	63.40	62.79
TiO_2	0.06	nd	0.02	nd	0.06	nd	0.02	nd	nd	nd	nd	0.01	0.04	0.06	0.10	0.02	0.01	nd	0.10	nd
Al_2O_3	23.22	23.42	22.89	22.25	22.65	24.43	22.33	21.94	22.36	23.38	23.00	23.67	23.32	22.91	23.33	22.93	23.01	22.80	23.00	22.85
FeO*	0.01	0.05	0.04	nd	nd	nd	0.14	nd	0.03	0.05	0.13	0.04	nd	0.04	nd	0.07	0.12	0.05	0.09	nd
MnO	nd	nd	nd	nd	nd	0.02	0.02	nd	0.03	nd	0.01	0.03	nd	nd	0.01	0.04	nd	0.04	0.04	nd
MgO	0.13	0.13	0.10	nd	nd	0.07	0.07	nd	0.08	0.04	0.14	0.10	0.11	0.10	0.12	0.09	0.21	0.09	0.05	0.08
CaO	4.52	4.72	4.38	3.93	3.94	4.56	3.92	3.65	3.93	4.97	4.57	4.91	4.85	4.45	4.91	4.36	4.44	4.39	4.42	4.59
Na_2O	9.12	9.37	9.36	9.07	9.24	9.65	9.00	9.23	9.24	8.95	9.09	9.03	9.14	9.02	8.96	9.33	9.28	9.19	9.33	9.34
K_2O	0.22	0.25	0.16	0.22	0.20	0.18	0.32	0.26	0.24	0.17	0.11	0.24	0.19	0.55	0.16	0.24	0.26	0.41	0.34	0.13
Total	99.86	101.22	100.13	99.77	100.48	106.06	99.61	99.77	99.87	100.25	99.93	100.89	100.66	100.12	100.09	99.93	100.53	100.58	100.76	99.77
Number of ions on the basis of 8 oxygen atoms:																				
Si^{4+}	2.777	2.774	2.794	2.831	2.827	2.799	2.827	2.845	2.828	2.772	2.786	2.763	2.775	2.790	2.768	2.788	2.786	2.802	2.790	2.789
Al^{3+}	1.214	1.210	1.193	1.168	1.172	1.200	1.167	1.153	1.165	1.218	1.201	1.227	1.210	1.196	1.218	1.198	1.196	1.183	1.193	1.196
Fe^{3+}	0.000	0.002	0.001	0.000	0.000	0.000	0.005	0.000	0.001	0.001	0.004	0.001	0.000	0.001	0.000	0.002	0.004	0.002	0.003	0.000
Ti^{4+}	0.002	0.000	0.001	0.000	0.002	0.000	0.001	0.000	0.000	0.000	0.000	0.000	0.001	0.002	0.003	0.001	0.000	0.000	0.003	0.000
Mn^{2+}	0.000	0.000	0.000	0.000	0.000	0.001	0.001	0.000	0.001	0.000	0.000	0.001	0.000	0.000	0.001	0.001	0.000	0.001	0.002	0.000
Mg^{2+}	0.008	0.009	0.007	0.000	0.000	0.004	0.005	0.000	0.005	0.003	0.009	0.006	0.007	0.007	0.008	0.006	0.014	0.006	0.003	0.005
Na^{+}	0.784	0.796	0.802	0.784	0.786	0.779	0.774	0.798	0.792	0.767	0.781	0.770	0.780	0.774	0.769	0.802	0.793	0.785	0.796	0.804
Ca^{2+}	0.215	0.221	0.207	0.187	0.186	0.204	0.186	0.174	0.186	0.235	0.217	0.231	0.229	0.211	0.233	0.207	0.210	0.207	0.208	0.218
K^{+}	0.012	0.014	0.009	0.012	0.011	0.009	0.018	0.015	0.013	0.010	0.006	0.014	0.011	0.031	0.009	0.014	0.015	0.023	0.019	0.007
Cation total	5.013	5.025	5.014	4.983	4.984	4.996	4.983	4.985	4.992	5.006	5.005	5.014	5.014	5.012	5.009	5.019	5.018	5.009	5.017	5.019
An	0.212	0.215	0.204	0.191	0.189	0.205	0.190	0.176	0.188	0.233	0.216	0.228	0.224	0.208	0.230	0.203	0.206	0.204	0.203	0.212
Ab	0.776	0.772	0.788	0.797	0.800	0.785	0.791	0.808	0.799	0.758	0.778	0.759	0.765	0.762	0.761	0.784	0.779	0.773	0.778	0.781
Or	0.012	0.013	0.009	0.012	0.012	0.010	0.019	0.015	0.014	0.010	0.006	0.013	0.011	0.031	0.009	0.013	0.014	0.023	0.019	0.007

Table C5. (*continued*)

Rock type	Pyroxene-bearing		Pyroxene-free granodiorites																	
Sample	Mat 59$_r$	Mat 62	Mat 3	Mat 3	Mat 9	Mat 9	Mat 14	Mat 14	Mat 22	Mat 22	Mat 22$_r$	Mat 22$_c$	Mat 22	Mat 22	Mat 22	Mat 22	Mat 22	Mat 22	Mat 22	Mat 22
SiO_2	63.10	63.36	65.11	64.77	63.26	64.80	64.10	63.93	63.77	62.87	62.08	62.18	58.33	63.99	63.53	63.66	63.30	63.19	63.31	63.33
TiO_2	nd	nd	0.02	nd	nd	nd	nd	nd	nd	0.01	nd	nd	nd	nd	nd	nd	nd	0.07	nd	nd
Al_2O_3	22.62	23.51	22.42	21.24	22.17	21.50	22.98	22.20	22.96	22.79	22.99	23.01	25.80	22.70	22.92	22.81	22.91	22.86	22.79	22.82
FeO*	nd	0.06	0.05	0.10	0.03	0.01	nd	nd	0.06	0.17	nd	0.05	1.15	0.07	nd	0.14	0.07	0.08	0.08	0.12
MnO	nd	0.01	0.08	nd	nd	0.01	nd	nd	nd	nd	nd	nd	nd	0.02	nd	nd	nd	nd	0.02	nd
MgO	0.11	0.16	nd	0.09	0.24	0.15	nd	nd	0.04	0.01	0.02	0.03	0.08	0.06	0.03	0.08	0.04	0.03	0.08	0.06
CaO	4.38	4.67	3.44	2.61	3.67	2.63	4.31	3.58	4.31	4.29	4.87	4.68	5.30	4.15	4.41	4.24	4.40	4.41	4.31	4.30
Na_2O	9.44	9.44	9.85	10.30	9.54	10.12	9.57	9.81	9.50	9.18	8.94	8.96	6.72	9.56	9.50	9.25	9.16	9.27	9.47	9.37
K_2O	0.08	0.20	0.09	0.08	0.16	0.09	nd	nd	0.20	0.22	0.17	0.28	2.56	0.48	0.13	0.50	0.18	0.11	0.15	0.13
Total	99.73	101.31	101.06	99.18	99.07	99.31	100.96	99.52	100.85	99.53	99.08	99.18	99.94	101.03	100.51	100.67	100.06	100.02	100.20	100.13
Number of ions on the basis of 8 oxygen atoms:																				
Si^{4+}	2.801	2.772	2.842	2.876	2.821	2.872	2.806	2.834	2.800	2.796	2.777	2.779	2.629	2.808	2.798	2.802	2.799	2.796	2.798	2.799
Al^{3+}	1.183	1.212	1.153	1.111	1.165	1.123	1.186	1.160	1.188	1.194	1.212	1.212	1.370	1.174	1.190	1.183	1.194	1.192	1.187	1.189
Fe^{3+}	0.000	0.002	0.001	0.003	0.001	0.000	0.000	0.000	0.002	0.006	0.000	0.002	0.039	0.002	0.000	0.005	0.002	0.003	0.003	0.004
Ti^{4+}	0.000	0.000	0.001	0.000	0.000	0.000	0.000	0.000	0.000	0.000	0.000	0.000	0.000	0.000	0.000	0.000	0.000	0.002	0.000	0.000
Mn^{2+}	0.000	0.000	0.003	0.000	0.000	0.000	0.000	0.000	0.000	0.000	0.000	0.000	0.000	0.001	0.000	0.000	0.000	0.000	0.001	0.000
Mg^{2+}	0.007	0.011	0.000	0.006	0.016	0.010	0.000	0.000	0.003	0.001	0.002	0.002	0.006	0.004	0.002	0.005	0.003	0.002	0.005	0.004
Na^{+}	0.813	0.801	0.834	0.886	0.825	0.870	0.812	0.843	0.808	0.791	0.776	0.776	0.588	0.814	0.811	0.789	0.785	0.795	0.811	0.803
Ca^{2+}	0.208	0.219	0.161	0.124	0.175	0.125	0.202	0.170	0.203	0.205	0.234	0.224	0.256	0.195	0.208	0.200	0.208	0.209	0.204	0.204
K^{+}	0.005	0.011	0.005	0.005	0.009	0.005	0.000	0.000	0.011	0.012	0.010	0.016	0.147	0.027	0.007	0.028	0.010	0.006	0.008	0.007
Cation total	5.017	5.027	5.000	5.012	5.013	5.004	5.007	5.007	5.015	5.005	5.010	5.010	5.034	5.024	5.016	5.012	5.001	5.005	5.017	5.010
An	0.203	0.212	0.161	0.122	0.174	0.125	0.199	0.168	0.198	0.203	0.229	0.220	0.258	0.188	0.203	0.196	0.208	0.207	0.199	0.201
Ab	0.792	0.777	0.834	0.873	0.817	0.870	0.801	0.832	0.791	0.785	0.761	0.764	0.593	0.786	0.791	0.776	0.783	0.787	0.793	0.792
Or	0.005	0.011	0.005	0.005	0.009	0.005	0.000	0.000	0.011	0.012	0.009	0.016	0.148	0.026	0.007	0.028	0.010	0.006	0.008	0.007

Table C5. (*continued*)

Rock type	Pyroxene-free																			
	granodiorites								granites with ≤71 wt.% SiO_2								granites with >71 wt.% SiO_2			
Sample	Mat 22	Mat 34	Mat 34	Mat 34	Mat 34	Mat 70_c	Mat 70_r	Mat 70	Mat 7	Mat 7	Mat 31	Mat 31	Mat 31	Mat 31	Mat 31	Mat 42	Mat 23	Mat 23	Mat 23	Mat 23
SiO_2	62.95	64.15	63.87	64.00	67.21	64.86	65.68	62.51	63.44	64.90	65.58	65.67	63.60	66.99	65.02	63.97	65.00	63.90	64.56	65.07
TiO_2	nd	nd	nd	nd	nd	0.02	0.08	0.03	0.05	nd	nd	nd	0.06	0.05	nd	0.11	nd	0.03	nd	nd
Al_2O_3	22.83	22.74	22.59	21.97	20.57	22.28	21.74	22.73	22.47	21.92	21.84	21.49	21.99	20.14	21.56	21.59	21.39	21.96	21.86	22.00
FeO*	0.05	0.07	nd	0.08	0.04	0.04	0.07	0.07	0.09	0.06	0.09	0.09	0.09	0.28	0.08	1.24	0.05	0.07	0.03	0.07
MnO	0.05	0.05	nd	nd	0.09	0.01	nd	nd	nd	0.03	0.00	0.05	0.01	nd	nd	0.01	nd	nd	0.06	0.02
MgO	0.08	0.04	0.03	0.04	nd	0.03	nd	0.03	0.03	0.09	0.07	0.07	0.05	0.05	0.02	0.31	nd	nd	nd	0.02
CaO	4.39	4.03	4.09	3.41	1.49	3.30	2.92	4.36	3.91	3.20	3.03	2.57	3.63	0.95	2.96	2.67	3.04	3.51	3.40	3.28
Na_2O	9.36	9.69	9.34	9.82	11.09	10.03	10.30	9.21	9.65	10.01	10.15	10.38	9.75	11.24	10.25	10.24	10.02	9.80	9.83	9.92
K_2O	0.21	0.10	0.11	0.08	0.04	0.10	0.12	0.13	0.13	0.07	0.04	0.07	0.06	0.04	0.10	0.17	0.14	0.13	0.13	0.13
Total	99.93	100.87	100.03	99.39	100.53	100.66	100.90	99.07	99.77	100.28	100.80	100.39	99.23	99.72	99.98	100.31	99.63	99.40	99.84	100.51
Number of ions on the basis of 8 oxygen atoms:																				
Si^{4+}	2.792	2.813	2.820	2.841	2.934	2.842	2.869	2.793	2.812	2.853	2.865	2.880	2.831	2.945	2.867	2.827	2.874	2.839	2.852	2.854
Al^{3+}	1.193	1.175	1.175	1.150	1.058	1.151	1.119	1.197	1.174	1.136	1.125	1.111	1.154	1.044	1.120	1.124	1.114	1.150	1.138	1.137
Fe^{3+}	0.002	0.002	0.000	0.003	0.001	0.001	0.002	0.002	0.003	0.002	0.003	0.003	0.003	0.009	0.003	0.041	0.002	0.002	0.001	0.002
Ti^{4+}	0.000	0.000	0.000	0.000	0.000	0.001	0.003	0.001	0.002	0.000	0.000	0.000	0.002	0.002	0.000	0.004	0.000	0.001	0.000	0.000
Mn^{2+}	0.002	0.002	0.000	0.000	0.003	0.000	0.000	0.000	0.000	0.001	0.000	0.002	0.000	0.000	0.000	0.000	0.000	0.000	0.002	0.001
Mg^{2+}	0.005	0.003	0.002	0.003	0.000	0.002	0.000	0.002	0.002	0.006	0.005	0.004	0.003	0.003	0.001	0.020	0.000	0.000	0.000	0.001
Na^{+}	0.805	0.824	0.799	0.845	0.939	0.852	0.873	0.798	0.829	0.853	0.860	0.883	0.842	0.958	0.876	0.877	0.859	0.844	0.842	0.844
Ca^{2+}	0.209	0.189	0.193	0.162	0.070	0.155	0.137	0.209	0.186	0.151	0.142	0.121	0.173	0.045	0.140	0.127	0.144	0.167	0.161	0.154
K^{+}	0.012	0.006	0.006	0.004	0.002	0.005	0.007	0.007	0.008	0.004	0.002	0.004	0.003	0.002	0.006	0.010	0.008	0.007	0.007	0.007
Cation total	5.019	5.013	4.995	5.007	5.007	5.009	5.008	5.009	5.016	5.006	5.002	5.007	5.011	5.007	5.013	5.030	5.001	5.010	5.003	5.001
An	0.204	0.186	0.194	0.160	0.069	0.153	0.134	0.206	0.182	0.149	0.141	0.120	0.170	0.045	0.137	0.125	0.142	0.164	0.159	0.153
Ab	0.785	0.808	0.800	0.836	0.929	0.842	0.859	0.787	0.811	0.847	0.857	0.876	0.827	0.953	0.858	0.865	0.850	0.829	0.834	0.840
Or	0.012	0.006	0.006	0.004	0.002	0.005	0.006	0.007	0.007	0.004	0.002	0.004	0.003	0.002	0.005	0.010	0.008	0.007	0.007	0.007

Table C5. (*continued*)

Rock type	Pyroxene-free granites with >71 wt.% SiO_2														Enclave in px-diorites2 diorites	
Sample	Mat 23	Mat 23	Mat 23	Mat 24	Mat 24	Mat 35	Mat 35	Mat 35	Mat 35	Mat 35	Mat 35	Mat 35	Mat 35	Mat 35	Mat 61_c	Mat 61_r
SiO_2	65.00	64.40	65.32	65.37	63.84	61.63	60.86	61.48	61.06	60.81	60.85	60.66	60.99	60.69	63.01	62.65
TiO_2	nd	nd	nd	nd	nd	0.10	0.02	0.02	nd	0.01	0.01	0.05	0.04	0.02	0.05	nd
Al_2O_3	21.69	22.11	21.80	22.34	22.49	23.90	24.05	24.16	24.15	24.17	24.11	24.32	23.93	24.06	23.17	23.34
FeO*	0.08	0.03	0.10	0.13	0.12	0.01	0.05	nd	0.03	0.03	nd	0.04	0.05	nd	0.03	0.11
MnO	0.01	0.01	nd	0.01	0.02	nd	nd	nd	nd	nd	nd	nd	nd	nd	0.04	0.06
MgO	0.02	0.02	0.03	nd	0.07	0.02	nd	0.01	nd	0.05	nd	0.03	0.04	0.02	0.05	0.20
CaO	3.07	3.57	3.08	2.80	4.00	5.64	5.97	5.89	6.00	5.96	6.03	6.07	5.96	5.82	4.77	4.73
Na_2O	10.05	9.82	10.10	10.05	9.53	8.59	8.23	8.43	8.20	8.20	8.20	8.27	8.36	8.21	9.21	8.96
K_2O	0.17	0.18	0.16	0.28	0.31	0.24	0.24	0.14	0.23	0.20	0.18	0.26	0.21	0.19	0.22	0.16
Total	100.08	100.13	100.59	100.97	100.37	100.12	99.43	100.13	99.66	99.43	99.38	99.70	99.57	99.01	100.54	100.22
Number of ions on the basis of 8 oxygen atoms:																
Si^{4+}	2.863	2.840	2.863	2.853	2.815	2.736	2.722	2.728	2.723	2.719	2.722	2.709	2.725	2.723	2.779	2.770
Al^{3+}	1.126	1.149	1.126	1.149	1.169	1.250	1.268	1.263	1.269	1.273	1.271	1.280	1.260	1.272	1.205	1.217
Fe^{3+}	0.003	0.001	0.003	0.004	0.004	0.000	0.002	0.000	0.001	0.001	0.000	0.001	0.002	0.000	0.001	0.004
Ti^{4+}	0.000	0.000	0.000	0.000	0.000	0.003	0.001	0.001	0.000	0.000	0.000	0.002	0.001	0.001	0.002	0.000
Mn^{2+}	0.000	0.000	0.000	0.000	0.001	0.000	0.000	0.000	0.000	0.000	0.000	0.000	0.000	0.000	0.002	0.002
Mg^{2+}	0.001	0.001	0.002	0.000	0.004	0.001	0.000	0.001	0.000	0.004	0.000	0.002	0.002	0.001	0.003	0.013
Na^{+}	0.858	0.839	0.858	0.850	0.815	0.740	0.714	0.725	0.709	0.711	0.711	0.716	0.724	0.714	0.788	0.769
Ca^{2+}	0.145	0.169	0.145	0.131	0.189	0.268	0.286	0.280	0.287	0.285	0.289	0.291	0.285	0.280	0.225	0.224
K^{+}	0.009	0.010	0.009	0.015	0.017	0.013	0.014	0.008	0.013	0.012	0.010	0.015	0.012	0.011	0.013	0.009
Cation total	5.006	5.010	5.006	5.003	5.014	5.012	5.006	5.006	5.002	5.005	5.003	5.014	5.011	5.002	5.016	0.009
An	0.143	0.166	0.143	0.131	0.185	0.263	0.282	0.276	0.284	0.283	0.286	0.285	0.279	0.278	0.220	0.224
Ab	0.848	0.824	0.848	0.853	0.798	0.724	0.704	0.716	0.703	0.705	0.704	0.701	0.709	0.711	0.768	0.767
Or	0.009	0.010	0.009	0.015	0.017	0.013	0.014	0.008	0.013	0.011	0.010	0.014	0.012	0.011	0.012	0.009

Table C6. Alkali feldspar composition for the rocks of the Matok pluton.

Rock type	Pyroxene-bearing																Pyroxene-free				
	diorites1		diorites2				granodiorites														
Sample	Mat 61	Mat 61	Mat 66	Mat 66	Mat 66	Mat 66	Mat 27	Mat 27	Mat 27	Mat 57	Mat 57	Mat 59	Mat 59	Mat 59_c	Mat 59_r	Mat 62	Mat 22	Mat 22	Mat 22	Mat 22	Mat 22
SiO_2	63.70	64.58	65.26	63.86	65.29	63.87	65.84	64.95	65.06	64.82	63.97	64.79	64.27	64.64	65.00	64.72	65.00	64.73	64.62	64.73	64.77
TiO_2	nd	nd	nd	0.04	nd	0.04	0.01	nd	nd	nd	0.05	nd	nd	nd	nd	0.02	nd	nd	nd	nd	nd
Al_2O_3	18.51	18.32	18.54	18.45	18.55	18.45	18.43	18.10	18.01	18.21	18.34	18.34	18.33	18.37	18.43	18.24	18.68	18.46	18.56	18.46	18.42
FeO*	0.09	0.12	nd	0.23	nd	0.23	0.14	0.03	0.06	0.01	0.34	0.10	0.04	nd	nd	0.11	0.01	nd	nd	nd	nd
MnO	nd	nd	nd	0.02	nd	nd	nd	0.01	0.04	0.03	nd	0.01	0.02	nd	nd	0.03	nd	0.05	0.03	0.05	nd
MgO	0.13	nd	nd	nd	nd	nd	0.25	nd	0.13	0.15	0.29	0.11	0.17	0.12	0.14	0.06	0.07	0.01	0.05	0.01	nd
BaO	0.35	0.34	0.41	0.48	0.41	0.48	0.18	0.14	0.17	nd	nd	0.21	0.28	0.21	0.20	0.26	0.01	nd	nd	nd	nd
CaO	nd	nd	nd	nd	nd	nd	nd	nd	nd	nd	nd	0.02	nd	nd	0.01	nd	nd	nd	nd	nd	nd
Na_2O	0.78	1.22	1.27	1.02	1.35	1.08	1.14	0.90	0.89	1.04	0.86	1.69	1.40	1.76	1.60	0.75	1.30	1.36	1.39	1.36	1.26
K_2O	15.62	15.07	15.31	15.25	15.31	15.25	14.73	15.10	15.05	15.50	15.73	14.57	15.02	14.54	14.72	15.89	15.44	15.32	15.35	15.32	15.21
Total	99.17	99.65	100.78	99.34	100.90	99.41	100.63	99.18	99.28	99.76	99.56	99.82	99.53	99.64	100.11	99.97	100.53	99.92	99.99	99.92	99.66
Number of ions on the basis of 8 oxygen atoms:																					
Si^{4+}	2.976	2.993	2.993	2.978	2.991	2.977	3.003	3.012	3.013	2.998	2.974	2.991	2.984	2.989	2.992	2.994	2.984	2.989	2.983	2.989	2.995
Al^{3+}	1.019	1.001	1.002	1.014	1.002	1.014	0.991	0.989	0.983	0.992	1.005	0.998	1.003	1.001	1.000	0.994	1.011	1.005	1.010	1.005	1.004
Fe^{3+}	0.003	0.004	0.000	0.008	0.000	0.008	0.005	0.001	0.002	0.000	0.012	0.003	0.001	0.000	0.000	0.004	0.000	0.000	0.000	0.000	0.000
Ti^{4+}	0.000	0.000	0.000	0.002	0.000	0.002	0.000	0.000	0.000	0.000	0.002	0.000	0.000	0.000	0.000	0.001	0.000	0.000	0.000	0.000	0.000
Mn^{2+}	0.000	0.000	0.000	0.001	0.000	0.000	0.000	0.000	0.001	0.001	0.000	0.000	0.001	0.000	0.000	0.001	0.000	0.002	0.001	0.002	0.000
Mg^{2+}	0.009	0.000	0.000	0.000	0.000	0.000	0.017	0.000	0.009	0.010	0.020	0.007	0.012	0.008	0.009	0.004	0.005	0.000	0.004	0.000	0.000
Na^{+}	0.070	0.109	0.112	0.092	0.120	0.098	0.101	0.081	0.080	0.093	0.077	0.151	0.126	0.157	0.143	0.067	0.116	0.122	0.124	0.122	0.113
Ca^{2+}	0.000	0.000	0.000	0.000	0.000	0.000	0.000	0.000	0.000	0.000	0.000	0.001	0.000	0.000	0.001	0.000	0.000	0.000	0.000	0.000	0.000
K^{+}	0.930	0.891	0.895	0.907	0.895	0.907	0.857	0.893	0.889	0.915	0.933	0.858	0.889	0.858	0.864	0.938	0.904	0.902	0.904	0.902	0.897
Ba^{2+}	0.006	0.006	0.007	0.009	0.007	0.009	0.003	0.003	0.003	0.000	0.000	0.004	0.005	0.004	0.004	0.005	0.000	0.000	0.000	0.000	0.000
Cation total	5.014	5.005	5.010	5.010	5.015	5.013	4.978	4.979	4.979	5.009	5.021	5.013	5.022	5.018	5.012	5.008	5.020	5.020	5.026	5.020	5.008
An	0.000	0.000	0.000	0.000	0.000	0.000	0.000	0.000	0.000	0.000	0.000	0.001	0.000	0.000	0.001	0.000	0.000	0.000	0.000	0.000	0.000
Ab	0.070	0.109	0.112	0.092	0.118	0.097	0.105	0.083	0.082	0.092	0.076	0.150	0.124	0.155	0.142	0.067	0.114	0.119	0.121	0.119	0.112
Or	0.930	0.891	0.888	0.908	0.882	0.903	0.895	0.917	0.918	0.908	0.924	0.850	0.876	0.845	0.858	0.933	0.886	0.881	0.879	0.881	0.888

Table C6. (*Continued*)

Rock type	Pyroxene-free																			
	granodiorites											granites with ≤71 wt.% SiO_2			granites with >71 wt.% SiO_2						
Sample	Mat 22	Mat 22	Mat 30	Mat 30	Mat 30	Mat 30	Mat 30	Mat 30	Mat 30	Mat 70	Mat 70	Mat 42_c	Mat 42_r	Mat 42	Mat 23	Mat 23	Mat 23	Mat 23	Mat 24	Mat 24	Mat 31
SiO_2	64.21	64.66	64.69	64.73	64.18	64.77	64.22	64.33	63.86	64.63	63.97	64.35	63.93	64.80	65.71	64.95	65.04	65.37	65.87	64.80	65.43
TiO_2	nd	nd	nd	0.26	0.31	0.34	0.36	nd	0.33	nd	0.02	0.04	nd	nd	nd	nd	nd	nd	nd	0.01	nd
Al_2O_3	18.32	18.35	18.22	18.20	18.14	18.31	18.19	18.18	18.07	18.65	18.22	18.32	18.20	18.03	18.40	18.07	18.06	18.32	18.30	18.15	18.35
FeO*	nd	0.07	nd	nd	nd	0.03	0.01	nd	0.04	0.03	0.01	0.07	nd	0.10	nd	0.01	0.04	0.05	0.00	0.01	0.07
MnO	nd	0.00	nd	nd	nd	nd	0.02	nd	nd	nd	0.00	nd	nd	nd	nd	0.10	nd	nd	0.08	nd	0.02
MgO	nd	0.02	0.02	0.05	0.01	0.02	0.06	0.04	0.03	0.13	0.02	0.12	0.12	0.03	nd	0.03	nd	0.01	0.02	0.04	0.00
BaO	nd	0.07	nd	nd	nd	nd	nd	nd	nd	0.52	0.49	0.34	0.35	0.42	0.10	0.03	0.08	0.11	0.12	0.19	0.18
CaO	nd	nd	nd	nd	nd	nd	nd	nd	nd	nd	nd	nd	nd	nd	nd	nd	nd	nd	nd	nd	nd
Na_2O	1.18	1.28	0.29	0.38	0.61	0.63	0.80	0.87	0.72	0.76	0.77	1.08	0.91	1.25	0.80	1.07	0.82	0.91	1.24	1.05	0.80
K_2O	15.54	15.34	16.70	16.69	16.41	16.37	15.99	15.78	16.04	15.73	15.56	15.38	15.59	14.81	16.35	15.46	15.72	15.90	15.20	15.78	16.20
Total	99.25	99.80	99.92	100.31	99.65	100.46	99.64	99.19	99.08	100.45	99.07	99.70	99.10	99.43	101.35	99.71	99.76	100.66	100.81	100.03	101.05
Number of ions on the basis of 8 oxygen atoms:																					
Si^{4+}	2.989	2.991	2.999	2.991	2.986	2.986	2.983	2.996	2.984	2.981	2.991	2.986	2.988	3.006	3.001	3.006	3.009	3.001	3.009	2.998	2.998
Al^{3+}	1.005	1.000	0.996	0.991	0.994	0.995	0.996	0.998	0.995	1.014	1.004	1.002	1.002	0.986	0.990	0.985	0.985	0.991	0.985	0.989	0.991
Fe^{3+}	0.000	0.003	0.000	0.000	0.000	0.001	0.000	0.000	0.002	0.001	0.000	0.003	0.000	0.003	0.000	0.000	0.001	0.002	0.000	0.000	0.002
Ti^{4+}	0.000	0.000	0.000	0.009	0.011	0.012	0.012	0.000	0.012	0.000	0.001	0.001	0.000	0.000	0.000	0.000	0.000	0.000	0.000	0.000	0.000
Mn^{2+}	0.000	0.000	0.000	0.000	0.000	0.000	0.001	0.000	0.000	0.000	0.000	0.000	0.000	0.000	0.000	0.003	0.000	0.000	0.002	0.000	0.001
Mg^{2+}	0.000	0.002	0.001	0.004	0.000	0.001	0.004	0.003	0.002	0.009	0.001	0.009	0.008	0.002	0.000	0.002	0.000	0.001	0.001	0.003	0.000
Na^{+}	0.106	0.114	0.026	0.034	0.055	0.056	0.072	0.078	0.065	0.068	0.070	0.097	0.083	0.112	0.070	0.096	0.074	0.081	0.109	0.094	0.071
Ca^{2+}	0.000	0.000	0.000	0.000	0.000	0.000	0.000	0.000	0.000	0.000	0.000	0.000	0.000	0.000	0.000	0.000	0.000	0.000	0.000	0.000	0.000
K^{+}	0.923	0.905	0.988	0.984	0.974	0.963	0.947	0.937	0.956	0.926	0.928	0.910	0.929	0.876	0.952	0.912	0.928	0.931	0.886	0.931	0.947
Ba^{2+}	0.000	0.001	0.000	0.000	0.000	0.000	0.000	0.000	0.000	0.009	0.009	0.006	0.006	0.008	0.002	0.000	0.001	0.002	0.002	0.003	0.003
Cation total	5.023	5.017	5.010	5.013	5.020	5.014	5.016	5.013	5.016	5.008	5.005	5.014	5.017	4.993	5.016	5.005	4.998	5.009	4.995	5.020	5.014
An	0.000	0.000	0.000	0.000	0.000	0.000	0.000	0.000	0.000	0.000	0.000	0.000	0.000	0.000	0.000	0.000	0.000	0.000	0.000	0.000	0.000
Ab	0.103	0.112	0.026	0.034	0.053	0.055	0.071	0.077	0.064	0.068	0.070	0.097	0.082	0.113	0.069	0.095	0.074	0.080	0.110	0.092	0.070
Or	0.897	0.888	0.974	0.966	0.947	0.945	0.929	0.923	0.936	0.932	0.930	0.903	0.918	0.887	0.931	0.905	0.926	0.920	0.890	0.908	0.930

Table C6. (*Continued*)

Rock type	Pyroxene-free granites with >71 wt.% SiO_2																			
Sample	Mat 35	Mat 35_c	Mat 35_r	Mat 35	Mat 35_r	Mat 35_c	Mat 35	Mat 35	Mat 35_r	Mat 35_c	Mat 35_c	Mat 35_r	Mat 35_c	Mat 35_r	Mat 35_r	Mat 35_c	Mat 35	Mat 35	Mat 35_c	Mat 35_r
SiO_2	64.88	64.63	64.46	64.52	64.67	64.74	65.56	64.42	64.51	64.67	65.41	65.43	65.51	65.48	65.25	65.40	65.37	65.47	65.33	65.16
TiO_2	0.18	0.14	nd	nd	0.04	nd	0.04	0.11	0.09	nd	nd	nd	0.01	0.15	0.04	nd	0.04	nd	0.10	0.08
Al_2O_3	18.22	18.05	18.00	18.06	17.92	18.00	18.32	18.21	18.09	18.05	18.46	18.19	18.26	18.11	18.48	18.26	18.37	18.38	18.17	18.21
FeO*	0.01	0.03	nd	0.08	0.03	nd	0.03	0.12	0.08	0.06	0.04	nd	nd	nd	0.08	nd	nd	nd	0.02	nd
MnO	nd	0.01	nd	0.00	nd	nd	0.02	nd	nd	nd	nd	0.01	0.02	0.05	0.01	nd	nd	0.02	nd	nd
MgO	0.06	0.02	0.05	nd	0.06	0.06	0.00	0.01	nd	0.01	0.01	0.05	0.02	0.03	nd	nd	0.06	0.02	nd	0.02
BaO	nd	nd	0.08	0.08	0.07	0.09	0.11	0.08	0.07	0.09	0.09	0.08	0.08	nd	0.11	0.10	0.08	0.10	0.09	0.08
CaO	nd	nd	nd	nd	nd	nd	nd	nd	nd	nd	nd	nd	nd	nd	nd	nd	nd	nd	nd	nd
Na_2O	0.86	0.82	0.63	0.53	0.58	0.85	0.40	1.12	0.69	0.92	0.80	0.96	1.17	0.85	0.88	0.76	0.76	1.11	0.94	0.90
K_2O	15.91	15.92	16.17	16.42	16.25	15.80	16.63	15.64	15.92	15.69	16.25	16.00	15.64	16.16	15.98	16.28	16.34	15.87	16.04	16.11
Total	100.11	99.64	99.38	99.69	99.60	99.55	101.09	99.71	99.44	99.49	101.06	100.72	100.71	100.81	100.84	100.79	101.01	100.96	100.69	100.56
Number of ions on the basis of 8 oxygen atoms:																				
Si^{4+}	2.995	2.999	3.002	3.000	3.005	3.005	3.003	2.989	2.999	3.003	2.996	3.004	3.003	3.004	2.993	3.003	2.996	2.998	3.001	2.999
Al^{3+}	0.991	0.987	0.988	0.990	0.981	0.985	0.989	0.995	0.991	0.988	0.996	0.984	0.987	0.979	0.999	0.988	0.992	0.992	0.984	0.988
Fe^{3+}	0.000	0.001	0.000	0.003	0.001	0.000	0.001	0.004	0.003	0.002	0.001	0.000	0.000	0.000	0.003	0.000	0.000	0.000	0.001	0.000
Ti^{4+}	0.006	0.005	0.000	0.000	0.001	0.000	0.001	0.004	0.003	0.000	0.000	0.000	0.000	0.005	0.001	0.000	0.001	0.000	0.003	0.003
Mn^{2+}	0.000	0.000	0.000	0.000	0.000	0.000	0.001	0.000	0.000	0.000	0.000	0.000	0.001	0.002	0.000	0.000	0.000	0.000	0.000	0.000
Mg^{2+}	0.004	0.002	0.004	0.000	0.004	0.004	0.000	0.001	0.000	0.001	0.000	0.003	0.001	0.002	0.000	0.000	0.004	0.001	0.000	0.001
Na^{+}	0.077	0.074	0.057	0.048	0.052	0.077	0.035	0.101	0.062	0.083	0.071	0.085	0.104	0.076	0.078	0.067	0.067	0.099	0.083	0.081
Ca^{2+}	0.000	0.000	0.000	0.000	0.000	0.000	0.000	0.000	0.000	0.000	0.000	0.000	0.000	0.000	0.000	0.000	0.000	0.000	0.000	0.000
K^{+}	0.937	0.942	0.960	0.974	0.963	0.935	0.971	0.926	0.944	0.930	0.949	0.937	0.914	0.946	0.935	0.954	0.955	0.927	0.940	0.946
Ba^{2+}	0.000	0.000	0.001	0.001	0.001	0.002	0.002	0.001	0.001	0.002	0.002	0.002	0.001	0.000	0.002	0.002	0.001	0.002	0.002	0.001
Cation total	5.010	5.010	5.013	5.015	5.010	5.008	5.004	5.021	5.003	5.008	5.016	5.015	5.012	5.012	5.011	5.014	5.018	5.019	5.015	5.018
An	0.000	0.000	0.000	0.000	0.000	0.000	0.000	0.000	0.000	0.000	0.000	0.000	0.000	0.000	0.000	0.000	0.000	0.000	0.000	0.000
Ab	0.076	0.073	0.056	0.047	0.051	0.076	0.035	0.098	0.061	0.082	0.070	0.083	0.102	0.074	0.077	0.066	0.066	0.096	0.082	0.079
Or	0.924	0.927	0.944	0.953	0.949	0.924	0.965	0.902	0.939	0.918	0.930	0.917	0.898	0.926	0.923	0.934	0.934	0.904	0.918	0.921

TableC7. Epidote composition for the px-free rocks of the Matok pluton.

Rock type	granodiorites																
textural relationship	Symplectitic/well developed																
Sample	Mat 3	Mat 3	Mat 3	Mat 9	Mat 9	Mat 9	Mat 9	Mat 9	Mat 14	Mat 14	Mat 14	Mat 14	Mat 14	Mat 14	Mat 14	Mat 14	Mat 14
SiO_2	36.59	37.44	37.41	37.69	36.87	36.48	36.85	36.46	37.60	37.91	36.60	37.23	36.98	37.71	37.29	37.36	37.65
TiO_2	0.17	0.07	0.14	0.14	0.15	nd	0.15	nd	nd	nd	nd	0.07	0.01	0.06	0.12	0.07	0.12
Al_2O_3	22.38	22.85	22.44	21.84	21.51	21.43	22.03	21.95	24.09	23.86	22.71	22.31	22.07	23.27	22.12	23.06	23.89
Y_2O_3	nd	0.48	0.64	0.37	0.21	nd	nd	nd	nd	nd	nd	nd	0.28	0.18	0.06	0.28	0.21
Ce_2O_3	nd	nd	nd	nd	nd	nd	0.21	nd	nd	nd	nd	nd	nd	0.10	nd	nd	nd
La_2O_3	nd	nd	nd	nd	nd	nd	nd	nd	nd	nd	nd	nd	nd	nd	nd	nd	nd
FeO*	12.91	13.32	14.01	14.65	14.50	14.37	13.96	13.83	12.24	12.53	12.94	14.20	14.30	12.89	14.64	13.08	12.39
MnO	0.21	0.10	0.16	0.13	0.20	0.05	0.20	0.05	0.26	0.31	0.17	0.20	0.19	0.22	0.13	0.13	nd
MgO	0.06	0.09	nd	0.06	0.02	0.01	0.02	0.01	nd	0.06	0.08	nd	0.05	0.03	0.03	0.02	0.05
CaO	22.47	23.18	23.61	24.26	23.57	23.63	22.87	22.93	23.51	23.37	23.21	23.53	23.17	23.46	23.39	23.46	23.61
Na_2O	0.06	0.04	0.05	0.11	0.08	0.05	0.08	0.05	0.12	0.14	0.09	nd	0.10	0.03	0.07	0.03	0.12
K_2O	nd	0.06	0.04	0.11	0.04	0.13	0.03	0.11	nd	nd	nd	nd	0.01	nd	nd	nd	nd
Total	94.85	97.63	98.50	99.36	97.15	96.15	96.40	95.39	97.81	98.18	95.80	97.54	97.15	97.94	97.84	97.49	98.02
Number of ions on the basis of 12 oxygen atoms:																	
Si^{4+}	2.963	2.955	2.945	2.954	2.953	2.951	2.959	2.956	2.939	2.954	2.940	2.953	2.952	2.957	2.955	2.948	2.940
Al^{3+}	2.135	2.126	2.082	2.017	2.030	2.042	2.084	2.097	2.219	2.191	2.150	2.086	2.077	2.151	2.066	2.145	2.198
Fe^{3+}	0.874	0.879	0.922	0.960	0.971	0.972	0.937	0.938	0.800	0.816	0.869	0.942	0.955	0.845	0.970	0.863	0.809
Ti^{4+}	0.010	0.004	0.008	0.008	0.009	0.000	0.009	0.000	0.000	0.000	0.000	0.004	0.000	0.004	0.007	0.004	0.007
Mn^{2+}	0.015	0.007	0.011	0.009	0.013	0.004	0.014	0.004	0.017	0.020	0.012	0.013	0.013	0.015	0.008	0.009	0.000
Mg^{2+}	0.007	0.010	0.000	0.007	0.002	0.001	0.002	0.001	0.000	0.007	0.009	0.000	0.006	0.003	0.004	0.003	0.005
Y^{3+}	0.000	0.020	0.027	0.016	0.009	0.000	0.000	0.000	0.000	0.000	0.000	0.000	0.012	0.008	0.002	0.012	0.009
Ca^{2+}	1.950	1.960	1.992	2.037	2.022	2.047	1.967	1.991	1.968	1.951	1.998	2.000	1.981	1.971	1.986	1.984	1.975
Ce3+	0.000	0.000	0.000	0.000	0.000	0.000	0.006	0.000	0.000	0.000	0.000	0.000	0.000	0.003	0.000	0.000	0.000
La3+	0.000	0.000	0.000	0.000	0.000	0.000	0.000	0.000	0.000	0.000	0.000	0.000	0.000	0.000	0.000	0.000	0.000
Na^{+}	0.010	0.006	0.007	0.017	0.012	0.007	0.013	0.008	0.018	0.022	0.014	0.000	0.015	0.004	0.011	0.004	0.018
K^{+}	0.000	0.006	0.004	0.011	0.004	0.013	0.003	0.012	0.000	0.000	0.000	0.000	0.001	0.000	0.000	0.000	0.000
Cation total	7.964	7.974	7.998	8.036	8.026	8.038	7.995	8.006	7.961	7.961	7.992	7.999	8.011	7.961	8.010	7.971	7.959
$Fe^{3+}/(Fe^{3+}+Al^{3+})$	29.04	29.26	30.70	32.25	32.36	32.25	31.01	30.90	26.50	27.14	28.78	31.10	31.49	28.21	31.95	28.69	26.90

Table C7. (*Continued*)

Rock type	granodiorites																	
textural relationship	Symplectitic/well developed																	
Sample	Mat 14	Mat 14	Mat 14	Mat 14	Mat 14	Mat 14	Mat 14	Mat 14	Mat 14	Mat 30	Mat 30	Mat 30	Mat 30	Mat 30	Mat 30	Mat 70	Mat 70	Mat 70
SiO_2	37.20	36.01	35.91	36.65	36.01	36.34	35.68	36.95	36.33	38.64	38.12	37.66	37.98	38.03	37.73	37.11	38.07	38.41
TiO_2	0.12	0.10	0.18	0.07	0.10	0.05	0.21	0.07	0.09	nd	nd	nd	nd	nd	nd	0.03	0.09	0.08
Al_2O_3	23.09	22.37	22.54	23.25	22.15	22.38	21.94	25.98	22.98	23.13	23.01	22.85	22.94	22.96	22.89	24.07	24.48	23.61
Y_2O_3	0.33	0.24	0.27	0.07	nd	0.33	0.19	0.35	0.30	nd	nd	nd	nd	nd	nd	nd	nd	nd
Ce_2O_3	0.08	nd	nd	0.09	nd	0.33	0.02	nd	nd	nd	nd	nd	nd	nd	nd	nd	nd	nd
La_2O_3	nd	nd	nd	0.12	nd	0.07	0.04	0.06	nd	nd	nd	nd	nd	nd	nd	nd	nd	nd
FeO*	13.01	12.56	11.80	11.58	12.30	12.00	12.35	7.79	12.02	13.62	13.46	13.77	13.66	14.01	13.51	11.79	11.96	13.08
MnO	0.17	0.18	0.15	0.19	0.14	0.14	0.19	0.09	0.15	0.20	0.23	0.20	0.29	0.17	0.19	0.08	0.08	0.11
MgO	0.11	0.03	0.07	0.10	nd	0.05	0.05	0.04	0.01	0.08	0.00	nd	nd	nd	0.10	0.05	0.03	0.09
CaO	23.41	22.82	22.71	22.97	22.29	22.27	22.62	23.20	22.59	23.83	23.50	23.23	23.31	23.29	22.97	23.23	23.74	23.86
Na_2O	0.09	0.10	0.09	0.11	0.11	0.16	0.11	0.10	0.12	0.05	0.09	nd	nd	nd	0.03	0.05	0.11	0.05
K_2O	nd	0.04	0.04	nd	nd	0.01	0.01	0.02	0.03	nd	nd	nd	nd	nd	nd	0.03	nd	0.02
Total	97.61	94.44	93.76	95.18	93.08	94.12	93.37	94.64	94.61	99.55	98.40	97.71	98.17	98.45	97.42	96.46	98.55	99.31
Number of ions on the basis of 12 oxygen atoms:																		
Si^{4+}	2.936	2.936	2.938	2.945	2.967	2.965	2.942	2.920	2.942	2.983	2.978	2.968	2.976	2.974	2.976	2.934	2.944	2.965
Al^{3+}	2.148	2.149	2.173	2.202	2.150	2.152	2.132	2.419	2.193	2.105	2.118	2.122	2.118	2.116	2.127	2.243	2.231	2.148
Fe^{3+}	0.858	0.856	0.807	0.778	0.847	0.819	0.851	0.515	0.814	0.880	0.879	0.908	0.895	0.916	0.891	0.779	0.773	0.844
Ti^{4+}	0.007	0.006	0.011	0.004	0.006	0.003	0.013	0.004	0.005	0.000	0.000	0.000	0.000	0.000	0.000	0.002	0.005	0.005
Mn^{2+}	0.011	0.012	0.010	0.013	0.009	0.010	0.013	0.006	0.010	0.013	0.015	0.013	0.019	0.011	0.013	0.006	0.005	0.007
Mg^{2+}	0.013	0.003	0.008	0.012	0.000	0.006	0.006	0.005	0.002	0.010	0.000	0.000	0.000	0.000	0.011	0.006	0.003	0.010
Y^{3+}	0.014	0.010	0.012	0.003	0.000	0.014	0.008	0.015	0.013	0.000	0.000	0.000	0.000	0.000	0.000	0.000	0.000	0.000
Ca^{2+}	1.979	1.993	1.991	1.977	1.967	1.948	1.998	1.964	1.959	1.971	1.967	1.961	1.957	1.951	1.941	1.968	1.967	1.973
Ce3+	0.002	0.000	0.000	0.003	0.000	0.010	0.001	0.000	0.000	0.000	0.000	0.000	0.000	0.000	0.000	0.000	0.000	0.000
La3+	0.000	0.000	0.000	0.003	0.000	0.002	0.001	0.002	0.000	0.000	0.000	0.000	0.000	0.000	0.000	0.000	0.000	0.000
Na^{+}	0.014	0.015	0.015	0.016	0.018	0.025	0.018	0.016	0.018	0.007	0.014	0.000	0.000	0.000	0.005	0.008	0.016	0.007
K^{+}	0.000	0.004	0.004	0.000	0.000	0.001	0.001	0.002	0.003	0.000	0.000	0.000	0.000	0.000	0.000	0.003	0.000	0.002
Cation total	7.982	7.987	7.968	7.952	7.961	7.955	7.983	7.867	7.960	7.968	7.970	7.972	7.965	7.968	7.963	7.948	7.944	7.961
$Fe^{3+}/(Fe^{3+}+Al^{3+})$	28.55	28.49	27.08	26.11	28.27	27.56	28.54	17.55	27.06	29.47	29.33	29.96	29.70	30.21	29.52	25.79	25.74	28.21

Table C7. (*Continued*)

Rock type	granites with ≤71 wt.% SiO_2														granodiorites			
textural relationship	Symplectitic/well developed														inclusion in feldspar			
Sample	Mat 7	Mat 7	Mat 7	Mat 7	Mat 7_r	Mat 7_c	Mat 7	Mat 7	Mat 7_r	Mat 7_c	Mat 7_c	Mat 7_r	Mat 7_c	Mat 7_r	Mat 14	Mat 14	Mat 14	Mat 14
SiO_2	36.60	37.35	36.82	36.94	37.22	36.81	36.96	36.58	37.36	36.80	36.92	37.20	36.79	36.94	38.90	38.28	38.02	37.17
TiO_2	0.19	0.18	0.10	0.12	0.09	0.30	0.06	0.19	0.18	0.10	0.12	0.09	0.30	0.06	nd	nd	nd	nd
Al_2O_3	22.98	25.20	22.17	21.64	22.28	21.44	21.92	23.54	25.82	22.71	22.16	22.81	21.95	22.44	25.61	25.23	25.11	25.82
Y_2O_3	0.37	0.40	0.14	0.10	nd	0.36	0.48	0.37	0.40	0.14	0.10	nd	0.36	0.48	nd	nd	nd	nd
Ce_2O_3	nd	nd	nd	nd	nd	nd	nd	nd	nd	nd	nd	nd	nd	nd	nd	nd	nd	nd
La_2O_3	nd	nd	nd	nd	nd	nd	nd	nd	nd	nd	nd	nd	nd	nd	nd	nd	nd	nd
FeO*	12.57	9.30	13.54	14.12	13.60	14.00	13.55	12.09	8.94	13.03	13.59	13.08	13.47	13.03	11.23	10.81	10.79	7.93
MnO	0.12	0.10	0.16	0.10	0.15	0.20	nd	0.12	0.10	0.16	0.10	0.15	0.20	nd	0.25	0.23	0.18	0.15
MgO	0.10	0.05	0.01	0.08	0.07	nd	0.10	0.09	0.05	0.01	0.07	0.07	nd	0.09	nd	nd	nd	0.04
CaO	23.71	24.18	23.70	23.60	23.74	23.57	23.31	23.01	23.46	23.00	22.90	23.03	22.87	22.62	23.10	23.62	23.57	23.19
Na_2O	0.12	0.11	0.04	0.11	0.08	0.09	0.09	0.13	0.12	0.04	0.13	0.09	0.10	0.10	nd	nd	nd	0.10
K_2O	nd	nd	0.09	nd	0.02	nd	nd	nd	nd	0.08	nd	0.02	nd	nd	nd	nd	nd	nd
Total	96.76	96.86	96.77	96.79	97.23	96.77	96.45	96.13	96.43	96.07	96.07	96.53	96.05	95.76	99.09	98.17	97.66	94.40
Number of ions on the basis of 12 oxygen atoms:																		
Si^{4+}	2.914	2.915	2.944	2.959	2.956	2.955	2.963	2.917	2.914	2.948	2.964	2.960	2.960	2.967	2.965	2.950	2.947	2.940
Al^{3+}	2.157	2.317	2.090	2.043	2.085	2.028	2.071	2.212	2.373	2.144	2.096	2.139	2.081	2.125	2.301	2.292	2.293	2.406
Fe^{3+}	0.837	0.607	0.905	0.946	0.903	0.940	0.908	0.806	0.583	0.873	0.912	0.871	0.906	0.876	0.716	0.696	0.699	0.524
Ti^{4+}	0.012	0.011	0.006	0.007	0.005	0.018	0.004	0.012	0.011	0.006	0.007	0.005	0.018	0.004	0.000	0.000	0.000	0.000
Mn^{2+}	0.008	0.006	0.011	0.007	0.010	0.014	0.000	0.008	0.006	0.011	0.007	0.010	0.014	0.000	0.016	0.015	0.012	0.010
Mg^{2+}	0.012	0.006	0.001	0.009	0.009	0.000	0.012	0.011	0.005	0.001	0.008	0.008	0.000	0.011	0.000	0.000	0.000	0.005
Y^{3+}	0.016	0.017	0.006	0.004	0.000	0.015	0.021	0.016	0.017	0.006	0.004	0.000	0.015	0.021	0.000	0.000	0.000	0.000
Ca^{2+}	2.023	2.022	2.031	2.025	2.020	2.027	2.002	1.966	1.961	1.974	1.969	1.963	1.971	1.946	1.886	1.950	1.957	1.964
Ce3+	0.000	0.000	0.000	0.000	0.000	0.000	0.000	0.000	0.000	0.000	0.000	0.000	0.000	0.000	0.000	0.000	0.000	0.000
La3+	0.000	0.000	0.000	0.000	0.000	0.000	0.000	0.000	0.000	0.000	0.000	0.000	0.000	0.000	0.000	0.000	0.000	0.000
Na^{+}	0.018	0.016	0.006	0.017	0.012	0.014	0.013	0.021	0.018	0.007	0.020	0.013	0.016	0.015	0.000	0.000	0.000	0.015
K^{+}	0.000	0.000	0.009	0.000	0.002	0.000	0.000	0.000	0.000	0.008	0.000	0.002	0.000	0.000	0.000	0.000	0.000	0.000
Cation total	7.997	7.916	8.010	8.018	8.003	8.012	7.994	7.968	7.889	7.978	7.988	7.972	7.982	7.964	7.884	7.904	7.907	7.865
$Fe^{3+}/(Fe^{3+}+Al^{3+})$	27.95	20.75	30.23	31.65	30.22	31.67	30.49	26.71	19.73	28.93	30.32	28.92	30.33	29.18	23.72	23.31	23.36	17.88

Table C7. (*Continued*)

Rock type	granodiorites																	
textural relationship	inclusion in feldspar																	
Sample	Mat 14	Mat 14	Mat 14	Mat 14	Mat 14	Mat 14	Mat 14	Mat 14	Mat 14	Mat 14	Mat 14	Mat 14	Mat 14	Mat 14	Mat 34	Mat 34	Mat 34	Mat 34
SiO_2	38.37	37.58	37.70	37.53	37.92	38.06	36.67	36.62	36.01	36.14	36.52	36.18	36.65	37.40	37.99	38.06	37.82	38.37
TiO_2	nd	nd	nd	nd	nd	nd	nd	0.15	0.37	0.13	0.11	0.04	nd	0.01	0.09	nd	nd	nd
Al_2O_3	25.84	23.37	26.95	24.08	25.32	26.35	23.26	22.28	22.67	23.14	23.05	22.94	24.09	23.98	24.19	26.60	24.43	26.22
Y_2O_3	nd	nd	nd	nd	nd	nd	nd	0.08	0.19	0.28	0.22	0.24	0.31	0.24	nd	nd	0.33	0.29
Ce_2O_3	nd	nd	nd	nd	nd	nd	nd	nd	nd	nd	nd	nd	nd	nd	nd	nd	nd	nd
La_2O_3	nd	nd	nd	nd	nd	nd	nd	0.17	nd	nd	nd	nd	0.11	nd	nd	nd	nd	nd
FeO*	9.76	12.14	7.23	11.57	10.16	8.82	11.60	13.00	11.71	11.14	11.82	11.92	10.67	11.26	11.91	8.84	11.16	9.80
MnO	0.17	nd	0.15	0.20	0.16	0.26	nd	0.21	0.30	0.21	0.14	0.12	0.13	0.17	0.23	0.15	0.16	0.13
MgO	nd	nd	nd	nd	nd	nd	nd	0.10	0.06	0.05	0.08	0.03	0.07	0.03	0.06		0.07	0.04
CaO	23.62	23.21	23.47	23.03	23.46	23.54	22.92	22.56	22.45	22.74	22.74	22.83	22.95	23.01	23.32	24.11	23.70	23.86
Na_2O	0.07	0.06	0.11	0.13	0.21	0.04	0.11	0.24	0.05	0.08	0.08	0.16	0.15	0.08	0.07	0.06	0.14	nd
K_2O	nd	nd	nd	nd	nd	nd	nd	0.02	nd	nd	0.01	nd	nd	nd	0.01	0.02	nd	0.03
Total	97.83	96.36	95.62	96.55	97.22	97.06	94.56	95.42	93.81	93.91	94.75	94.47	95.13	96.18	97.86	97.85	97.79	98.75
Number of ions on the basis of 12 oxygen atoms:																		
Si^{4+}	2.950	2.976	2.929	2.958	2.944	2.936	2.957	2.957	2.939	2.938	2.948	2.935	2.931	2.958	2.957	2.917	2.944	2.928
Al^{3+}	2.341	2.181	2.468	2.237	2.317	2.396	2.211	2.120	2.180	2.217	2.193	2.194	2.270	2.235	2.219	2.403	2.241	2.357
Fe^{3+}	0.628	0.804	0.469	0.763	0.659	0.569	0.782	0.877	0.799	0.757	0.798	0.809	0.713	0.744	0.775	0.567	0.727	0.625
Ti^{4+}	0.000	0.000	0.000	0.000	0.000	0.000	0.000	0.009	0.023	0.008	0.006	0.002	0.000	0.001	0.005	0.000	0.000	0.000
Mn^{2+}	0.011	0.000	0.010	0.013	0.010	0.017	0.000	0.014	0.021	0.014	0.009	0.009	0.009	0.011	0.015	0.010	0.010	0.008
Mg^{2+}	0.000	0.000	0.000	0.000	0.000	0.000	0.000	0.012	0.007	0.006	0.009	0.004	0.008	0.004	0.007	0.000	0.008	0.005
Y^{3+}	0.000	0.000	0.000	0.000	0.000	0.000	0.000	0.003	0.008	0.012	0.009	0.010	0.013	0.010	0.000	0.000	0.014	0.012
Ca^{2+}	1.946	1.968	1.953	1.944	1.951	1.945	1.980	1.951	1.963	1.980	1.966	1.985	1.966	1.949	1.945	1.979	1.976	1.951
Ce3+	0.000	0.000	0.000	0.000	0.000	0.000	0.000	0.000	0.000	0.000	0.000	0.000	0.000	0.000	0.000	0.000	0.000	0.000
La3+	0.000	0.000	0.000	0.000	0.000	0.000	0.000	0.005	0.000	0.000	0.000	0.000	0.003	0.000	0.000	0.000	0.000	0.000
Na^{+}	0.010	0.010	0.017	0.020	0.031	0.006	0.017	0.037	0.009	0.012	0.012	0.025	0.024	0.013	0.010	0.008	0.020	0.000
K^{+}	0.000	0.000	0.000	0.000	0.000	0.000	0.000	0.002	0.000	0.000	0.001	0.000	0.000	0.000	0.001	0.002	0.000	0.003
Cation total	7.885	7.939	7.846	7.934	7.913	7.869	7.946	7.989	7.949	7.945	7.951	7.972	7.938	7.925	7.934	7.886	7.939	7.889
$Fe^{3+}/(Fe^{3+}+Al^{3+})$	21.14	26.93	15.98	25.43	22.15	19.19	26.14	29.27	26.82	25.46	26.67	26.94	23.91	24.99	25.89	19.09	24.48	20.97

Table C7. (*Continued*)

Rock type	granodiorites		granites with ≤71 wt.% SiO_2							
textural relationship			inclusion in feldspar							
Sample	Mat 34	Mat 70	Mat 31	Mat 31	Mat 31	Mat 31	Mat 31	Mat 31	Mat 31	Mat 31
SiO_2	38.49	38.51	39.41	37.81	37.02	38.36	37.81	36.16	38.01	38.06
TiO_2	nd	0.14	0.13	nd	nd	0.01	0.09	nd	0.12	0.06
Al_2O_3	25.90	24.54	24.48	24.13	23.37	24.60	25.72	22.83	24.83	25.73
Y_2O_3	0.35	nd	nd	0.34	0.57	0.50	0.32	0.47	nd	nd
Ce_2O_3	nd	nd	nd	nd	nd	nd	nd	nd	nd	nd
La_2O_3	nd	nd	nd	nd	nd	nd	nd	nd	nd	nd
FeO*	9.96	12.16	11.50	12.31	12.75	11.27	10.04	11.44	10.98	10.18
MnO	0.06	0.11	0.16	0.21	0.23	0.18	0.12	nd	0.17	0.23
MgO	0.07	nd	0.07	0.05	0.00	0.05	0.05	0.09	0.05	0.06
CaO	23.85	23.99	23.26	23.75	23.35	23.37	23.81	22.10	23.31	23.64
Na_2O	0.07	0.15	0.38	0.16	0.04	0.17	0.04	0.07	0.14	0.05
K_2O	nd	0.01	nd	0.06	0.01	nd	nd	0.01	0.01	0.03
Total	98.74	99.60	99.40	98.81	97.33	98.49	97.99	93.16	97.64	98.03
Number of ions on the basis of 12 oxygen atoms:										
Si^{4+}	2.939	2.949	3.004	2.933	2.928	2.961	2.916	2.962	2.950	2.930
Al^{3+}	2.331	2.214	2.199	2.206	2.178	2.238	2.338	2.204	2.271	2.334
Fe^{3+}	0.636	0.778	0.733	0.798	0.843	0.728	0.647	0.783	0.713	0.655
Ti^{4+}	0.000	0.008	0.008	0.000	0.000	0.000	0.005	0.000	0.007	0.004
Mn^{2+}	0.004	0.007	0.010	0.014	0.015	0.011	0.008	0.000	0.011	0.015
Mg^{2+}	0.008	0.000	0.008	0.005	0.000	0.005	0.006	0.011	0.006	0.007
Y^{3+}	0.014	0.000	0.000	0.014	0.024	0.020	0.013	0.021	0.000	0.000
Ca^{2+}	1.951	1.968	1.899	1.973	1.979	1.932	1.967	1.939	1.938	1.950
Ce3+	0.000	0.000	0.000	0.000	0.000	0.000	0.000	0.000	0.000	0.000
La3+	0.000	0.000	0.000	0.000	0.000	0.000	0.000	0.000	0.000	0.000
Na^{+}	0.010	0.022	0.056	0.024	0.007	0.025	0.006	0.010	0.021	0.007
K^{+}	0.000	0.001	0.000	0.005	0.001	0.000	0.000	0.001	0.001	0.003
Cation total	7.893	7.948	7.917	7.972	7.975	7.921	7.906	7.931	7.919	7.904
$Fe^{3+}/(Fe^{3+}+Al^{3+})$	21.43	26.01	25.00	26.57	27.90	24.53	21.69	26.23	23.89	21.92

Table C8. Ilmenite composition for the rocks of the Matok pluton.

Rock type	Pyroxene-bearing																	
	diorites1							diorites2								granodiorites		
Sample	Mat 44	Mat 44	Mat 44	Mat 44	Mat 44	Mat 44	Mat 67	Mat 66	Mat 66	Mat 66	Mat 66	Mat 18	Mat 52	Mat 52c	$Mat\ 52_r$	$Mat\ 57_c$	$Mat\ 57_r$	Mat 57
TiO_2	48.88	49.39	47.48	45.17	46.60	46.62	48.25	48.36	48.82	48.54	49.33	50.39	46.74	48.78	48.66	47.36	46.40	47.87
SiO_2	0.16	0.12	0.15	0.30	0.41	0.67	0.19	0.20	0.28	0.28	0.20	nd	0.24	0.27	0.24	0.31	0.31	0.28
Al_2O_3	0.29	0.43	0.30	0.27	0.37	0.58	0.15	0.18	0.12	0.21	0.19	nd	0.25	0.16	0.17	0.34	0.28	0.24
V_2O_3	0.62	0.51	0.47	nd	0.55	0.45	0.53	0.54	0.47	nd	0.58	nd	0.44	0.36	0.53	0.65	0.52	nd
FeO*	45.41	44.68	46.97	50.36	47.87	48.82	49.17	48.76	48.08	48.50	49.22	40.23	49.49	49.16	49.11	50.63	50.43	49.58
MnO	3.52	3.68	3.33	2.69	1.49	2.05	1.97	1.83	1.91	2.09	2.06	9.02	2.01	2.07	1.98	1.67	1.77	1.80
MgO	0.08	0.12	0.05	nd	nd	nd	0.03	0.07	0.05	0.01	0.08	nd	0.10	0.12	0.04	0.07	nd	nd
CaO	0.13	0.44	0.25	0.09	0.13	0.17	0.15	0.03	0.06	0.06	0.05	nd	0.04	0.14	0.23	0.09	0.29	0.20
Na_2O	0.15	0.09	0.16	0.19	0.06	0.36	nd	nd	0.08	0.11	0.10	nd	0.10	0.15	0.01	0.18	0.06	0.16
K_2O	0.01	nd	nd	nd	nd	0.02	nd	nd	0.02	nd	nd	nd	0.01	nd	0.02	0.03	nd	0.02
Total	99.24	99.45	99.16	99.07	97.47	99.73	100.45	99.98	99.90	99.81	101.81	99.64	99.40	101.19	100.99	101.32	100.04	100.15
Ti^{4+}	0.928	0.935	0.900	0.855	0.900	0.874	0.906	0.913	0.922	0.917	0.913	0.957	0.885	0.907	0.909	0.878	0.872	0.898
Si^{4+}	0.004	0.003	0.004	0.008	0.010	0.017	0.005	0.005	0.007	0.007	0.005	0.000	0.006	0.007	0.006	0.008	0.008	0.007
Fe^{3+}	0.122	0.105	0.181	0.276	0.159	0.209	0.162	0.148	0.132	0.151	0.152	0.085	0.207	0.168	0.154	0.214	0.225	0.187
Cr^{3+}	0.000	0.000	0.000	0.000	0.000	0.000	0.000	0.000	0.000	0.000	0.000	0.000	0.000	0.000	0.000	0.000	0.000	0.003
Al^{3+}	0.009	0.013	0.009	0.008	0.011	0.017	0.005	0.005	0.004	0.006	0.006	0.000	0.007	0.005	0.005	0.010	0.008	0.007
V^{3+}	0.013	0.010	0.010	0.000	0.011	0.009	0.011	0.011	0.010	0.000	0.012	0.000	0.009	0.007	0.010	0.013	0.010	0.000
Fe^{2+}	0.856	0.852	0.840	0.836	0.897	0.846	0.893	0.901	0.900	0.893	0.887	0.777	0.871	0.878	0.893	0.868	0.870	0.880
Mn^{2+}	0.075	0.078	0.071	0.057	0.032	0.043	0.042	0.039	0.041	0.044	0.043	0.193	0.043	0.043	0.042	0.035	0.037	0.038
Mg^{2+}	0.003	0.004	0.002	0.000	0.000	0.000	0.001	0.003	0.002	0.000	0.003	0.000	0.004	0.004	0.001	0.002	0.000	0.000
Ca^{2+}	0.003	0.012	0.007	0.002	0.003	0.005	0.004	0.001	0.002	0.002	0.001	0.000	0.001	0.004	0.006	0.002	0.008	0.005
Na^{+}	0.007	0.004	0.008	0.009	0.003	0.017	0.000	0.000	0.004	0.005	0.005	0.000	0.005	0.007	0.000	0.009	0.003	0.008
Cation total	2.020	2.017	2.031	2.051	2.028	2.037	2.029	2.026	2.023	2.026	2.026	2.012	2.037	2.029	2.027	2.039	2.041	2.033

Table C8. (*Continued*)

Rock type	Pyroxene-bearing											Pyroxene-free					
	granodiorites													granites with ≤71 wt.% SiO_2			
Sample	Mat 57_c	Mat 57_r	Mat 57	Mat 58_c	Mat 58_r	Mat 58	Mat 58	Mat 59	Mat 59	Mat 59	Mat 59	Mat 3_c	Mat 3_r	Mat 42_r	Mat 42_c	Mat 42	Mat 42
TiO_2	47.48	47.60	49.45	48.59	47.16	47.82	47.15	46.09	48.40	49.85	49.79	46.09	47.24	46.70	49.66	48.49	48.06
SiO_2	0.17	0.19	0.23	0.45	0.33	nd	1.30	2.32	0.31	0.11	0.40	0.30	0.87	3.21	0.30	0.33	0.20
Al_2O_3	0.48	0.36	0.17	0.51	0.27	0.42	1.25	1.38	0.24	0.24	0.44	0.30	0.34	1.59	0.23	0.19	0.20
V_2O_3	0.45	nd	0.24	nd	nd	nd	nd	0.48	0.54	0.41	nd	nd	nd	nd	nd	nd	nd
FeO*	50.43	50.15	49.45	43.80	47.78	48.14	45.63	41.62	43.60	47.24	46.12	46.71	43.69	44.39	47.62	48.20	48.81
MnO	1.61	1.73	1.91	4.65	1.32	1.29	1.48	2.68	2.18	2.27	2.22	4.79	4.81	2.55	2.56	2.36	2.45
MgO	0.06	0.00	0.02	0.04	0.08	0.12	0.42	0.11	0.04	0.04	0.15	0.05	nd	0.70	0.13	nd	0.06
CaO	0.01	0.11	0.04	0.10	0.09	0.03	0.02	0.10	0.06	0.08	0.06	0.07	1.03	0.05	0.08	0.07	0.07
Na_2O	0.04	0.16	0.29	0.10	0.07	0.10	0.18	0.14	0.11	0.09	0.96	0.13	0.15	0.16	0.06	0.02	0.16
K_2O	0.01	nd	0.03	0.17	nd	nd	0.12	0.28	nd	0.00	0.01	nd	0.03	0.54	nd	nd	nd
Total	100.74	100.30	101.83	98.41	97.08	97.92	97.54	95.20	95.49	100.33	100.15	98.44	98.14	99.91	100.64	99.66	100.01
Ti^{4+}	0.887	0.892	0.913	0.931	0.915	0.920	0.902	0.905	0.957	0.938	0.925	0.880	0.902	0.868	0.930	0.918	0.904
Si^{4+}	0.004	0.005	0.006	0.011	0.008	0.000	0.033	0.061	0.008	0.003	0.010	0.008	0.022	0.079	0.007	0.008	0.005
Fe^{3+}	0.196	0.203	0.165	0.099	0.148	0.153	0.097	0.015	0.057	0.108	0.163	0.223	0.149	0.049	0.121	0.143	0.183
Cr^{3+}	0.000	0.000	0.000	0.000	0.000	0.000	0.000	0.000	0.000	0.000	0.000	0.000	0.000	0.000	0.000	0.000	0.000
Al^{3+}	0.014	0.011	0.005	0.015	0.008	0.013	0.037	0.042	0.007	0.007	0.013	0.009	0.010	0.046	0.007	0.006	0.006
V^{3+}	0.009	0.000	0.005	0.000	0.000	0.000	0.000	0.010	0.011	0.008	0.000	0.000	0.000	0.000	0.000	0.000	0.000
Fe^{2+}	0.887	0.879	0.880	0.849	0.909	0.903	0.889	0.896	0.911	0.899	0.816	0.806	0.802	0.876	0.891	0.897	0.871
Mn^{2+}	0.034	0.036	0.040	0.100	0.029	0.028	0.032	0.059	0.049	0.048	0.046	0.103	0.103	0.053	0.054	0.050	0.052
Mg^{2+}	0.002	0.000	0.001	0.002	0.003	0.005	0.016	0.004	0.002	0.001	0.006	0.002	0.000	0.026	0.005	0.000	0.002
Ca^{2+}	0.000	0.003	0.001	0.003	0.002	0.001	0.001	0.003	0.002	0.002	0.002	0.002	0.028	0.001	0.002	0.002	0.002
Na^{+}	0.002	0.008	0.014	0.005	0.003	0.005	0.009	0.007	0.006	0.004	0.046	0.006	0.007	0.008	0.003	0.001	0.008
Cation total	2.035	2.037	2.029	2.016	2.026	2.027	2.016	2.002	2.009	2.018	2.027	2.038	2.024	2.008	2.020	2.025	2.032